Triphenylene-based Polymers for Organic Electronics

Dissertation

zur Erlangung des Grades

“Doktor der Naturwissenschaften”

am Fachbereich Chemie, Pharmazie und Geowissenchaften der

Johannes Gutenberg-Universität Mainz

vorgelegt von

Moussa Saleh

geboren in Tripolis, Libyen

Mainz, 2010

Table of contents

Index of Abbreviations

CIE	Commission Internationale de L'Eclairage
DCM	dichloromethane
DSC	differential scanning calorimetry
EL	electroluminescence
ETL	electron transporting layer
FD MS	field desorption mass spectroscopy
FRET	Forster resonance energy transfer
GPC	Gel permeation chromatography
h	hour
HBC	hexa-peri-hexabenzocoronene
HBL	hole blocking layer
HOMO	highest occupied molecular orbital
ITO	indium tin oxide
I-V-L	current density and luminescence versus voltage
LUMO	lowest unoccupied molecular orbital
MALDI-TOF	matrix-assisted laser desorption ionization –time of flight
MeOH	methanol
min	minute
MS	mass spectroscopy
NMR	nuclear magnetic resonance
OLED	organic light emitting diode
PAH	polycyclic aromatic hydrocarbons
PEDOT:PSS	poly(styrene sulphonic ester) doped poly(ethylenedioxy-thiophene)

PF	polyfluorene
PL	photoluminescence
PLED	Polymeric light emitting diode
RGB	red, green, and blue
RT	room temperature
STM	scanning tunneling microscopy
TBAF	tetrabutylammonium fluoride
TCNQ	7,7,8,8-tetracyanoquinodimethane
TGA	thermogravimetric analysis
THF	tetrahydrofuran
UV-vis	ultraviolet/visible
WAXS	wide angle X-ray scattering

Chapter 1

Foreword

With the invention of the transistor around the middle of the 20th century, inorganic semiconductors like silicon started to take over the role as principal materials in electronics from the before customary metals. By more development in the field of semiconductors, inorganic based microelectronics became ubiquitous in our everyday life by the end of the last century. Now at the beginning of the 21st century we are in front of a new electronics revolution that has become possible due to the development and understanding of a new class of materials, commonly known as *Organic Semiconductors*. The promise of inexpensive electronics has fuelled widespread interest in the field of organic electronics. Although organic device performances are still low compared to the existing silicon technology (Figure 1.1), they offer interesting alternatives in a number of niche electronics applications such as large-area, low-cost, and flexible electronics.

Strictly speaking organic semiconductors are not new, they have been synthesized and studied for over five decades[1]. In the 1950s, drift mobility measurements and the photoconductivity response of small molecules such as anthracene were examined[1] and although these materials showed semiconducting properties (i.e., conductivities in the range of 10^{-9}-10^{-6} Scm^{-1})[2], their performance and stability were poor.

Following that, the research scope extended from organic small molecules to cover polymeric materials, and a new type of material was firstly discovered, known as conducting polymers. Such polymers evolved from a rather esoteric occupation to a lively field of activity ever since the discovery in 1977 by the 2000 Chemistry Nobel Laureates, Alan J. Heeger, Alan G. MacDiarmid and Hideki Shirakawa, of electrical conductivity in the simple hydrocarbon polymer polyacetylene upon doping. [3-5]

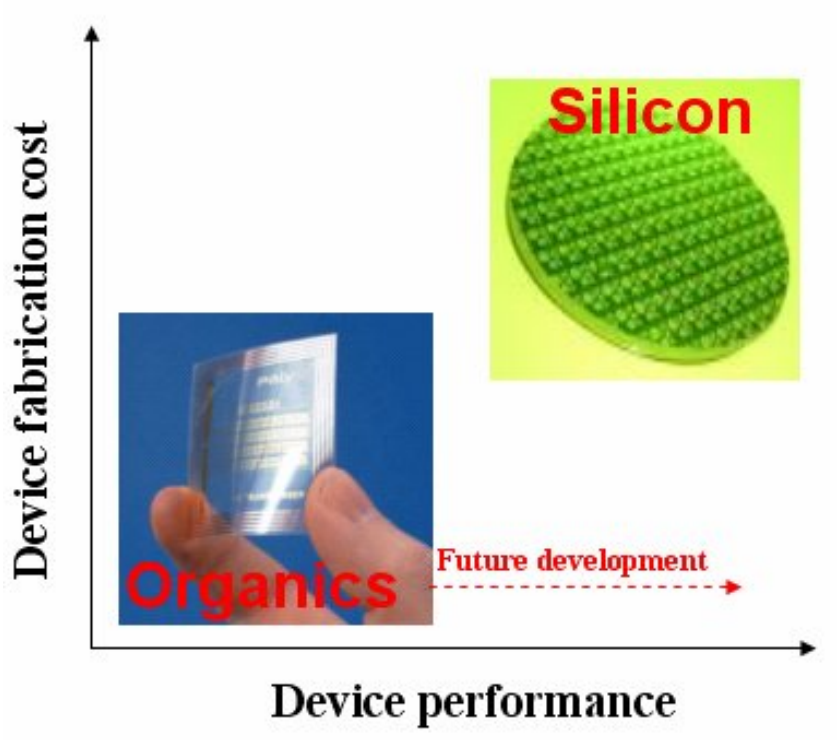

Figure 1.1 Comparison between silicon and organic electronics.

Later on, after the discovery by the Cambridge groups of R. Friend and A. Holmes, of electroluminescence of poly(phenylenevinylene) in 1990,[6] a dramatic development in the field of conjugated polymers occurred which opened the way to the development of polymer light emitting diodes. As a result, the research activities in the 1990s focused on the semiconductor properties of un-doped conjugated polymers rather than on metal conduction, and on the development of organic semiconductor devices.

Because of their unique properties, conjugated polymers lend themselves to a myriad of applications such as polymeric light emitting diodes (PLEDs),[7-16] photovoltaic devices,[17-21] and field-effect transistors.[22-27] This introduction is not intended as a comprehensive survey of conjugated polymer-based devices, since many general review articles have appeared in the literature.[28] Instead it will concentrate on the precedents that have shaped and provided motivation behind this work. I shall begin with a concise overview of conjugated polymers, and then discuss some of the most popular blue-emitting semiconducting polymers with a

brief description of their synthetic routes. We will then move on to talk about organic light emitting diodes (OLEDs) and their working principles. In addition the concept of converting 3D-conjugated polymers into 2D-graphene nanoribbons will be shortly introduced.

1.1 Background on π-Conjugated Polymers

Conjugated polymers are organic macromolecules which consist at least of one chain of alternating double- and single-bonds. Theses polymers are characterized by a conjugated π-electron system formed by the p_z-orbitals of the sp^2 hybridized C-atoms in the molecules (see Figure 1.2). As compared to the σ-bond linkages in the backbone of the polymers, the π-bonding is significantly weaker. Therefore, the lowest electronic excitations of conjugated molecules are the π-π* transitions leading to light absorption or emission corresponding to the molecular energy band gaps. One of the main advantages of these materials is the way they are processed to form thin films. Whereas conventional inorganic semiconductors are usually deposited from the gas phase by sublimation or evaporation, conjugated polymers can only be

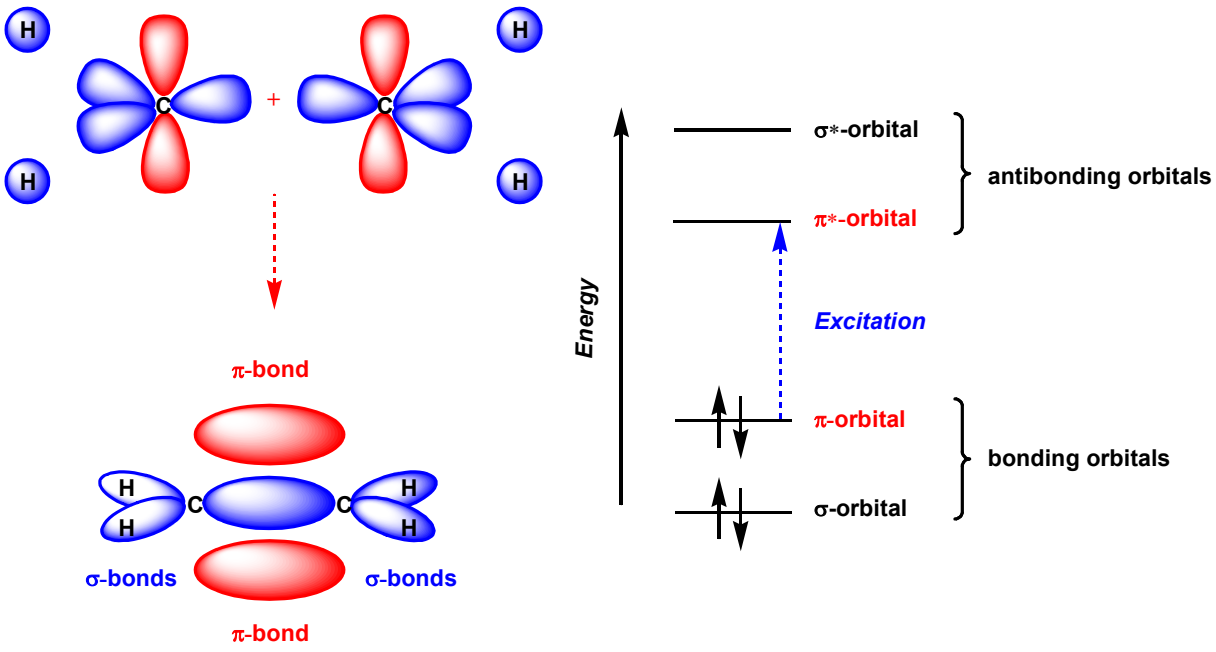

Figure 1.2 Left: σ- and π-bonds in ethene, as an example for the simplest conjugated π-electron system. The right viewgraph shows the energy levels of the ethene molecule.

processed from solution (e.g. by spin-coating or printing techniques). That makes this class of materials combine the optoelectronic properties of semiconductors with the mechanical properties and processing advantages of plastics.

As mentioned above a new era of scientific research launched with the discovery of the metallic conductivity in polyacetylene (**PA**).[5] Nevertheless **PA** itself suffered from three major drawbacks: its insolubility, unprocessibility, and structural defects (by oxidation). To overcome these problems several synthetic approaches were reported at that time for preparing malfunction free **PAs**.[29,30] Such synthetic procedures represented innovative strategies in macromolecular synthesis and were responsible for the chemical revolution of the semiconducting polymer field. Consequently, a large number or research teams all over the world were engaged in the search for new organic semiconductors materials that could provide the desired properties of stability and ease of processing.

Shortly after, new polymers such as poly(pyrrole) (**PPy**), poly(thiophene) (**PT**), poly(p-phenylene) (**PPP**), poly(p-phenylenevinylene) (**PPV**), poly(fluorene) (**PF**), poly(indenofluorene) (**PIF**) poly(carbazole) (**PCz**) and poly(phenanthrene) (**PPh**) (Figure 1.3), were introduced and their chemical modification were developed even faster, proving in only a few years, by the beginning of the 1990s, that controlling the molecular structures induced changes in very important physical parameters such as optical properties, thermal stability, and 3D arrangements of the materials. It was also found that fine tuning of the polymers' band gaps can be done by the appropriate selection of the monomers, of the side chain length and/or of the degree steric hindrance.

By controlling the size of polymer's band gap, it was possible to tune the color emitted form the polymer upon optical or electrical excitation. In the following section some of the most famous blue-emitting (large band gap) conjugated polymers will be presented and discussed.

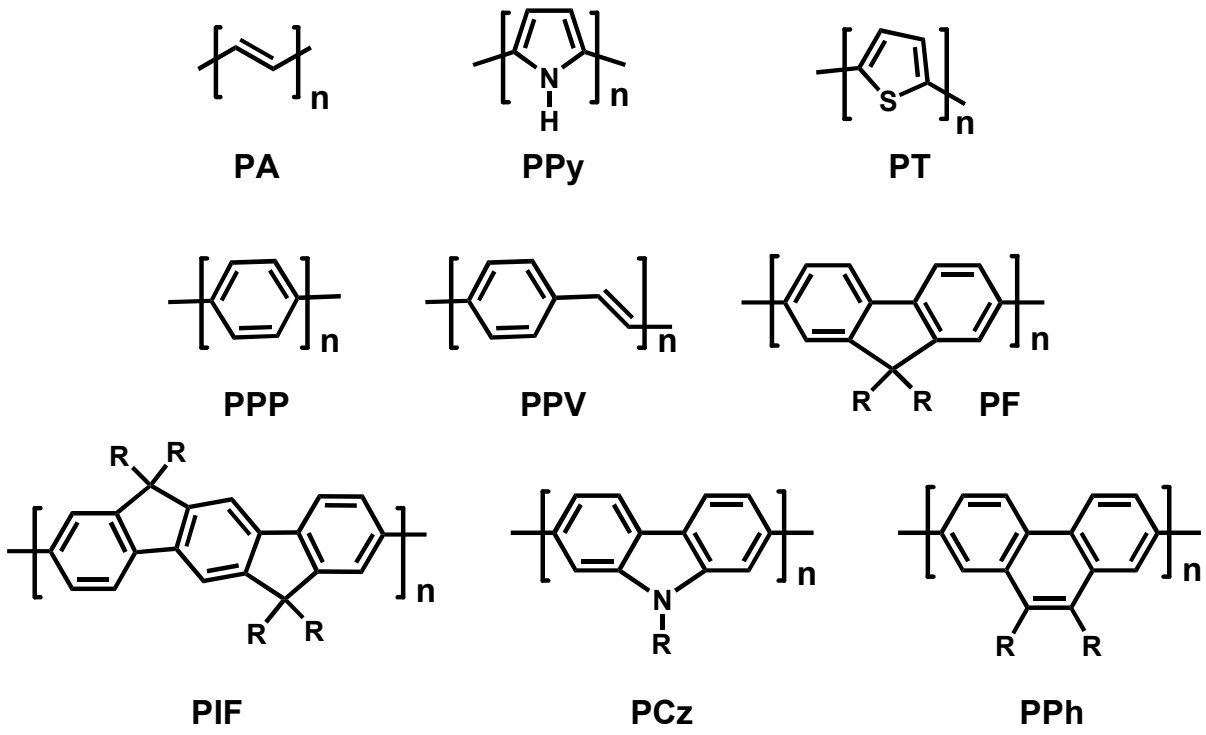

Figure 1.3 Molecular structure of some conjugated polymers.

1.2 Poly(para-phenylene)-Type Polymers as Blue-emitters

As part of the display applications based on conjugated polymers, significant attention has been directed to attain stable blue electroluminescence (EL) from poly(para-phenylene)-type (**PPP**-type) polymers[31-33]. The importance of blue light generation is not only because of its essential role as one of the constituents in the red–green–blue (RGB) full color light-emitting devices, but it can also be transformed into red and green light by internal[34] or external color conversion[35].

During the last decade, great consideration has been given to the polyphenylene-based materials. Among this class of materials, special attention was given to the highly emissive polyfluorenes (**PFs**) as a promising class of conjugated polymers, which can be used as blue light-emitting materials in PLEDs. The first report on the synthesis of soluble poly(9,9-dialkylfluorene)s from the corresponding fluorene monomers with 9,9-alkyl chains up to C_{12} using $FeCl_3$ as the oxidative coupling agent was given by Yoshino and coworkers in 1989[36,37],

and first blue EL from such poly(9,9-dialkylfluorene) was shown by the same group two years later[38]. After these initial experiments, a broad variety of efficient synthesis of **PFs** has been developed, especially by Suzuki- and Yamamoto-type aryl–aryl couplings. The excellent optical and electronic properties of 9,9-disubstituted **PFs**, polyindenofluorenes (PIF)[39], and fluorene- based copolymers[40,41]have brought this class of materials into the focus of scientific and industrial interest. The photophysics of **PF**-type polymers has been intensively studied and impressive improvements concerning color purity and device stability of **PF**-based devices have been made. Still, the strict requirements for commercialization demanding tens of thousands of hours of operation are a hard to reach goal for blue-emitting PLEDs.

Due to the hope that **PFs**, **PIFs**, **PPP**-type ladder polymers (**LPPPs**), and other bridged **PPPs** hold as a very promising class of blue emitters of PLEDs[42-44], widespread studies concerning the synthetic routes, characterization, and application of such aromatic polymers have been done in the last decade.

There is too immense an amount of scientific publication to give a complete overview of blue-emitting PLEDs which fit in the scope of this thesis. Therefore in the following sections a short overview that summarizes some of the most attractive outcomes and trends in the field in the last few years will be presented. Moreover, this overview will only touch on the related topic of aromatic copolymers containing bridged oligophenyl segments as one structural component. Such copolymers present excellent examples of conjugated polymers that have been successfully applied in electronic devices[45-49].

1.3 Synthetic Approaches to Poly(para-Phenylene)- Type Polymers

Unsubstituted **PPP** is insoluble in common organic solvents. The lack of solubility and fusibility prevent both the obvious characterization and the processing of **PPP**. Moreover, the intractability of unsubstituted **PPP** materials has thwarted any serious commercial development of the polymer.

Several synthetic routes were suggested to synthesis **PPP**-type polymers, such methods include: The use of soluble, nonconjugated precursor polymers[50,51], the electrochemical polymerization of benzene[52], oxidative condensation of aromatic hydrocarbons[53] and transition metal-mediated coupling reactions.[54] The last two classes of reactions represent the major synthetic routs for the **PPP**- type polymers and they will be discussed in the following paragraphs.

1.3.1 Oxidative condensation of aromatic hydrocarbons

The first attempts to generate poly(*para*-phenylene) were undertaken in the 1960s. Kovacic et al.[53] reported that the oxidative treatment of benzene with copper(II) chloride in the presence of strong Lewis acids (aluminium trichloride) led to a condensation of the aromatic rings. This reaction proceeded through the formation of reactive radical cation intermediates that subsequently attack neutral benzene molecules. The maximum degree of condensation

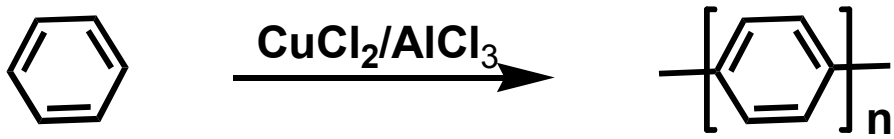

Scheme 1.1 Kovacic's route for the synthesis of **PPP**.[53]

was ca. 10–12, where the benzene subunits were preferentially connected in the 1,4-position (Scheme 1.1). Other reactions like cross-linking and oxidative condensation to more highly condensed, aromatic hydrocarbon building blocks happened as side reactions. By the adaptation of the original procedure of Kovacic et al., several other substituted benzene derivatives and other aromatic hydrocarbon monomers were coupled to oligo- and polyarylenes. Katsuya et al.[55] reported the oxidative coupling of 2,5-dimethoxybenzene using the binary system copper(II) chloride, aluminum chloride to form poly(2,5-dimethoxy-1,4-phenylene) (Scheme 1.2). The polymer obtained was only soluble in concentrated sulfuric

acid, and was fusible at 320°C. Ueda et al.[56] reported also the same coupling reaction for the same monomer by using different binary system (iron(III) chloride/aluminum chloride). However, the gained polymers were not totally *para*-linked.

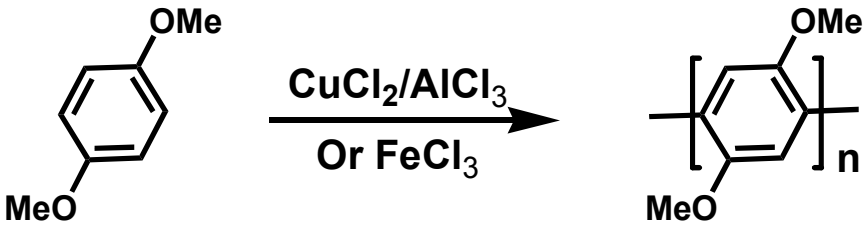

Scheme 1.2 Katsuya and Ueda's approaches for the synthesis of **PPP**-derivatives.[56]

In 1993 Yoshino et al.[57] reported the synthesis of 9,9-disubstituted poly(fluorene)s (**PFs**) (Scheme 1.3), in which the solubilizing substituents were introduced in the form of a di-*n*-hexylmethylene bridge, that spans the neighboring rings in pairs and enforces a planar arrangement. The soluble and fusible poly(9,9-di-*n*-hexylfluorene-2,7-diyl)s were obtained by oxidative coupling of 9,9-di-*n*-hexylfluorene with iron(III) chloride.

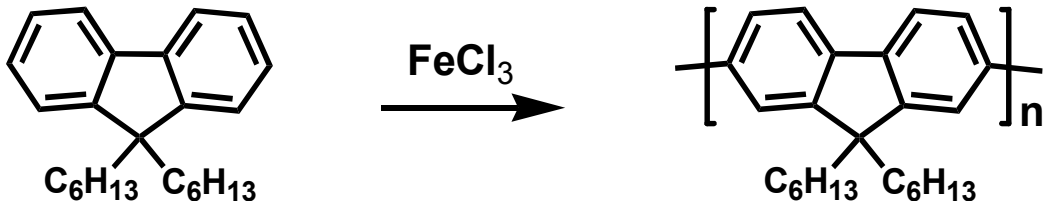

Scheme 1.3 Synthetic route of 9,9-disubstituted poly(fluorene)s by Yoshino et al.[57]

Characterization of the obtained polymers depicted that they had number average molecular weight (M*n)* up to a maximum of 5000 g/mol. The absorption maxima (λ_{max}) of the polymers were centred at about 388 nm. As a result of the partial flattening of the **PPP** backbone to a "stepladder" polymer, the long-wave-length absorption maxima were bathochromically shifted by about 50 nm relative to that of the parent **PPP** structure.

An unsatisfactory aspect of this synthesis is the quite low degree of polymerization: a maximum of 20 aromatic rings. Moreover, in addition to the predominant 2,7-coupling of the

building blocks, other types of coupling can occur leading to structural defects.

1.3.2 Transition metal-mediated coupling reactions

Although, several approaches have been investigated (see section 1.3) for the preparation of **PPP**-type polymers, only the introduction of alkyl, alkoxy, ester, keto, or ionic side groups in a ‘‘hairy rod’’ approach that was initially developed by Schlüter and Wegner and coworkers[58-77] has enabled the solubilization of the **PPP**-type polymers in common organic solvents. Moreover, the availability of newer, more effective methods for aryl-aryl coupling has been an important driving force for the development of new synthetic strategies for poly(para-phenylene)-type polymers. This bundle of available synthetic methods today includes the Suzuki cross coupling[78] of arylboronic acids or esters with chloro-, bromo-, iodo-, or tosylaryls (Scheme 1.4), Yamamoto homocoupling[79] of chloro-, bromo-, or iodoaryls, and Stille cross coupling[80] of trialkylstannylaryls with haloaryls. The application of such original transition metal-mediated aryl–aryl coupling reactions together with the ‘‘hairy rod’’

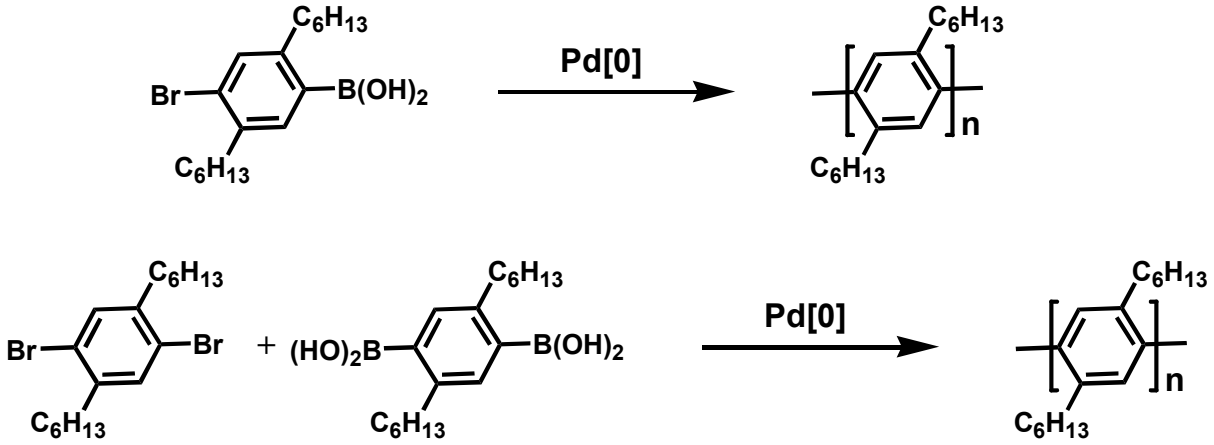

Scheme 1.4 Synthesis of poly(2,5-dialkyl-1,4-phenylene) after Schlüter and Wegner.[54]

approach has enabled the design and the synthesis of nearly defect-free soluble **PPP** derivatives of high molecular weight (Mn = 300,000 g / mol). However, the key shortcoming of such substituted **PPPs** is the distinct decrease of the main chain conjugative interaction that is caused by the steric bulkiness of the substituents. The effect is most pronounced for alkyl

groups in the 2- and 5-positions of the 1,4-phenylene units (mutual distortion of neighboring aryl units of up to 80°) and somewhat lesser pronounced for alkoxy groups.[81]

A strategy which overcomes this shortcoming was first proposed and developed by Scherf and Müllen, and includes the bridging of adjacent phenylenes by methylene bridges.[82-84] These bridges force neighboring aryl units into a coplanar arrangement and guarantee a full conjugative interaction of the aromatic moieties of the conjugated PPP main chain. A complete execution of this synthetic strategy led to ladderized **PPP** (**LPPPs**) (Scheme 1.5).

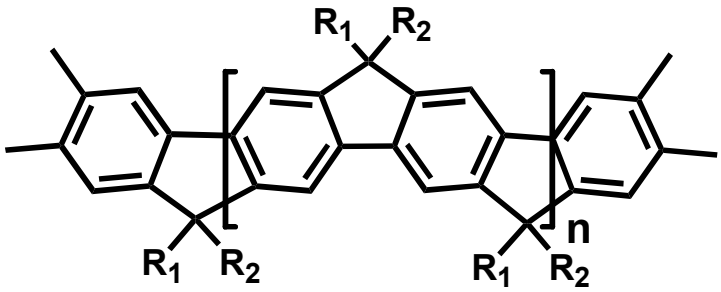

Scheme 1.5 Structure of a ladderized **PPP** (**LPPP**).[82]

Afterward several synthetic strategies toward well-defined ladder polymers have been developed.[85-87] The pioneer work of Müllen and Scherf, where they developed a precursor strategy toward **LPPPs** (Scheme 1.6) including the generation of suitably substituted **PPP** precursors and their polymer-analogous cyclization to **LPPPs**[82] was the platform for other aromatic building blocks. Naphthalene, anthracene, thiophene, and carbazole have been also incorporated into the main chain of such planarized arylene-type ladder polymers (Scheme 1.7). This novel synthetic strategy (Scheme 1.6) with the optimized substitution pattern of the single-stranded precursors allows for a regioselective and quantitative cyclization without the occurrence of unfavorable interchain cross-linking.[82]

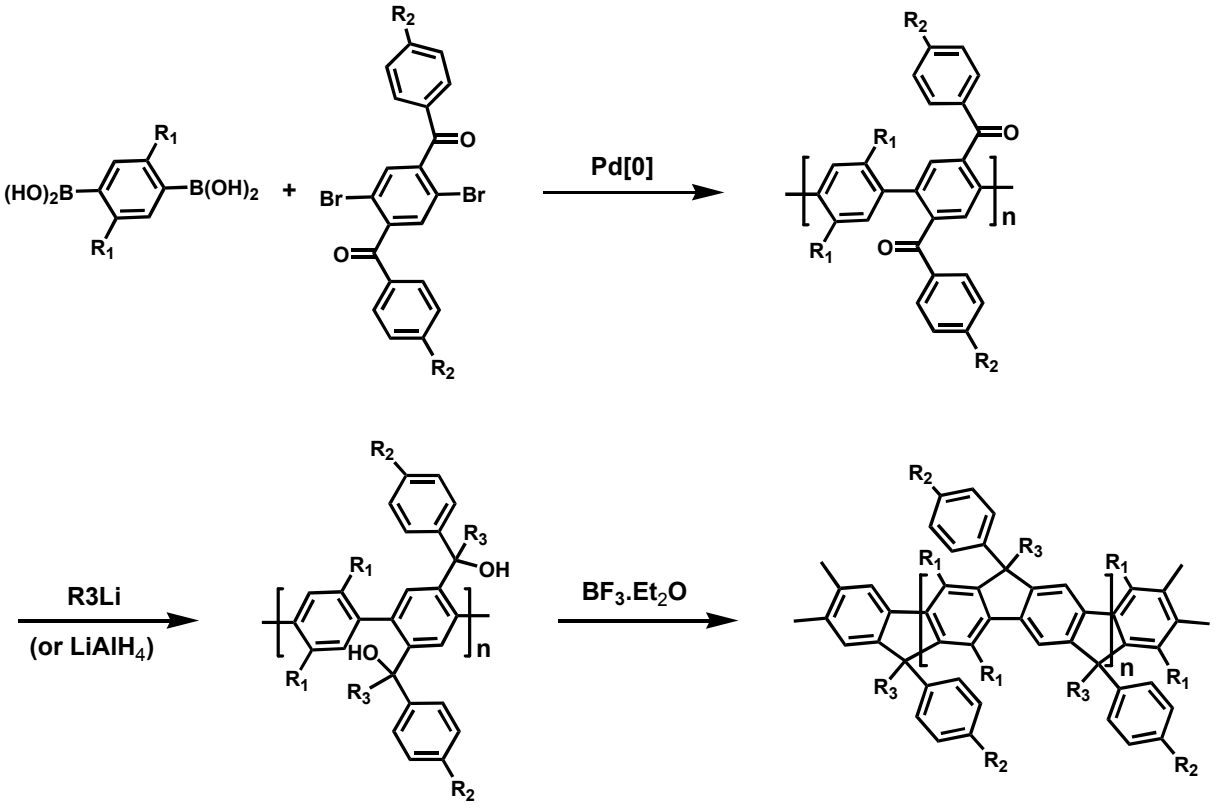

Scheme 1.6 Synthesis of **LPPPs** after Scherf and Müllen[82]

(R_1 and R_2 = C_6-C_{10}, while R_3 = H or CH_3).

Due to the high regioselective reaction products the metal mediated aryl–aryl coupling reactions offer, the method was applied for the synthesis of **PFs**. Polyfluorenes those were initially synthesized by Yoshino[57] by the oxidative coupling of 9,9-dialkylfluorene monomers

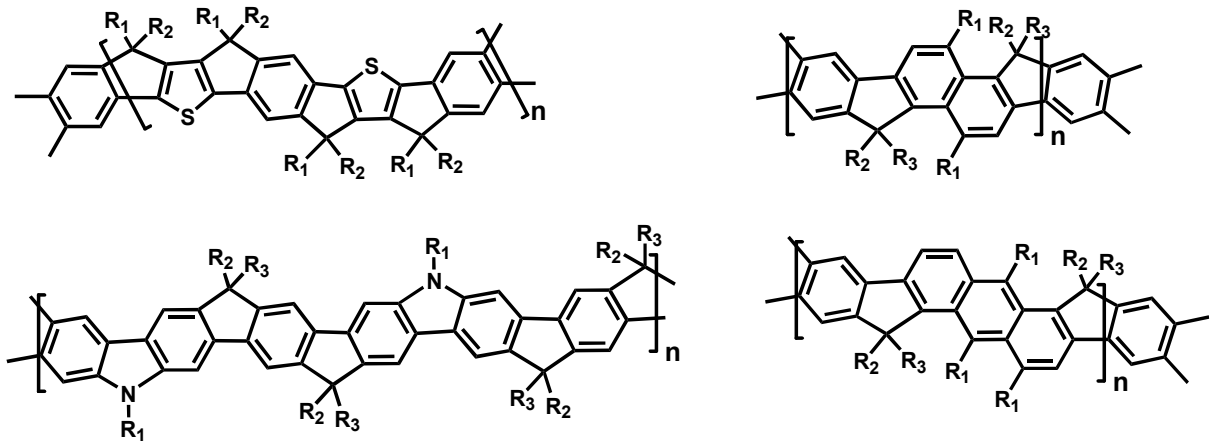

Scheme 1.7 Structures of related **LPPPs**-type polymers with main chain thiophene, carbazole, naphthalene, and anthracene units.[88-91]

with $FeCl_3$ and were characterized by unselective coupling at the 2- and 7-positions of the fluorene core were obtained in well-defined chemical structure (regioselective coupling at the 2- and 7-positions of the fluorene core) by using the metal mediated aryl–aryl coupling reactions.

A group at DOW Chemicals first developed and patented an approach based on the Suzuki-type cross coupling of 9,9-dialkylfluorene-2,7-diboronic esters and 9,9-dialkyl-2,7-dibromofluorenes toward high molecular weight, soluble poly(9,9-dialkylfluorene-2,7-diyl)s[92,93] (Scheme 1.8).

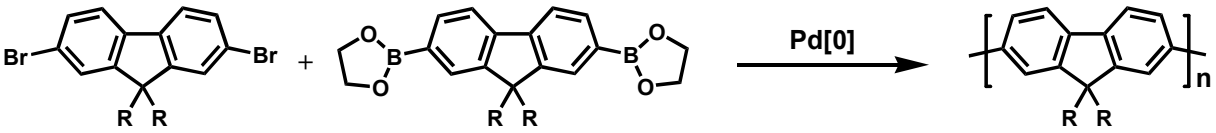

Scheme 1.8 Synthesis of poly(9,9-dialkylfluorene-2,7-diyl) described by DOW Chemicals.[92,93]

As previously mentioned the electronic properties of conjugated polymers are adversely affected by changes in conformation due to the substituents, which can lead to a marked mutual twisting of the aromatic subunits followed by a drastic reduction in the conjugative interaction.[81] Thus the decisive step in the realization of this principle is the preparation of a **PPPs** in which the aromatic subunits could be obtained in a planar or only slightly twisted conformation (in which the π-conjugation remains fully intact) in spite of the introduction of substituents. While the synthesis of the **LPPP**-type polymers using the palladium-mediated Suzuki cross coupling reaction was able to afford products with such requirements, it was logical to combine this principle for the preparation of "stepladder" structures possessing a minimized twist between consecutive phenylene units with new, efficient and selective methods for aryl-aryl couplings.

A first attempt at this was by Yamamoto et al.[94] They coupled 2,7-dibromo-9,10-dihydrophenanthrene to give an ethano-bridged poly(*para*-phenylene) derivative (poly(9,10-

dihydrophenanthrene-2,7-diyl)) (Scheme 1.9) by way of low-valent nickel complexes, which were used either stoichiometrically as a reagent ($Ni(COD)_2$) or were generated electrochemically in the reaction mixture. As a result of the insufficient solubilization of the ethano substituents only the oligomer fraction with Mn < 1000 was soluble, while the polymeric products precipitated out as an insoluble powder. The value of λ_{max} for the soluble fraction was about 360 nm. Building on this, it was expected that combining the synthetic procedure of Yamamoto et al.[94] with the introduction of more extended solubilizing substituents would be an advance. Accordingly, several alkyl-substituted monomer precursors were used in the Yamamoto aryl-aryl coupling reaction.

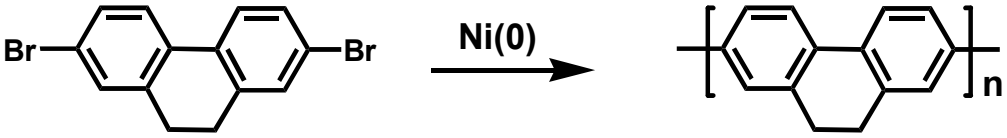

Scheme 1.9 Synthesis of poly(9,10-dihydrophenanthrene-2,7-diyl).[94]

In 1995 Müllen et al. applied the Yamamoto-type coupling for the synthesis of pyrene derivatives. The reaction was done by reacting 2,7-dibromo-4,9-dialkyl-4,5,9,10-tetrahydropyrene with Ni(COD) in DMF/toluene that gave a poly(4,9-dialkyl-4,5,9,10-tetrahydropyrene-2,7-diyl) (**PTHP**) (Scheme 1.10).[95] The polymer represented a new, completely soluble type of **PPP** derivative with a "stepladder" structure, in which each pair of neighboring aromatic rings is doubly bridged with ethano linkages.

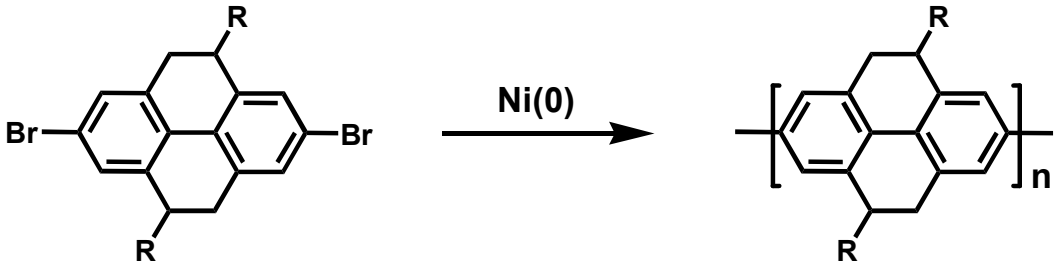

Scheme 1.10 Synthesis of poly(4,9- dialkyl-4,5,9,10-tetrahydropyrene-2,7-diyl) by Müllen.[95]

In the first coupling experiments the monomer was used as a *cis*/*trans* diastereomeric mixture.[95] When the diastereoisomers were separated the polymer was obtained in stereoregular PTHPs. The polymers depicted UV-vis absorption (λ_{max}) of 385 nm, which was almost identical with the value for the "stepladder" polyfluorenes reported by Yoshino et al.[57] In solution PTHP showed an intense blue photoluminescence (PL) (λ_{max} = 425 nm) with a Stoke shift between absorption and emission of 40 nm. In the solid state the PL was slightly bathochromically shifted to λ_{max} ca. 457 nm, probably as a result of aggregation. Applying the polymer as an active layer in PLEDs showed the appearance of a quite intense blue-green electroluminescence (EL) with a quantum yield of 0.1–0.15% (single layer construction ITO/PTHP /Ca).

Due to the success the Yamamoto homocoupling reaction showed, the method utility was extended to produce several other PPP-type polymers. After the Suzuki coupling-based synthesis of poly(9,9-dialkylfluorene-2,7-diyl) that was presented by DOW Chemicals,[92,93] Nothofer and Scherf developed in 1999 an alternative approach for the synthesis of PF based on the Yamamoto-type homocoupling of 9,9-dialkyl-2,7-dibromofluorene (Scheme 1.11).[96]

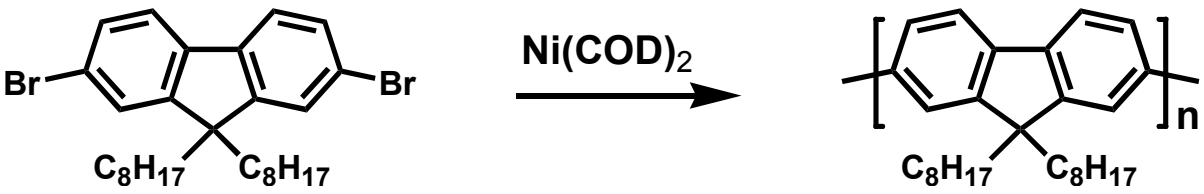

Scheme 1.11 Synthesis of **PFO** after Nothofer and Scherf.[96]

Both methods, if properly done, lead to the highest-quality PFs with a number average molecular weight of up to 300000 g/mol, corresponding to a coupling of several hundreds of repeat units.[42] Poly(9,9-dialkylfluorene-2,7-diyl)s have been intensively studied for their potential application as blue emitters in polymer-based OLEDs.[42,97] **PFs** show a very rich variety of structures in the condensed state, including nematic LC mesophases and crystalline phases.[97,98] It was found that the substituents at the 9-position strongly influence the solid

state packing behavior of the materials, accordingly many PF-derivatives with linear and branched alkyls as well as aryls including dendritic oligophenyl and spirobifluorene-type side chains were synthesised and investigated.[99-100].

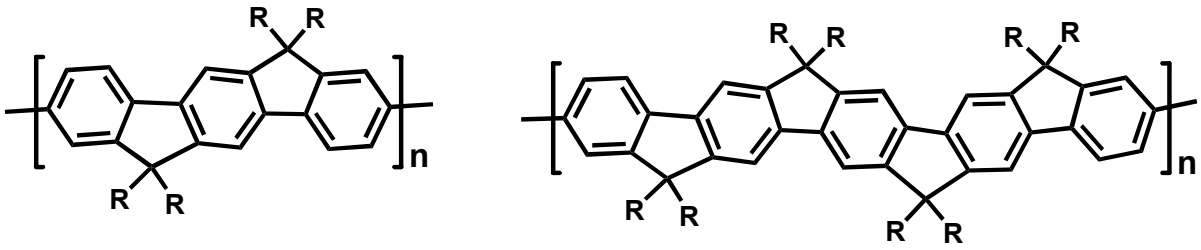

Scheme 1.12 Structures of polyindenofluorene (left) and a poly(para-phenylene) (right) with bridged pentaphenyl units.[101-103]

In parallel, Müllen and Grimsdale have varied the pattern of bridged and nonbridged biphenyl units in **PPP**-type polymers by synthesizing **PIFs** (2 of 3 aryl–aryl linkages are bridged),[101,102] and **PPPs** containing ladder-type pentaphenyl segments (5 aryl–aryl linkages are bridged) as shown in Scheme 1.12.[103] In that way, the authors filled the ‘‘gap’’ between **PFs** and **LPPPs**. Now, a complete series of **PPP**-type structures with increasing degree of bridging is available.

After the extensive synthetic work during the last decade, now a whole series of **PPPs** with increasing degree of methylene bridging is available ranging from the nonbridged poly(2,5-dialkyl-1,4-phenylene)s by **PFs**, **PIFs**, and **PPPs** with bridged pentaphenyl units toward fully bridged **LPPPs**. Table 1.1 gives molecular weight as well as optical data (absorption and emission) of this series of aromatic, conjugated polymers.

Table 1.1 Poly(para-Phenylene)s with different degree of Aryl–Aryl bridging.

Polymer	**$\lambda_{max.,abs}$ (nm)**	**$\lambda_{max.,em}$ (nm)**	**M_n (g/mol)**	**PDI**
Poly(2,5-dihexyl-1,4-phenylene)[64]	+	-	16000	4.5
Poly(2,5-dibutoxy-1,4-phenylene)[74]	336	404	6600[a]	-
Poly[9,9-bis(2-ethylhexyl) fluor-ene-2,7-diyl][42]	383	413 (Film 416)	83500	1.9
Polyindenofluorene[102]	417	428 (Film 434)	66400	3.8
Poly(para-phenylene) with bridged pentaphenyl units[103]	434	445 (Film 445)	136000	2.2
Ladder-type 11-mer [104]	442	452	4116.73[b]	-
Para-phenylene ladder polymer[85]	453	455 (Film 456)	22500	2.1

Note: PDI: polydispersity, + no significant absorption detectable at $\lambda > 300$ nm, [a] M_n from measured by vapor pressure osmosis, [b] calculated mass.

As seen from the data of the **PPPs**-based materials (Table 1.1), the planarization of the π-electron system was increased with the increase of the degree of bridging. Poly(2,5-dialkyl-1,4-phenylene)s display only a negligible degree of conjugative interaction in the main chain (no significant absorption was deteted at $\lambda > 300$ nm). In the same time the partial planarization was accompanied by an increasing conjugative interaction of the aromatic subunits as seen for the absorption as well as for the emission data.

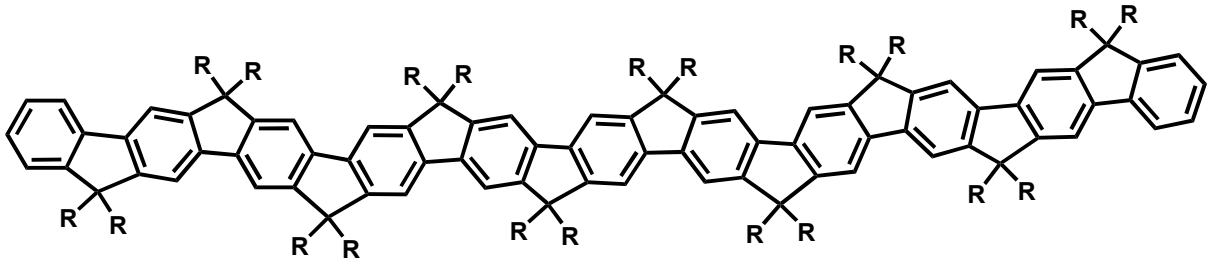

Scheme 1.13 Structure of a ladder-type para-phenylene 11-mer. (the 10 methylene bridges carry different aryl and alkyl substituents, for simplicity all substituents are given as –R).[104]

The data of the recently synthesized ladder-type paraphenylene 11-mer seen in Scheme 1.13 (reported by Müllen and Grimsdale[104]) reflect that, the electronic properties of MeLPPP[65,104] are reached, especially in emission (polymer and undecamer showed emission maxima around 450 nm, with almost identical spectral width). This finding illustrates the occurrence of a relatively short length of the effectively conjugated segments in ladder-type poly- and oligophenylenes of only 10–12 phenyls as proposed already 10 years ago in a study of a series of shorter LPPP oligomers up to the 7-mer.[105]

Nevertheless, despite the fact that the optical and electronic properties already converge for relatively short chain lengths of 10-12 phenyls, there are a couple of simple reasons to favour polymers over defined oligomers, such as the ladder-type phenylene 11-mer in ‘‘practical’’ applications: (1) in most cases, the synthetic effort toward the defined oligomers is enormous (extensive multistep procedures); and (2) only polymers with a certain molecular weight (favorable > 10,000–20,000) allow the processing into high-quality, flexible thin films by solution techniques as favored for the production of ‘‘polymer electronic’’ devices.

Blue polymer-based LEDs represent an attractive target, as blue-emitting LEDs based on inorganic semiconducting materials are not easily accessible. As a result of their band gap energy of 2.7–3.2 eV,[102-104] **PPP** derivatives are particularly suitable as blue emitters.

In the following sections the basic operations of organic light emitting diodes (OLEDs) will be discussed to provide a full understanding of the meaning of the device characteristics that will be presented in the next chapters. Following that the general motivation of this work will be presented.

1.4 Organic Light Emitting Diodes

Electroluminescent devices based on organic materials (OLEDs) are a very attractive class of electronic devices due to their unique characteristics and potential applications to flat panel displays and illumination devices.[106] Organic materials and specially conducting polymers have been considered to have outstanding potential for replacing inorganic light-emitting materials such as used in large area, lightweight, flexible displays. As compared to conventional fluorescent materials, conducting polymers offer the following advantages: [10,107-111]

- The characteristics of conducting polymers can be tuned by chemically altering the polymer backbone.
- They can be processed in the form of thin films and have potential for the production of flexible devices.
- They can be uniformly illuminated over a large area
- Output colors can span the whole visible spectrum.
- The polymeric materials have the potential for low cost.

Understanding how OLED devices function needs the awareness of several principles and technical terms, which will be briefly explained in the upcoming sections.

1.4.1 Electroluminescence

The basic operation in OLEDs is the electroluminescence (EL) which can be described as the electrically driven emission of light from a material. This phenomena was firstly found in inorganic semiconductors, particularly in 1936 when Destriau recorded the electroluminescence of ZnS-Phosphors.[112] In the early 1960s, organic electroluminescence from single crystals of anthracene was reported by Pope et.al.[113] They observed the EL from the single anthracene crystals (few tens of micrometers) at very high voltages above about 400 V. After this discovery, extensive studies were done with the aim of improving the organic thin-film electroluminescence with the study of thin-film devices. At the end of the 1980s, the work by Tang and Van Slyke[114] on the electroluminescence (EL) of aluminum 8-hydroxyquinoline (**Alq3**) stimulated a great amount of efforts worldwide on the generation of light by electrical excitation in organic materials. It was in 1990 that Friend and co- workers[6] presented the first electroluminescent polymeric device able to emit at 2.2 eV with an external quantum efficiency of 0.05%. The light emitting diode (LED) was formed by a single layer of PPV sandwiched between an indium tin oxide (ITO)-coated glass and an aluminum cathode which was vacuum evaporated on the top of the polymer film. Injection of electrons takes place at the cathode, while holes are injected at the anode.

In the following years, the number of scientific contributions on polymeric LEDs increased consistently. Different strategies were developed, all addressed to understanding the basic mechanism of the injection of opposite charges in the polymers, their travelling in the thickness of the layer, and their radiative decay, all these factors being fundamental for the increase of efficiency and lifetime.

1.4.2 Basic processes and parameters in electroluminescent devices

In this section, some basic information on operative guidelines for light emitting diodes is provided, as a general understanding of the device parameters is essential for the

work presented in this thesis. OLEDs are devices that transform electrical signals into optical signals. The typical structure of a single-layer polymer-based OLED is shown in Figure 1.4. A glass substrate coated by indium tin oxide (ITO) is used as a transparent (positive) electrode. A polymer layer is deposited onto the substrate by a spin coating technique. On top of the polymer is deposited, by vacuum evaporation, a metallic layer which forms the negative electrode. With the assistance of a bias voltage at the electrodes, light emission is obtained through the transparent anode.

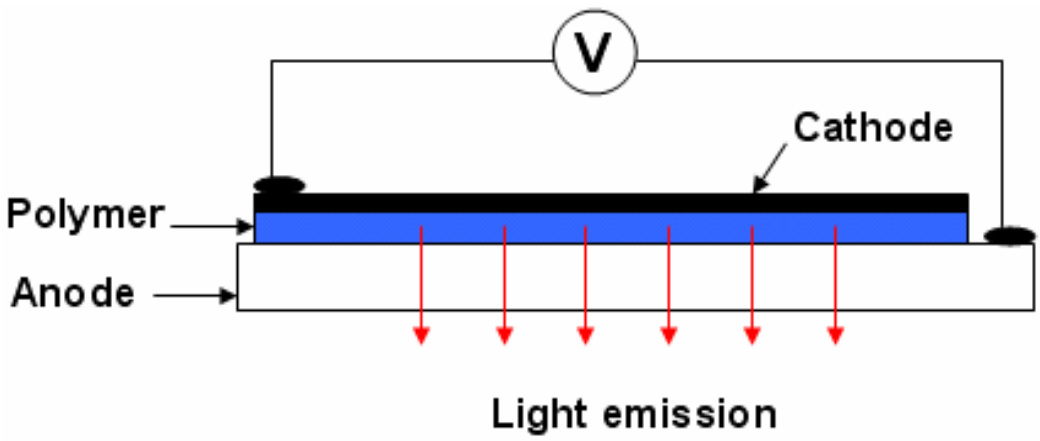

Figure 1.4 Scheme of single layer Polymer-based OLED.

The working mechanism of a LED consists of four main steps:

(1) By applying a bias voltage, charge carriers of opposite signs (positive and negative) are injected in the active material (organic layer).

(2) The positive (negative) charge carriers move in the material towards the negative (positive) electrode, driven by the applied electric field.

(3) Charge carriers of opposite sign couple to generate the excitons (excited species).

(4) The excitons decay radiatively by photon emission.

Some considerations can be made on each of the four steps in order to increase the device performances:

(i) Charge injection The number of injected positive and negative charges must be similar. This is obtained if the electrode metals have work function such that the potential barriers for positive and negative charge injection are similar. Commonly ITO with work function around 4.5 eV.[115,116] is used as the positive electrode (anode), while low work function alkali metals such as Ca, Mg, Ba, or Al are generally used as the negative electrode (cathode).[117]

(ii) Charge transport Since most conjugated polymers are better hole than electron transporters, the positive and negative charge transport in the organic layer should be always balanced for better device performance.[118-120]

(iii) Exciton generation and decay The efficiency of exciton generation can be optimized by increasing the interaction between the charge carriers, through a good balance of positive and negative charges in a restricted active volume, which can be achieved when the emissive layer is sandwiched between two other materials (heterostructures).[119] Excitons are short lived excited species which on radiative decay emit light corresponding to the band gap of the organic emitting material. The efficiency of the radiative decay can be maximized by reducing the quenching centers, for that the active area of the organic material must be far from the electrodes, where a high concentration of quenching interfacial defects are present.[121-123] This is generally obtained by confining the active layer within a heterostructure.

The performance of an OLED can be measured by means of several parameters. The most common ones are:

• **Internal efficiency (η_{int})** Which is the number of photons emitted per electron injected. While it is the most common measure of quantum efficiency, the measurement is complicated and cannot be measured directly.

• **External efficiency (η_{ext})** Since not all the emitted light can be observed by the viewers, the external efficiency is lower than the internal efficiency by a factor of $2n^2$, where n is the

refractive index of the polymer (organic active layer). Typical values for the external quantum efficiency range between 0.1-5 %.[124]

$$\eta_{int} = 2n^2 \eta_{ext}$$

• **Power efficiency (η_{pow})** Is the ratio of light power output to the electric power input, and measured in cdA^{-1}. η_{pow} can be calculated by multiplying the external efficiency by the ratio of the mean photon energy (Ep) and the drive voltage (U). High power efficiency is required for long device lifetimes.

$$\eta_{pow} = Ep\ U^{-1} \eta_{ext}$$

• **Luminous efficiency** The luminous efficiency, measured in lumens per watt (lmW^{-1}) takes into account that the human eye is more sensitive to certain colours. The luminous efficiency is determined by multiplying the power efficiency by the luminous efficacy (S), as defined by the Commission de L'Eclairage (CIE).[125]

$$\eta_{lum} = \eta_{pow} S$$

• **Luminance** It describes the amount of light that is emitted (brightness) from a device. luminance is measured in cdm^{-2}, and also used to estimate the efficiencies of an OLED. The Luminance is sometimes reported as a function of current density (current per cross-sectional area). An average laptop display has a luminance in the order of 100 cdm^{-2}.[7,118]

As earlier mentioned, charge carrier mobility in the polymer active layer is an important parameter on which the OLED device performance depends, for that balanced charge carriers migration is a crucial issue. In the polymer layer holes have generally higher mobility compared to electrons.[118] As a result; excitons tend to be formed close to the cathode-polymer interface, which due to the high concentration of quenching interfacial defects[121-123] reduce the lifetimes and efficiencies of the devices. To overcome this problem the device construction must be such that the electron-hole recombination zone is shifted more to the centre of the emitting layer. One technique to do that is to use multilayer devices.

1.4.3 Multilayer PLED devices

In the single layer device configuration (Figure 1.4) the emitting layer (conjugated polymer) was directly sandwiched between the cathode and the anode. However, the multilayer devices can be obtained by inserting an electron transporting layer (ETL) between the cathode and polymer, and/or hole transporting layer (HTL) between the anode and polymer (Figure 1.5). Several materials can be used as ETL or HTL, while fabricating a PLED device. The type of the used materials depends totally on the intrinsic properties of the polymer emitting layer used.

1.4.3.1 Electron transport layer in PLEDs

The exciton nonradiative quenching that takes place at the polymer/cathode interface is one of the major drawbacks a PLED could have. This quenching effect can be minimized by the introduction of an ETL between the polymer layer and the cathode. A good match between the LUMO levels of the polymer, electron transporting material, and the work function of the metal cathode is necessary in order to end up with a low electron-injection barrier. Consequently, the electron injection into the emissive layer is facilitated, which is needed for effective device performance. One of the most commonly used electron transporting material used in multilayer PLED devices is shown in Figure 1.5.

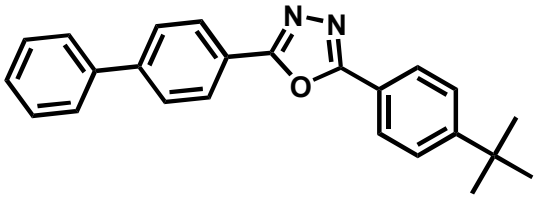

Figure 1.5 2-Biphenyl-4-yl-5-(4-tert-butyl-phenyl)-[1,3,4]oxadiazole.

1.4.3.2 Hole transporting layer in PLEDs

A low turn-on voltage (V_{on}) is one of the requirements an efficient PLED device needs. V_{on} should be as low as possible so that the power consumption and hence the Joule heating of the devices is reduced. Such generated high temperature due to the high bias voltage during

the device operation can in turn lead to thermal quenching effects of the excited species. One solution for that is decreasing the V_{on} value, which can be done by decreasing the hole-injection barrier between the polymer layer and the anode. The reduction in the barrier height can be achieved by inserting a HTL between the polymer layer and the anode. The HOMO levels of the polymer and the hole transporting material should have a proper matching with the work function of the anode. Some of the more common hole transporting materials are shown in Figure 1.6.

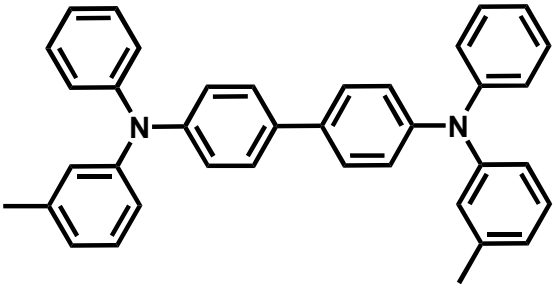

iii

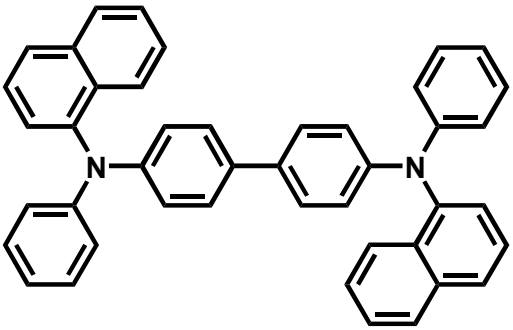

iv

Figure 1.6 Examples of hole-transporting materials. iii) N^4,$N^{4'}$-diphenyl-N^4,$N^{4'}$-dim-tolylbiphenyl-4,4'-diamine (**TPA**), iv) N,N'-bis(1- naphthyl)N,N'-diphenyl-1,1'-biphenyl-4,4'-diamine (**NPB**).

1.5 General motivation

Although extensive scientific activities on the field of polymeric light emitting diodes have been reported in the last few years, several questions still opened and need to be answered. One of these questions is how to obtain a stable blue-emitting polymer, which is an essential component for RGB full color displays.

As previously reviewed, several **PPP**-based type polymers such as **PFs**, **PIFs**, **LPPPs** have been introduced as blue emitters for PLED applications.[42-44] However, to date, the generation of stable blue PLEDs remains hindered by several problems. Specifically, the family of blue-emitting **PPP**-type polymers, particularly **PFs**, is prone to oxidation resulting in a green emission band located at 2.2–2.3 eV as a result of a bulk polymer defect. The cause of these low-energy photoluminescence and EL peaks was firstly attributed to an aggregate or excimer emission.[98,126-129] This primary assignment led to various synthetic efforts, such as copolymer generation, attachment of dendronic substituents[130-132], endcapping[127], and spiro-linking[133] in order to modify and stabilize the bulk emission properties. Frequently, the observed improvements of the bulk PL properties have then been related to the variations of the chemical structure of single polymer chains.

Recently the low-energy emission bands in **PF**-type polymers were identified as the emission from an exciton and / or charge trapping on-chain emissive keto defect. The formation of the keto-type defects in **PF** derivates is found to be the result of an oxidative degradation process that is occurring during the synthesis as a consequence of the chemical structure of the monomer units.[42] The investigations showed that two possible way can lead to the keto-defect formation: 1) Photo- or electro- oxidation: As shown in the solid state PL and EL spectra of a 9,9-dialkyl-**PF** under ambient conditions, which depicted a clear increase in the relative amount of low-energy emission with respect to time.[42,134] 2) Chemical stability of the monomer unit: For instance the 9-monoalkyl-**PF** (formed due to incomplete alkylation of fluorene) degrades much more rapidly than the 9,9-dialkyl-**PF**.[42,134] That can be attributed to

the reduced chemical stability of 9-monoalkyl-**PF** due to the presence of the relatively weakly bound, acidic methylene bridge hydrogen. It has been proposed that small traces of monoalkyl monomers can result in the generation of fluorenone defects in the corresponding polymer.

As shown in Scheme 1.14 the highly active Ni[0]-species used in the reductive coupling of the dibromo monomers reduce a certain amount of the 9-monoalkyl fluorene (I) to the fluorenyl anions (II) with the release of hydrogen. These anions can form hydroperoxide anions (III) with atmospheric oxygen during the work-up of the reaction mixture. The hydroperoxide anions then undergo a final rearrangement to fluorenone moieties (IV).[42,134]

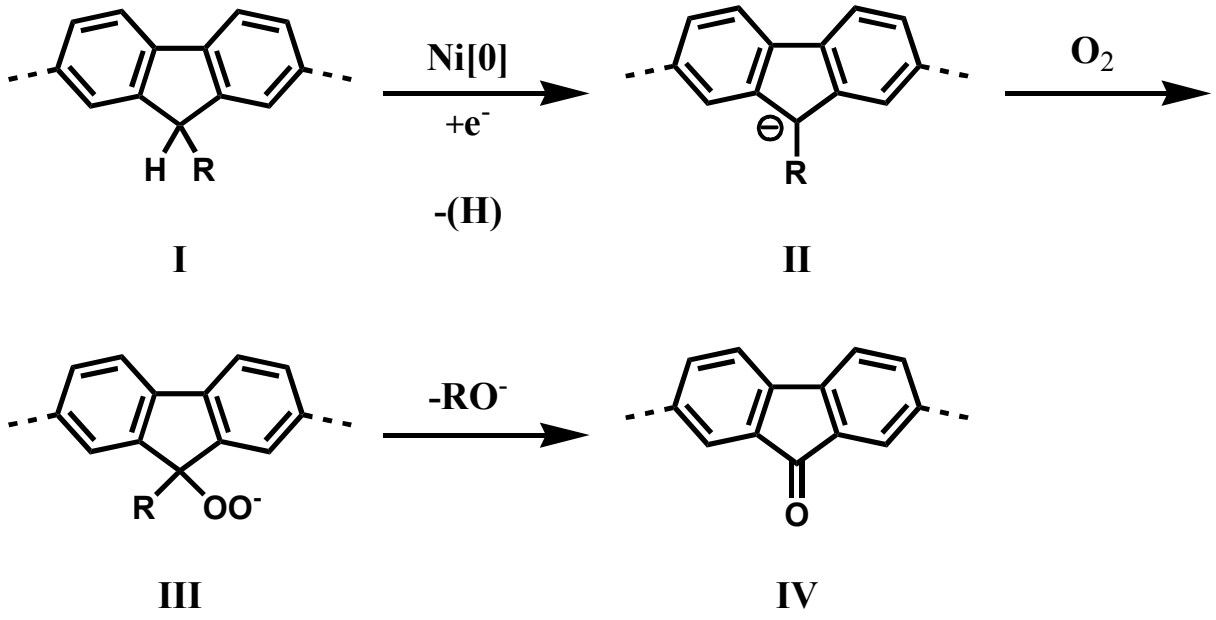

Scheme 1.14 Proposed mechanism for the generation of keto defect in **PF**.

It was shown that by incorporating keto defects into the polymer backbone the emissive characteristics of oxidatively degraded **PFs**, especially the appearance of the 530 nm band (2.3 eV) was reproducible.[135] The absence of any concentration dependence of the 530 nm bands' intensity in solution as well as the appearance of a vibronic structure in the 530 nm band at low temperatures support the picture of an emissive on-chain defect as the origin of this particular spectral feature.[136] These fluorenone defects on the **PF**-backbone reduced the efficiency of the energy migration process, which is strongly confined to the fluorene unit,

and led to a significant alteration in the optical properties of **PF** films even at low defect concentrations.[137] The formation of keto-type defects is, however, not limited to the **PF**-type polymers. Further evidence for this process also taking place in **LPPPs** is found when the methyl group in **MeLPPP** is replaced by hydrogen.[138] There the polymer with the hydrogen displays a broad emission band between 2.0 and 2.5 eV, that can be attributed to on-chain keto-type emission. From this point of view the defect formation mechanism presented for **PF** has to be extended to all bridged **PPP**-type polymers.

Beside the above mentioned possible keto-type defect in **PPP**-type polymers, most wide band gap polymers used in the fabrication of blue-PLEDs require low work function metal cathodes (e.g., Ca or Mg / Al) to afford appropriate electron-injection. As shown recently, chemical reactions of these **PPP**-linked polymers lead to defects on the polymer / metal interface that also shift the emission color under device operation.[14,139]

Several attempts have been presented in the past few years with the aim of attaining a stable blue emission form the **PPP**-type polymers. It was shown that shielding a **PF** backbone with Müllen-type dendronic side chains drastically reduces the interchain interactions and thus exciton migration to defect sites or emission from ketonic defect sites.[130-132] Few years later Müllen et al. demonstrated that shielding the bridgeheads by full substitution with aryl groups shows remarkably improved resistance to oxidative degradation at the 9-position,[140] which confirms that improving the chemical stability of the bridgeheads in bridged **PPP**-type polymers is one of the key steps toward stable blue-emitting **PPP**-type polymers. However, one drawback of utilizing the aryl substituents on the physical properties of the polymers is to hinder chain packing as demonstrated by the lack of liquid crystalline phases, and the absence of any signs of organization in the polymer films when studied by atomic force microscopy (AFM).[141]

Based on the above mentioned investigations, it was obvious that the need for new wide band gap polymers that can afford a stable blue emission is vital. Such polymers should basically overcome the former problems and offer:

i) High chemically and thermally stable structures for stable blue emission.

ii) Good macroscopic organization for better charge transport.

iii) High solubility to permit solution processability for easy PLEDs fabrication.

In this thesis, the synthesis and characterization of a novel series of blue emitting conjugated polymers for PLED application will be introduced. Furthermore, the concept of graphene nanoribbons (thin strips of (graphene) a one-atom-thick planar sheet of sp^2-bonded carbon atoms that are densely packed in a hexagonal crystal lattice) will be introduced in chapter 4, and the synthesis and characterization of their triphenylene-based derivatives will be discussed in details. The thesis will be presented as the following:

i) In chapter 2, novel architectures for blue light emitting triphenylene-based conjugated co- and homo-polymers together with their related PLED devices are presented. The polymers were synthesized from a new type of building blocks, 6,11- dibromo-1,2,3,4-*substituted*-triphenylenes (Scheme 1.15).

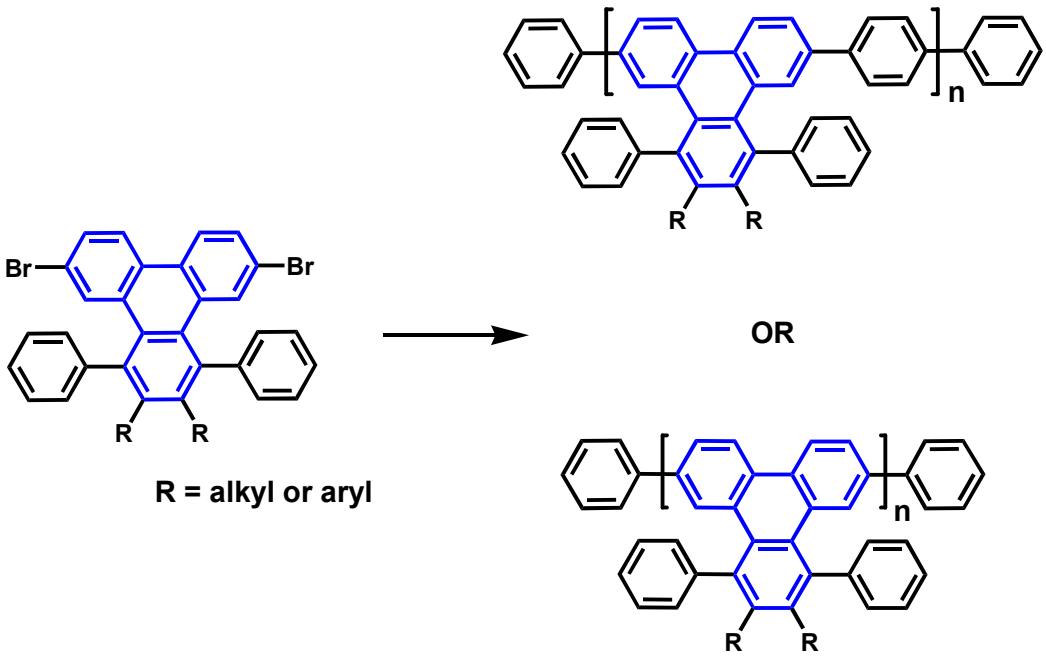

Scheme 1.15 Synthesis of blue-emitting triphenylene-based conjugated polymers.

ii) In chapter 3, a unique design of triphenylene-pyrene, triphenylene-fluorene, and triphenylene-carbazole co-polymers are presented (Scheme 1.16). Although several homo- and co-polymers incorporating these chromophors were already announced, such combinations were never reported so far. The PLED devices based on these copolymers will also be discussed.

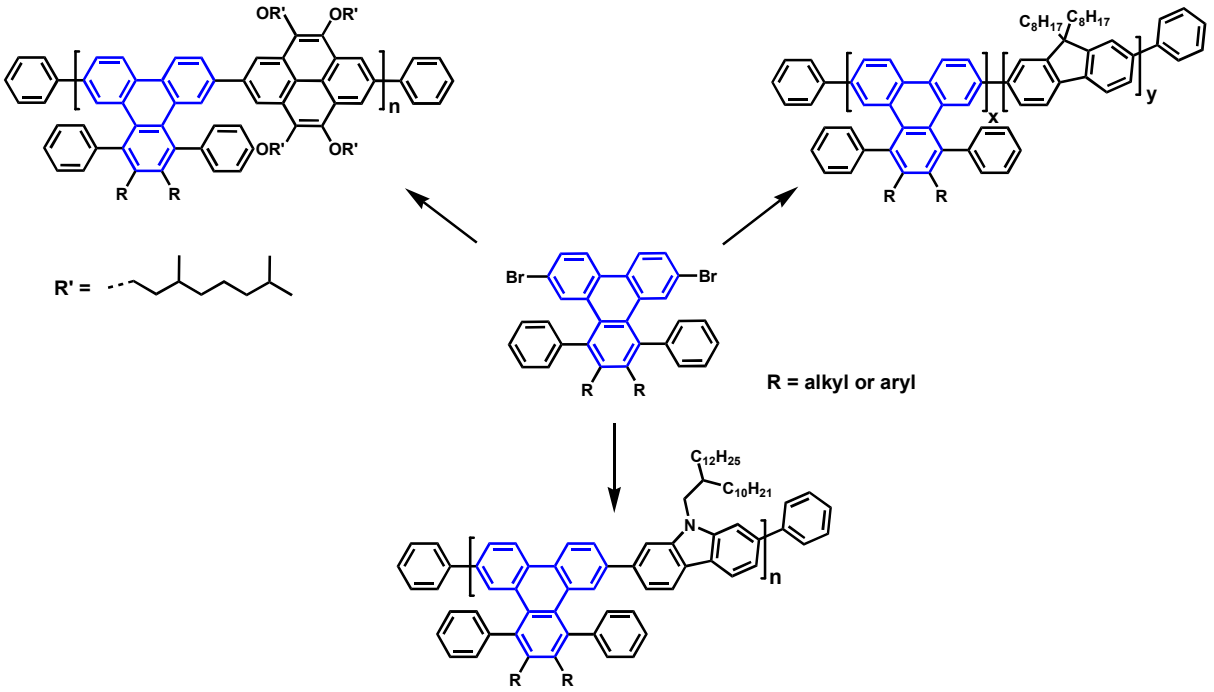

Scheme 1.16 Synthesis of blue-emitting triphenylene-pyrene, triphenylene-fluorene, and triphenylene-carbazole co-polymers.

iii) In chapter 4, new two dimensional graphene nanoribbons (Scheme 1.17) will be demonstrated. Such graphene molecules were synthesized using chemical and physical cyclodehydrogenation routes to convert the 3D-triphenylene based-polymers into 2D-planarized graphene nanoribbons.

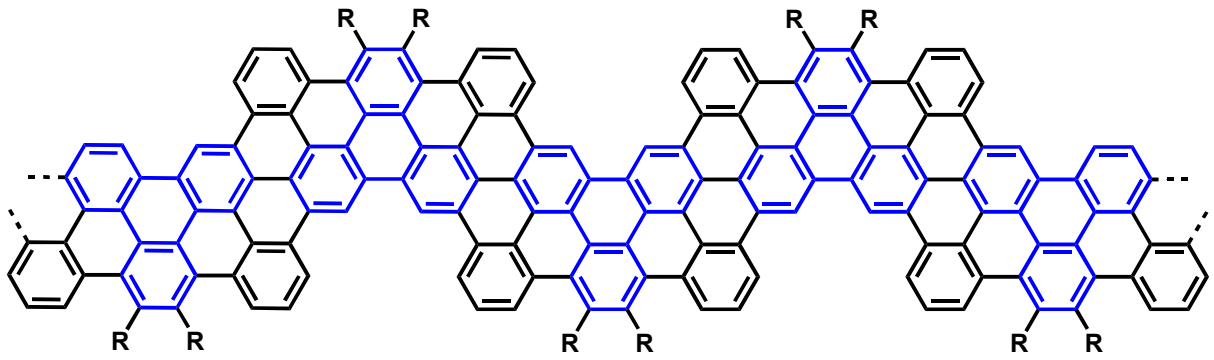

Scheme 1.17 Structure representation of triphenylene based- graphene nanoribbons.

1.6 References

(1) Gutmann, F.; Lyons, L. E. *Organic Semiconductors* John Wiley & Sons, Inc, **1967**

(2) Garnier, F. *Scope and limits of organic-based thin-film transistors* Phil. Trans.,**1997**, 355,815–827.

(3) Chiang, C. K.; Druy, M. A.; Gau, S. C.; Heeger, A. J.; Louis, E. J.; MacDiarmid, A. G.; Park, Y. W.; Shirakawa, H. *J. Am. Chem. Soc.***1978**, 100, 1013.

(4) Chiang, C. K.; Fischer, C. R.; Park, Y. W.; Heeger, A. J.; Shirakawa, H .; Louis, E. J.; Gau, S. C.; MacDiarmid, A. G.; *Phys. Rev. Lett.***1977**,39 , 1098.

(5) Shirakawa, H.; Louis, E. J.; MacDiarmid, A. G.; Chiang, C. K.; Heeger, A. J. *J. Chem. Soc. Chem. Com mun.***1977**, 579.

(6) Burroughes, J. H.; Bradley, D. D. C.; Brown, A. R.; Marks, R. N.; Friend, R. H.; Bum, P. L.; Holmes, A. B. *Nature* **1990**, 347, 539.

(7) Kraft, A.; Grimsdale, A. C.; Holmes, A. B., *Angew. Chem., Int. Ed. Engl*. **1998**, 37, (4), 402.

(8) Burroughes, J. H.; Bradley, D. D. C.; Brown, A. R.; Marks, R. N.; Mackay, K.; Friend, R. H.; Burns, P. L.; Holmes, A. B., *Nature* **1990**, 347, 539.

(9) Jacob, J.; Zhang, J. Y.; Grimsdale, A. C.; Müllen, K.; Gaal, M.; List, E. J. W. *Macromolecules* **2003**, 36, (22), 8240.

(10) Friend, R. H.; Gymer, R. W.; Holmes, A. B.; Burroughes, J. H.; Marks, R. N.; Taliani, C.; Bradley, D. D. C.; Dos Santos, D. A.; Bredas, J. L.; Logdlund, M.; Salaneck, W. R., *Nature* **1999**, 397, (6715), 121.

(11) Sheats, J. R.; Chang, Y. L.; Roitman, D. B.; Stocking, A., *Acc. Chem. Res*. **1999**, 32, (3), 193.

(12) Partridge, R. H., *Polymer* **1983**, 24, (6), 733.

(13) Jacob, J.; Sax, S.; Piok, T.; List, E. J. W.; Grimsdale, A. C.; Müllen, K., *J. Am. Chem. Soc.* **2004**, 126, (22), 6987.

(14) Akcelrud, L., *Progress in Polymer Science* **2003**, 28, (6), 875.

(15) Jacob, J.; Sax, S.; Gaal, M.; List, E. J. W.; Grimsdale, A. C.; Müllen, K., *Macromolecules* **2005**, 38, (24), 9933.

(16) Gong, X.; Robinson, M. R.; Ostrowski, J. C.; Moses, D.; Bazan, G. C.; Heeger, A. J., *Adv. Mater*. **2002**, 14, (8), 581.

(17) Sariciftci, N. S.; Smilowitz, L.; Heeger, A. J.; Wudl, F., *Science* **1992**, 258, 1474.

(18) Morita, S.; Zakhidov, A. A.; Yoshino, K., *Solid state Commun*. **1992**, 82, 249.

(19) Xue, J. G.; Uchida, S.; Rand, B. P.; Forrest, S. R., *Appl. Phys. Lett*. **2004**, 84, (16), 3013.

(20) Christoph, J.; Brabec, J.; Sariciftci, N. S.; Hummelen, J. C., *Adv. Funct. Mater.* **2001**, 11, 15.

(21) Li, J. L.; Dierschke, F.; Wu, J. S.; Grimsdale, A. C.; Müllen, K., *J. Mater. Chem.* **2006**, 16, (1), 96.

(22) Ong, B. S.; Wu, Y. L.; Liu, P.; Gardner, S., *J. Am. Chem. Soc*. **2004**, 126, (11), 3378.

(23) Bao, Z., *Adv. Mater.* **2000**, 12, 227.

(24) Gelinck, G. H.; Geuns, T. C. T.; Leeuw, D. M. d., *Appl. Phys. Lett*. **2000**, 77, 1487.

(25) Huitema, H. E. A.; Gelinck, G. H.; van der Putten, J.; Kuijk, K. E.; Hart, C. M.; Cantatore, E.; Herwig, P. T.; van Breemen, A.; de Leeuw, D. M., *Nature* **2001**, 414, (6864), 599.

(26) Garnier, F.; Hajlaoui, R.; Yassar, A.; Srivastava, P., *Science* **1994**, 265, 1684.

(27) Dimitrakopoulos, C. D.; Mascaro, D. J., *Adv. Mater*. **2002**, 14, 99.

(28) For leading reviews, see (a) Kim, J. *Pure App. Chem*. **2002**, 21, 585.589. (b) Bradley, D. D. C. *Synth. Mat.* **1993**, 54, 401-415. (c) Friend, R. H. *Synth. Mat*. **1992**, 51, 357.

(29) Boweley, H. J.; Gerrard, D. L.; Maddams, W. F.; *Makromol. Chem*. 1985, 186, 715.

(30) Haberkorn, H**.;** Heckman, W.; Kohler, G.; Naarmann, H.; Schlag, J.; Simak, P.; Theophilou, N.; Voelkel, R. *Eur. Polym. J.* **1988**, 24, 497.

(31) Grem, G.; Leditzky, G. ; Ullrich, B.; Leising, G. *Synth. Met.* **1992**, 51, 383.

(32) Grem, G.; Leditzky, G. ; Ullrich, B.; Leising, G. *Adv. Mater.* **1992**, 4, 15.

(33) Grüner, J.; Hamer, P.J.; Friend, R.H.; Huber, H.J.; Scherf, U.; Holmes, A.B. *Adv. Mater.* **1994**, 6, 748.

(34) Tasch, S.; List, E.J.W. ; Hochfilzer, C.; Leising, G.; Schlichting, P.; Rohr, U.; Geerts, Y.; Scherf, U.; Müllen, K. *Phy.s Rev. B.* **1997**, 56, 4479.

(35) Tasch, S.; Brandstätter, C.; Meghdadi, F.; Leising, G.; Athouel, L.; Froyer, G. *Adv. Mater.* **1997**, 9, 33.

(36) Fukuda, M.; Sawada, K.; Yoshino, K. *Jpn. J. Appl. Phys.* **1989**, 28, 1433.

(37) Fukuda, M.; Sawada, K.; Yoshino, K. *Polym. Sci. A.* **1993**, 31, 2465.

(38) Ohmori, Y.; Uchida, M.; Muro, K.; Yoshino, K., *Jpn. J Appl. Phys.* **1991**,11, 1941.

(39) Grimsdale, A.C.; Lecle`re, P.; Lazzaroni, R.; Mackenzie, J. D.; Murphy, C.; Setayesh, S.; Silva, C.; Friend, R. H.; Müllen, K. *Adv. Func.t Mater.* **2002**,12, 729.

(40) Campbell, A. J.; Bradley, D.D.C.; Antoniadis, H.; Inbasekaran, M.; Wu, W.W.; Wu, E.P *Appl. Phys. Lett.* **2000**, 76, 1734.

(41) Campbell, A. J.; Bradley, D.D.C.; Antoniadis, H. *J. Appl. Phys.* **2001**, 89, 3343.

(42) Scherf, U.; List, E.J.W. *Adv. Mate.*, **2002**,14, 477.

(43) Neher, D. *Macromol. Rapid. Commun.* **2001**, 22, 1365.

(44) Gamerith, S.; Gadermaier, Ch.; Scherf, U.; List, E. J. W. *Physics of organic semiconductors, ed. H. Bütting. Weinheim: Wiley-VCH* **2005**, 153.

(45) Sirringhaus, H.; Kawase, T.; Friend, R.H.; Shimoda, T.; Inbasekaran, M.; Wu, W.; Woo, E.P. *Science* **2000**, 290, 2123.

(46) Gaylord, B.S.; Heeger, A. J.; Bazan, G.C. *Proc Natl. Acad. Sci*. **2000**, USA 99:10954.

(47) Dimitrakopoulos, C. D.; Malenfant, P.R.L. *Adv. Mater*.**2002**, 14, 99.

(48) Ramsdale, C. M.; Barker, J. A.; Arias, A. C.; McKenzie, J. D.; Friend, R. H.; Greenham, N.C. *J. Appl. Phys.* **2002**, 92, 4266.

(49) Kietzke, T.; Neher, D.; Kumke, M.; Montenegro, R.; Landfester, K.; Scherf, U. *Macromolecules* **2004**, 37, 4882.

(50) Ballard, D.G.H.; Courtis, A.; Shirley, I. M.; Taylor, S.C. *J. Chem. Soc. Chem. Commun*. **1983**, 17, 954.

(51) Ballard, D.G. H., Curtis, A.; Shirley, I. M.; Taylor, S.C. *Macromolecules* **1987**, 21, 1787.

(52) Tabata, M.; Satoh, M.; Kaneto, K.; Yoshino, K. *J. Phys. C.* **1986**, 19, L101.

(53) Kovacic P, Jones M. B. *Chem. Rev.* **1987**, 87, 357.

(54) Rehahn, M.; Schlüter, A.-D.; Wegner, G.; Feast, W. J. *Polymer* **1989**, 30, 1054.

(55) Katsuya, M.; Teshirogi, T.; Kuramato, N.; Kitamura, T. *J. Polym. Sci., Polym. Chem. Ed.* **1995**, 23, 1259.

(56) Ueda, M.; Abe, T.; Awano, H. *Macromolecules* **1992**, 25, 5125.

(57) Fukuda, M.; Sawada, K.; Yoshino, K. *J. Polym. Sci A.* **1993**, 31, 2465.

(58) Ueda, M.; Miyaji, Y.; Ito, T. *Macromolecules* **1991**, 24, 2694.

(59) Colon, I.; Kwiatkowski, G. T. *J. Polym. Sci. A.* **1990**, 28, 367.

(60) Huber, J.; Scherf, U. *Macromol. Chem. Phys*. **1994**, 15, 897.

(61) Fiesel, R.; Huber, J.; Apel, U.; Enkelmann, V.; Hentschke, R.; Scherf, U.; Cabrera, K. *Macromol. Chem. Phys*. **1997**, 198, 2623.

(62) Yamamoto, T.; Hayashi, Y.; Yamamoto, A. *Bull. Chem. Soc. Jpn.* **1978**, 51, 2091.

(63) Noll, A.; Siegfield, N.; Heitz, W. *Makromol. Chem. Rapid. Commun.* **1990**, 11, 485.

(64) Park, L.R., Dodd, L. R.; Levon, K.; Kwei, T. K. *Macromolecules* **1996**, 29, 7149.

(65) Scherf, U.; Müllen, K. *Makromol. Chem. Rapid. Commun.* **1991**, 12, 489.

(66) Child, A.D.; Reynolds, J. R. *Macromolecules* **1994**, 27, 1975.

(67) Rau, U.I.; Rehahn, M. *Acta. Polymer* **1994**, 45, 3.

(68) Rehahn, M.; Schlüter, A.-D.; Wegner, G.; Feast, W. J. *Polymer* **1989**, 30, 1060.

(69) Ueda, M.; Ichikawa, F. *Macromolecules* **1990**, 23, 926.

(70) Percec, V.; Okita, S.; Weiss, R. *Macromolecules* **1992**, 25, 1816.

(71) Yamamoto, T.; Morita, A.; Miyazaki, Y.; Maruyama, T.; Wakayama, H.; Zhou, Z.; Nakumura, Y.; Kanbara, T.; Sasaki, S.; Kubota, K. *Macromolecules* **1992**, 25, 1214.

(72) Phillips, R. W.; Sheares, V. V.; Samulski, E. T.; DeSimone, J. M, *Macromolecules* **1994**, 27, 2354.

(73) Chaturvedi, V.; Tanaka, S.; Kaeriyama, K. *Macromolecules* **1993**, 26, 2607.

(74) Vahlenkamp, T.; Wegner, G. *Macromol. Chem. Phys.* **1994**, 195, 1933.

(75) Kanbara, T.; Saito, N.; Yamamoto, T.; Kubota, K.*Macromolecules* **1991**, 24, 5883.

(76) Wallow, T. I.; Novak, B. M. J. *J. Am. Chem. Soc.* **1991**, 113, 741.

(77) Rulkens, R.; Schultze, M.; Wegner, G. *Macromol. Rapid. Commun*. **1994**,15, 669.

(78) Miyaura, M.; Yanagi, T.; Suzuki, A. *Synth. Commun*. 1981, 11, 513.

(79) Kanbara, T.; Saito, N.; Yamamoto, T.; Kubota, K. *Macromolecules* **1991**, 24, 5883.

(80) Stille, J. K. *Angew. Chem*. **1986**, 98, 504.

(81) Park, L. R.; Dodd, L. R.; Levon, K.; Kwei, T. K. *Macromolecules* **1996**, 29, 7149.

(82) Scherf, U.; Müllen, K. *Makromol. Chem. Rapid. Commun*. **1991**, 12, 489.

(83) Scherf, U.; Bohnen, A.; Müllen, K. *Makromol. Chem*. **1992**, 193, 1127.

(84) Scherf, U.; *J. Mater. Chem*. **1999**, 9, 1853.

(85) Scherf, U. *Handbook of conducting polymers, 2nd ed.* **1997**.

(86) Scherf, U. *Topics in current chemistry: Carbon rich compounds II, Vol. 201, ed. A*. **1999**, 163.

(87) Scherf, U.; Müllen, K. *Semiconducting polymers, eds. G. Hadziioannou, and P.F. vanHutten. Heidelberg: Wiley-VCH*, **1999**, 37.

(88) Grimsdale, A. C.; Lecle`re, P.; Lazzaroni, R.; Mackenzie, J. D.; Murphy, C.; Setayesh, S.; Silva, C.; Friend, R. H.; Müllen, K. *Adv. Funct. Mater*. **2002**, 12, 729.

(89) Campbell, A. J.; Bradley, D. D. C.; Antoniadis, H.; Inbasekaran, M.; Wu, W.W.; Wu, E. P. *Appl. Phys. Lett*. **2000**, 76, 1734.

(90) Campbell, A. J., Bradley, D. D. C.; Antoniadis, H. *J Appl Phys*. **2001**, 89, 3343.

(91) Neher, D. *Macromol. Rapid. Commun.* **2001**, 22, 1365.

(92) Inbasekaran, M.; Wu, W.; Woo, P. *US Patent 5*, **1998**, 777, 070.

(93) Bernius, M.T.; Inbasekaran, M.; OBrien, J.; Wu, W. *Adv. Mater.* **2000**, 12, 1737.

(94) Saito, N.; Kanbara, T.; Sato, T.;Yamamoto, T. *Polym. Bull*. **1993**, 30, 285.

(95) Kreyenschmidt, M.; Uckert, F.; Müllen, K.Macromolecules 1995, 28, 4577.

(96) Grell, M.; Knoll, W.; Lupo, D.; Meisel, A.; Miteva, T.; Neher, D.; Nothofer, H.-G.; Scherf, U.; Yasuda, A. *Adv. Mater.* **1999**, 11, 671.

(97) Grell, M.; Bradley, D.D.C.; Inbasekaran, M.; Woo, E. P. *Adv. Mater.* **1997**, 9, 798.

(98) Grell, M.; Bradley, D. D. C.; Ungar, G.; Hill, J.; Whitehead, K. S. *Macromolecules* **1999**, 32, 5810.

(99) Kanbara, T.; Saito, N.; Yamamoto, T.; Kubota, K. *Macromolecules* **1991**, 24, 5883.

(100) Yamamoto, T.; Morita, A.; Miyazaki, Y.; Maruyama, T.; Wakayama, H.; Zhou, Z.; Nakumura, Y .; Kanbara, T.; Sasaki, S.; Kubota, K. *Macromolecules* **1992**, 25, 1214.

(101) Setayesh, S.; Marsitzky, D.; Müllen, K. *Macromolecules* **2000**, 33, 2016.

(102) Jacob, J.; Zhang, J.; Grimsdale, A. C.; Müllen, K.; Gaal, M.; List, E. J. W. *Macromolecules* **2003**, 36, 8240.

(103) Jacob, J.; Sax, S. ; Piok, T.; List, E. J. W.; Grimsdale, A. C.; Müllen, K. *J. Am. Chem. Soc.* **2004**, 126, 6987.

(104) Schindler, F.; Lupton, J. M.; Feldmann, J.; Scherf, U.; Jacob, J.; Grimsdale, A.; Müllen, K. *Angew. Chem.* **2005**, 117, 1544.

(105) Grimme, J.; Kreyenschmidt, M.; Uckert, F.; Müllen, K.; Scherf, U. *Adv. Mater.* **1995**, 7, 292.

(106) Colle, M.; Dinnebier, R. E.; Brutting, W. *Chem. Commun.* 2002, 23, 2908.

(107) Heeger, A. J. *Solid State Commun.* **1998**, 07, 673.

(108) Tada, K.; Onoda, M.; Zakhidov, A. A.; Yoshino, K. *Japan. J. Appl. Phys.* **1997**, 36, 306.

(109) Bharathan, J.; Yang, Y. *Appl. Phys. Lett.* **1998**, 72, 2660.

(110) Roges, J. A. ; Bao, Z.; Dhar, L. *Appl. Phys. Lett.* **1998**, 73, 294.

(111) Tada, K.; Onoda, M.; Nakayama, H. *Japan. J. Appl. Phys.* **1998**, 37, 1181.

(112) Destriau, G. *J. Chem. Phys*. **1936**, 33, 587.

(113) Pope, M.; Kallmann, H. P.; Magnante, P. *J. Chem. Phys*. **1963**, 38, 2042.

(114) Tang, C. W.; Van Slyke, S. A. *Appl. Phys. Lett.* **1987**, 51, 913.

(115) Heeger, A. J.; Parker, I. D.; Yang, Y. *Synth. Met.* **1994**, 67, 23

(116) Yang, Y.; Heeger, A. J. *Appl. Phys. Lett.* **1994**, 64, 10, 1245.

(117) Jonda, Ch.; Mayer, A. B. R.; Grothe, W. *J. Appl. Phys.* **1999**, 85, 9, 6884.

(118) Mitschke, U.; Bauerle, P. *J. Mater. Chem.* **2000**, 10, 1471.

(119) Baigent, D. R.; Greenham, N. C.; Grüner, J.; Marks, R. N.; Friend, R. H.; Moratti, S. C.; Holmes, A. B. *Synth. Metals.* **1994**, 67, 3.

(120) Cacialli, F.; Friend, R. H.; Haylett, N.; Daik, R.; Feast, W. J.; Dos Santos, D. A.; Brédas, J. L. *Synth. Metals.* **1997**, 84, 643.

(121) Dannetum, P. ; Boman, M. ; Stafström, S.; Salaneck, W.; Lazzaroni, R.; Fredriksson, C.; Brédas, J. L.; Zamboni, R.; Taliani, C. *J. Chem. Phys.* **1993**, 99, 1, 664.

(122) Becker, H.; Burns, S. E.; Friend, R. H. *Phys. Rev. B* **1997**, 56, 4, 1893.

(123) Birgerson, J.; Fahlman, M.; Bröms, P.; Salaneck, W. R. *Synth. Metals.* **1996**, 80,125.

(124) Greenham, N. C.; Friend, R. H.; Bradley, D. D. C. *Adv. Mater*. **1994**, 6, 491.

(125) Sheats, J. R.; Antoniadis, H.; Hueschen, M.; Leonard, W.; Miller, J.; Moon, R.; Roitman, D.; Stocking, A., *Science* **1996**, 273, 884.

(126) Lemmer, U.; Heun, S.; Mahrt, R. F.; Scherf, U.; Hopmeier, M.; Siegner, U.; Göbel, E.O.; Müllen, K.; Bässler, H. *Chem. Phys. Lett.* **1995**, 240, 373.

(127) Lee, J. I.; Klärner, G.; Miller, R. D. *Chem. Mater.* **1999**, 11, 1083.

(128) Weinfurter, K. H.; Fujikawa, H.; Tokito, S.; Taga, Y. *Appl. Phys. Lett*. **2000**, 76, 2502.

(129) Bliznyuk, V. N.; Carter, S.A.; Scott, J. C.; Klärner, G.; Miller, R.D. *Macromolecules* **1999**, 32, 361

(130) Setayesh, S.; Grimsdale, A. C.; Weil, T.; Enkelmann, V.; Müllen, K.; Meghdadi, F.; List, E. J. W.; Leising, G. *J. Am. Chem. Soc*. **2001**,123, 946.

(131) Lupton, J. M.; Schouwink, P.; Keivanidis, P. E.; Grimsdale, A. C.; Müllen, K. *Adv. Funct. Mat* .2000, 13, 154.

(132) Pogantsch, F.; Wenzl, P.; List, E. J. W.; Leising, G.; Grimsdale, A. C.; Müllen, K. *Adv. Mater.* **2002**, 14, 1061.

(133) Nakazawa, Y. K.; Carter, S. A.; Nothofer, H.-G. ; Scherf, U.; Lee, V.Y.; Miller, R. D.; Scott, J. C. *Appl. Phys. Lett.* **2002**, 80, 3832.

(134) List, E. J. W.; Guentner, R.; de Freitas, P. S.; Scherf, U. *Adv. Mater.* **2002**, 14, 374.

(135) Scandiucci de Freitas, P.; Scherf, U.; Collon, M.; List, E. J. W.*e-polymers no.0009* **2002**.

(136) Romaner, L.; Pogantsch, A.; Scandiucci de Freitas, P.; Scherf, U.; Gaal, M.; Zojer, E.; List, E. J. W. *Adv. Funct. Mat*. **2003**, 13, 597.

(137) Zojer, E.; Pogantsch, A.; Hennebicq, E.; Beljonne, D.; Bre´das, J. L.; Scandiucci de Freitas, P.; Scherf, U.; List, E. J. W. *J. Chem. Phys*. **2002**, 117, 6794.

(138) Romaner, L.; Heimel, G.; Wiesenhofer, H.; Scandiucci de Freitas, P.; Scherf, U.; Bre´das, J. L.; Zojer, E.; List, E. J. W. *Chem. Mater*. **2004**, 16, 4667.

(139) Gamerith, S.; Nothofer, H.-G.; Scherf, U.; List, E. J. W. *Jpn. J. Appl. Phys*. **2004**, 43, 891.

(140) Jacob, J.; Grimsdale, A. C.; Müllen, K.; Sax, S.; Gaal, M.; List; E. J. W. *Macromolecules* **2005**, 38, 9933.

(141) Surin, M.; Hennebicq, E.; Ego, C.; Marsitzky, D.; Grimsdale, A . C.; Müllen, K.; Bredas, J.-L.; Lazzaroni, R.; Leclere, P. *Chem. Mater*. **2004**, 16, 994.

Chapter 2

Triphenylene-Based Conjugated Polymers for Blue Polymeric Light Emitting Diodes

In this chapter, the synthesis and characterization of a novel series of conjugated blue emitting polymers containing triphenylene as repeating unit for PLEDs are presented. The synthesis was developed to prepare di-bromotriphenylene monomers; using these di-bromo-functionalities the monomers were polymerized by the palladium-catalyzed Suzuki -Miyaura and the nickel-catalyzed Yamamoto polycondensation reactions to result in a series of co- and homopolymers, respectively. The resulting polymers are discussed in the light of photophysical and electrochemical properties and compared with other blue emitting polymers reported in literature. Supramolecular organizations of the polymers were also investigated using two-dimensional wide-angle X-ray scattering (2D-WAXS). Finally, the polymers were tested in polymeric light emitting diodes (PLEDs).

2.1 Introduction

Triphenylene (TP) (Figure 2.1) is a symmetric aromatic hydrocarbon in which three benzene rings fuse to form a common fourth ring has been known in the chemical literature for more than a century. It was first isolated from the pyrolytic products of benzene by Schmidt and Schultz.[1] Triphenylene is a ubiquitous combustion effluent that pollutes the environment, into which it is released from various sources such as, coal burning, refineries and internal combustion engines. Due to its fully-benzenoid nature triphenylene is much more resonance stabilized than its isomers chrysene, tetraphene, benzo[c]phenanthrene and

tetracene (Figure 2.2a). This makes it much more difficult to hydrogenate to the saturated hydrocarbon (octadecahydro-triphenylene) (Figure 2.2b).[2]

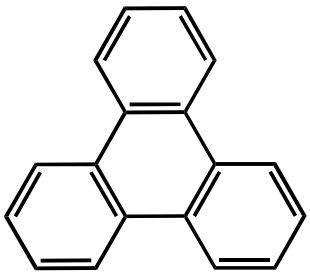

triphenylene

Figure 2.1 The molecular structure of triphenylene.

a)

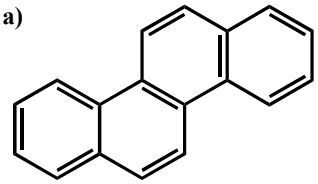

chrysene

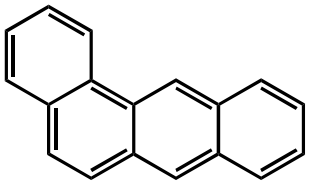

tetraphene

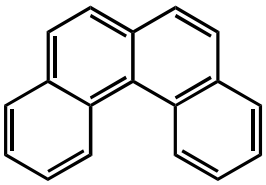

benzo[*c*]phenanthrene

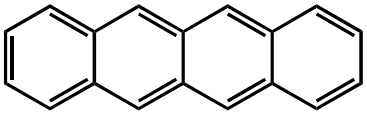

tetracene

b)

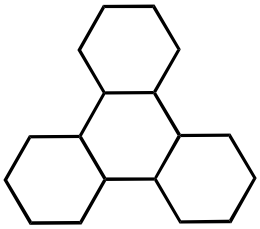

Octadecahydro-triphenylene

Figure 2.2 a) The molecular structure of triphenylene isomers. b) The structure of octadecahydro-triphenylene.

Several synthetic methods were reported in literature for the production of this trisannulated benzene system. In the early twentieth century, an easy way of synthesis was presented by Mannich by dehydrogenation with selenium of dodecahydrotriphenylene**,** which is formed in relatively small yields on treating cyclohexanone with methyl alcoholic sulfuric acid.[3] Following that several methods for the synthesis of triphenylene were developed,[4,5] including the self-condensation of cyclohexanone using polyphosphoric acid followed by dehydrogenation of the formed dodecahydrotriphenylene using copper, palladium-charcoal and selinium.[6-9] Triphenylene was also synthesized by the action of lithium on 1-bromo-2-iodo-benzene (Scheme 2.1)[2] and on ortho-diiodobenzene[10] or magnesium on o-bromofluoro-benzene,[11] and by the dehydrogenation of o-terphenyl.[12]

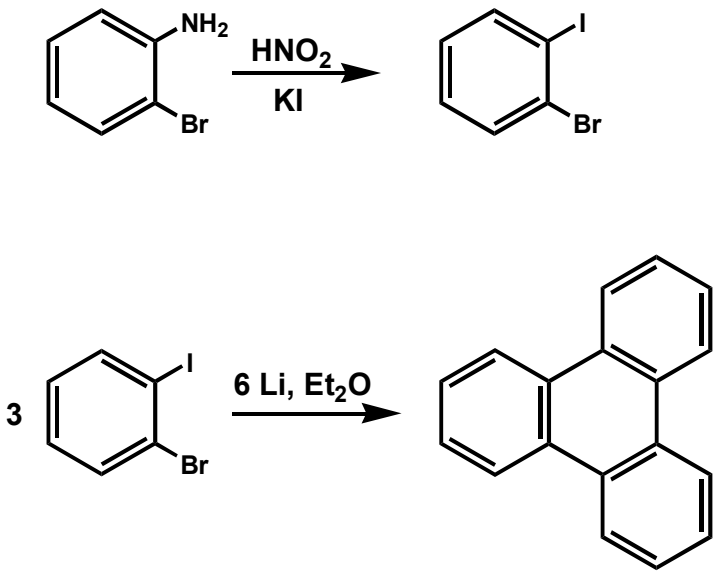

Scheme 2.1 Synthesis of triphenylene.[2]

Although the synthesis of triphenylene was already introduced in the early 20th century, the material gained increased scientific interest only after 1978. In particular after the work of Billard *et al*. when he introduced this tetracyclic aromatic hydrocarbon as a novel core for discotic liquid crystals (DLCs).[13] Triphenylene became an attractive core for DLCs for several reasons: (i) it possesses C_3 symmetry, (ii) its chemistry is relatively accessible, (iii) its

derivatives are thermally as well as chemically stable and they show a variety of mesophases.[13] Consequently, several triphenylene containing small molecules and oligomers have been synthesized.[14-33] In addition some triphenylene-based polymers have been presented by different research group.[34-45] However, these polymers were mostly non-conjugated or were not used for blue-PLED applications, which are the main focus of this thesis, thus they will not be discussed here.

As formerly discussed in chapter 1, in the field of blue-PLED, several PPP-based polymers[46-56] have been reported. However, these systems suffered from several problems such as: i) poor charge injection and transport, ii) the tendency to oxidize at the bridge-head positions.[50,51] Therefore, finding new materials for blue-PLEDs that do not suffer from these problems was of great importance.

In addition to the above mentioned attractive physical properties of triphenylene such as its discotic liquid crystalline nature and chemical and thermal stabilities,[13] this molecule emits blue.[2] Moreover, the triphenylene-based systems show other very interesting physical properties including one-dimensional charge migration,[57] one-dimensional energy migration,[58] electroluminescence,[59] ferroelectric switching,[60] alignment, and self-assembling behavior on surfaces.[61,62] All these properties motivated us to use the triphenylene chromophore as the basic building block in a new type of solution processable conjugated polymers.

In this work we present for the first time a series of triphenylene-*alt*-arylene copolymers and polytriphenylene homopolymers with different alkyl or alkoxy chains as the solubilizing units. The synthetic protocols, characterization as well as the application of these novel polymers in PLED devices are discussed below.

2.2 Synthesis and characterization of conjugated polytriphenylenes

An efficient synthesis has been developed toward a novel series of conjugated blue emitting polymers containing triphenylene as repeating unit for PLEDs. Soluble 1,2,3,4-tetraphenyltriphenylene, 2,3-bis(4-octylphenyl)-1,4-diphenyltriphenylene, 2-heptyl-1,3,4-triphenyltriphenylene, 2-decyl-3-(4-octylphenyl)-1,4-diphenyltriphenylene, 2,3-diheptyl-1,4-diphenyltriphenylene, 2,3-bis(4-dodecylphenyl)-1,4-diphenyltriphenylene, and 2,3-bis(4-(2-decyltetradecyl)phenyl)-1,4-diphenyltriphenylene-based co- and homo-polymers have been synthesized by the microwave assisted (MA) palladium-catalyzed Suzuki-Miyaura and the nickel-catalysed Yamamoto polycondensation reactions, respectively. Following the successful synthesis the optical properties, thermal stabilities, and supramolecular organization of the obtained polymers were investigated.

2.2.1 Monomer synthesis

The synthetic approaches toward the new triphenylene-based conjugated polymers started with a novel synthesis of the corresponding triphenylene-based monomers (Scheme 2.2).

The desired monomers were synthesized in two steps starting from the Knoevenagel condensation reaction[63] between 2,7-dibromophenanthrene-9,10-dione (**1**) and 1 equivalent of 1,3-diphenylpropan-2-one (**2**) using ethanol as a solvent and a solution of potassium hydroxide in methanol as the required base for the reaction. The reaction afforded 5,10-dibromo-1,3-diphenyl-2H-cyclopenta[l]phenanthren-2-one (**3**) in 40 % yield. Such moderate yield can be attributed to the incomplete reaction between the starting materials, due to the insufficient solubility of compound **1** in ethanol. It is worth here to mention that the reaction was also done using different solvents such as *t*-butyl alcohol, however the target molecule was only obtained when ethanol was used. Following that, compound **3** was subjected to a series of Diels-Alder reactions[64] with 1,2-di-*substituted*-ethynes **4** using diphenylether as

solvent to give monomers **5a-5g** in yields in the range of 10 % to 50 %. These relatively low reaction yields can be explained based on two main reasons: i) the steric hindrance between the aryl groups on compound **3** and the aryl and/or alkyl groups on compound **4**, and ii) the debromination of the desired product **5** due to the high temperature and the long time of the Diels-Alder reactions. In order to improve these yields a series of reactions to produce compound **5e** and **5d** were run in a microwave reactor at decreased temperatures (to reduce the degree of debromination) of 160°C, 190°C, and 220°C for 18 hours each. At the same time, the maximum power (300W) of the reactor was applied with the aim of minimizing the steric hindrance effect by exciting the reactants to an extreme extent. The obtained results showed that utilizing temperatures of 160°C and 190°C was not enough to afford the desired products. On the other hand using 220°C gave the desired products in similar yields as those obtained using the conventional reaction conditions (refluxing in diphenylether), which can be ascribed to the same reasons mentioned above. Further optimization of these reactions for example by changing the solvent system used was not done; because this needs demanding experimental work and our main goal was obtaining the precursor monomers for the subsequent polymerization steps.

It is important to mention that the synthesis of several 1,2-di-*substituted*-ethynes **4** with different alkyl chain lengths and types (linear and branched) was vital to afford the monomers with the required solubility, which is needed to achieve soluble high molecular weight polymers. Moreover, the optical properties of the resulting polymers can be eventually studied based on the different kinds of alkyl chains. For instance, polymers with bulky long branched alkyl chains usually result in less aggregation when compared to polymers substituted with short linear alkyl chains. Such possibly formed aggregations have usually a pronounced effect on the PL spectra of the polymers and result in red-shifted emission bands.[50,54] Compounds **4a**, **4d**, and **4e** were commercially available. In contrast, 1-(dodec-1-ynyl)-4-octylbenzene (**4b**) and 1,2-bis(4-octylphenyl)-ethyne (**4c**) were obtained for the first time by Sonogashira

coupling reaction.[57] **4b** was prepared from the reaction between 1- dodecyne and 0.86 equivalent of 1-bromo-4-octyl-benzene (**6**) in the presence of $Pd(PPh_3)_4$/CuI as catalyst to give the desired product in 70 % yield (Scheme 2.3). The purity of the material was tested by checking its carbon and hydrogen contents by using elemental analysis, which demonstrated C = 87.73 % and H = 12.0 % that was in agreement with the percentages of C and H calculated for **4b** (C = 88.06 % and H = 11.94 %). The Hagihara coupling reaction[57] among **8** and 1.2 equivalent of **6** with the assist of $Pd(PPh_3)_4$/CuI gave compound **4c** in 59 % yield (Scheme 2.3). Elemental analysis results showed that the found carbon and hydrogen contents in the obtained sample were in accordance with the calculated values for **4c**: found: C = 89.01 %, H = 10.34 %; calculated: C = 89.49 %, H = 10.51 %, which proved the purity of the product. Moreover, the previously reported compounds **4f** and **4g** have been synthesized according to literature procedure.[65,66] (for preparation details see experimental section).

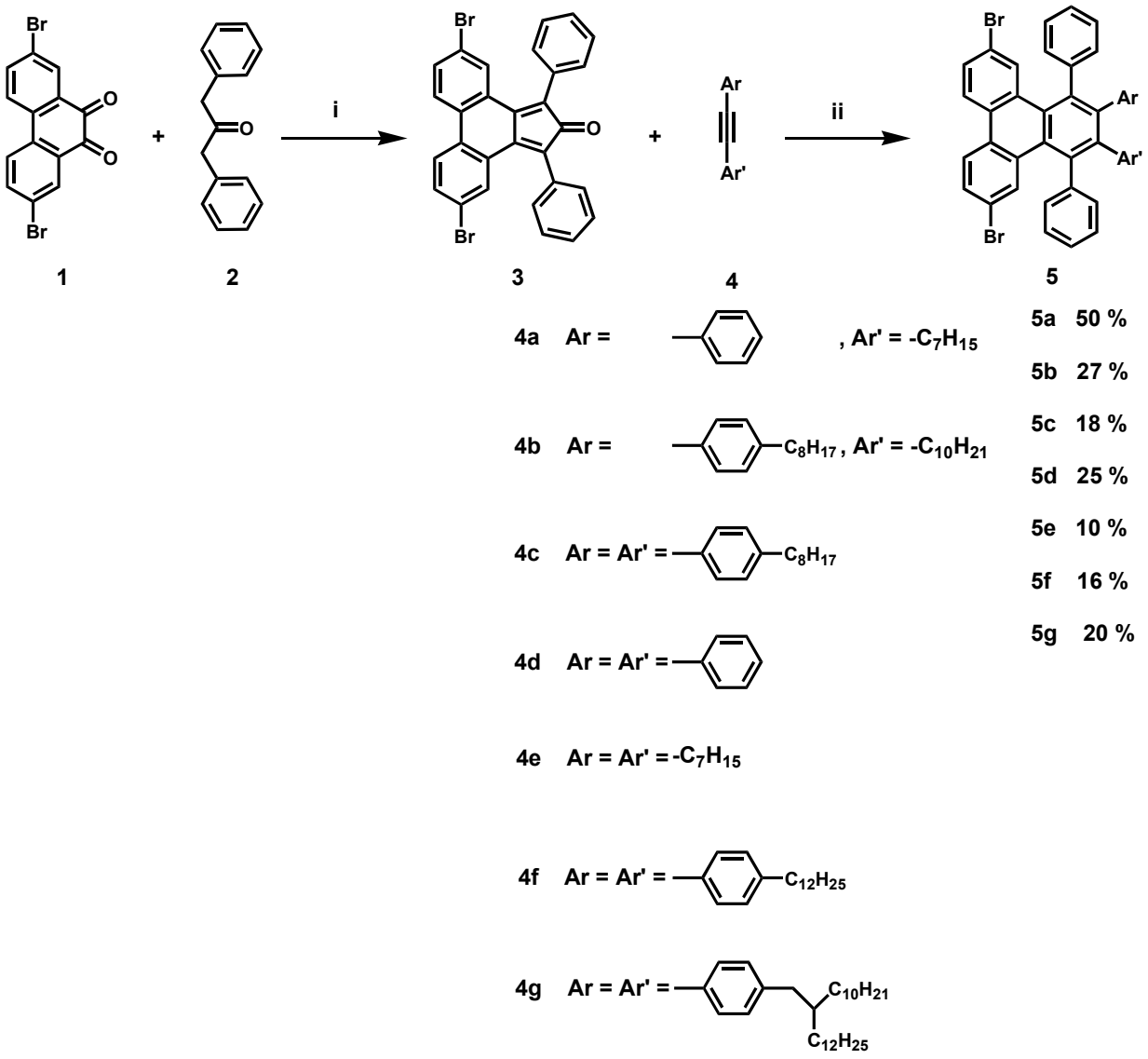

Scheme 2.2 Synthetic routes toward 6,11-dibromo-1,2,3,4-*substituted*-triphenylene monomers. Compound **1** was obtained from Ciba Inc., compound **2** was commercially available. (i) KOH, MeOH, EtOH, 80^{o}C, 40 %. (ii) Ph_2O, reflux.

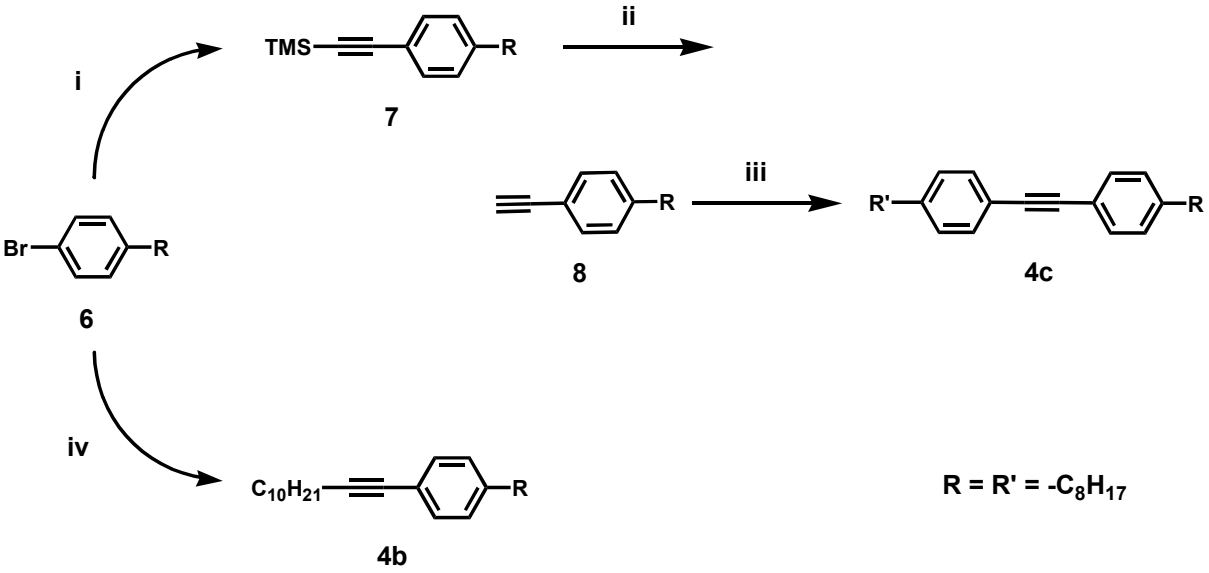

Scheme 2.3 Synthesis of 1-(dodec-1-ynyl)-4-octylbenzene (**4b**) and 1,2-bis(4-octylphenyl)-ethyne (**4c**)[a]. [a] Reagents and conditions: (i) Pd^0, ethynyltrimethylsilane, CuI, piperidine, 80°C, 91 %. (ii) TBAF, THF, 61%. (iii) Pd^0, 1-bromo-4-octyl-benzene, CuI, piperidine, 70°C, 59%. (iv) Pd^0, 1-dodecyne, CuI, piperidine, 50°C, 70%.

2.2.2 Polymer synthesis

2.2.2.1 Suzuki-Miyaura approach

For the polymerization protocols, we decided first to use the Pd-catalyzed Suzuki-Miyaura polycondensation reaction, which is one of the most powerful methods for preparing conjugated polymers.[67] **Polymers P_1-P_6** were synthesized using the MA-Suzuki–Miyaura polymerization of monomers **5a-5f** in high yields in the range of 50 % up to 81.5 % (Scheme 2.4). For this AB type polymerization highly accurate stoichiometric ratios (1:1) of the reactants are necessary to attain high molecular weight polymers. While the monomers were purified by column chromatography, 1,4-bis(4,4,5,5-tetramethyl-1,3,2-dioxaborolan-2-yl)benzene and its derivatives were always recrystallized from hot hexane prior to their use.

The purity of the monomers was tested by using several methods such as ^{1}HNMR and ^{13}CNMR spectroscopy and elemental analysis (see experimental section). The ^{1}H-NMR

spectrum of 6,11-dibromo-1,2,3,4-tetraphenyltriphenylene (**5d**) is presented here as one example (Figure 2.3). The spectrum was recorded in CD_2Cl_2 at room temperature. Only four types of aromatic protons (Ha, Hb, Hc, and Hd) were found in the spectrum, which was in accordance with the structure of the molecule. The aromatic signals assigned to the two protons Hb were found as doublets (J = 8.73 Hz) due to the presence of only one proton (Ha) in its direct neighborhood, the signals showed a down-field shift around 8.24 ppm. The two

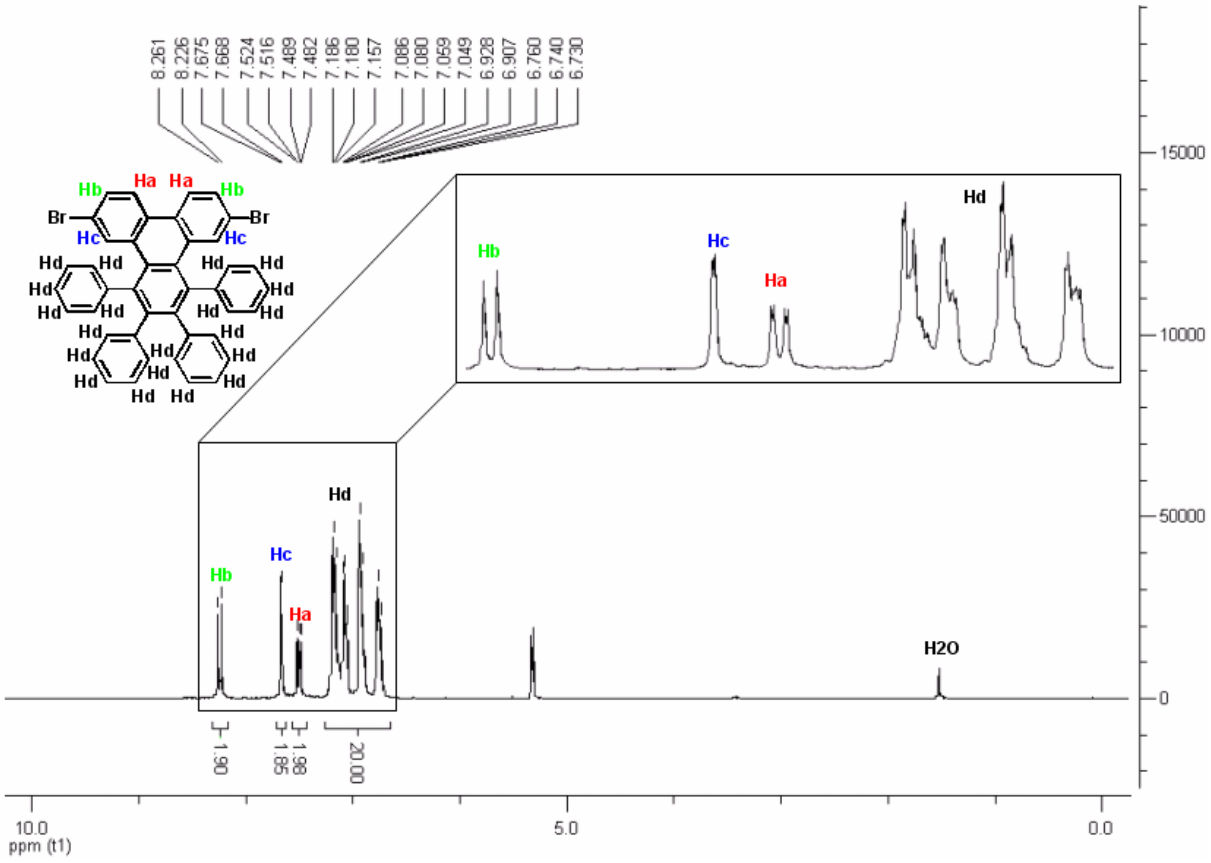

Figure 2.3 ^{1}HNMR spectrum of 6,11-dibromo-1,2,3,4-tetraphenyltriphenylene (**5d**).

protons of Hc depicted splitted singlet peaks (due to the possible meta-coupling between Hc and Hb with coupling constant of 1.74 Hz, and a chemical shift of 7.67 ppm. Similar to Hb, the signals of the two protons of Ha appeared as doublets (J = 8.65 Hz) with chemical shift of 7.51 ppm. Finally, the twenty protons of Hd were found as multiply splitted signals, and acquired a chemical shift of 7.19-6.73 ppm.

The MA-reactions commonly give different results from one system to the other. Consequently, it was difficult to find the most suitable conditions (power, temperature, and time) for the MA-Suzuki-Miyaura reaction to be used in our synthesis. Finally, it was found that 50 W at 100^{o}C for 1 hour were the suitable conditions for our system. In the general polymerization reaction a suspension of the monomer, 1,4-bis(4,4,5,5-tetramethyl-1,3,2-dioxaborolan-2-yl)benzene (or its derivatives), aqueous potassium carbonate, and the catalyst tetrakis (triphenylphosphine) Palladium in toluene was charged in a microwave tube equipped with a magnetic stirrer bar. The tube was then flashed with argon for about 2 minutes and finally sealed, and the mixture was vigorously stirred in a CEM Discover microwave at 50 W and activated cooling; keeping the temperature at 100°C for 1 h. The reaction was finally quenched (to end cap polymer chains) by the successive addition of bromobenzene and benzene boronic acid, and the whole reaction mixture was stirred at 100^{o}C for additional ½ h. The organic layer was then extracted with toluene and washed with aqueous sodium cyanide in order to remove the non reacted catalyst. The organic layer was then concentrated in vacuo until a highly viscous solution was obtained which by the slow addition to 300 ml methanol afforded the desired product as yellow precipitate. The polymer was filtered off and sequentially washed with methanol, water, acetone, and methanol. The polymer was dissolved again in toluene and vigorously stirred in aqueous sodium cyanide (1 %, 100 ml) at 90°C for 2 h to remove as much as possible the remaining traces of the catalyst. The organic phase was extracted, concentrated, and finally poured into excess of methanol. The polymer was again filtered off, and the oligomeric fractions were removed by extraction (Soxhlet apparatus / acetone or ethyl acetate).

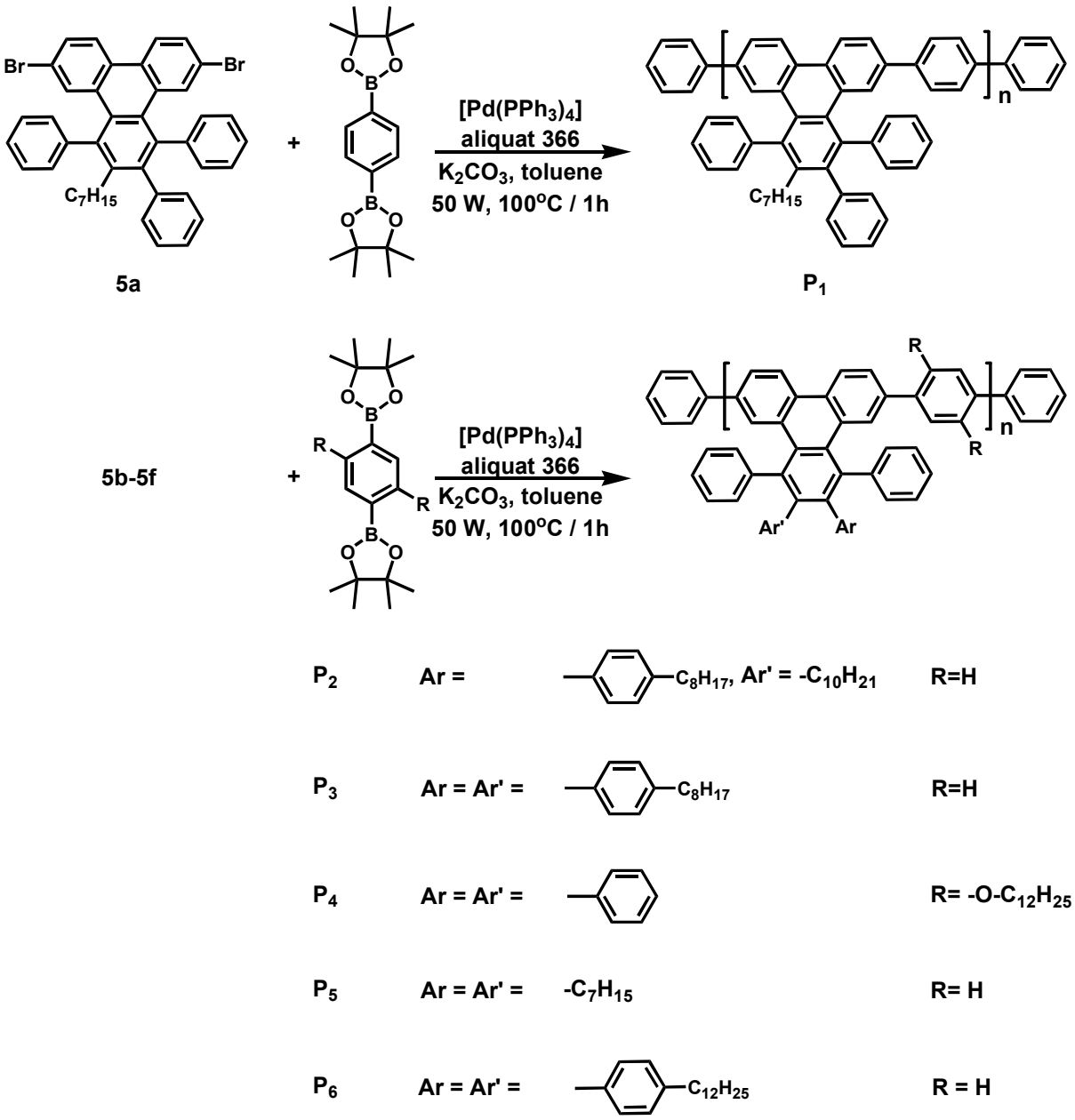

Scheme 2.4 Synthetic route toward polymers $\mathbf{P_1}$-$\mathbf{P_6}$ via Suzuki-Miyaura coupling reaction.

The molecular weight of the polymer was detected by using gel permeation chromatography (GPC). The measurement was done initially against polystyrene standard (soluble); however the GPC curves were recalculated using PPP standard (insoluble) in order to have more realistic results, since the molecular structure shows that the TP-based polymer can be also considered as PPP-type polymer (upper periphery of the polymer chain). That is expected to result in comparable degree of stiffness between our system and PPP but not to

polystyrene (more flexible). In addition this method of molecular weight determination has been widely used to estimate the molecular weight of several PPP-type polymers such as poly(fluorene),[46] and poly(ladder-type pentaphenylene).[48] Consequently, The presented polymers here showed weight average molecular weight of $M_w = 15 \times 10^3$ up to 63×10^3 g mol^{-1}, with polydispersity indices (PDI) ranging from 1.4 to 3.6. The polymers exhibited very good solubility in common organic solvents (>10 mg / 1 ml) such as chloroform ($CHCl_3$), tetrahydrofurane (THF), and toluene. The molecular weights and PDI of the resulting polymers are summarized in Table 2.1.

2.2.2.2 Yamamoto approach

The Suzuki-Miyaura polycondensation reactions presented here were successful in affording the desired target polymers. Nevertheless, these AB type polymerizations need always very accurate stoichiometries (1:1) of the reacting materials, where small deviation can lead to dramatic decrease in the molecular weight of the resulting polymers. On the other hand, the preparation and purification (several times recrystallization) of the arylenediboronic ester derivatives require considerable synthetic efforts, especially when scale-up is needed. These drawbacks of the Suzuki approach to prepare copolymers motivated us to search for simpler but comparatively powerful and robust methods for the preparation of the functionalized TP-based polymers. A promising alternative was the Yamamoto polycondensation.[68] In this synthetic route, dibromo-functionalized starting materials are the only monomers required and stoichiometric quantities of nickel complexes take over the role of the organometallic counterpart. The purity of the monomers was studied by ^{1}HNMR, ^{13}CNMR, and elemental analysis (see experimental section). As example, the elemental analysis of monomer **5e** showed carbon and hydrogen contents of 71.65 % and 6.34 % that was in agreement with the theoretical calculated values C = 71.94 %, and H = 6.31 %.

Because of the simplicity of the Yamamoto approach, and the fact that it has previously shown to be highly valuable for the synthesis of constitutionally homogeneous,

high molecular weight polyaromatics,[68] we decided to utilize this method also in our synthesis.

Using the nickel (0) mediated MA-Yamamoto polymerization (Scheme 2.5) of monomers **5e**, **5c**, and **5g** resulted in the homopolymers $\mathbf{P_7}$, $\mathbf{P_8}$, and $\mathbf{P_9}$ in 93 %, 91 %, and 79 % yield, respectively. In this synthetic approach equal molar ratios of Bis(1,5-cyclooctadiene)nickel, 1,5-cyclooctadiene, and 2,2'-bipyridine were dissolved in a mixture of dry toluene and dry *N*,*N*dimethylformamide (1:1). The mixture was then charged under argon in a microwave tube equipped with a magnetic stirrer bar, and heated at 80°C for 30 min to generate the catalyst. A solution of the monomer in dry toluene was then added and the reaction mixture was vigorously stirred in a CEM Discover microwave at 80 W and activated cooling; keeping the temperature at 80°C for 1 h. The reaction was finally quenched (end capping of polymer chains) with the addition of bromobenzene in excess followed by heating at 80°C for additional ½ h. The reaction mixture was then stirred for 4 h in a blend of methanol and concentrated hydrochloric acid (1:1) to destroy the remaining catalyst. Finally, a yellow fibre like precipitate was formed, which was again dissolved in toluene and stirred in a saturated aqueous ethylenediaminetetraacetate (EDTA) solution for 12 h to remove the traces of the residual catalyst in the attained polymer. The organic layer was then extracted with toluene and the polymer reprecipitated in methanol, filtrated, sequentially washed with methanol, water, and acetone. At the end the oligomeric fractions were removed by extraction (Soxhlet apparatus / ethyl acetate). From the GPC analysis (recalculated against PPP standard), polymers $\mathbf{P_7}$, $\mathbf{P_8}$, and $\mathbf{P_9}$ demonstrated high molecular weights of $M_w = 224 \times 10^3$, 112×10^3, and 77×10^3 g mol^{-1}, respectively. Polymers $\mathbf{P_7}$ and $\mathbf{P_8}$ showed PDI value of 2.7, while $\mathbf{P_9}$ had a value of 2 (Table 2.1). The three polymers displayed high solubility (10 mg / 1 ml) in common organic solvents ($CHCl_3$, THF, and toluene).

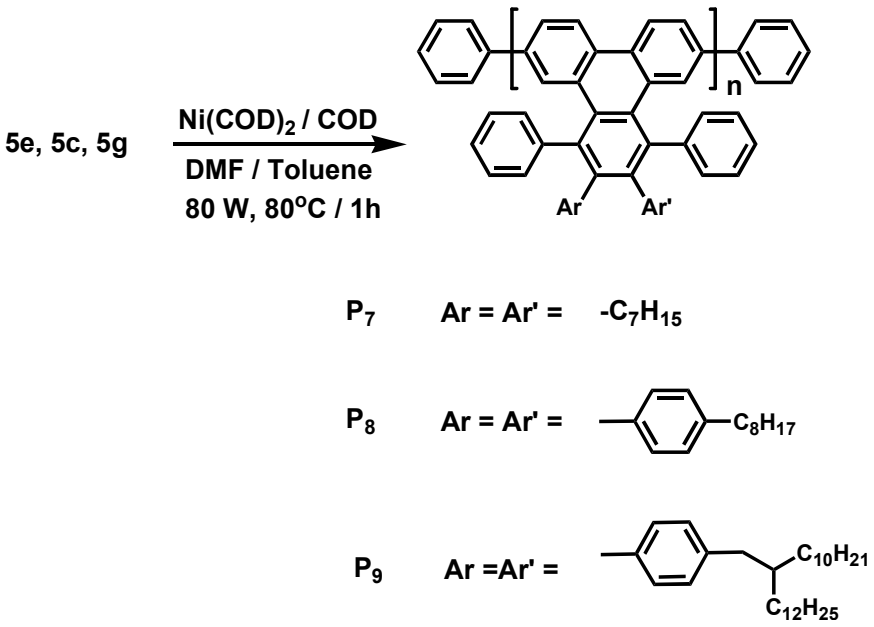

Scheme 2.5 Synthetic route of polymers $\mathbf{P_7}$-$\mathbf{P_9}$ via Yamamoto coupling reaction.

The above results showed that the Suzuki and the Yamamoto polymerization reactions were able to afford the desired TP-polymers with high degree of solubility in the common organic solvents. Moreover the GPC analysis demonstrated higher molecular weights for the homopolymers compared to the copolymers (Table 2.1). That can be attributed to the fact that the Yamamoto polymerization does not need very exact stoichiometries as the Suzuki polymerization does. This fact makes the homocoupling reaction more effective in producing high molecular weight polymers than the heterocoupling one, since any small deviation from the 1:1 reactants' molar ratios in the Suzuki coupling reaction can lead to dramatic decrease in the molecular weight.

As the direct coupling of the TP-chromophors in the homopolymers is expected to result in new properties compared to the copolymers in which the arylene units are used as spacers between the triphenylene moieties. It was important to study the effect of the TP-coupling mode on the photophysical characteristics of the obtained polymers.

Table 2.1 Molecular weights and PDI of Polymers **P_1- P_9**[a]

Polymer	Yield (%)	M_w	PDI
P_1	68	27×10^3	2.7
P_2	55	36×10^3	1.4
P_3	67	15×10^3	1.9
P_4	65	18×10^3	1.6
P_5	81.5	63×10^3	3.6
P_6	50	19×10^3	1.5
P_7	93	224×10^3	2.7
P_8	91	112×10^3	2.7
P_9	79	77×10^3	2.0

[a] Estimated from GPC analysis (standard = PPP, eluent = THF, temperature = 25^{o}C).

2.3 Photophysical properties of triphenylene-based monomers and polymers

2.3.1 Absorption and photoluminescence of triphenylene monomers

In order to have a complete study of the optical properties of the synthesized TP-based systems, the investigation started with studying the UV-Vis absorption and PL spectroscopy of the synthesized monomers in dichloromethane (DCM) solutions.

Figure 2.4 depicts the UV-Vis absorptions spectra of monomers **5a**-**5g**. The absorption spectra were very similar in shape with unresolved absorption maxima and high energy shoulder. The absorption maxima of the monomers were found to be between 283 and 289 nm. These values reflect how the similarity in the chemical structure can result in comparable optical behavior.

For instance monomers **5a** and **5e** that have alkyl chains of only seven carbon atoms attached directly to the triphenylene edges exhibited the same absorption maxima at 283 nm. In addition, **5a** and **5e** showed similar molar extinction coefficient (ε) values of 95238 and 91743 $M^{-1}.Cm^{-1}$, respectively. Compound **5b** which has similar structure as **5a** but with longer alkyl

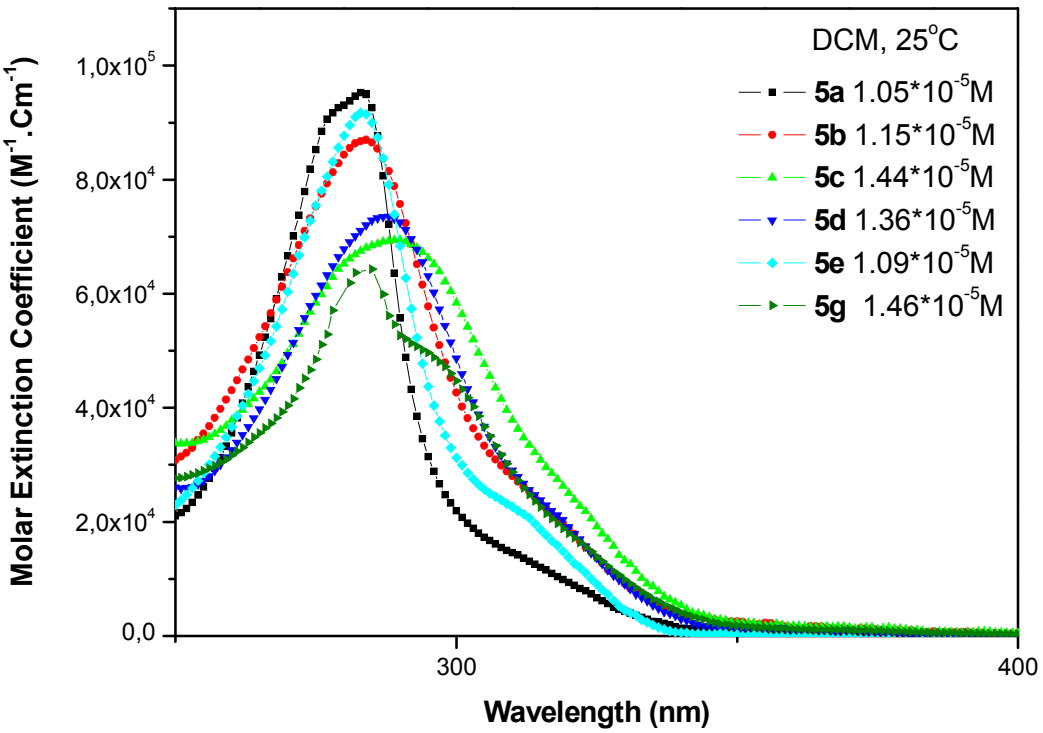

Figure 2.4 UV-Vis spectra of monomers **5a-5g** in DCM at 25°C.

chains showed maximum absorption of 284 nm and ε value of 86957 $M^{-1}.Cm^{-1}$.

Finally, monomers **5c**, **5d**, and **5g** in which the triphenylene moiety is totally surrounded by aryl units depicted slightly red-shifted absorption maxima of 289, 288, and 285 nm, respectively. That can be attributed to the small increment in the degree of conjugation when compared to monomers **5a**, **5b**, and **5e** due to the presence of extra aryl units around the triphenylene moiety. Furthermore, lower molar extinction coefficient degree of 69443, 73529, and 64269 $M^{-1}.Cm^{-1}$ were reported for **5c**, **5d**, and **5g**, respectively. Such lower values

compared to those of **5a**, **5b**, and **5e** can be ascribed to the dilution of the absorption efficiency of the triphenylene unit with the increased amount of aryl and long alkyl chains around the chromophore. Figure 2.5 presents the emission spectra of the monomers. **5d**, **5e**, and **5g** exhibited emission maxima of 415, 416, and 430 nm, respectively. That was bathochromically-shifted compared to those of **5a**, **5b**, and **5c** (405, 408, and 411 nm). Table 2.2 outlines the UV-Vis absorption and photoluminescence of all monomers (**5a-5g**).

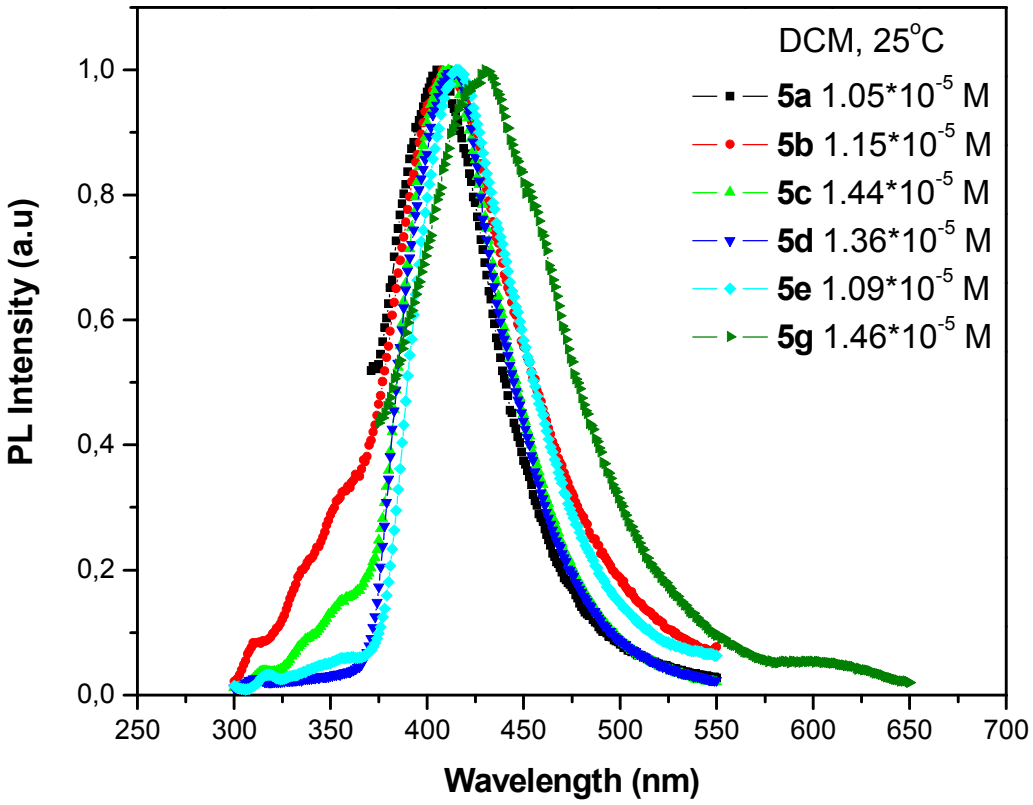

Figure 2.5 PL spectra of monomers **5a-5g** in DCM at 25°C.

Table 2.2 UV-Vis absorption and PL behavior of monomers **5a**–**5g** (solvent = DCM, concentration ~ 1-2 × 10^{-5} M, temperature = 25°C).

Monomer	$\lambda_{abs.\ sol}$ [a] (nm)	$\lambda_{PL.\ sol}$ [b] (nm)	Monomer	$\lambda_{abs.\ sol}$ [a] (nm)	$\lambda_{PL.\ sol}$ [b] (nm)
5a	283	405	**5d**	288	415
5b	284	408	**5e**	283	416
5c	289	411	**5g**	285	430

2.3.2 Optical properties of triphenylene-based polymers

2.3.2.1 Absorption and PL in Solution

In the following sections the optical properties of polymers **P_1**-**P_9** will be discussed as well as compared with other blue emitting polymers reported in the literature.

The UV-Vis absorption spectra of the synthesized polymers in solution (THF) are depicted in Figure 2.6. Polymers **P_1**, **P_2**, and **P_3** exhibited two bands in the solution absorption, with the absorption maxima at 391, 408, and 388 nm, respectively, while the second bands were at 409, 392, 405 nm, respectively. Polymers **P_1** and **P_3** showed hypsochromically shifted absorption maxima compared to **P_2** that can be attributed to the lower molecular weight and consequently the smaller conjugation length for **P_1** and **P_3**. However the three polymers showed almost identical PL maxima in solution at 429, 428 nm, and 427 nm, respectively (Figures 2.6 and 2.7).

The PL spectra were characterized by steep onsets and by well-resolved vibrationally split maxima at higher wavelengths but with lower intensities (453 and 481nm for **P_1**, 453 and 480 nm for **P_2**, and 452 and 479 nm for **P_3**) which resulted from the vibrational splitting. The UV-Vis spectrum of the alkoxy substituted polymer **P_4** in solution was characterized by

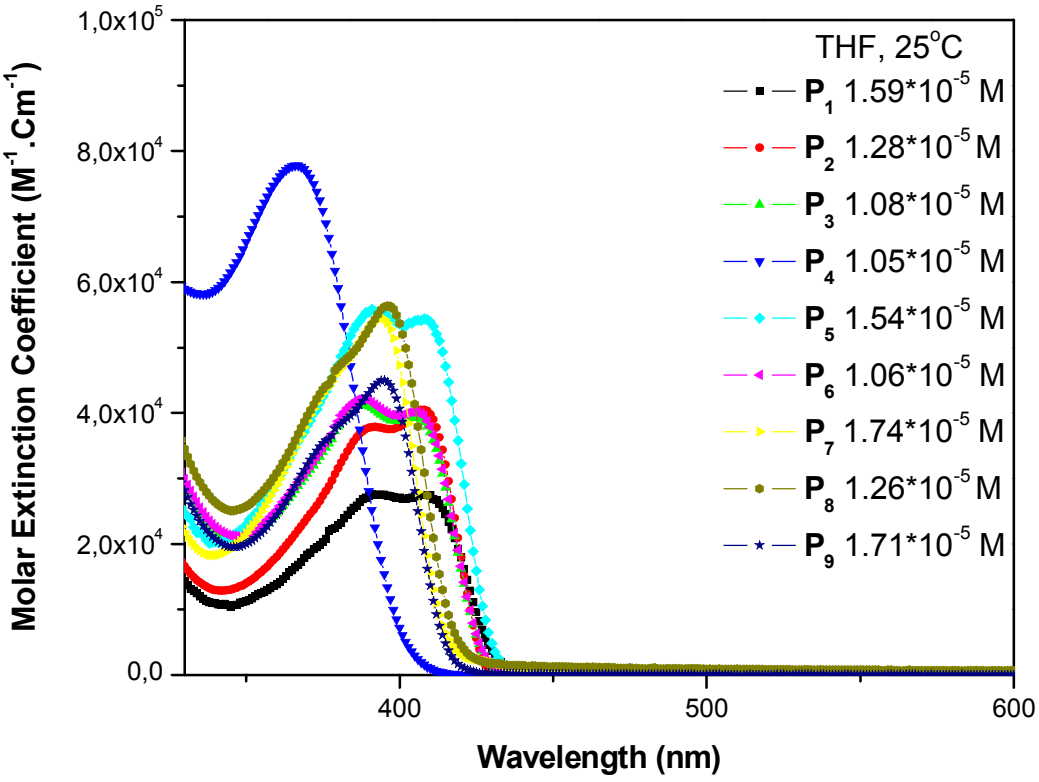

Figure 2.6 UV-Vis spectra of polymers in THF at 25°C.

featureless π–π* transition (one band) at 367 nm which was blue-shifted compared to the absorption maxima of the other polymers. This is most probably due to the alkoxy groups on the poly(arylene)s backbone which usually lead to an increase of the dihedral angle of consecutive aromatic units, which reduces electronic conjugation leading to an increased band gap.[69] In order to semi quantify this effect, the dihedral angles in the two model compounds 1,4,6-triphenyl-triphenylene and 6-(2,5-dimethoxy-phenyl)-1,4-diphenyl-triphenylene (Figure 2.8) that are representing our systems were calculated using the DFT/B3LYP method. The study was done by Dr. Martin Baumgarten at Max Planck institute for Polymer Research in Mainz. The DFT B3LYP - basis set 6-31G* gave 38 degree of twisting for benzene and 47.7 degrees for bisalkoxybenzene. Although, the two compounds showed only a small difference

in the dihedral angles, these values should be taken twice into account for next triphenylene unit. Therefore, this study supports the idea that introducing alkoxy units to the backbone of polymer **P4** should result in reduced conjugation length. Unlike **P1**, **P2**, and **P3**, polymer **P4** demonstrated one PL maximum at 422 nm in solution with unresolved shoulder at 445 nm. Polymer **P5** showed absorption maxima at 391 nm with a second band at 408 nm, while the PL maximum was observed at 429 nm. **P5** exhibited also a second higher wavelength but less intense PL maximum at 454 nm which was homologous to the absorption and PL maxima of polymer **P1**.

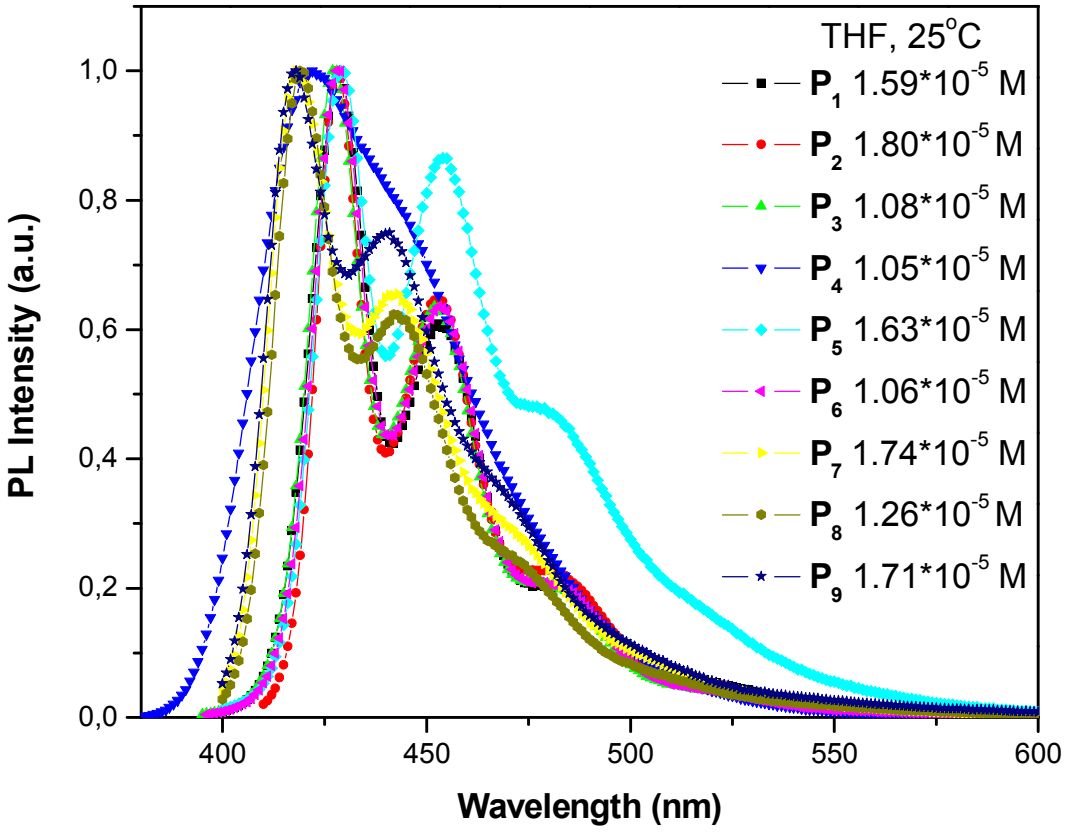

Figure 2.7 PL spectra of polymers in THF at 25°C.

The UV-Vis spectrum of polymer **P6** was almost identical to that of polymer **P3**. This can be ascribed to their very close chemical structure, since the only difference between the

two polymers was the length of the alkyl chains attached to the polymer repeating unit (**P_3** has octyl-chains, while **P_6** has dodecyl- chains). **P_6** exhibited absorption maximum at 388 nm with a second peak appeared at 405 nm. In addition, **P_6** showed PL maximum at 428 nm with another lower energy maximum at 453 nm. These values were in agreement with those of polymer **P_3**.

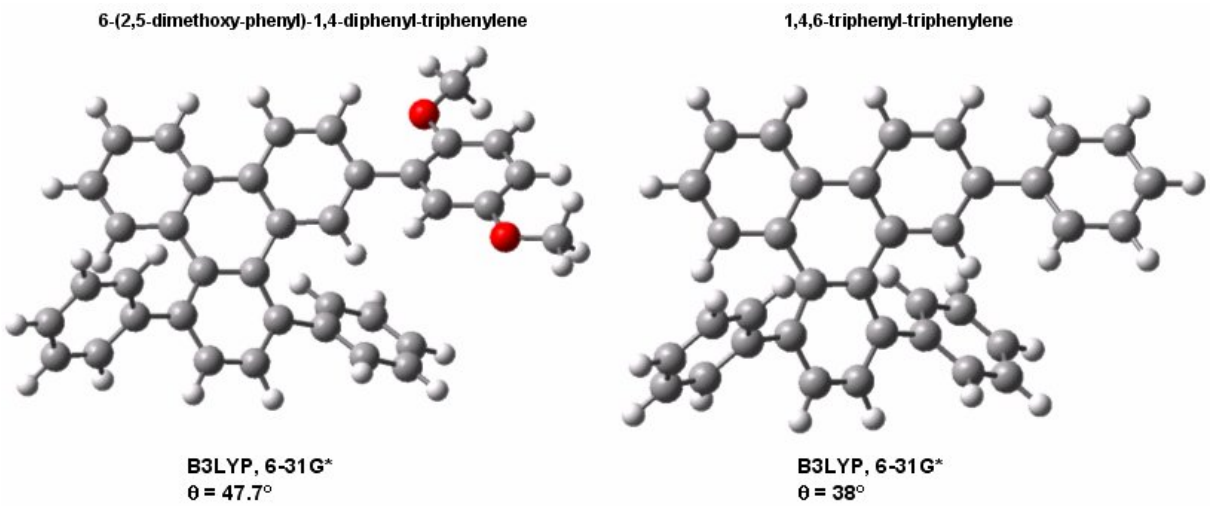

Figure 2.8 DFT/B3LYP studies for the model compounds 1,4,6-triphenyl-triphenylene and 6-(2,5-dimethoxy-phenyl)-1,4-diphenyl-triphenylene.

Polymers **P_7**, **P_8**, and **P_9** showed absorption maxima at 394 nm, 396 nm, and 395 nm, respectively with PL maxima at 418 nm in solution. The PL spectra were similar to those of polymers **P_1**-**P_6** and characterized also by steep onsets with second vibrationally split maxima at 442 nm for **P_7** and 441 nm for **P_8**, and **P_9**, respectively. Furthermore, the observed PL spectra for **P_7**, **P_8**, and **P_9** suggest that decreasing the number of the aryl units around the triphenylene moiety has no significant effect in solution. The observed PL maxima of ~420 nm for **P_1**-**P_9** compares very well with that of dialkylpolyfluorene (PL maximum ~ 415 nm)[62] which has been widely studied as an active material in blue PLED.

2.3.2.2 Absorption and PL in thin Films

The thin films of the presented polymers were prepared by spin coating from toluene solutions (~ 1×10^{-5} M) at 1000 rpm over quartz substrates. As shown in Figures 2.9 and 2.10, polymers **P_1** and **P_2** showed comparable absorption in film and nearly the same PL spectra in both solution and film. On the other hand polymer **P_3** exhibited an almost identical absorption and PL spectra in both solution and film. In addition a solid state related broadening of the spectra was observed in the three polymers. Polymer **P_4** depicted also nearly indistinguishable emission spectra in solution and in film and showed in both cases emission maxima about 420 nm. In contrast to **P_1**, **P_2**, and **P_3**, polymer **P_4** showed smaller solid state related broadening in the film PL spectrum. From these results one can conclude that there is no significant change in the conformations of the four polymers in going from solution to film, and since the PLED device is basically a thin film of the emitting polymer, **P_1-P_4** can be introduced as promising blue emitters for PLED applications. Moreover, **P_4** with its tiny broadening in the film PL spectra displays a clear advantage over **P_1**, **P_2**, and **P_3** in terms of emitting more deep and pure blue color.

While polymer **P_5** revealed identical absorption maxima in solution and film (391 nm), the PL spectrum exposed a broad bathochromically shifted emission band of 30 nm in film (459 nm) compared to solution (429 nm). This bathochromic shift can be ascribed to the molecular structure of the polymer, which has two small and short alkyl chains on the periphery of the triphenylene core that were not able to suppress aggregation in the solid state. It worth to mention that, such red shift was not noticed in polymers **P_1-P_4** since the four polymers contain at least one bulky aryl unit instead of one of the two alkyl chains found in **P_5**, which effectively prevented any aggregation in the solid state.

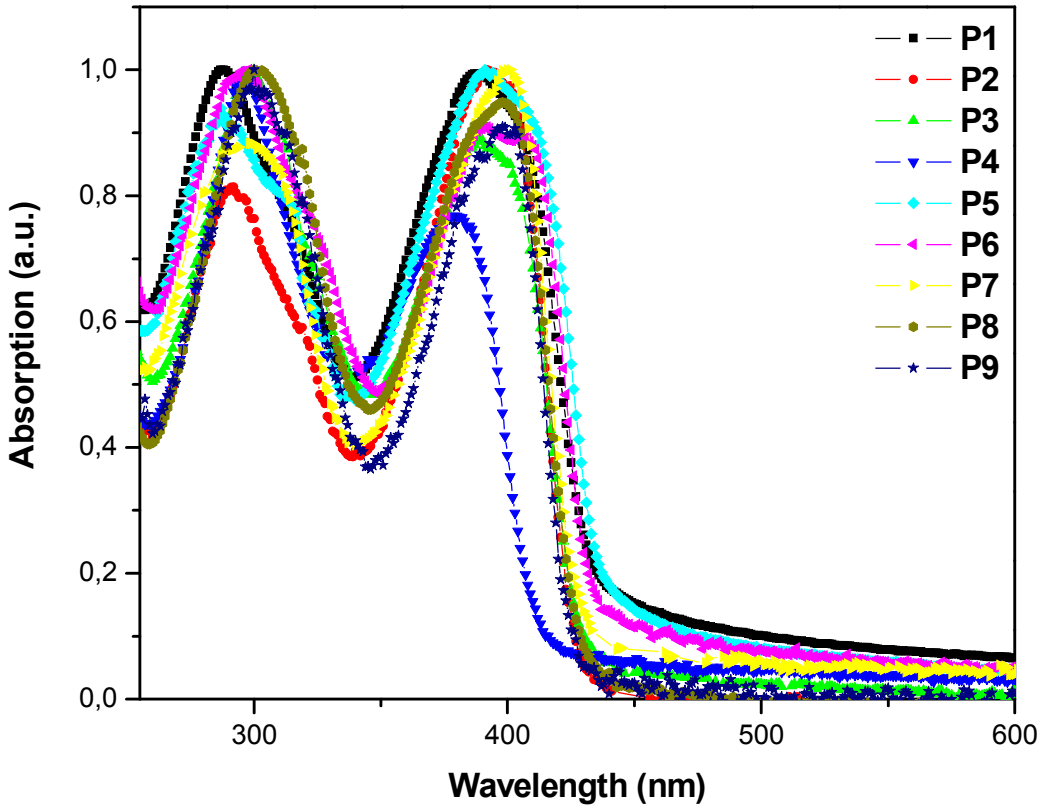

Figure 2.9 UV-Vis spectra of polymer thin films.

Polymer $\mathbf{P_6}$ showed comparable absorption and emission behavior as $\mathbf{P_3}$. The film absorption and PL maxima were at 392 nm, and 428 nm, respectively. That was nearly the same as in the solution spectra, but with a solid state related broadening in the film case. These results suggest that there is no considerable variation in the conformations of $\mathbf{P_6}$ in going from solution to film. Moreover, the film PL spectrum of the polymer did not reveal any huge red shift as evidence of aggregation that can be attributed to the presence of bulky aryl groups surrounding the triphenylene moiety. Therefore, polymer $\mathbf{P_6}$ could be a possible emitter for blue-PLED.

The absorption spectra of polymer $\mathbf{P_7}$ in solution and in film exhibited approximately the same behavior. Nevertheless the PL spectrum showed a broader bathochromically shifted

maximum of about 40 nm in film compared to solution. These results were similar to the obtained spectral results for polymer **P_5**. This resemblance, despite containing a different π-conjugated backbone (the inclusion of a phenyl spacer), support our previous explanation that the small solublizing alkyl side chains found on the edge of the polymer result in the broadening and the bathochromic shift by promoting polymer aggregation. Accordingly polymers **P_5** and **P_7** with their more pronounced green emission can not be considered as good blue emitters.

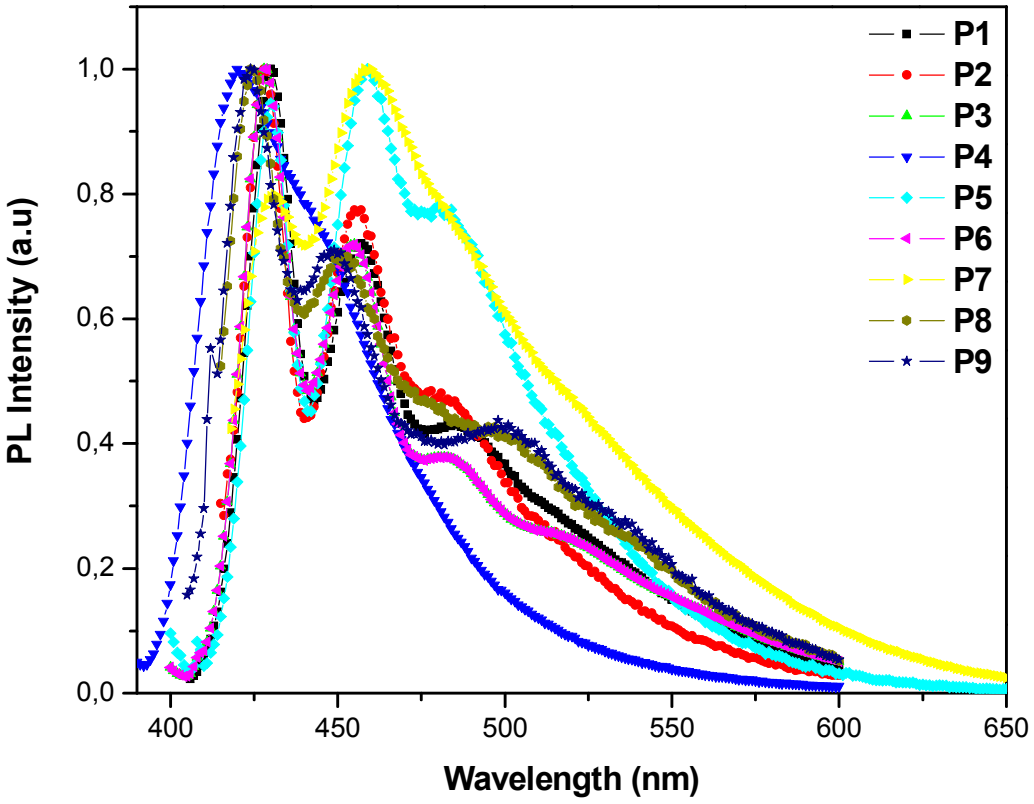

Figure 2.10 PL spectra of polymer thin films.

Polymers **P_8** and **P_9** exhibited identical film absorption and emission maxima of 398 nm and 424 nm, respectively. While the absorption maxima were very close to those obtained

in solution, the film PL spectra showed solid state related broadening with ~6 nm bathochromically shifted emission maxima.

Comparing the PL spectra of polymers **P_8** and **P_3** showed roughly identical PL behavior aside from a broadening in the PL spectra of polymer **P_8**. These results suggest that the direct coupling between the triphenylene repeating units in the homo-polymers did not hinder the conjugation in the polymers backbones due to the probable increased twisting of the different phenyl rings on the sequential triphenylene moieties. Instead it led to analogous optical spectra for polymers **P_8** and **P_3**. The optical data of all polymers are illustrated in table 2.3.

2.3.2.3 Quantum yield

The quantum yields of the polymers in solution were investigated by using 9,10-diphenylanthracene (Φ_{PL} = 0.9) as a standard.[70] For that the UV-vis absorption spectra of the polymers in THF were recorded in a 1 cm cuvette. In order to minimize re-absorption effects the absorbance never exceeded 0.1 at the excitation wavelength of the used standard (here 365 nm). The PL spectra of the same solutions were recorded in a 1 cm cuvette, and the integrated fluorescence intensities were calculated and noted. The quantum yield values were then calculated according to the equation[70]: $\phi_{unk} = : \phi_{std} (I_{unk} / A_{unk})(A_{std} / I_{std}) (\eta_{unk} / \eta_{std})^2$, where ϕ_{unk} is the quantum yield of the sample, ϕ_{std} is the quantum yield of the standard (0.9 in cyclohexane), I_{unk} and I_{std} are the integrated emission intensities of the sample and the standard, respectively. A_{unk} and A_{std} are the absorbance of the sample and the standard at the excitation wavelength, respectively. η_{unk} and η_{std} are the refractive indexes of the corresponding solvents. Multiple measurements indicated a precision of about 5 % for the quantum yield values determined.

Polymers **P_1**, **P_2**, **P_5**, **P_7**, **P_8** and **P_9** exhibited high quantum efficiencies (Φ_{PL}) in solution, which were found to be 0.65, 0.84, 0.66, 0.67, 0.85 and 0.65, respectively. These values were close to or even in case of **P_2** and **P_8** higher than polyfluorene containing bis(2,2-

diphenylvinyl)fluorene (Φ_{PL} = 0.75).[71] The values were also close and in case of **P_8** equal to the quantum yield of POF (Φ_{PL} = 0.85).[72]

The PL quantum yield in film was also estimated relative to a thin film quantum efficiency of POF. Sample polymer and reference POF were dissolved in toluene and spin coated over quartz (1 min at 2000 rpm and 15 s at 5000 rpm) then by comparing the sample fluorescence intensity to that of a thin film sample of POF polymer that was excited at 380 nm (Φ_{PL} = 0.55) the quantum efficiency was determined.[71, 72]

We estimated the PL quantum yield of **P_2**, **P_4**, **P_5**, **P_7**, and **P_8** in films to be 0.34, 0.34, 0.31, 0.21, and 0.17, respectively. The lower quantum efficiencies of **P_2**, **P_5**, **P_7**, and **P_8** in film compared to solution might be due to the formation of intermolecular species, i.e. excimer formation or aggregates as in case of **P_5** and **P_7**[72] that was in agreement with our previous explanation that decreasing the number of aryl units around the triphenylene moieties in case of **P_5** and **P_7** resulted in aggregate formation.

Table 2.3 UV-Vis Absorption, PL, and quantum yields (Φ_{PL}) of polymrs **P_1–P_9** (solvent = THF, concentration ~ 1-2 × 10^{-5} M, temperature = 25°C).

Polymer	$\lambda_{abs.\ sol}$ [a] (nm)	$\lambda_{abs.\ film}$ [a] (nm)	band gap[b] (eV)	$\lambda_{PL.\ sol}$ [a] (nm)	$\lambda_{PL.\ film}$ [a] (nm)	$\Phi_{PL\ film}$ [c]	$\Phi_{PL\ solution}$ [d]
P_1	391	387	2.87	429	430	e	0.65
P_2	408	392	2.91	428	428	0.34	0.84
P_3	388	389	2.90	427	427	e	e
P_4	367	380	3.02	422	420	0.34	e
P_5	391	391	2.83	429	459	0.31	0.66
P_6	388	392	2.90	428	428	e	e
P_7	394	401	2.91	418	458	0.21	0.67
P_8	396	398	2.90	418	424	0.17	0.85
P_9	395	398	2.98	418	424	e	0.65

[a] Wavelength of the maximum absorbance or PL. [b] Band gaps were calculated from the onsets of UV-Vis absorption spectra of polymer solutions.[c] Relative to thin-film quantum efficiency of poly(9,9-dioctylfluorene) POF (sample polymer and reference POF were dissolved in toluene and spin coated over quartz (1min 2000 rpm and 15sek 5000 rpm). [d] Determined in THF relative to 9,10-diphenylanthracene in cyclohexane (Φ_{PL} = 0.9) with excitation at 365 nm. [e] not measured.

2.4 Electrochemical properties of triphenylene-based polymers

To investigate the redox properties, cyclic voltammograms were recorded for the polymer thin films against Ag/AgCl with a ferrocene standard (Figure 2.11). All polymers showed only anodic peaks with irreversible oxidation, which was in agreement with the general case of conjugated polymers, where often only reduction or oxidation is observed or where only one process is found to be reversible.[73-75] For that reason direct estimation of the

LUMO levels were not possible. Subsequently the HOMO levels, optical band gaps, and the LUMO levels of the reduced polymers (were deduced from the HOMO values and the polymers optical band gaps) were calculated as described by *Janietz et al*.[73] Polymers **P_1-P_9** showed irreversible oxidation peaks at potentials ranging from 1.57 to 1.87 V (Table 2.4) and onset potentials of oxidation between 1.39 and 1.68 V in the anodic scan. This could be attributed to the electron rich nature of the polymers (due to the presence of several alkyl chains or alkoxy groups on the periphery of the polymers that can act as an electron source) which may make it easier to oxidize rather than being reduced.[76,77] Compared with all polymers, the oxidation onset potential of **P_4** showed the lowest value which could be due to the high electron-donating property of the alkoxy group on the polymer backbone.

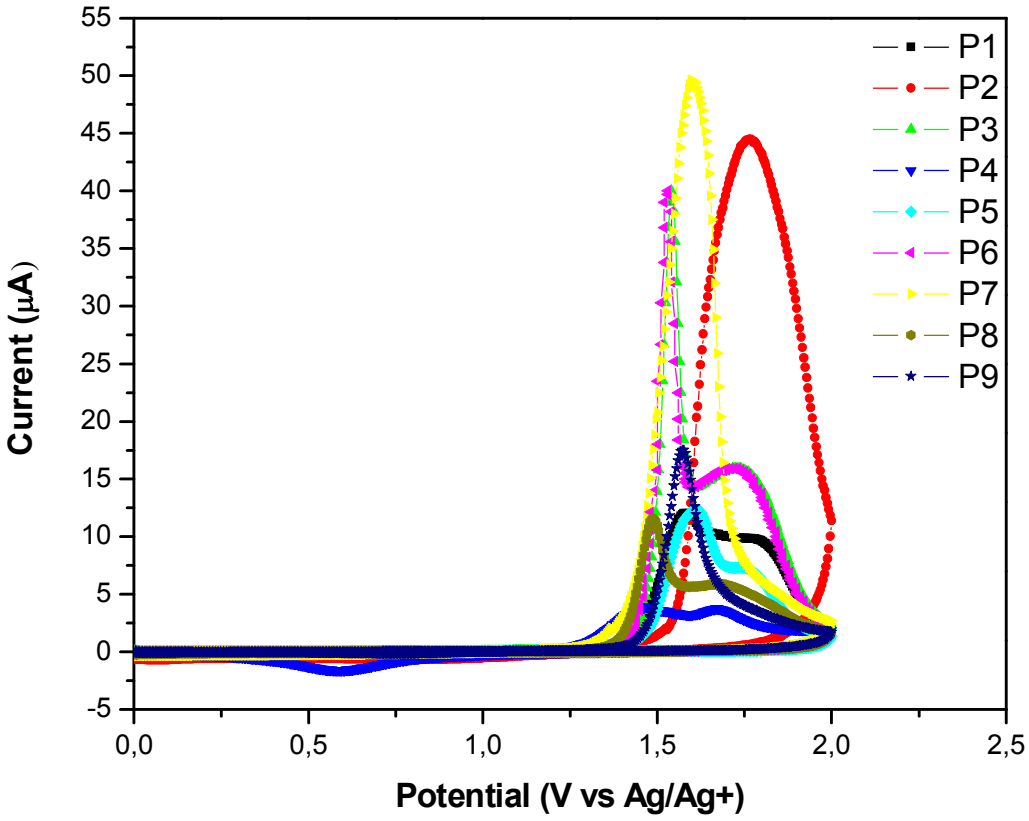

Figure 2.11 Cyclic voltammograms of drop casted polymer films from toluene solution on Pt-electrode in 0.1 M $TBAClO_4$ in acetonitrile solution vs Ag/Ag^+. Scanning rate100 mV/s.

All polymers exhibited HOMO and LUMO values in the range of 6.0 and 3.0 eV, respectively. These results were analogous to the obtained results for PFO which showed HOMO and LUMO values of 5.8 and 2.85 eV (estimated), respectively.[73]

Table 2.4 HOMO and LUMO energies and electrochemical properties of polymers **P_1-P_9** (corrected to Ag/AgCl reference electrode).

Polymer	$E^{ox/onset}$ (V)	$E^{ox/peak}$ (V)	E^{HOMO} (eV)	E^{LUMO} (eV)
P_1	1.55	1.68	5.95	3.08
P_2	1.68	1.87	6.08	3.17
P_3	1.56	1.65	5.96	3.06
P_4	1.39	1.57	5.79	2.77
P_5	1.56	1.71	5.96	3.13
P_6	1.54	1.64	5.94	3.07
P_7	1.54	1.71	5.94	3.03
P_8	1.50	1.59	5.90	3.0
P_9	1.57	1.68	5.97	3.04

2.5 Thermogravimetric analysis (TGA)

The thermal stabilities of polymers **P_2**, **P_4**, **P_5**, **P_6**, **P_8**, and **P_9** were investigated by thermogravimetric analysis (TGA). The thermal stability of each sample under nitrogen atmosphere was determined by measuring its weight loss while heating at a rate of 10^{o}C/min. All polymers exhibited good thermal stabilities with onset degradation temperatures above 300^{o}C that can be ascribed to the loss of the alkyl chains on the polymer backbone. These values were lower than the value reported for the blue emitting polymer Spiro-DPVF-

Containing Polyfluorenes, which showed thermal stabilities up to 423°C.[71] The TGA curve of polymer **P_6** is shown in Figure 2.12. The TGA curve showed that polymer **P_6** was thermally stable until 300°C, after this temperature a degradation process was detected till a temperature of 670°C. The measured total weight loss was about 40 % that was close to the weight percentage of the alkyl chains (36 %) in the repeating unit of the polymer. Therefore, this weight loss can be attributed to the loss of the alkyl chains from the polymer chains.

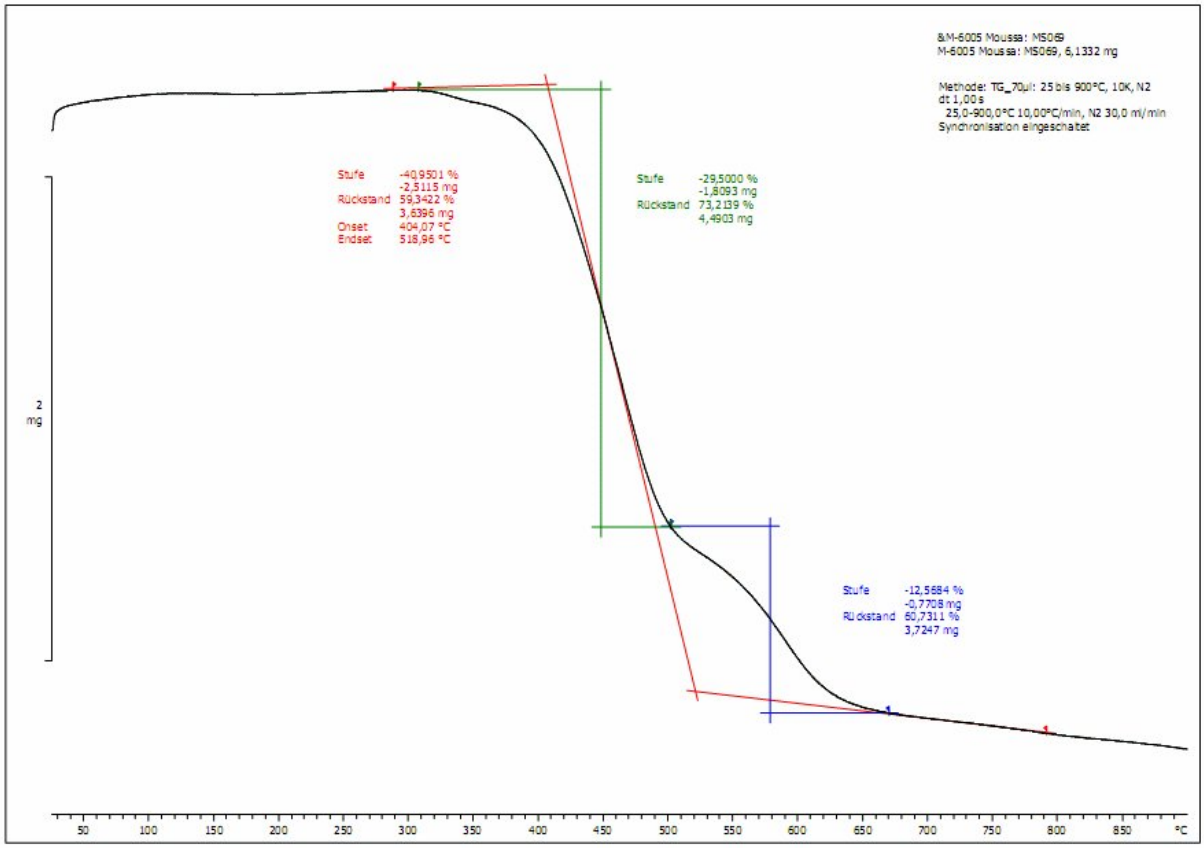

Figure 2.12 Thermogravimetric analysis (TGA) results of polymer **P_6**.

2.6 Supramolecular organization of triphenylene-based polymers

In this section the supramolecular organization of polymers **P_2**, **P_4**, **P_5**, and **P_7-P_9** in solid-state was studied by X-ray scattering method on extruded filaments using two-dimensional wide angle detector (2D-WAXS) as appropriate to the distribution of the

scattering centers.[78] This investigation was done by Dr. Wojciech Pisula and Alexey Mavrinskiy at Max Planck Institute for Polymer Research.

The sample preparation was carried out by using a home-built mini-extruder as illustrated in Figure 2.13. The extrusion was done at different temperatures for each polymer sample (Table 2.5), to reach a phase at which the material became plastically deformable and could be extruded as a thin filament of 0.7 mm diameter. Although the 2D-WAXS patterns were obtained at different temperatures, no changes in these diffractograms were observed.

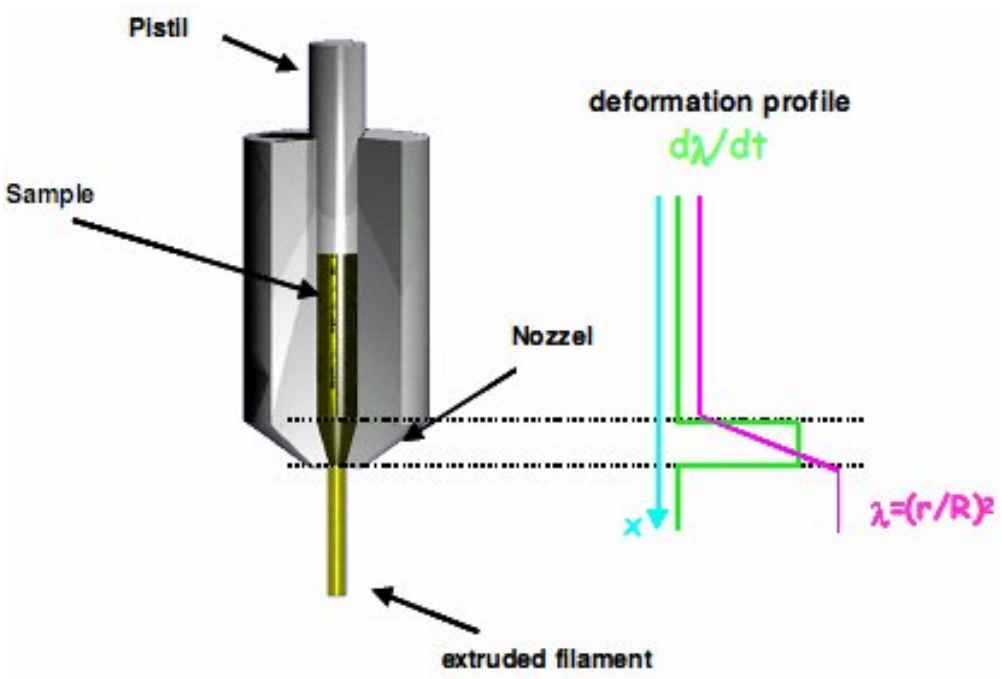

Figure 2.13 Schematic illustration of the alignment by mechanical extrusion.

(Pisula et al. *Chem. Mater.* **2005**, 17, 4296).[78]

The extruded filament was positioned perpendicular to the incident X-ray beam and vertical toward the 2D-WAXS detector (Figure 2.14). The distribution of the reflections over the scattering pattern allowed the conclusion about the relative arrangement of the building units within the supramolecular organization.

Table 2.5 Filament extrusion temperature for polymers.

Polymer	Extrusion temperature (^{o}C)
P_2	190
P_4	180
P_5	230
P_7	210
P_8	210
P_9	120

The X-ray patterns of all compounds revealed three typical reflections. The reflection in the wide-angle scattering range was related to an average value of 0.45 nm which corresponds to the noncovalent interaction between polymer chains. This interaction represents the indication for the lamellae packing. Two reflections in the equatorial small-angle scattering range were attributed to the chain-to-chain spacing between lamellae structures in which the polymers were packed.

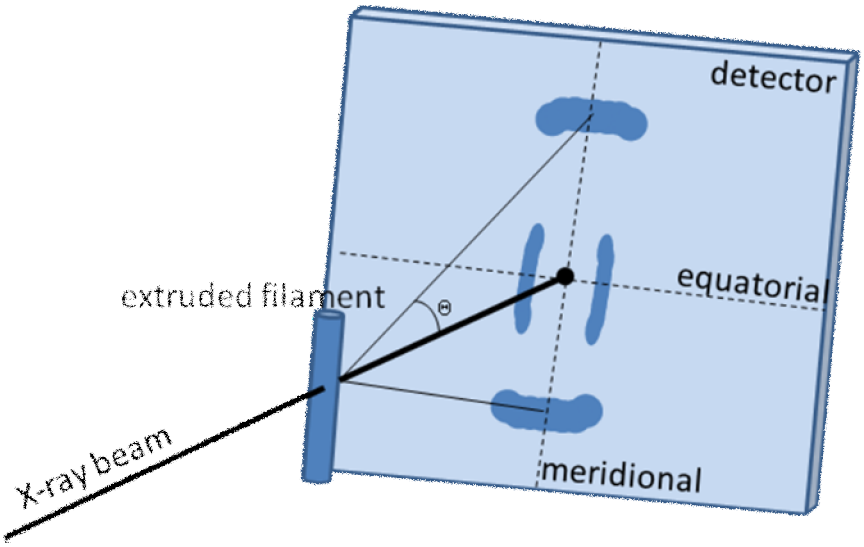

Figure 2.14 Schematic demonstration of the experimental setup.

2.6.1 Supramolecular organization of triphenylene-*alt*-arylene copolymers (P_2, P_4, P_5)

Figures 2.15-2.17 show the typical 2D-WAXS patterns of polymer **P_2**, **P_4**, and **P_5**.The intense and distinct reflections indicate a pronounced to sufficient organization of the polymers with a strong alignment of the chains along the shearing direction and thus along the filament. In general, the criteria by which the degree of organization can be evaluated are the size and the intensity of the peaks (reflexes). While, the solid concentric reflex corresponds to a disorder (isotropic) state of molecules, the smaller reflex reveals a higher degree of organization. In the figures (2.15-2.17) it is clear that all reflexes are located strictly on the axes (meridional or equatorial), which means all molecules have preferential orientation. In addition, the position and location of the reflection within the pattern gives information about the corresponding periodicities and orientation of the polymer chains in the sample. A detailed analysis for each pattern will be presented below.

If one compares the 2D-WAXS patterns of the three polymers, it will be obvious that polymer **P_5** (Figure 2.17) reveals better organization from all samples. This was apparent from the more sharp reflexes and the appearance of second order reflexes in the small angle region in the X-ray pattern of **P_5**. The wide-angle equatorial scattering intensity (marked in the pattern with arrows as "1") is attributed to a stacking distance of 0.43 nm of the adjacent molecules, confirming that the polymer chains are aligned along the extrusion direction of the sample as illustrated in Figure 2.18. This value is close to the distance found for different polyfluorene derivatives which should result in identical charge carrier transport for this material.[79-81]

The d-distance for the reflection "2" is 2.03 nm and corresponds to the interlamellae distance. The appearance of the second equatorial peaks in the small-angle region (marked as "3") indicates the formation of well-defined periodic structures. The meridional reflection "4" of 1.25 nm correlates to the distance between monomer units along the polymer chain. The derived supramolecular organization in the extruded fiber of this compound is schematically

shown in Figure 2.18. For polymer **P_2** (Figure 2.15) the macroscopic organization remains sufficiently pronounced (reflexes on the X-ray pattern remains quite sharp) and similar to compound **P_5**. But the absence of the second-order reflections indicates weak periodicity as compared with **P_5**. This slightly lower degree of order can be seen from the number of reflexes on the axes, since if a pronunced periodical structure exists, more number of reflexes will appear. In polymer **P_5** on the equatorial axis 2 order of reflexes in the small angel area can be seen. On the other hand polymer **P_2** has only one reflex. That can be attributed to the longer side chains and the introduction of an additional phenyl ring at the side group in **P_2**. Two sharp equatorial reflections were observed in the small-angle region and wide-angle region, respectively, corresponding to chain-to-chain spacing of 2.18 nm and 0.44 nm, while the meridional scattering intensity was related to 1.24 nm. The larger chain-to-chain distance confirms the steric demand of the additional phenyl ring in the backbone periphery, while, as expected, the period of the monomer units does not change.

The change in the position of the side chains in compound **P_4** compared to **P_5** (see structure) reveals also an improvement of the macroscopic organization. Thereby, a chain-to-chain of 1.84 nm and packing distance of 0.43 nm were determined (Figure 2.16). The period between repeating units of 1.25 nm remained unchanged.

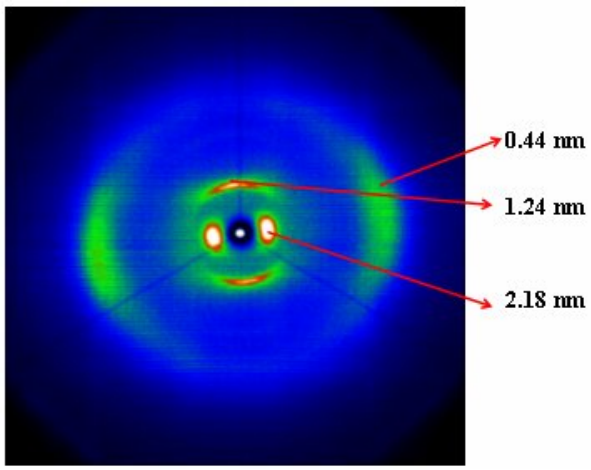

Figure 2.15 2D-WAXS pattern of **P_2** with the corresponding distances of the reflections.

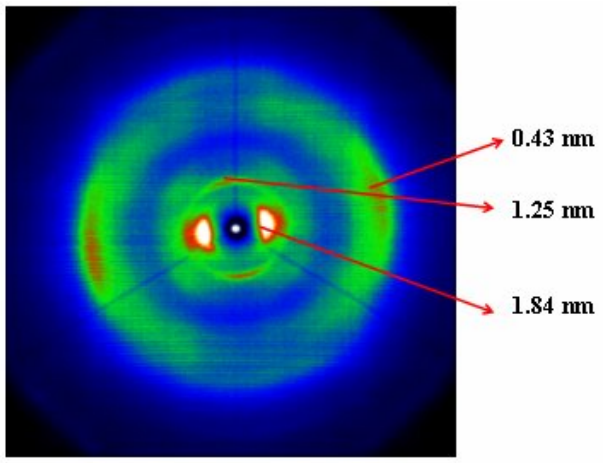

Figure 2.16 2D-WAXS pattern of $\mathbf{P_4}$ with the corresponding distances of the reflections.

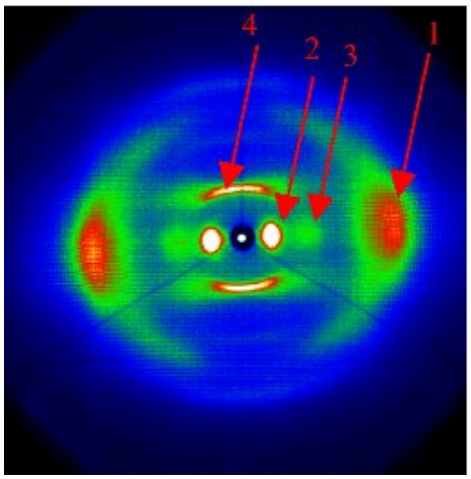

Figure 2.17 2D-WAXS pattern of $\mathbf{P_5}$ with the corresponding distances of the reflections.

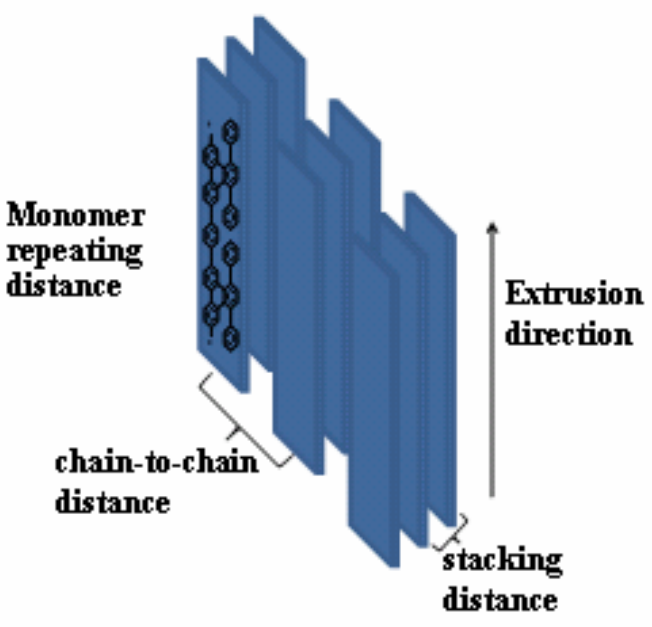

Figure 2.18 Schematic representation of the supramolecular organization of $\mathbf{P_2}$, $\mathbf{P_4}$, and $\mathbf{P_5}$.

2.6.2 Supramolecular organization of polytriphenylene homopolymers ($\mathbf{P_{8\ and}\ P_9}$)

All above described polymers consist of triphenylene moieties spaced by arylene units from each other. In contrast to this, polymers $\mathbf{P_8}$, and $\mathbf{P_9}$ do not contain such a spacer in the backbone. These polymer structures led to a decrease in the distance between the monomer units within the polymer chain and finally to a more pronounced intrachain twisting due to stronger steric interaction between the phenyl rings of adjacent side groups. In the two cases, the reflections were almost isotropic indicating local order, however, poor macroscopic orientation (Figure 2.19 and 2.20). Such results reflect that the two polymers could not be suitable to be used in PLED devices, since such isotropic behavior can result in poor charge carrier mobility between the polymer chains.

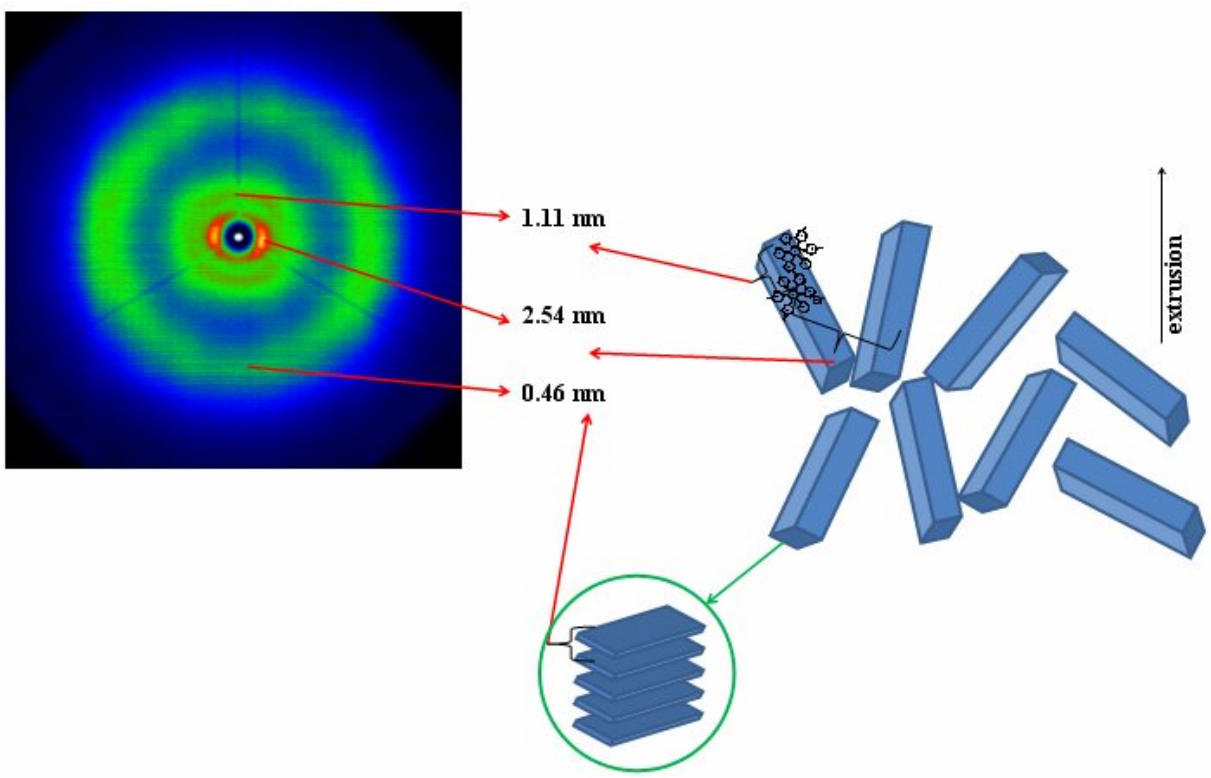

Figure 2.19 2D-WAXS pattern of $\mathbf{P_8}$ with the corresponding distances of the reflections.

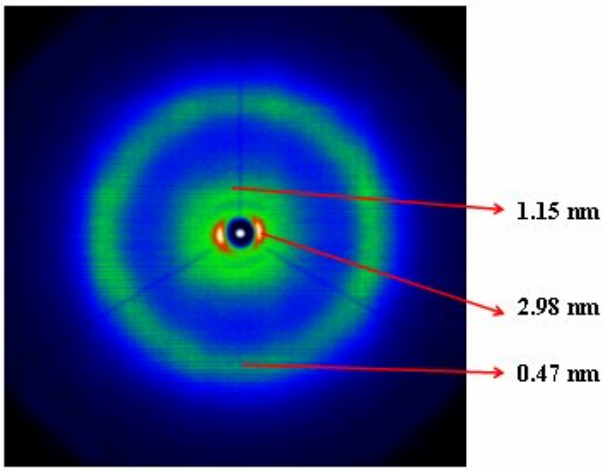

Figure 2.20 2D-WAXS pattern of $\mathbf{P_9}$ with the corresponding distances of the reflections.

2.7 Application of triphenylene-based polymers in polymeric light emitting diodes (PLEDs)

In PLEDs the three primary colors (red, green, and blue) for full color displays have been demonstrated, however only green and red PLEDs presently meet the requirements for commercial applications.[82] In the field of blue-PLEDs, various kinds of conjugated polymers have been proposed.[72-75] However, they are not yet adequate for practical displays due to their short life time, low efficiency, and insufficient color purity.[76,77]

In this section, we present the application of some of the formerly presented made available triphenylene-based conjugated polymers as novel candidates for blue polymeric light emitting diodes.

The following investigations were performed by Moussa Saleh and Young-Seo Park at the Department of Materials Science and Engineering the ‘‘OLED Center’’, in the group of Prof. Dr. Jang-Joo Kim, Seoul National University in Seoul, S. Korea.

The properties of the materials were tested by incorporating the polymers in devices similar in structure to the one shown in Figure 2.21. In such device, indium tin oxide (ITO) coated with layer of poly(styrene sulphonic ester) doped poly(ethylenedioxythiophene) (PEDOT: PSS) was used as the anode while LiF/Al was used as the cathode.

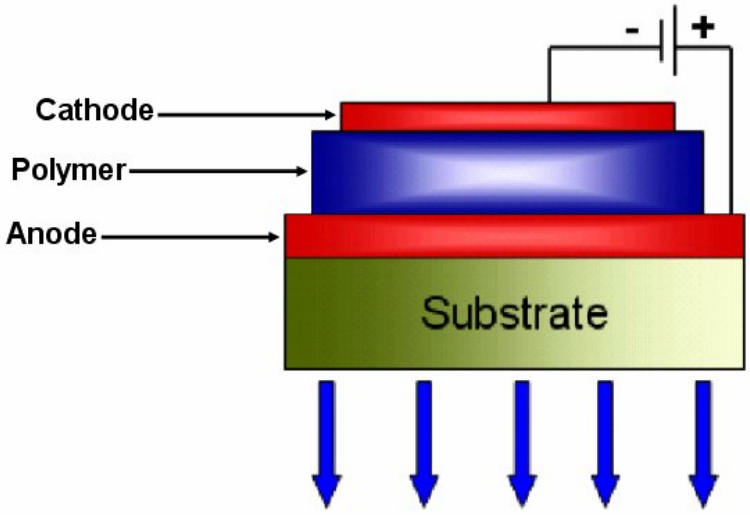

Figure 2.21 Schematic representation of the PLED device used in this study.

The general device fabrication process was made by spin-coating and thermal evaporation onto a cleaned glass substrate precoated with indium tin oxide (ITO). Prior to organic layer deposition, the ITO substrates were exposed to UV-ozone flux for 10 min following cleaning in acetone and isopropyl alcohol. A 40 nm-thick layer of poly(styrene sulphonic ester) doped poly(ethylenedioxythiophene) (PEDOT: PSS) was spin-coated onto the precleaned ITO substrates. The PEDOT:PSS layer was firstly dried at 200^{o}C for 5 min to remove residual water and cooled slowly for 40 min. In this study three polymers (**P_2**, **P_6**, and **P_9**) were used as the emitting materials in the PLED devices. Depending on the materials added to the polymers (Figure 2.22), two different device setups were obtained: i) setup 1, in which a blend of the polymer and the electron transporting material ***t*-PBD** (2-(4-biphenyl)-5-(4-tert-butylphenyl)-1,3,4,-oxadiazole) was used as the emissive layer (EML); ii) setup 2, the EML was formed by mixing the polymer with ***t*-PBD** together with the hole transporting material **NPB** (N,N'-bis(1- naphthyl)N,N'-diphenyl-1,1'-biphenyl-4,4'-diamine). The EML was then coated on the PEDOT: PSS layer from their toluene solution in a glove box filled with N_2 gas. Finally, successive deposition of 10 nm thick (hole- blocking layer) **BPhen** (4,7-Diphenyl-[1,10]phenanthroline), 1 nm thick LiF and 100 nm thick Al cathode under a vacuum of $<5 \times 10^{-7}$ Torr completed the device fabrication.

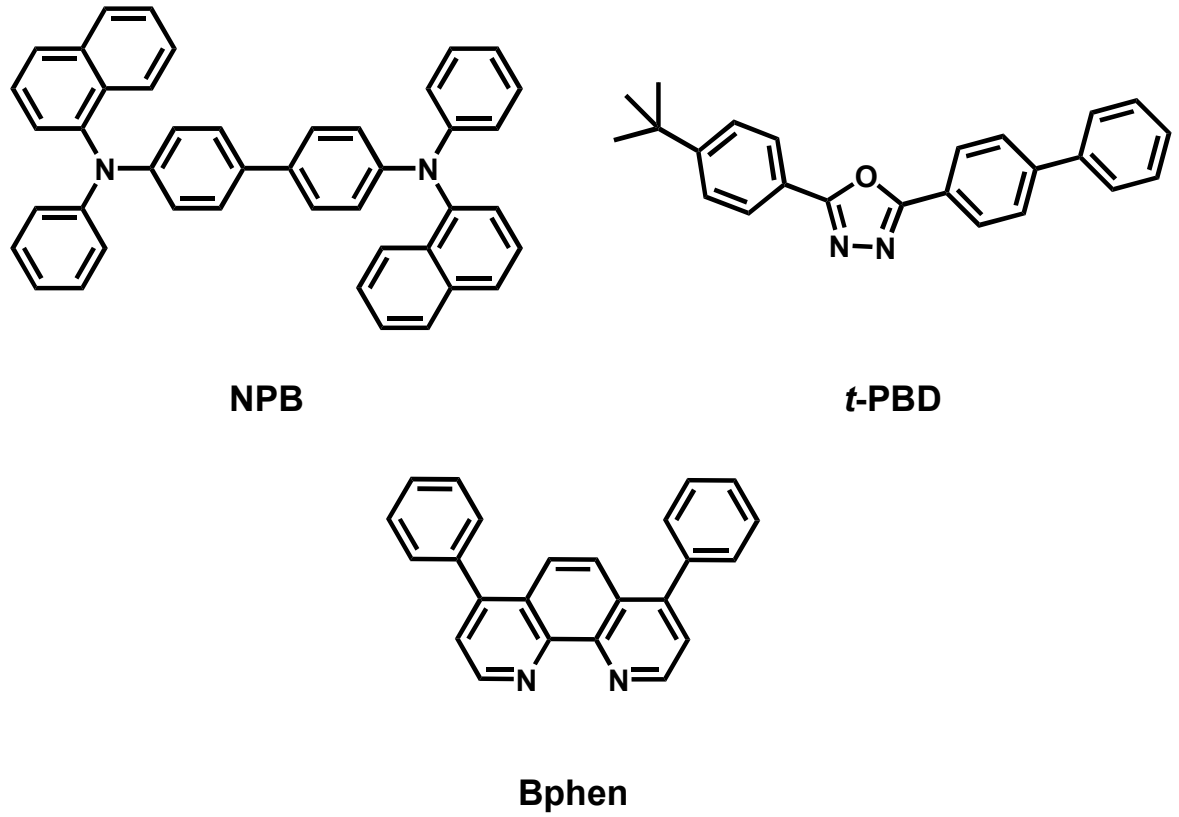

Figure 2.22 Molecular structure of the additives used in the PLED devices

In the following section six PLED devices based on setups 1 and 2 will be presented. Using setup 1 polymer $\mathbf{P_2}$ was used in the fabrication of devices 1, 2, and 3. While devices 4, 5, and 6 were formed from polymers $\mathbf{P_2}$, $\mathbf{P_6}$, and $\mathbf{P_9}$ using setup 2. In order to have a direct comparison between setup 1 and 2, the performances of device 1, 2, 3, and 4 were combined together in two graphs (Figure 2.24 and 2.26).

The device tests started with setup 1 (Figure 2.23). In this setup a blend of polymer $\mathbf{P_2}$ and ***t*-PBD** with weight ratio of 70:30 was used as the EML, while **Bphen** was used as hole blocking layer. The device has the general structure: Al (100 nm) / LiF (1 nm) / Bphen (10 nm) / polymer + *t*-PBD (70 nm) / PEDOT:PSS (40 nm) / ITO (150 nm).

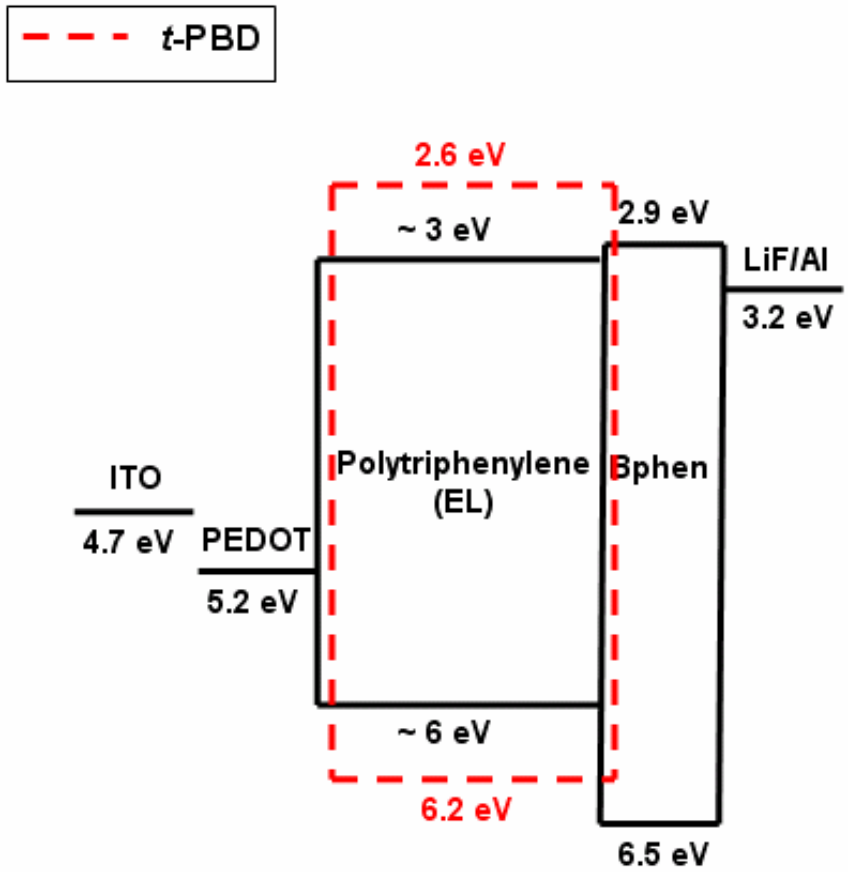

Figure 2.23 Hypothetical band diagrams of the devices based on setup 1.

Figure 2.25 depicts the characteristics of devices 1, 2, and 3. Each device was dried at different conditions after spin coating: at room temperature under vacuum for 48 h, at 90°C under N_2 for 10 min, at 150°C under N_2 for 10 min for device 1, 2 and 3, respectively. All the device characteristics are summarized in table 2.6.

Table 2.6 Results of devices 1-3.

Parameters / **Device no.**	**Max.η_L** (cd/A)	**Max.η_{pow}** (lm/W)	**V_{on}** (V)
Device 1	0.34	0.08	13.0
Device 2	0.71	0.25	8.4
Device 3	0.55	0.23	6.8

Figure 2.24 (a) shows the current density–voltage–luminance characteristics of the device 1-4. The turn-on voltage (defined as the voltage at which luminance of 1 cd /m^2 was detected) of the device 1, 2 and 3 are 13.0 V, 8.4 V and 6.8 V, respectively. The turn-on voltage is lowered and current density and luminance are increased as the baking temperature increases. It means the charge transporting ability of the polymer is improved with increasing baking temperature. This strong dependence of the charge (holes and electrons) transporting ability of the polymer blend films on baking processes is an interesting phenomenon and can be possibly explained based on kinetics. If baking temperature is low, there is enough time until the polymer film dried completely. Therefore, polymer chains and ***t*-PBD** can move and adjust their position during this time to lower the total energy so that morphological change such as phase separation or aggregation can take place, which cause the obstruction of charge transport.[83] However, if baking temperature is high, the solvent in the polymer film is dried quickly so that there is no time for phase separation or aggregation. Homogeneous mixing would give rise to better charge transport by hopping.

Figure 2.24 (b) displays the efficiencies of the device 1-4. Maximum luminance efficiencies are, 0.34 cd/A, 0.71 cd/A and 0.55 cd/A, and maximum power efficiencies are 0.08 lm/W, 0.25 lm/W and 0.23 lm/W for device 1, 2 and 3, respectively.

The triphenylene moiety usually is considered to be electron rich and it has hole transporting property.[84,85] However, the HOMO energy level difference between PEDOT:PSS and polymer $\mathbf{P_2}$ is quite large so that hole injection into the EML is expected to be hindered. This difficulty of hole injection resulted in unbalanced number of electrons and holes in the emitting layer, which led to low luminance efficiencies in the devices.

To solve the hole injection problem the hole-transporting material **NPB** was introduced in the EML of device 4-6. The hole injection barrier between PEDOT:PSS/NPB is only 0.2 eV thus holes can very efficiently be injected into the EML.

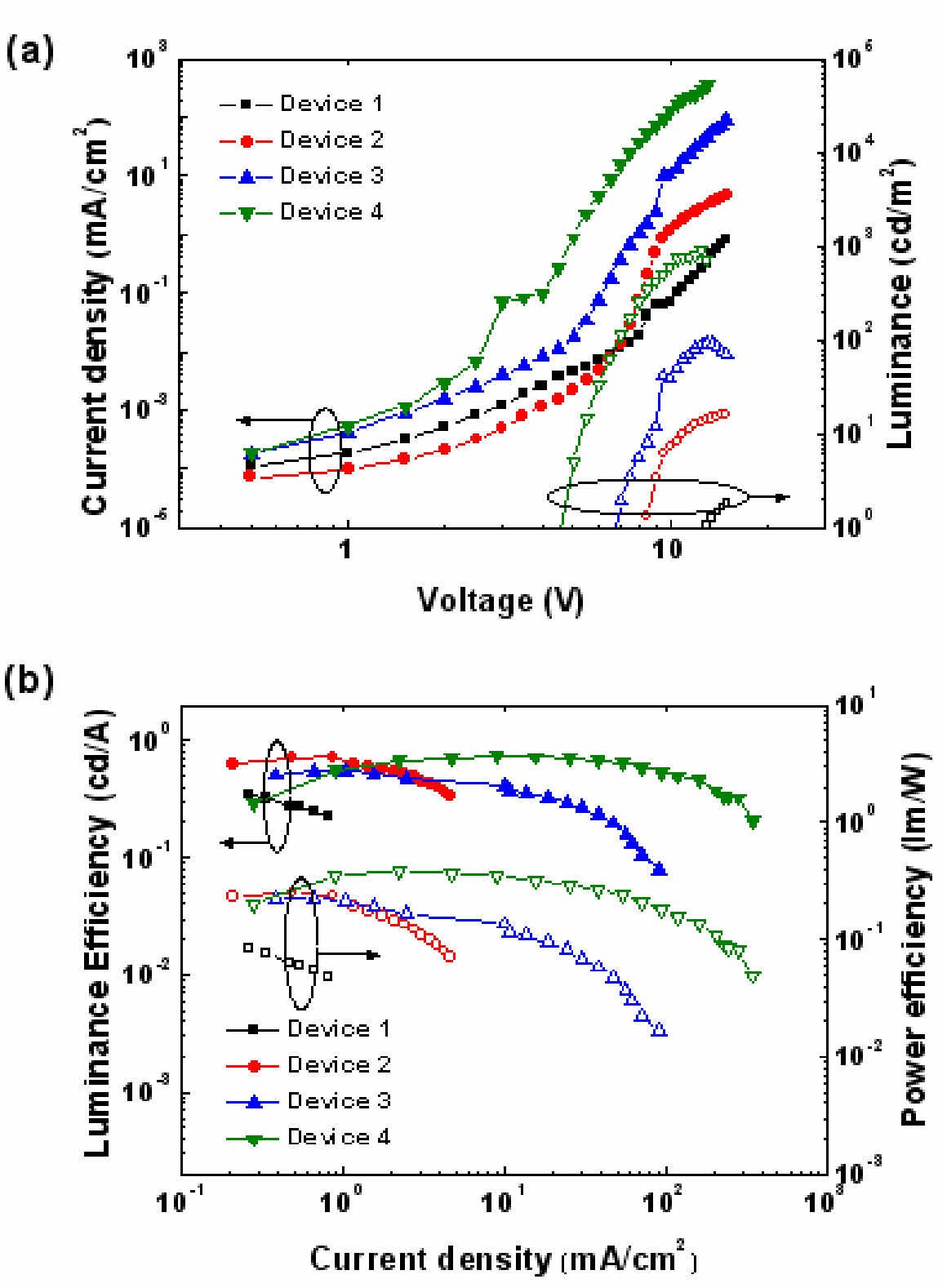

Figure 2.24 **(a)** Current density–voltage–luminance characteristic of the device 1-4.

(b) Luminance efficiency and power efficiency of the devices1-4.

For devices 4-6 a blend of an emitting polymer, ***t*-PBD** and **NPB** with a weight ratio of 52:26:22 was used to form an EML from their toluene solution. Figure 2.25 illustrates a schematic representation of the materials energy levels.

The general device structure was: Al (100nm) / LiF (1 nm) / Bphen (10 nm) / polymer + *t*-PBD + NPB (70 nm) / PEDOT:PSS (40 nm) / ITO (150 nm).

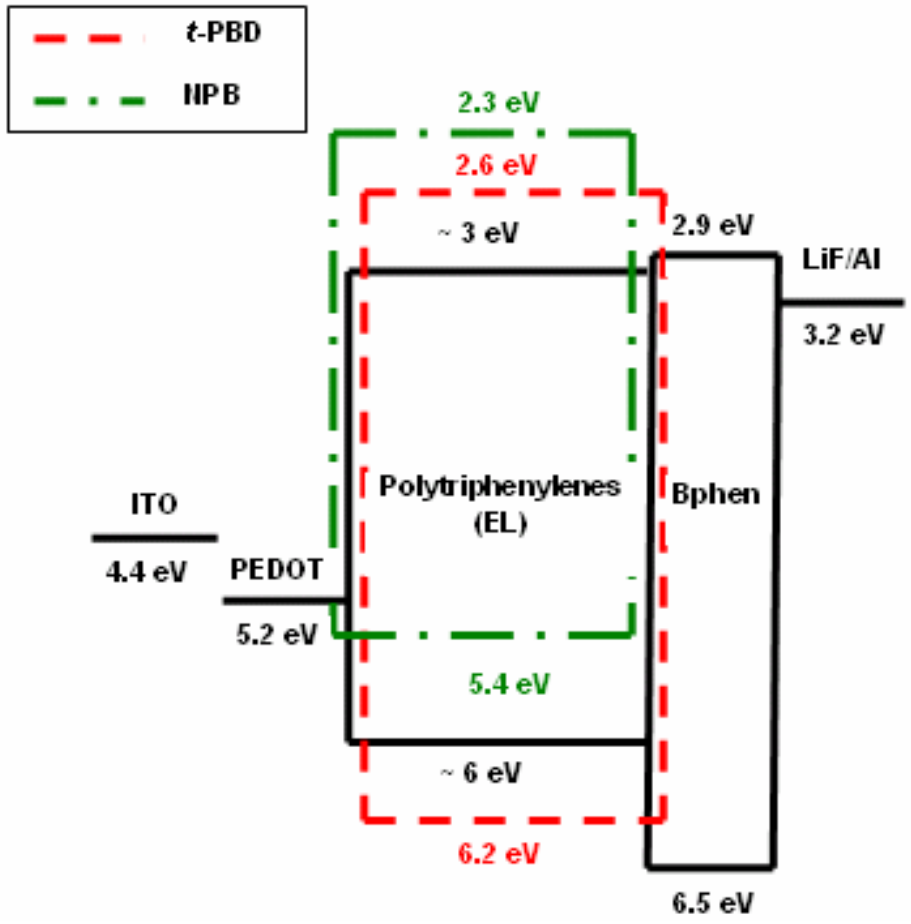

Figure 2.25 Energy level diagram of the materials.

All the results of devices 4-6 are presented in table 2.7. The device 4 yielded the turn-on voltage of 4.6 V, a maximum luminance efficiency of 0.73 cd/A, and a maximum power efficiency of 0.38 lm/W. Thus the device 4 exhibited lower turn-on voltage and higher efficiency than other devices because NPB assist the hole injection and transport, resulting in improved balance between holes and electrons.

Table 2.7 Results of devices 4-6.

Parameters / Device no.	Max.η_L (cd/A)	Max.η_{pow} (lm/W)	V_{on} (V)
Device 4	0.73	0.38	4.6
Device 5	0.49	0.23	5.3
Device 6	0.45	0.26	5.5

Figure 2.26 shows the normalized EL spectra of the devices. The EL spectra exhibited two peaks, 428 nm and 456 nm and some broad emission between 500 and 600 nm. The relative intensity of the peak at 428 nm in device 1 is higher than in device 2 or 3 and is similar to the device 4, indicating that the recombination zone of electrons and holes in the devices 1 and 4 is closer to the cathode than in the devices 2 or 3. This could be expected because hole injection is improved by blending NPB into the EML so that the recombination zone is formed closer to the cathode. The broad emission in the green region appears in the EL spectra and the origin of the emission is not yet clear. One possible reason is that the electron transport in the devices 2–4 is higher than in the device 1, resulting in stronger emission at longer wavelength.

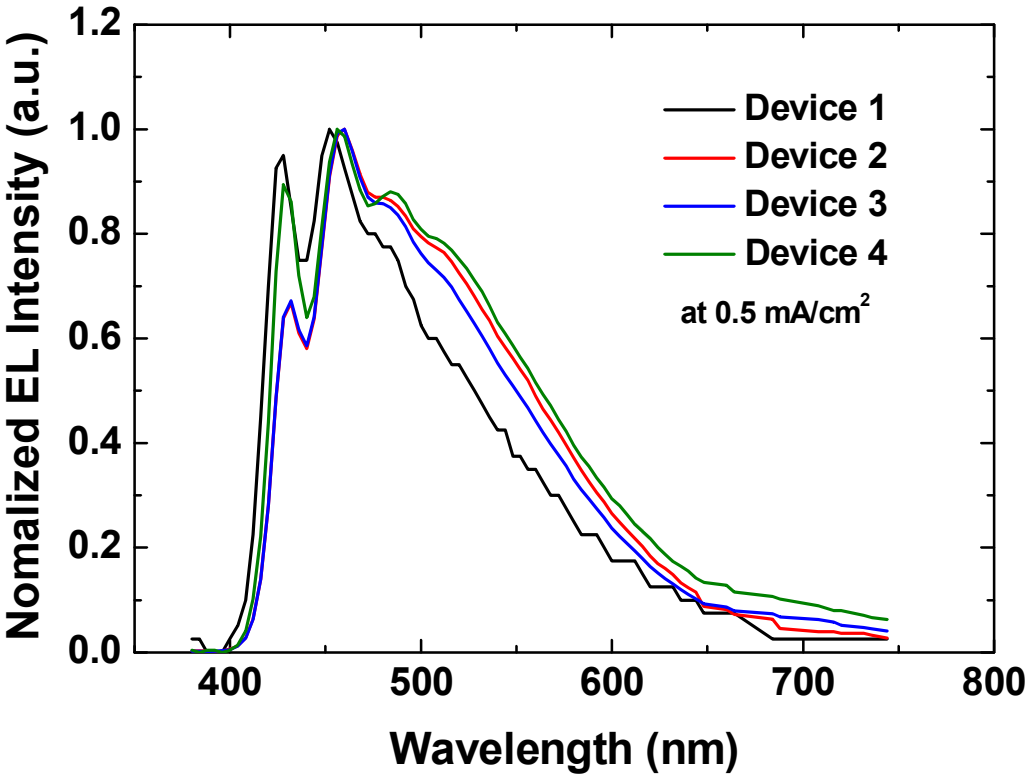

Figure 2.26 Normalized EL spectra of the devices at 0.5 mA/cm^2.

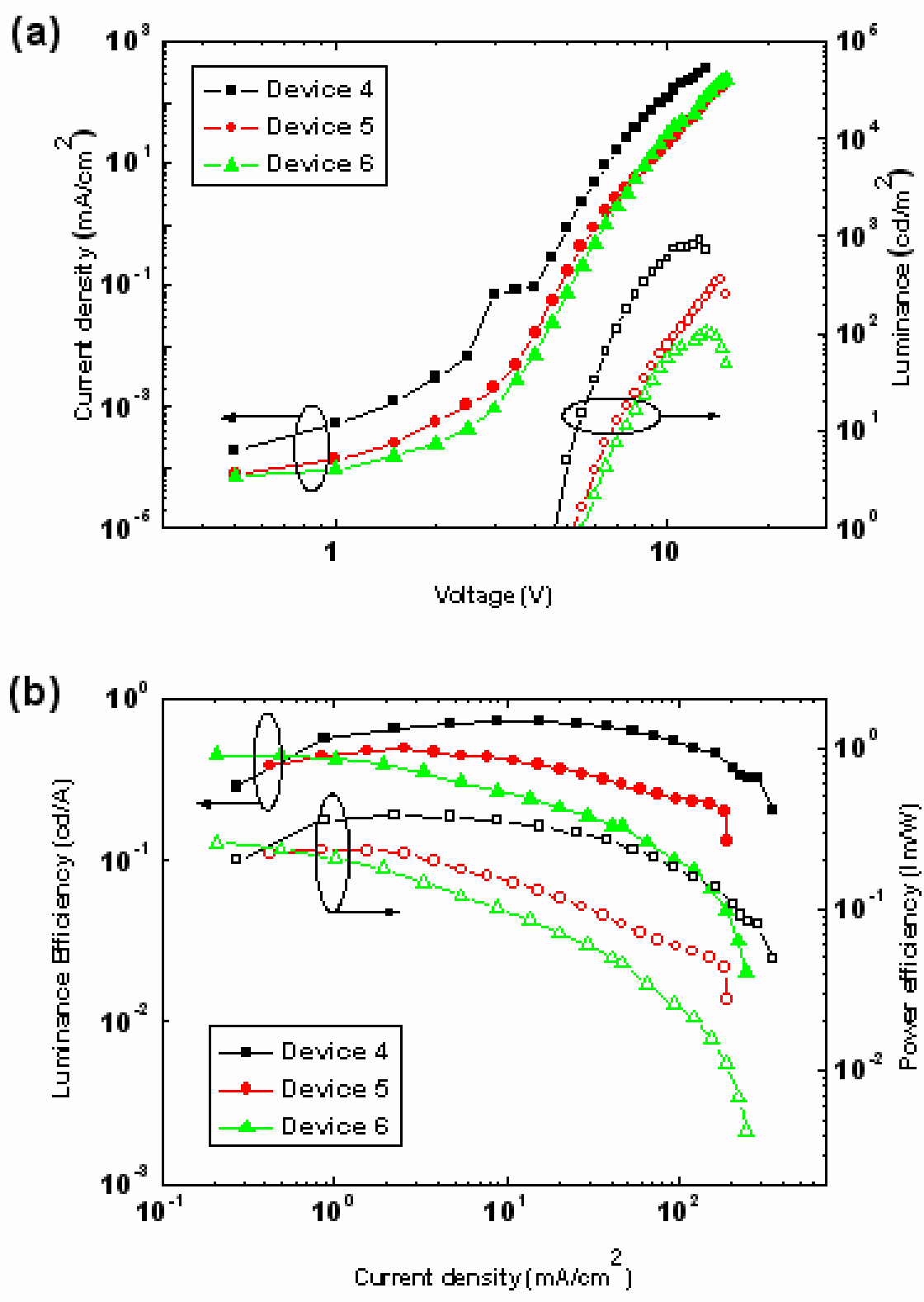

Figure 2.27 (a) Current density–voltage–luminance characteristic of the device 4-6. (b) Luminance efficiency and power efficiency of the devices 4-6.

Figure 2.27 displays current density–voltage–luminance characteristics and efficiencies of the devices 4–6. The turn-on voltages were 5.3 and 5.5 V, with maximum

luminance efficiencies of 0.49 and 0.45 cd/A, and maximum power efficiencies of 0.23 and 0.26 lm/W for the devices 5 and 6, respectively.

Polymers **P_6** and **P_9** have longer alkyl chains than **P_2**. These long alkyl chains enhance the solubility of the polymers, but increase the distance between molecules due to their bulkiness and thereby retard the intermolecular charge transport. This may also be the reason for the increased turn-on voltages for polymers **P_6** and **P_9** compared to **P_2**.

2.8 Conclusions

A novel series of blue light emitting triphenylene based polymers in good yields, based on Suzuki-Miyaura and Yamamoto polycondensation reactions. All of the polymers showed deep blue emission in solution with PL maxima centred around 420 nm. However the film UV-Vis absorption and PL spectra were diverse, that can be ascribed to the number of aryl units around the triphenylene moiety. Since in case of the less aryl substituted polymers **P_5** and **P_7** large bathochromic shifts of 30 nm and 40 nm, respectively were observed in the PL maxima (~ 460 nm), while in the more aryl substituted polymers **P_1**, **P_2**, **P_3**, **P_4**, **P_6**, **P_8** and **P_9** the PL maxima were centered around 430 nm to show deep blue emission .This suggests that decreasing the number of aryl units around the triphenylene moiety is not suitable to afford the desired blue emission (420-440 nm), which can be attributed to the formation of polymer aggregates. A possible evidence of such aggregates can be seen from the 2DWAXS results of polymer **P_5** that showed the best organization between all other polymer samples. This was obvious from the more sharp reflexes and the existence of second order reflexes in the small angle region in the X-ray pattern of **P_5**.

From the solution UV-Vis absorptions and PL spectra of the homo- and co-polymers it was shown that polymers did not show distinct differences, which may suggest similar conjugation interactions along the polymers backbones.

From the 2D-WAX studies we also found that the triphenylene-*alt*-arylene co-polymer **P2**, **P4**, and **P5** were related to a well-aligned macroscopic organization in the extruded sample, which was not obvious for the polytriphenylene homo-polymer **P8**, and **P9**. This difference in the macroscopic organization can be attributed to the present extra arylene groups between the triphenylene repeating units in the co-polymer which reduced the twist in the polymer backbone and result in well organized structure.

Finally, some of our novel synthesized TP-based conjugated polymers were tested in organic light emitting diodes. In order to find the optimum device structure that could result in good device performance two device setups were used. setup 1: Al (100nm) / LiF (1 nm) / Bphen (10 nm) / polymer + *t*-PBD (70 nm) / PEDOT:PSS (40 nm) / ITO (150 nm), and setup 2: Al (100nm) / LiF (1 nm) / Bphen (10 nm) / polymer + *t*-PBD + NPB (70 nm) / PEDOT:PSS (40 nm) / ITO (150 nm). To have a direct comparison, setup1 and 2 were used in the fabrication of two PLEDs (device 3 and 4, respectively) from polymer **P2** using backing temperature of 150^{o}C. The obtained device characteristics (table 2.6 and 2.7) clearly showed that setup 2 was more efficient than setup 1. The reported Max.η_L were 0.73 and 0.55 cd/A for setups 2 and 1, respectively. Moreover, the turn on voltage was improved to show 4.6 V for setup 2 compared to 6.8 V for setup 1. This reported higher device performance for setup 2 can be attributed to the presence of the hole-injection compound NPB, which reduced the hole injection barrier between PEDOT:PSS/NPB to 0.2 eV, therefore holes can effectively be injected into the EML. It was also proved that the supramolecular organization of the polymers have greatly influenced the device performance. This can be seen from the performances reported for the PLEDs fabricated from the co-polymers **P2** and the homo-polymer **P9**. As the 2D-WAXS results showed **P2** was of higher degree of macroscopic organization compared to **P9** that showed isotropic reflections. Such difference between the two polymers suggested better charge carrier mobility and thus higher device performance for **P2** compared to **P9**. The obtained results for device 3 (using polymer **P2**) and device 6 (using polymer **P9**) showed

Max.η_L of 0.55 and 0.45 cd/A, respectively. That clearly proves that **P_2** with its higher degree of macroscopic organization resulted in better device performance compared to **P_9**.

The above demonstrated results exhibit the success in producing novel blue-emitting materials that showed good performances in PLED devices in terms of luminance efficiency and turn on voltage. As intentionally planned the triphenylene systems presented here did not show the problem of the keto-defect emission that was mostly found in blue-OLEDs,[48-50] which add other values to our TP-based polymers, which are the chemical and thermal stabilities. In addition the recorded device performances of our systems were higher than the reported carbon- and nitrogen-bridged poly(ladder-type tetraphenylene) (PPP-type polymers) presented by Mishra et al.,[50] which showed a maximum luminance efficieny around 0.1 cd/A with turn-on voltage of 5.5 and 4 V, respectively. These results suggest that our TP-based conjugated polymers were more efficient than the carbon- and nitrogen -bridged poly(ladder-type tetraphenylene) to be used as active materials in blue-PLEDs.

2.9 References

(1) Schmidt, H.; Schultz, G. Ann., **1880**, 118, 203.

(2) Heaney, H.; Millar, I. T. Org. Synth. **1973**, 5, 1120.

(3) Mannich, C. *Ber*. **1907**, 40,159.

(4) Buess, C.M.; Lawson, D.D. *Chem. Rev.* **1960**, 60, 313-.330.

(5) Perez, D.; Guitian. E. *Chem. Soc. Rev*. **2004**, 33, 274-283.

(6) Bavin, P. M. G.; Dewar, M. J. S. *J. Chem. Soc.*, **1955**, 4479.

(7) Plesek, J.; Munk, P.; *Chem. Listy.***1957**, 51, 980.

(8) Barker, C. C.; Emmerson, R. G.; Periam, J. D. *J. Chem. Soc.* **1958**,1077.

(9) Diels, O.; Karstens, A. *Ber*. **1927**, 60, 2323.

(10) Heaney, H.; Mann, F. G.; Millar, I. T. *J. Chem. Soc.* **1956**, 1.

(11) Bartle, K. D.; Heaney, H.; Jones, D. W.; Lees, P. *Tetrahedron*, **1965**, 21, 3289.

(12) Copeland, P. G.; Dean, R. E.; McNeil, D. *J. Chem. Soc.* **1960**, 1687.

(13) Billard, J.; Dubois, J.C.; Tinh, N.H.; Zann, A. *Nouv. J. Chimie*, **1978**, 2, 535.

(14) Kreuder, W.; Ringsdorf, H.; Schonherr, O.H.; Wendorff. J.H. *Angew. Chem. int. Ed.* **1987**, 26, 1249.

(15) Rego, J.A.; Kumar, S.; Ringsdorf, H. *Chem. Mater.* **1996**, 8, 1402.

(16) Freudenmann, R.; Behnisch, B.; Hanack, M. *J. Mater. Chem.* **2001**, 11, 1618-1624.

(17) Praefcke, K.; Eckert, A.; Blunk, D. *Liq. Cryst*. **1997**, 22, 113.

(18) Kumar, S.; Manickam, M.; Balagurusamy, V.S.K.; Schonherr, H. *Liq. Cryst.* **1999**, 26, 1455.

(19) Kumar, S.; Varshney, S.K. *Liq. Cryst.* **2001**, 28, 161.

(20) Kumar, S.*Liq. Cryst.* **2004**, 31, 1037.

(21) Boden, N.; Bushby, R.J.; Cammidge, A.N.; Duckworth, S.; Headdock, G. *J. mater. Chem.* **1997**, 7, 601.

(22) Kumar, S.; Naidu, J.J.; Varshney, S.K. *Mol. Cryst. liq. Cryst.* **2004**, 411, 355.

(23) Kranig, W.; Huser, B.; Spiess, H.W.; Kreuder, W.; Ringsdorf, H.; Zimmermann, H. *Adv. Mater.* **1990**, 2, 36.

(24) Boden, N.; Bushby, R.J.; Cammidge, A.N.; Martin, P.S. *J. mater. Chem.* **1995**, 5, 1857.

(25) Kumar, S.; Manickam, M. *Liq. Cryst.* **1999**, 26, 939.

(26) Markovitsi, D.; Marguet, S.; Gallos, L.; Sigal, H.; Millie, P.; Argyrakis, P. ; Kumar, S.; Ringsdorf, H. *Chem. Phys. Lett.* **1999**, 306, 163.

(27) Kumar, S.; Schuhmacher, P.; Henderson, P.; Rego, J.; Ringsdorf, H. Mol. *Cryst. liq. Cryst.* **1996**, 288, 211.

(28) Maliszewskyj, N.C.; Heiney, P.A.; Josefowicz, J.Y.; Plesnivy, T.; Ringsdorf, H.; Schuhmacher, P. *Langmuir* **1995**, 11, 1666.

(29) Markovitsi, D. ; Marguet, S.; Bondkowski, J.; Kumar, S. *J. phys. Chem. B* **2001**, 105, 1299.

(30) Haarer, D.; Simmerer, J.; Adam, D.; Schuhmacher, P.; Paulus, W. ; Etzbach, K.; Siemensmeyer, K.; Ringsdorf, H. Mol. *Cryst. Liq. Cryst.* **1996**, 283, 63.

(31) Janietz, D.; Festag, R.; Schmidt, C.; Wendorff, J.H. *Liq. Cryst.* **1996**, 20, 459.

(32) Plesnivy, T. ; Ringsdorf, H. ; Schuhmacher, P.; Nutz, U.; Diele. S. *Liq. Cryst.* **1995**, 18, 185.

(33) Qin, T.; Zhou, G.; Scheiber, H.; Bauer, R. E.; Baumgarten, M.; Anson, C. E.; List, E. J. W. ; Müllen, K. *Angew. Chem. int. Ed.* **2008**, 120 , 8416 –84 20.

(34) Kreuder, W.; Ringsdorf, H. *Makromol. Chem. rapid Commun.* **1983**, 4, 807.

(35) Huser, B.; Spiess, H.W. Makromol. *Chem. rapid. Commun.* **1988**, 9, 337.

(36) Ringsdorf, H.; Wustefeld, R.; Zerta, E.; Ebert, M.; Wendorff, J.H. *Angew. Chem. int. Ed.* **1989**, 28, 914.

(37) Werth, M.: Spiess, H.W. *Makromol. Chem. rapid. Commun.* **1993**, 14, 329.

(38) Weck, M.; Mohr, B.; Maughon, B.R.; Grubbs, R.H. *Macromolecules* **1997**, 30, 6430.

(39) Imrie, C.T.; Inkster, R.T.; Lu, Z.; Ingram, M.D. *Mol. Cryst. liq. Cryst*. 2004, 408, 33.

(40) Boden, N.; Bushby, R.J.; Cammidge, A.N. *J. Am. chem. Soc.* **1995**, 117, 924.

(41) Henderson, P.; Ringsdorf, H.; Schuhmacher, P. *Liq. Cryst* **1995**, 18, 191.

(42) Wenz, G. *Makromol. Chem. rapid. Commun.* **1985**, 6, 577.

(43) Kreuder, W.; Ringsdorf, H.; Tschirner, P. *Makromol. Chem. rapid Commun.* **1985**, 6, 367.

(44) Boden, N. ; Bushby, R.J.; Eichhorn, H.; Lu, Z.B. ; Abeysekera, R.; Robardes, A.W. *Mol. Cryst. liq. Cryst.* **1999**, 332, 293..

(45) Rose, A.; Lugmair, C. G.; Swager, T. M. *J. Am. Chem. Soc.* **2001**, 123, 11298-11299.

(46) Neher, D. *Macromol. Rapid Commun.* **2001**, 22, 1365-1385.

(47) Setayesh, S.; Marsitzky, D.; Müllen, K. *Macromolecules* **2000**, 33, 2016-2020.

(48) Jacob, J.; Sax, S.; Piok, T.; List, E. J. W.; Grimsdale, A. C.; Müllen, K. *J. Am. Chem. Soc.* **2004**, 126, 6987-6995.

(49) Scherf, U. *J. Mater. Chem.* **1999**, 9, 1853-1864.

(50) Mishra, A. K.; Graf, M.; Grasse, F.; Jacob, J.; List, E. J. W.; Müllen, K. *Chem. Mater.* **2006**,18, 2879-2885.

(51) List, E. J. W.; Guentner, R.; De Freitas, P. S.; Scherf, U. *Adv. Mater.* **2002**, 14, 374-378.

(52) Setayesh, S.; Grimsdale, A. C.; Weil, T.; Enkelmann, V.; Mü1llen, K.; Meghdadi, F.; List, E. J. W.; Leising, G. *J. Am. Chem. Soc.* **2001,** 123, 946-953.

(53) Ego, C.; Grimsdale, A. C.; Uckert, F.; Yu, G.; Srdanov, G.; Müllen, K. *Adv. Mater* . **2002**, 14, 809-811.

(54) Jacob, J.; Zhang, J. Y.; Grimsdale, A. C.; Müllen, K.; Gaal, M.; List, E. J. W. *Macromolecules* **2003**, 36, 8240-8245.

(55) Jacob, J.; Sax, S.; Gaal, M.; List, E. J. W.; Grimsdale, A. C.; Müllen, K. *Macromolecules* **2005**, 38, 9933-9938.

(56) Surin, M.; Hennebicq, E.; Ego, C.; Marsitzky, D.; Grimsdale, A. C.; Müllen, K. Brédas, J.-L.; Lazzaroni, R.; Leclère, P. *Chem. Mater.* **2004**, 16, 994-1001.

(57) Bayer, A.; Zimmermann, S.; Wendorff, J. H. Mol. *Cryst. liq. Cryst.* **2003**, 396, 1-22.

(58) Marguet, S.; Markovitsi, D.; Millie, P.; Kumar, S.; Sigal, H. *J. Phys. Chem. B.* **1998**, 102, 4697-4710.

(59) Seguy, I.; Destruel, P.; Bock, H. *Synth. Met.* **2000**, 111–112,15-18.

(60) Heppke, G.; Krüerke, D.; Löhning, C.; Lötzsch, D.; Moro, D.; Müller, M.; Sawade, H. *J. Mater.Chem.* **2000**, 10, 2657-2661.

(61) Terasawa, N.; Monobe, H. *Liq. Cryst.* **2007**, 34, 447–455.

(62) a) Kumar, S. *Liq. Cryst.* **2005**, 32, 1089–1113. b) Boden, N.; Bushby, R.J. ; Cammidge, A.N.; El- Mansoury, A.; Martin, P.S.; Lu. Z. *J. mater. Chem.* **1999**, 9, 1391.

(63) Hann, A. C. O.; Lapworth, A. *J. Chem. Soc.* **1904**, 46-56.

(64) Diels, O.; Alder, K. *Ber.* **1929**, 62, 2081-2087.

(65) a) Pisula, W.; Kastler, M.; Wasserfallen, D.; Pakula, T.; Müllen, K. *J. Am. Chem. Soc.* **2004**, 128, 26. b) Wasserfallen, D.; Kastler, M.; Fogel, Y.; Pisula, W.; Wang, Z.; Hofer, W. A.; Müllen, K. *JACS* **2006**, 128, 1334. c) Ph. D thesis of Andreas Fechtenkötter. **2001**.

(66) Hou, S. *Org.Lett.* **2003**, 5, 4.

(67) Rehahn, M.; Schlüter, A. D.; Wegner, G. Makromol. Chem. 1990, 1991– 2003.

(68) Yamamoto, T.; Yamamoto, A. Chem. Lett. 1977, 353–356.

(69) Schlüter, A. D. *J. Polym. Sci. Part A: Polym. Chem.* **2001**, 39, 1533-1556.

(70) Joshi, H. S.; Jamshidi, R.; Tor, Y. *Angew. Chem.Int. Ed.* **1999**, 38, 18.

(71) Su, H-J.; Wu, F-I.; Shu, C-F. *Macromolecules* **2004**, 37, 7197-7202.

(72) Su, H-J.; Wu, F-I.; Tseng, Y-H.; Shu, C-F. *Adv. Funct. Mater.* **2005**,15,1209-1216.

(73) Janietz, S.; Bradley, D. D. C.; Grell, M.; Giebeler, C.; Inbasekaran, M.; Woo, E. P. *Appl. Phys.Lett.* **1998**, 73, 2453-2455.

(74) Schulz, B.; Janietz, S.; Sava, I.; Bruma, M. *Polym. Adv. Technol.* **1996**, 7, 514-518.

(75) Osaheni, J. A.; Jenekhe, S. A. *J. Am. Chem. Soc.* **1995**, 117, 7389-7398.

(76) Fabre, B. *Electrochem. Commun.***2001**, 3, 549-552.

(77) Naka, K.; Uemura, T.; Santiago, A. G.; Chujo, Y. *Macromolecules* **2002**, 35, 3806-3809.

(78) Pisula, W.; Tomovic, Z.; Simpson, C.; Kastler, M.; Pakula, T.; Müllen, K. *Chem. Mater.* **2005**,17, 4296–4303.

(79) Lieser, G.; Oda, M.; Miteva, T.; Meisel, A.; Nothofer, H.-G.; Scherf, U.; Neher, D. *Macromolecules* **2000**, 33, 4490–4495.

(80) Grell, M.; Bradley, D. D. C.; Ungar, G.; Hill, J.; Whitehead, K. S.*Macromolecules* **1999**, 32, 5810–5817.

(81) Kudla, C. J.; Koenen, N.; Pisula, W.; Scherf, U. *Macromolecules* **2009**, 42, 3483–3488.

(82) D. Y. Kim, H. N. Cho, C. Y. Kim, *Prog. Polym. Sci.* **2002**, 25, 1089.

(83) Braun, D.; Heeger, A. J. *Applied Physics Letters* **1991**, *58*, 1982.

(84) Heeger, A. J. *Solid State Communications* **1998**, *107*, 673.

(85) Tang, C. W.; Vanslyke, S. A. *Applied Physics Letters* **1987**, *51*, 913.

Chapter 3

Triphenylene-Pyrene, Triphenylene-Fluorene, and Triphenylene-Carbazole-based Copolymers for OLED applications

In this chapter, synthesis and characterization of solution processable triphenylene-pyrene (**TP-Py**), triphenylene-fluorene (**TP-F**), and triphenylene-carbazole (**TP-Cz**) copolymers are presented.

The photophysical and electrochemical properties of the obtained polymers are described. 2D-WAXS investigations were performed on extruded samples of polymers to understand the supramolecular organization in the solid-state. Finally the polymers were incorporated into PLED devices and their performances are discussed.

3.1 Introduction

In chapter 2, several TP-based conjugated polymers have been synthesized and tested in PLED devices. With the manipulation of the device structure by introducing electron-transporting, hole-transporting, and hole-blocking materials the polymers demonstrated good device performances with maximum luminance efficiency of 0.73 cd/A and turn on voltage of 4.6 V.

As discussed in chapter 2, the TP-based PLED device performances were enhanced by altering the device structure (see device setup 1 and 2), which was done by incorporating the hole transporting material (NPB) that result in reduced hole injection barrier between the anode and the EML. Other possible method that could also improve the performance of the devices can be achieved through the introduction of other promising blue chromophores with high PLQYs into the polymer's backbone, in such a way that the two blue emitting moieties alternate in one conjugated polymer chain.

A number of π-conjugated polymers, which show high quantum yield, such as poly(fluorene)s,[1-5] poly(carbazole)s,[6-9] and poly(pyrene)s,[10] have been developed. Due to their unique chemical, optical and electrical properties these materials have been used as a functional building block or substituents in the construction of organic molecules for the use in OLEDs. However, none of these systems are yet sufficient for practical displays due to their short life time (less than 10000 hours) and insufficient color purity (emission changes to green (530-565 nm) due to oxidative degradation and keto-defects).

In this work, our motivation was to synthesize new TP-Py (**P_{10}**), TP-F (**P_{11}** and **P_{12}**), and TP-Cz (**P_{13}**) copolymers (Figure 3.1) to study the effect of these chromophore combinations on the properties of the desired polymers, with the aim of enhancing the efficiency of TP-based blue PLEDs. Similar study was presented by Qin et al. in our group, where he synthesized pyrene cored polytriphenylene dendrimers with the intention of improving the efficiency of his polytriphenylene dendrimer-based blue LED. It was found that the maximum luminescence (500 cd/m^2) and current efficiency (0.12 cd/A) of the pyrene-triphenylene dendrimer (**PYG2**) were five times higher than those of the triphenylene dendrimer (**TPG2**), indicating that the pyrene core could improve not only the emissive quantum yield, but also the charge injection and transportation properties of polytriphenylene dendrimers, which was further proved by the lower turn-on voltage of electroluminescence of **PYG2** device at 3.8 V.[11]

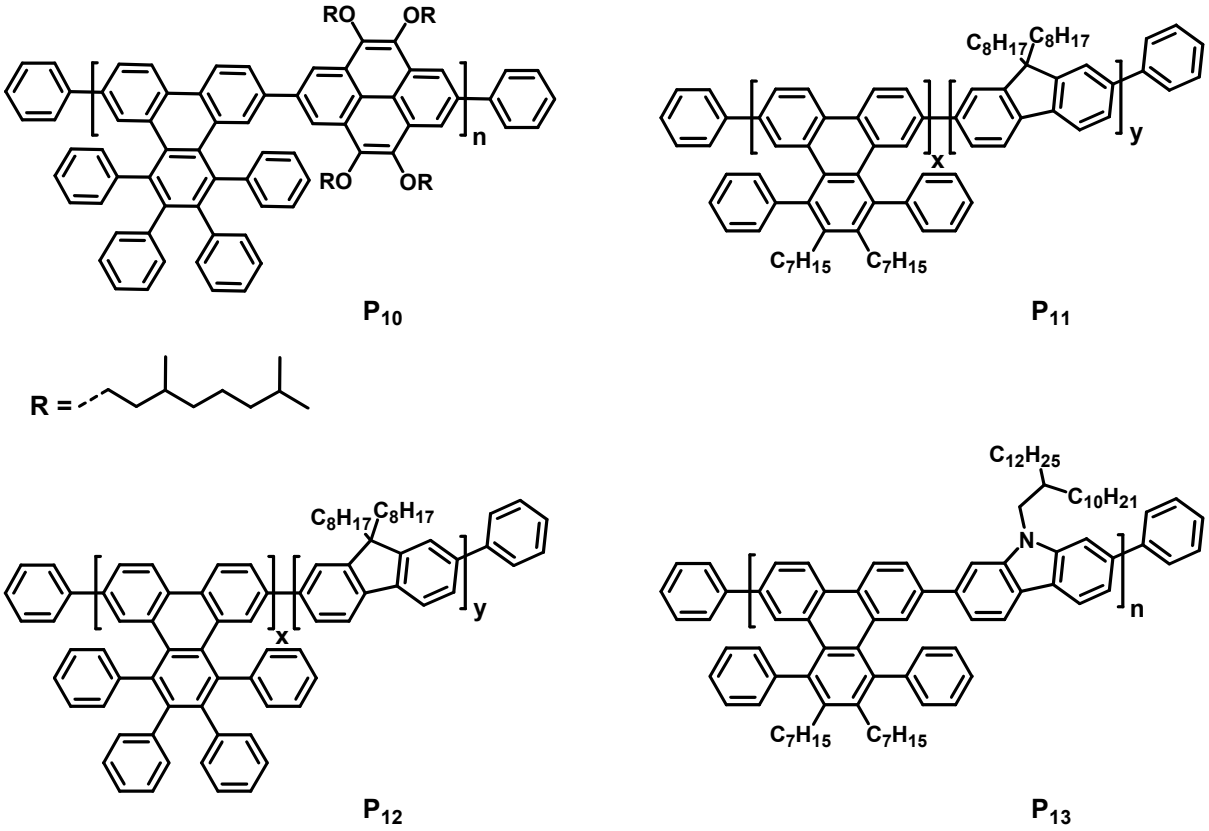

Figure 3.1 Molecular structures of the TP-Py (**P_{10}**), TP-F (**P_{11}** and **P_{12}**), and TP-Cz (**P_{13}**) copolymers.

3.2 Triphenylene-Pyrene copolymer (P_{10})

3.2.1 Synthesis and characterization

Synthesis of polymer **P_{10}** was performed by using the MA-palladium-catalyzed Suzuki-Miyaura coupling of 2,2'-(9,10,11,12-tetraphenyltriphenylene-2,7-diyl)-bis(4,4,5,5-tetramethyl-1,3,2-dioxaborolane) **(12)** and 2,7-dibromo-4,5,9,10-tetrakis-(3,7-dimethyl-octyloxy)-pyrene **(13)**.

The synthesis of **12** was accomplished via the reaction between **5d** (described in chapter 2) and 2.2 equivalent of bis(pinacolato)diboron in the presence of $[PdCl_2(dppf)]CH_2Cl_2$ as catalyst to afford **12** in 80% yield (Scheme 3.1).

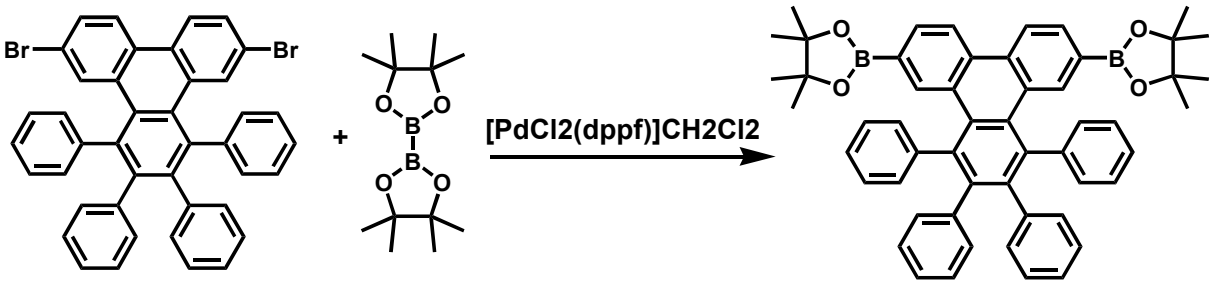

5d **12**

Scheme 3.1 Synthesis of 2,2'-(9,10,11,12-tetraphenyltriphenylene-2,7-diyl)-bis-(4,4,5,5-tetramethyl-1,3,2-dioxaborolane) **(12)**.

2,7-Dibromo-4,5,9,10-tetrakis-(3,7-dimethyl-octyloxy)-pyrene **(13)** was synthesized according to the literature procedures described by Kawano et al.[10a] and received from Kohei Kojima in 200 mg amounts.

The Pd (0) mediated MA-Suzuki polymerization reaction of monomers **12** and **13** at 50 W, 100°C for 1 h, resulted in polymer $\mathbf{P_{10}}$ in good yield of 53 %. The reaction pathway is presented in scheme 3.2.

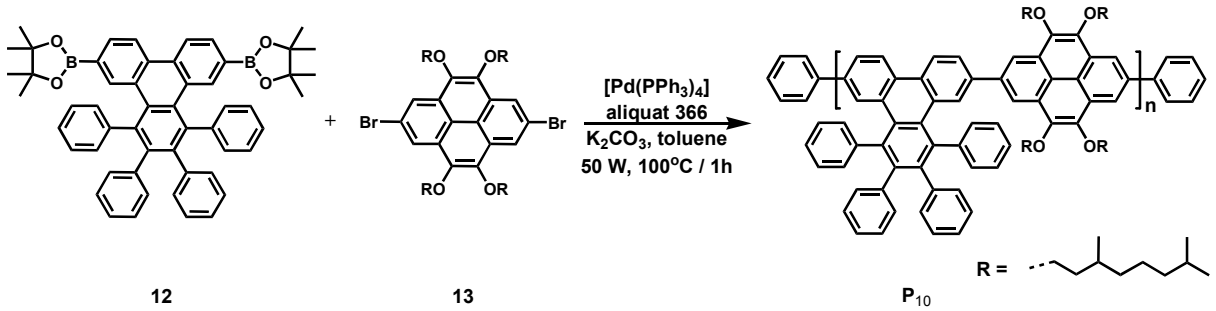

12 **13** $\mathbf{P_{10}}$

Scheme 3.2 Synthesis of polymer $\mathbf{P_{10}}$ via Suzuki-Miyaura coupling reaction.

The reaction procedure was the same as the general route described for polymers $\mathbf{P_1}$-$\mathbf{P_6}$ in chapter 2. After the reaction finished, bromobenzene and benzene boronic acid were added sequentially to the reaction mixture (to end cap polymer chains), and the whole mixture was stirred at 100°C for further ½ h. The organic layer was extracted with toluene and washed with aqueous sodium cyanide (to remove the catalyst). The polymer was precipitated by the slow addition of a concentrated polymer solution to 300 ml methanol. The precipitated

polymer was washed for several times with methanol, water and acetone. To remove the residuals of the catalyst, the polymer was once more dissolved in toluene and stirred in aqueous sodium cyanide (1 %, 100 ml) at 90°C for 2 h. Finally, the polymer was separated by reprecipitation in methanol. In order to get rid of the small molecular weight fractions (oligomers) formed during the reaction, the polymer was washed by ethyl acetate overnight (using a soxhlet apparatus).

GPC analysis was conducted to detect the molecular weight of the obtained polymer using polystyrene as a standard; however the GPC curves were recalculated against PPP-standard to have more reasonable results (see chapter 2 for more details). Accordingly, **P_{10}** showed M_w = 12 $\times 10^3$ g mol^{-1}, with PDI of 1.3. The resulting polymer was of very good solubility in common organic solvents (>10 mg / 1 ml) like chloroform, tetrahydrofurane, and toluene.

To study the optical properties of **P_{10}**, the UV-Vis absorption and PL of the polymer were studied in solution and in film, and are presented in the following section.

3.2.2 Photophysical properties of polymer P_{10}

In contrast to the formerly presented triphenylene polymers **P_1-P_9** (see chapter 2) that contained only the blue emitting triphenylene chromophore, polymer **P_{10}** composed of two blue emitting moieties, the pyrene and the triphenylene. Thus, intramolecular energy transfer between the two chromophores could basically occur when one unit acts as a donor while the other works as an acceptor,[12] which will be explained later in detail.

The photophysical characteristics of **P_{10}** were studied by UV-Vis absorption and PL spectroscopy in both solutions (THF) and films. The thin film was prepared by spin coating from toluene solutions (~ 1 × 10^{-5} M) at 1000 rpm over quartz substrates.

The absorption spectra of polymers **P_{10}** in solution as well as in film are shown in Figures 3.2 and 3.3, respectively. The absorption spectra were characterized by unresolved absorption

maxima, which was 20 nm red-shifted in film (386 nm), compared to solution (366 nm). In the solution absorption spectrum it was clear that the spectra composed of three main peaks, one at about 300 nm and two peaks at 347 nm and (a maximum) at 366 nm. This spectrum can apparently reflect the combination of the triphenylene and the pyrene chromophors in such a way: While the peak around 300 nm was attributed to the bathochromically-shifted absorption maximum of the triphenylene unit (initially around 280 nm)[13] due to the increased conjugation in the polymer chain, the second two observed peaks in the low energy region at 347 and 366 nm were related to the absorption of the pyrene moiety.

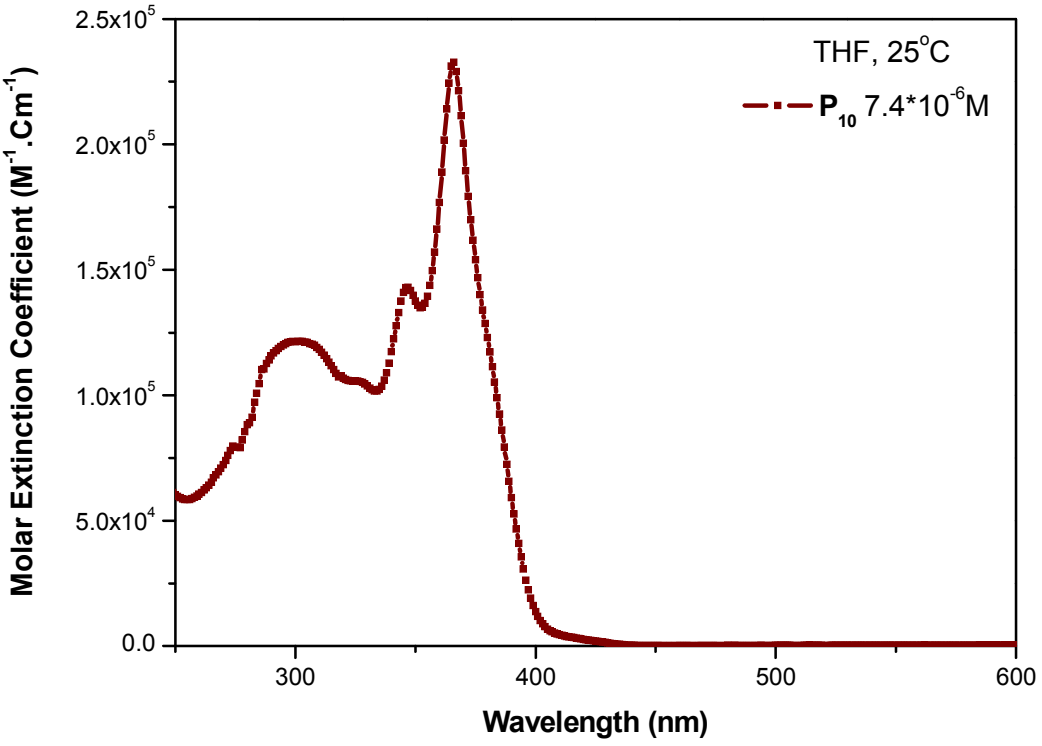

Figure 3.2 UV-Vis spectra of polymer $\mathbf{P_{10}}$ in THF at 25°C.

The absorption maximum of $\mathbf{P_{10}}$ at 366 nm was 9 nm blue-shifted compared to the 375 nm absorption maximum of the tetraalkoxy-pyrene polymer (**PPyr2**) that was reported by Kawano et al.[10a] Such hypsochromic-shift can be explained as result of the increased reduction

in the electronic conjugation in **P_{10}** compared to **PPyr2** due to the higher steric demands arose from the direct coupling of the triphenylene and the tetraalkoxypyrene moieties leading to an increased band gap.[14]

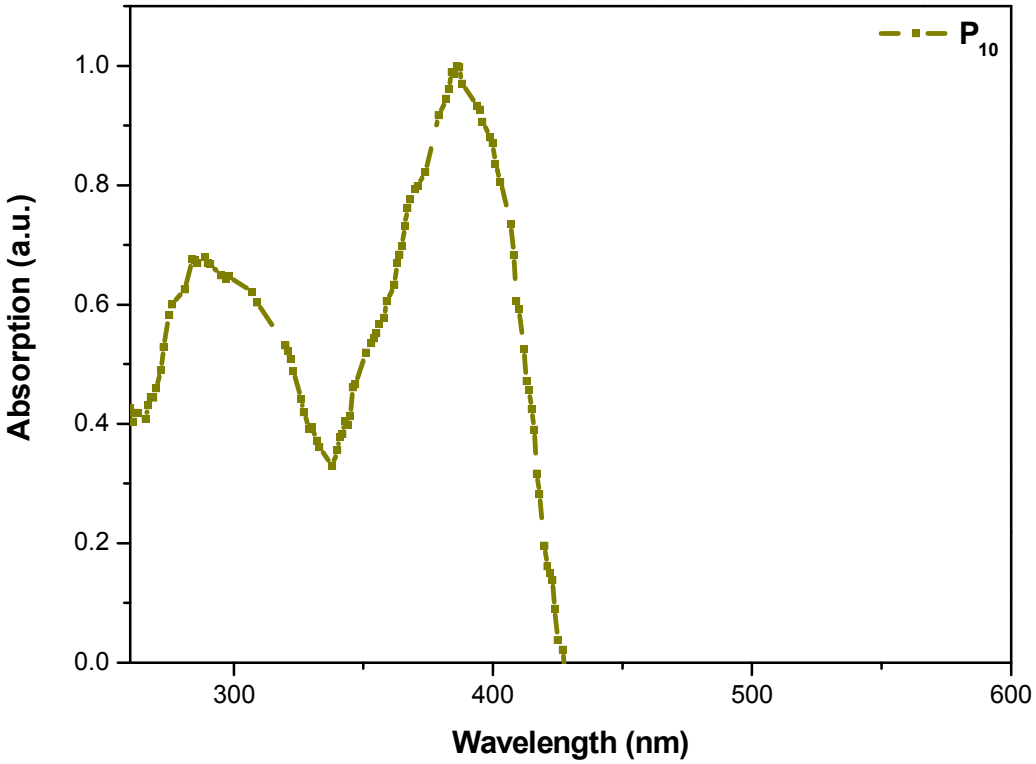

Figure 3.3 UV-Vis spectra of polymer **P_{10}** in thin films.

Figure 3.4 demonstrates the PL spectra of **P_{10}** in solution and in thin film. The emission spectra were characterized by steep onsets and by well-resolved vibrational split maxima at higher wavelengths. **P_{10}** depicts PL maxima at 442 nm and 430 nm for solution and thin film, respectively. The emission spectra were characterized by a second low energy peak at 468 nm for solution and 457 nm in film. Moreover the PL in film shows a broad band extending up to 700 nm.

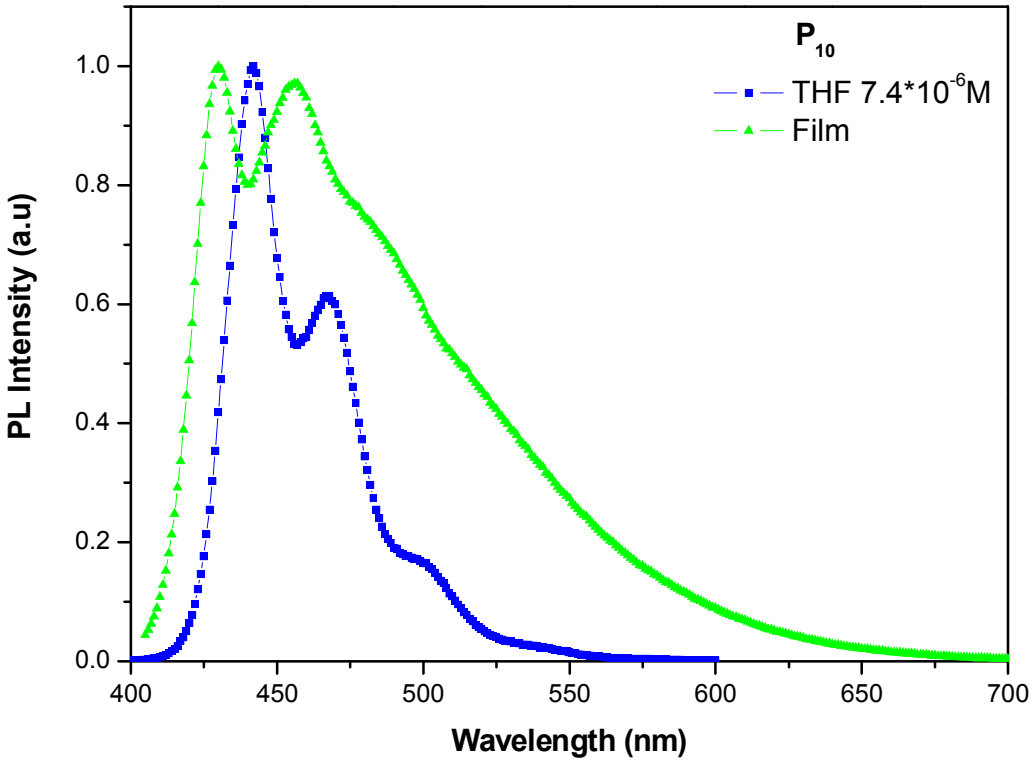

Figure 3.4 PL spectra of polymer $\mathbf{P_{10}}$ in solution and in thin film.

As formerly mentioned the existence of the two chromophores, triphenylene and pyrene in polymer $\mathbf{P_{10}}$ can lead to Förster energy transfer (FRET). In general, FRET can be detected by the appearance of fluorescence of the acceptor or by quenching of donor's emission.[12]

The solution PL spectra of $\mathbf{P_{10}}$ was almost identical with that of the **PPyr2** homo-polymer in which the emission was exclusively coming from the pyrene unit.[10a] In the same time the emission was 23 nm red-shifted compared to the previously presented homo-triphenylene polymer $\mathbf{P_8}$ (consists only of the triphenylene unit used in $\mathbf{P_{10}}$, but with two extra alkyl chain to afford solubility, see chapter 2, Scheme 2.5), in which the emission was only coming from the triphenylene moieties (Figure 3.5b). These results suggested that the

emission of the polymer was coming only from the pyrene unit (**P_8** emission was quenched). However, the solution emission spectrum of **P_{10}** was measured by exciting the polymer solution at 366 nm, which is the absorption maximum of **P_{10}** that was before attributed to the absorption of the pyrene unit in the polymer backbone. Therefore, these results alone could not prove the FRET operation in our system, since by using the 366 nm as the excitation wavelength it is possible that we were only exciting the pyrene moiety in the polymer and as a result the emission was only coming from the pyrene chromophore.

To solve this problem an excitation map was done for **P_{10}** in which the polymer was excited at a range of wavelengths (250 to 450 nm) (Figure 3.5a), which covers the maximum absorption of the triphenylene unit (~300 nm) and the pyrene chromophore (~366 nm). The observed PL spectra revealed only one type of emission that was again in agreement with the PL spectrum of the pyrene homopolymers **PPyr2**.[10a] These results finally proved that the energy was totally transferred from the triphenylene moiety to the pyrene unit, since the emission was only coming from the pyrene chromophore even if we excite the triphenylene unit at about 300 nm (Figure 3.5a). Therefore, polymer **P_{10}** can be described as a single molecular light-harvesting system with the triphenylene units in the polymer backbone act as donors, while the pyrene chromophors serve as acceptors.

The quantum efficiency in solution was measured for polymer **P_{10}** following the same procedure described in chapter 2. The polymer exhibited low quantum efficiencies in solution, which were upon excitation at 365 nm in THF, using 9,10-diphenylanthracene as a standard[15] found to be Φ_{PL}= 0.06 (multiple measurements indicated a precision of about 5 %). This value was close to the value reported for poly(2,7-pyrenylene) **P3b** that showed Φ_{PL} = 0.09.[10b]

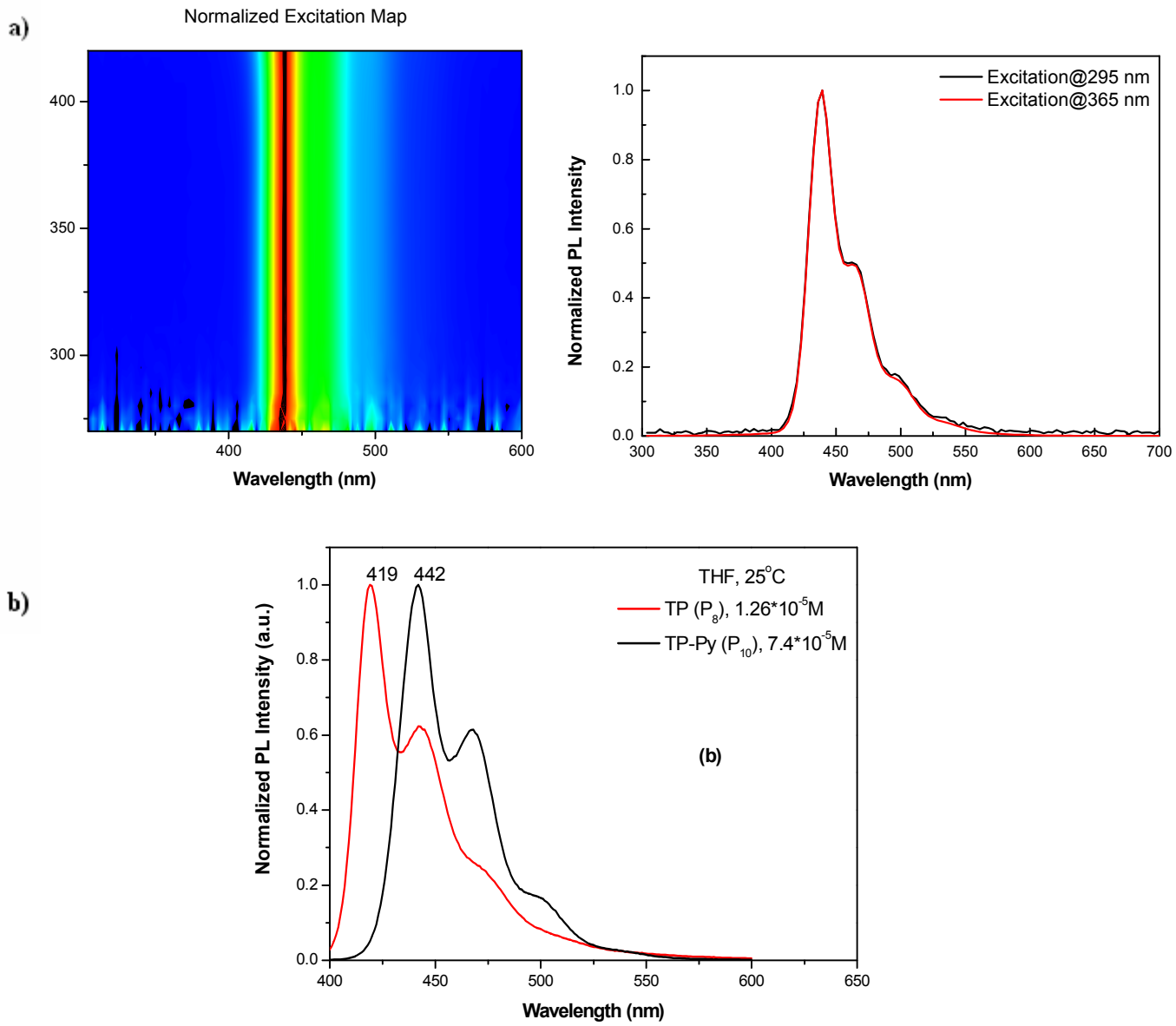

Figure 3.5 a) excitation map for $\mathbf{P_{10}}$ (left), PL spectra recorded at 295 and 365 nm (right). (b) emission spectra of polymer $\mathbf{P_{10}}$ compared to polymer $\mathbf{P_8}$.

Following the photophysical studies, it was needed to understand the electrochemical behavior of $\mathbf{P_{10}}$, for that cyclic voltammetry investigation was performed.

3.2.3 Electrochemical properties of polymer $\mathbf{P_{10}}$

The cyclic voltammogram was recorded for the polymer thin films against Ag/AgCl with a ferrocene standard (Figure 3.6). $\mathbf{P_{10}}$ showed only an anodic peak with irreversible

oxidation, which can be attributed to the electron rich nature of the polymers (due to the presence of several alkoxy groups on the edges of the polymers that can work as an electron source), which may make it easier to oxidize rather than being reduced. For that reason direct estimation of the LUMO level was not possible. Subsequently the HOMO level, optical band gap, and the LUMO level of the reduced polymer (was deduced from the HOMO value and the polymer optical band gap) was calculated as described by *Janietz et al.*[16]

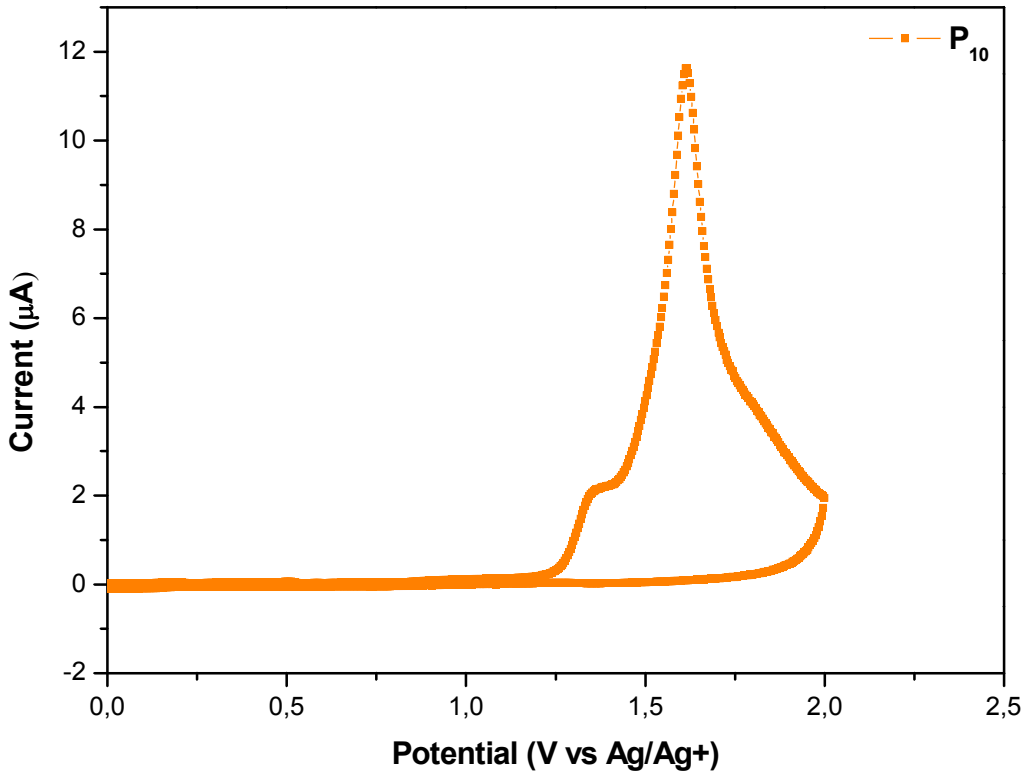

Figure 3.6 Cyclic voltammograms of drop casted polymer films from toluene solution on Pt-electrode in 0.1 M $TBAClO_4$ in acetonitrile solution vs Ag/Ag^+. Scanning rate100 mV/s.

Polymer **P_{10}** showed irreversible oxidation peak at 1.72 V with onset potential of oxidation at 1.38 V in the anodic scan. This low oxidation onset potential can be again ascribed to the electron rich nature of the polymer arising from the electron-donating property

of the alkoxy groups on the polymer backbone.[17] Polymer **P_{10}** exhibited a HOMO and LUMO values of 5.78 and 2.89 eV, respectively with optical band gab of 2.89 eV. These values were close to those obtained for the poly(2,7-pyrenylene) **P3b**, which showed HOMO and LUMO values of 5.66 and 3.4 eV,[10b] respectively.

3.2.4 Application of Triphenylene-Pyrene co-polymer (P_{10}) in blue PLEDs

This work was performed by Moussa Saleh and Young-Seo Park, at the group of professor Jang-Joo Kim at SNU. With our previous experience in fabricating triphenylene-based blue PLEDs (refere to chapter 2), the device set up shown in figure 3.7 was considered.

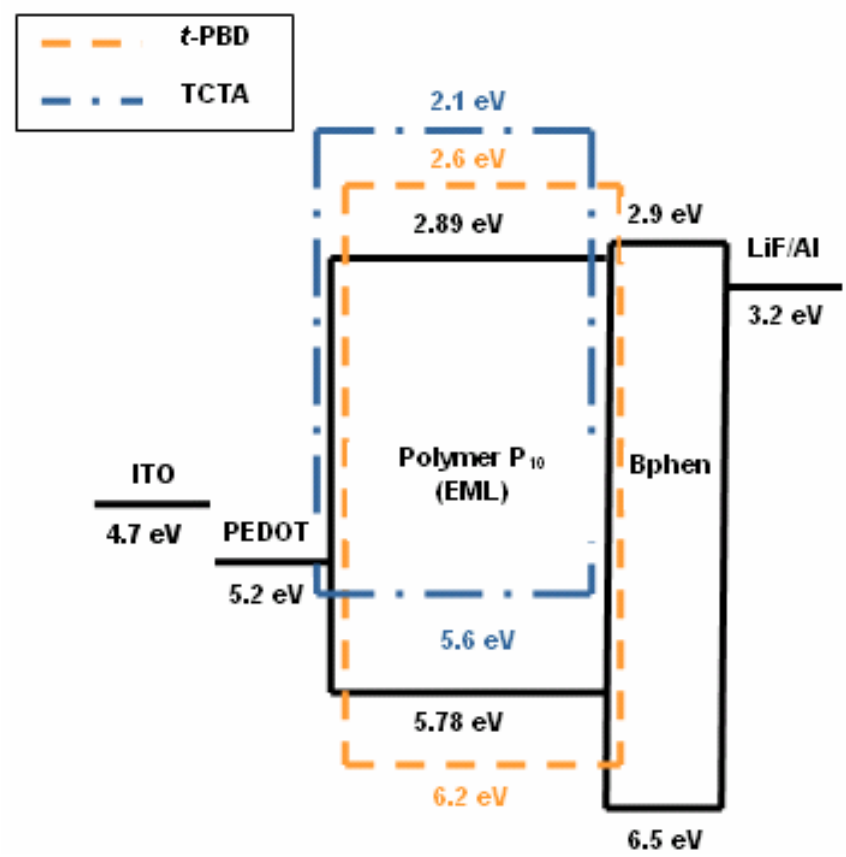

Figure 3.7 Energy levels diagram of the PLED of polymer **P_{10}**.

For the device construction in order to obtain good interlayer matching of the HOMO and LUMO properties, a blend of **P_{10}**, the electron transporting material ***t*-PBD** and the hole

transporting material Tris-(4-carbazol-9-yl-phenyl)-amine (**TCTA**) with a weight ratio of 52:26:22 was used to form an EML by spin coating from their toluene solution. The molecular structure of **TCTA** is shown in figure 3.8.

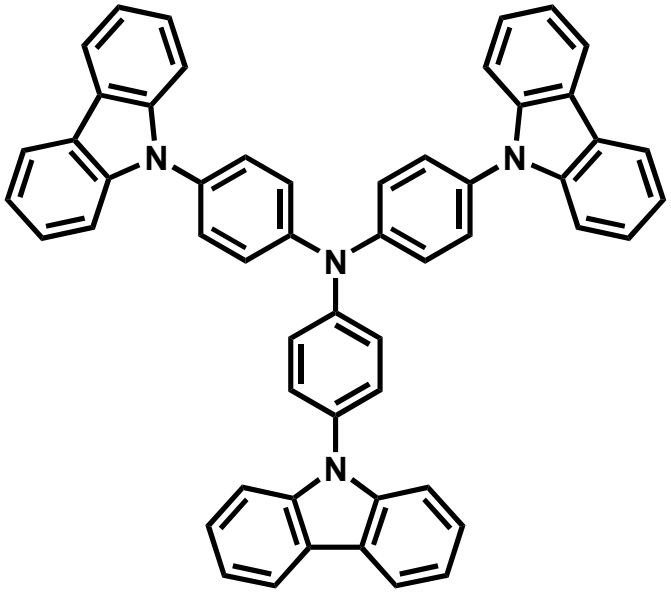

TCTA

Figure 3.8 Molecular structures of **TCTA** used in the PLED device of $\mathbf{P_{10}}$.

After spin coating, the device was dried at 150°C under N_2 for 10 min. A successive deposition of the hole blocking layer **BPhen** and the LiF/Al cathode completed the device construction.

The general device structure was: Al (100 nm) / LiF (1 nm) / Bphen (10 nm) / polymer + *t*-PBD + TCTA (80 nm) / PEDOT:PSS (40 nm) / ITO (150 nm).

Figure 3.9a shows the current density- voltage-luminance and current density-luminance efficiency-power efficiency characteristics of the PLEDs. The current density increased exponentially with increasing forward bias voltage, which is a typical diode characteristic. The turn-on voltage was found to be approximately 9 V. The PLED demonstrated maximum luminance efficiency (Max.η_L) of 0.22 cd/A corresponding to a bias of 13.2 V (Figure 3.9b). The electroluminescence spectrum (Figure 3.10) showed a maximum

EL peak at 444 nm that corresponds to a deep blue color and was analogous to the reported PL spectrum. **P_{10}** demonstrated Max. ELQE of 0.20 % with CIE color coordinates of x = 0.16, y = 0.12.

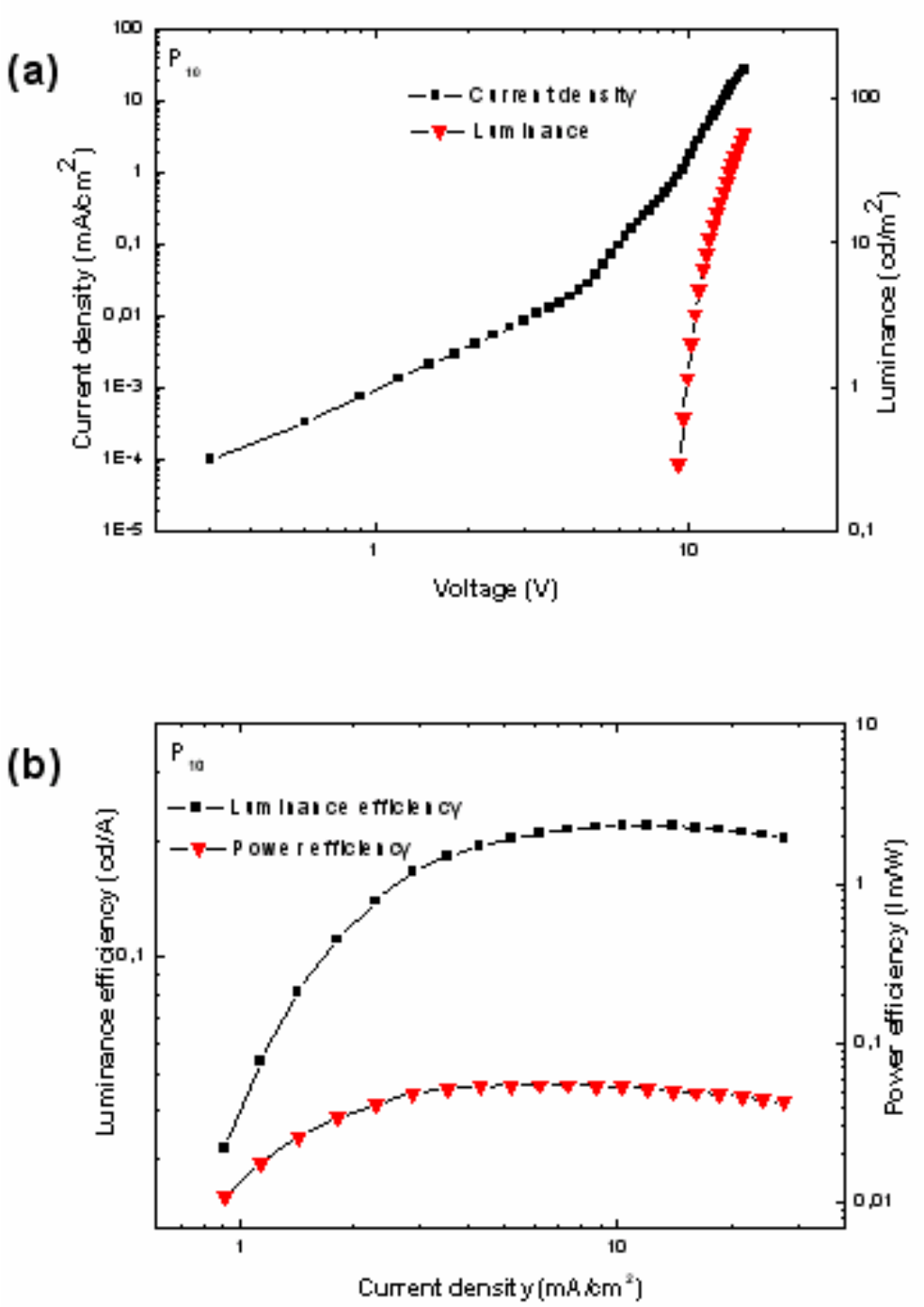

Figure 3.9 Current density–voltage–luminance characteristic of the device of **P_{10}** (a). Luminance efficiency and power efficiency of the PLED of **P_{10}** (b).

These results present polymer **P$_{10}$** as a promising emitter for blue PLEDs, since the device of the polymer was effectively able to produce deep blue electroluminescence (see color coordinates). However, the efficiency of the device was of moderate value and the turn on voltage was quite high. The reported device efficiency is most probably attributed to the use of TCTA, which was not forming adequate homogeneous mixture with the polymer and *t*-PBD because the solubility of the polymer and *t*-PBD were higher than TCTA in the toluene solution at the used concentrations. That can afford unbalanced ratios between the polymer and the additives in the device, which can result in unbalanced number of electrons and holes in the emitting layer that gave rise to such luminance efficiency and high turn-on voltage in the device. Therefore, the device efficiency could be improved by choosing more appropriate hole-transporting materials.

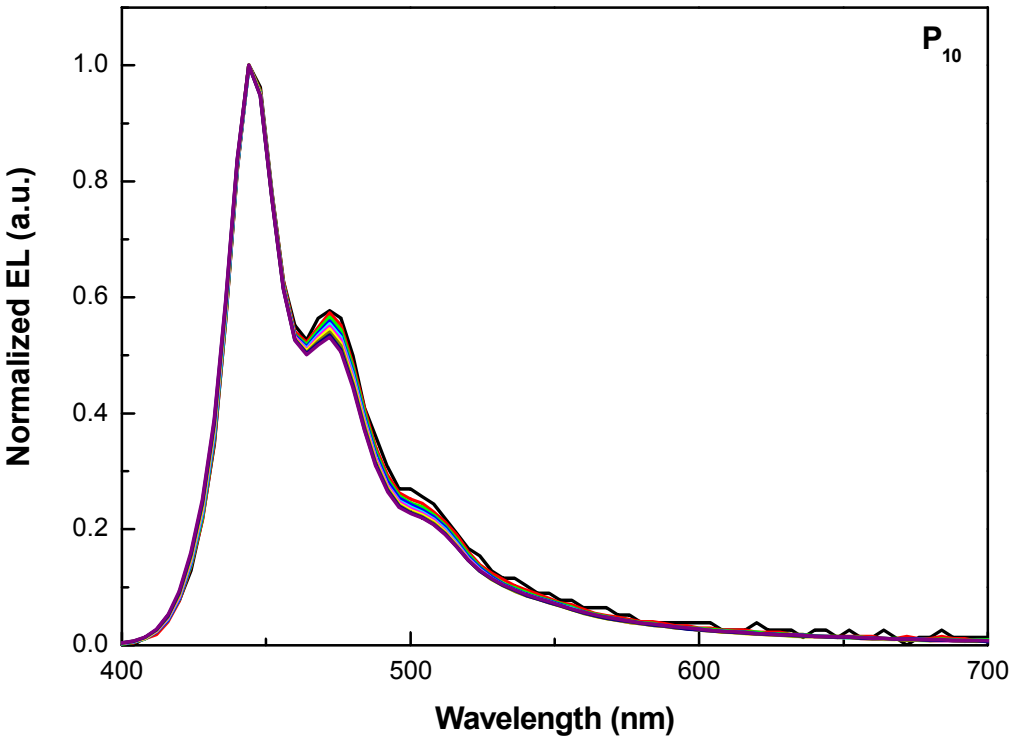

Figure 3.10 Normalized EL spectra of the device of **P$_{10}$**.

3.3 Triphenylene-Fluorene co-polymers (P_{11} and P_{12})

3.3.1 Synthesis and Characterizations

Following the synthesis of the TP-Py copolymer **(P_{10})**, which can be considered as a promising candidate for blue-PLEDs, incorporating other blue chromophores in the triphenylene polymer backbone was of major interest. Fluorene that represents the most vigorously studied moiety for blue emitting PLEDs was our second candidate to form TP-F polymers (P_{11} and P_{12}). We were aware of the possibly formed keto defect arising from the oxidation of the fluorene unit (refer to chapter 1), however due to the novelty of these copolymers (P_{11} and P_{12}) it was exciting to synthesize them and to study their associated properties. Polymers P_{11} and P_{12} were synthesized using the nickel (0) mediated MA-Yamamoto polycondensation reaction (Scheme 3.3). Monomers **5d** and **5e** (refer to chapter 2) were reacted with 1 equivalent of the commercially available 2,7-dibromo-9,9-dioctyl-9H-fluorene **(14)** at 80 W, 80^{o}C for 1 hour to afford polymers P_{11} and P_{12} in 80 % and 78 % reaction yields, respectively.(for a full description of the synthesis, work up, and purification procedures refer to the Yamamoto general synthetic route in chapter 2). From the GPC analysis using PPP as a standard, polymers P_{11} and P_{12} demonstrated molecular weights of M_w = 100 × 10^3 and 19 × 10^3g mol^{-1}, respectively. Polymers P_{11} and P_{12} showed PDI value of 2.3 and 1.6. The two polymers displayed high solubility (>10 mg / 1 ml) in common organic solvents ($CHCl_3$, THF, and toluene).

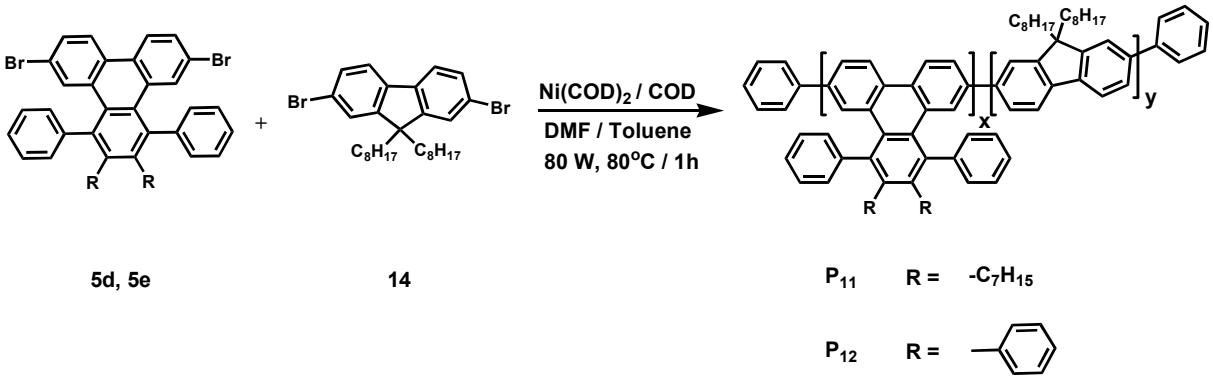

Scheme 3.3 Synthetic route of polymers P_{11} and P_{12} via Yamamoto coupling reaction.

After the successful synthesis of two **TP-F** polymers, studying their related optical and electrochemical properties as well as their supramolecular organization and PLED devices was essential.

3.3.2 Photophysical properties of polymers P_{11} and P_{12}

Polymers $\mathbf{P_{11}}$ and $\mathbf{P_{12}}$ represent two examples of polymers in which two blue emitting chromophors (triphenylene and fluorene) exist. Therefore the previously discussed FRET process should be also applicable here.

Figure 3.11 and 3.12 depicts the UV-Vis absorption spectra of polymers $\mathbf{P_{11}}$ and $\mathbf{P_{12}}$ in solution (THF) and in film, respectively. Polymer $\mathbf{P_{11}}$ with less aryl groups around the

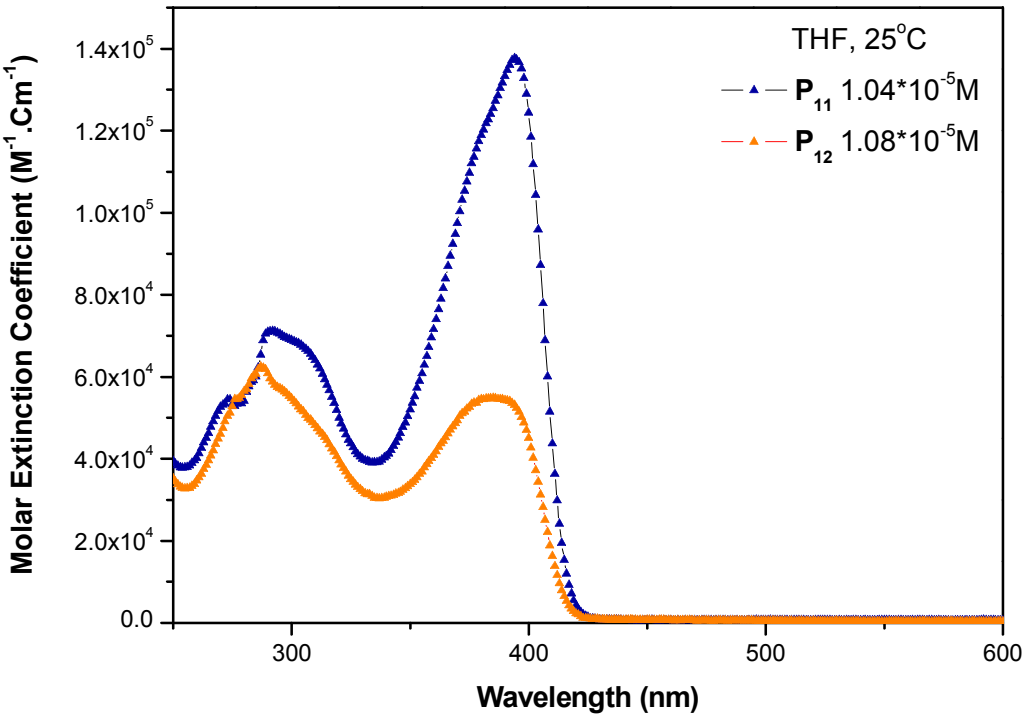

Figure 3.11 UV-Vis spectra of polymers $\mathbf{P_{11}}$ and $\mathbf{P_{12}}$ in THF at 25°C.

triphenylene moiety exhibited absorption maxima of 394 nm in solution and 400 nm in film. These values were identical with the absorption of the triphenylene homo-polymer $\mathbf{P_7}$

(consisting only of the triphenylene unit used in **P_{11}**, see chapter 2, Scheme 2.5 and Table 2.3) and was red-shifted compared to the values of PFO that showed absorption of 389 nm in solution and 387 nm in film.[18] The absorption spectra of polymer **P_{12}** displayed absorption maxima of 385 nm in both solution and film. These values were very similar to those of **PFO** and blue shifted compared to those of polymers **P_8** and **P_{11}**.

Polymers **P_{11}** and **P_{12}** displayed nearly identical behavior in the PL spectra of solution (Figure 3.13) and film (Figure 3.14). They showed solution emission maxima at 420 nm and 419 nm, respectively. That was accompanied by a shoulder at 443 nm. Again these results were matching the solution emission of **PFO** (418 nm, with shoulder at 442 nm).[18]

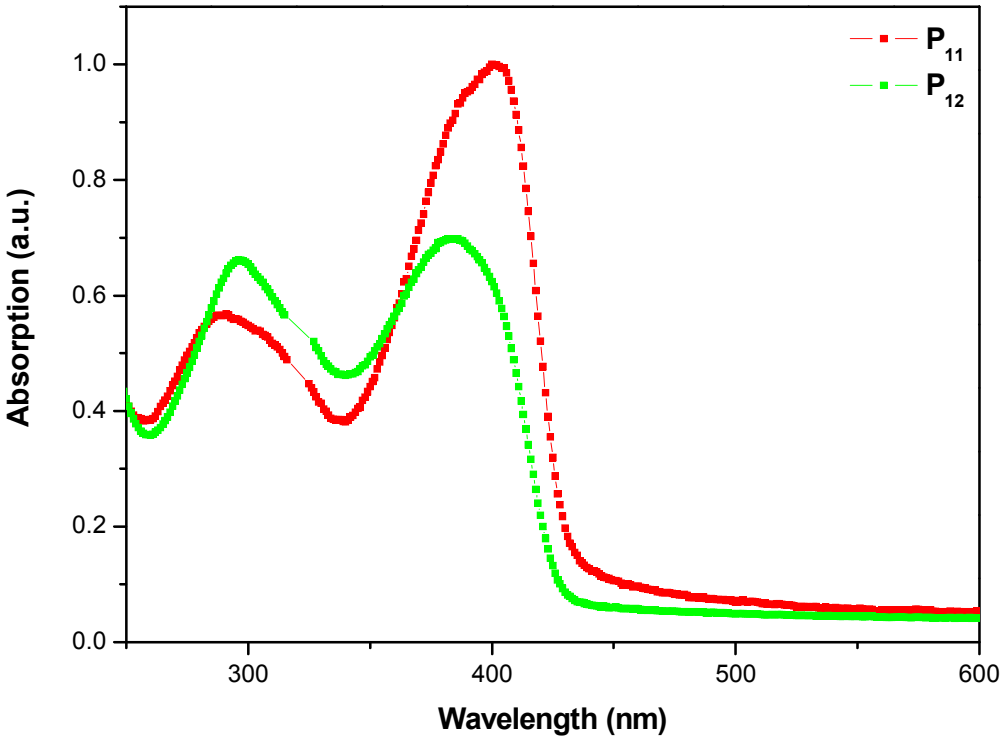

Figure 3.12 UV-Vis spectra of **P_{11}** and **P_{12}** thin films.

The film emission of $\mathbf{P_{11}}$ and $\mathbf{P_{12}}$ exhibited emission maxima at 429 nm, with pronounced shoulders at 456, and 495 nm, respectively, and revealed a solid state related broadening. The film PL of the two polymers were bathochromically shifted compared to that of **PFO** (424 nm, with shoulder at 448 nm).[18]

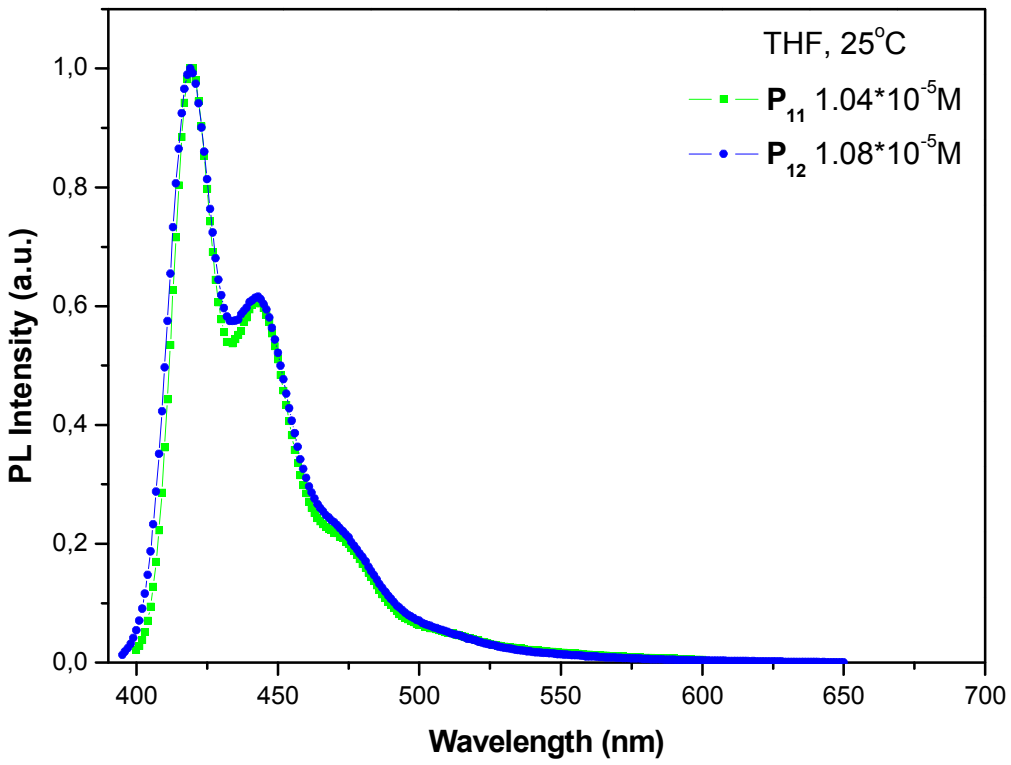

Figure 3.13 PL spectra of polymers $\mathbf{P_{11}}$ and $\mathbf{P_{12}}$ in THF at 25°C.

Since the two polymers demonstrated similar absorption and emission. Polymer $\mathbf{P_{11}}$ was used to study the FRET process in the **TP-F** polymers. This was done by comparing the emission spectrum of $\mathbf{P_{11}}$ with the PL spectrum of homo-triphenylene polymer $\mathbf{P_7}$ (consists only of the triphenylene unit used in $\mathbf{P_{11}}$). Both PL spectra were recorded by using 394 nm as the excitation wavelength, because $\mathbf{P_{11}}$ and $\mathbf{P_7}$ showed the same absorption maxima at 394 nm in solution. Accordingly, the solution PL spectra of $\mathbf{P_{11}}$ and $\mathbf{P_7}$ (Figure 3.15) depicted nearly identical emission behavior, which was at the same time almost matching with that of **PFO**

(emission maximum at 418 nm).[18] Due to this similarity between the spectra of the three systems it was not possible to distinguish the emitting chromophore.

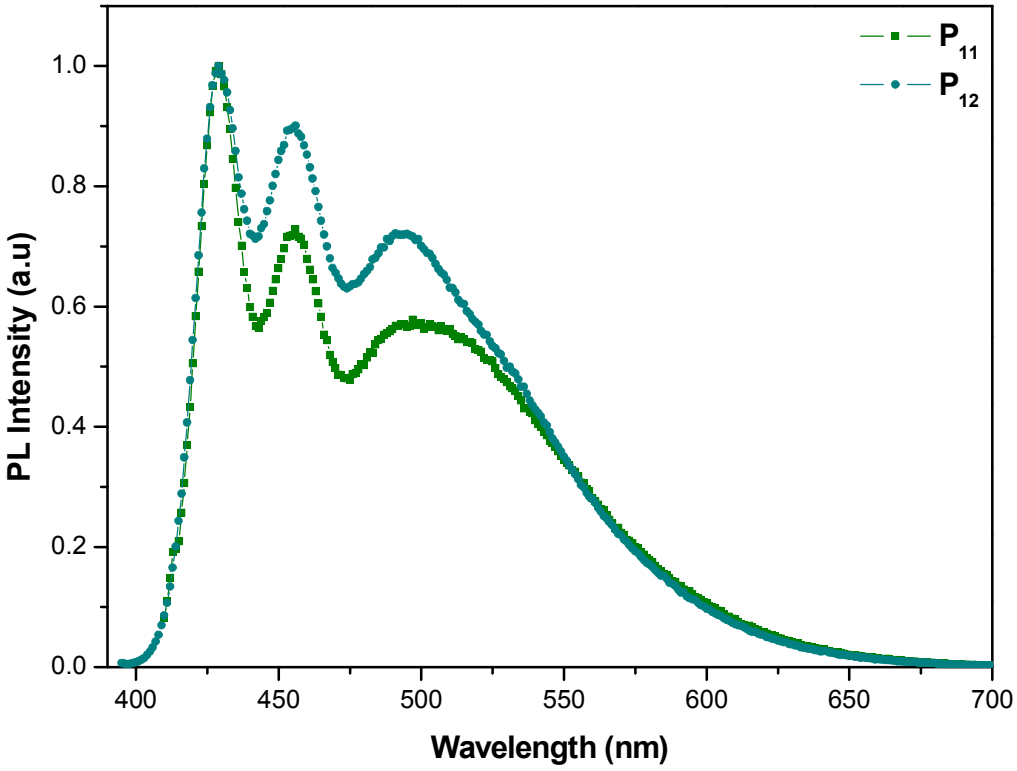

Figure 3.14 PL spectra of polymers $\mathbf{P_{11}}$ and $\mathbf{P_{12}}$ thin films.

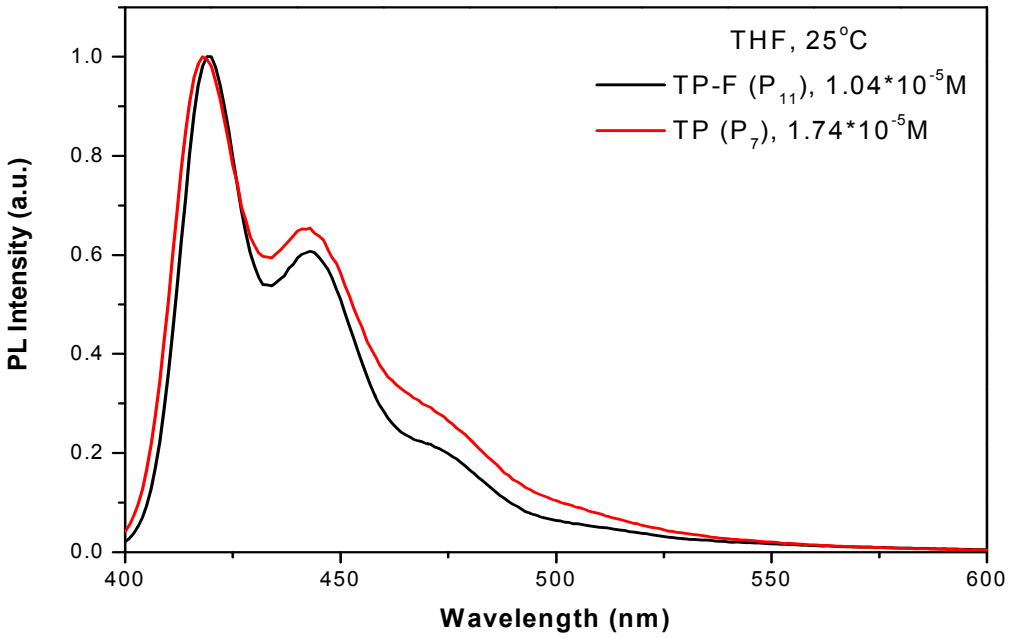

Figure 3.15 Emission spectra of polymer $\mathbf{P_{11}}$ compared to polymer $\mathbf{P_7}$.

The film PL quantum efficiencies of polymers $\mathbf{P_{11}}$ and $\mathbf{P_{12}}$ were measured using an integrating sphere.[19] The experiment was performed by Young-Seo Park, at the group of professor Jang-Joo Kim at Seoul National University.

The measurements were done by using:

- Excitation source : He/Cd laser (325 nm)
- 6" integrating sphere coated with $BaSO_4$
- PMT with monochromator as detector.
- Deuterium tungsten lamp as calibration source.

The measurement results showed that polymer $\mathbf{P_{11}}$ and $\mathbf{P_{12}}$ exhibited low PLQY of 16 % and 18 %, respectively. Such low quantum yield values can be ascribed to excimer formation in both polymers that can be seen from the more pronounced emission peaks at higher wavelengths in the film emission spectrum compared to the solution PL.

3.3.3 Electrochemical properties of polymers P_{11} and P_{12}

The cyclic voltammogram was recorded for the polymer thin films against Ag/AgCl with a ferrocene standard (Figure 3.16).The two polymers showed only anodic peaks with irreversible oxidation, which can be explained based on the electron rich nature of the polymers as a result of the presence of the alkyl groups attached to the periphery of the two polymers, which have an electron donating effect. That makes the polymers easier to oxidize rather than being reduced. The HOMO and LUMO levels were calculated as described by *Janietz et al*.[16]

Polymer **P_{11}** exhibited an irreversible oxidation peak at 1.67 V with an onset oxidation potential of 1.49 V. The HOMO and LUMO values were at 5.89 and 3.01 eV, respectively with an optical band gap of 2.88 eV. Similarly the oxidation peak and the onset potential of oxidation of polymer **P_{12}** were at 1.69 V and 1.53 V, respectively. The polymer optical band gap was of 2.9 eV, while the HOMO and LUMO were at 5.93 and 3.03 eV, correspondingly.

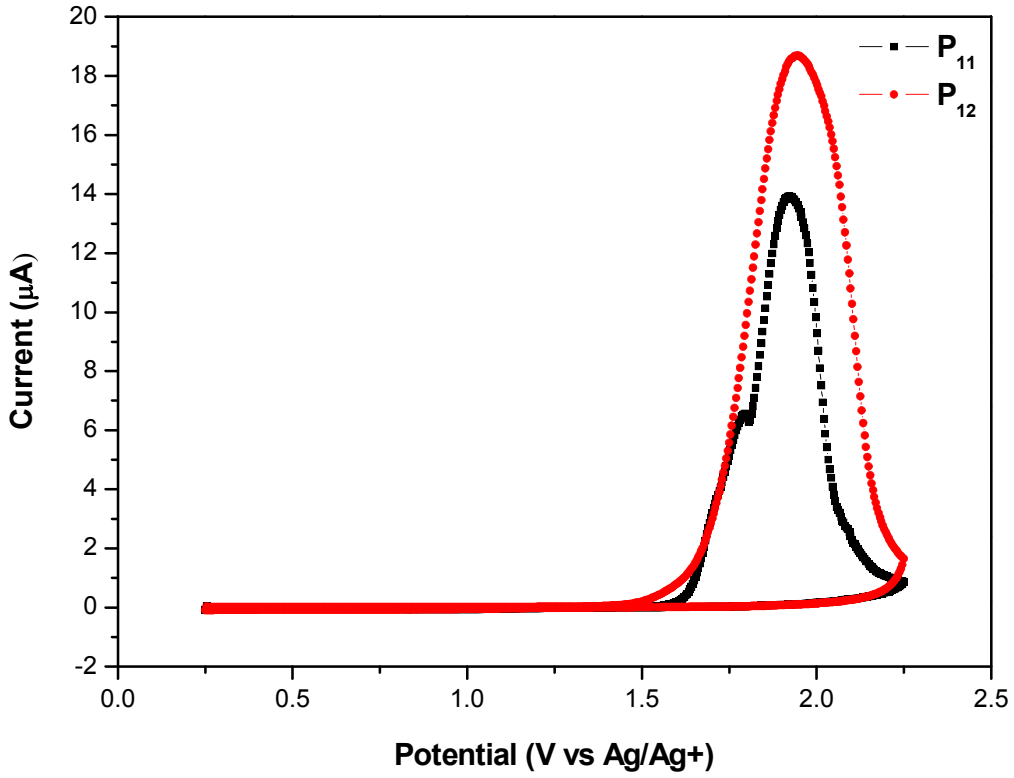

Figure 3.16 Cyclic voltammograms of drop caste films of $\mathbf{P_{11}}$ and $\mathbf{P_{12}}$ from toluene solution on Pt-electrode in 0.1 M $TBAClO_4$ in acetonitrile solution vs Ag/Ag^+. Scanning rate100 mV/s.

These results were analogous to the reported results for polymers $\mathbf{P_1}$-$\mathbf{P_9}$ (see chapter 2), and for **PFO** that showed HOMO of 5.8 eV and LUMO of 2.85 eV.[16]

3.3.4 Differential scanning calorimetry (DSC)

To study the thermal properties of the polymers DSC measurements were conducted. The DSC measurements did not reveal any phase transitions for the investigated polymers $\mathbf{P_{11}}$ and $\mathbf{P_{12}}$ within a temperature range of –150 °C to 300 °C. The two polymers showed almost identical DSC curves. Figure 3.17 displays the DSC results for polymer $\mathbf{P_{11}}$. The results

indicate an absence of structural changes in a wide temperature interval, which is a reported behavior for several PPP-based conjugated polymers.[5]

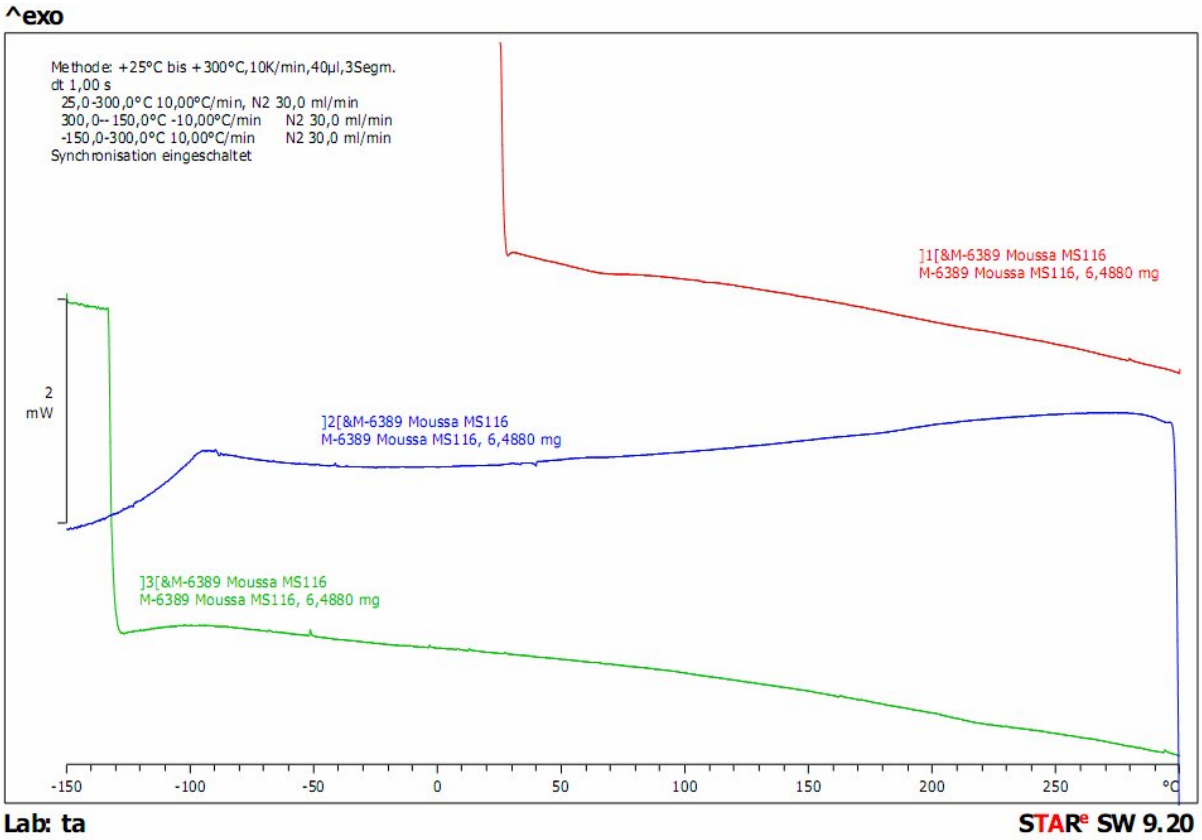

Figure 3.17 DSC curve for polymer $\mathbf{P_{11}}$ that showed no phase transition.

3.3.5 Thermogravimetric analysis (TGA)

The thermal stabilities of polymers $\mathbf{P_{11}}$ and $\mathbf{P_{12}}$ were investigated by TGA analysis. The thermal stability of each sample under nitrogen atmosphere was determined by measuring its weight loss while heating at a rate of 10°C / min. $\mathbf{P_{11}}$ and $\mathbf{P_{12}}$ exhibited good thermal stabilities with onset degradation temperatures above 300°C, which can be attributed to the loss of the alkyl chains on the polymer backbone. These values were comparable to those of polymers $\mathbf{P_1}$-$\mathbf{P_9}$ described in chapter 2. The TGA curve of polymer $\mathbf{P_{11}}$ (Figure 3.18) showed that polymer $\mathbf{P_{11}}$ was thermally stable until 340°C, after this temperature a degradation process was observed till a temperature of 700°C. The measured total weight loss was about

43 % that was close to the weight percentage of the alkyl chains (44 %) in the repeating unit of the polymer. Therefore, this weight loss can be ascribed to the loss of the alkyl chains from the polymer chains.

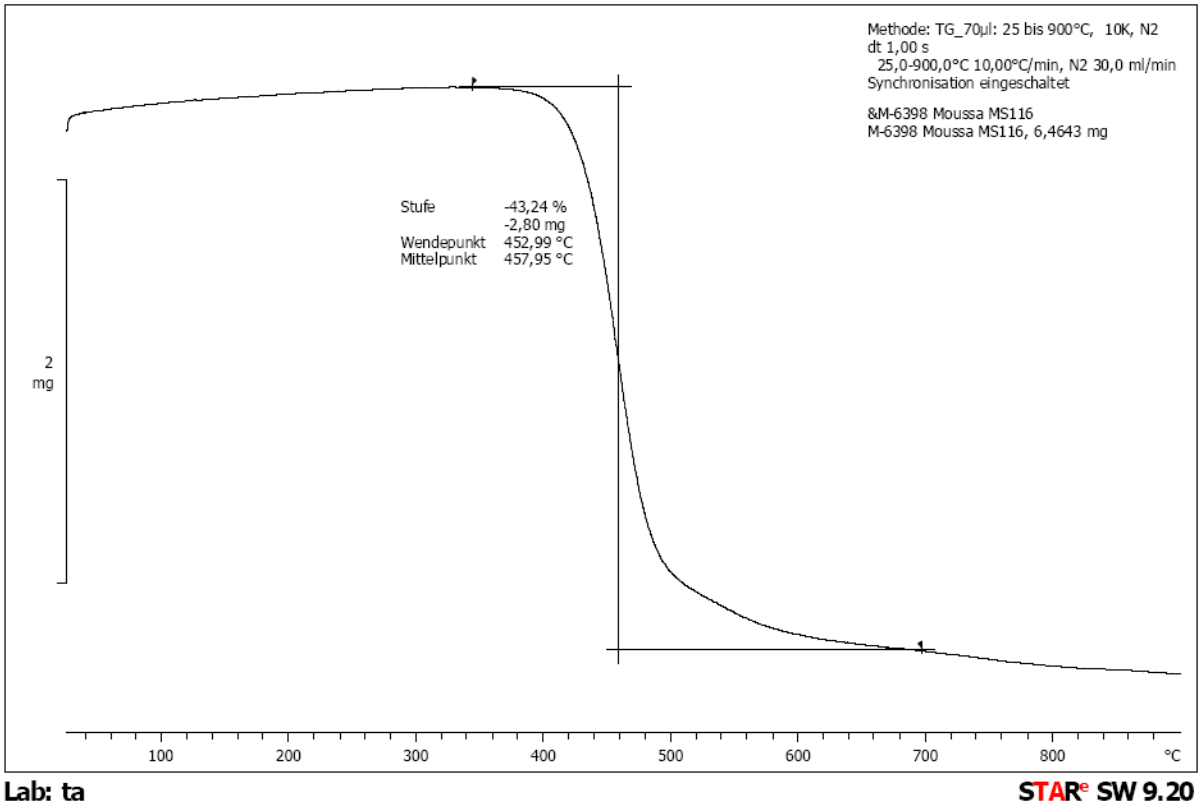

Figure 3.18 Thermogravimetric analysis results of polymer $\mathbf{P_{11}}$.

3.3.6 Supramolecular organization of polymers P_{11} and P_{12}

The supramolecular organization of both polymers on the macroscopic level was studied on a filament extruded sample by using two-dimensional wide-angle X-ray scattering (2D- WAXS). The investigation was done by Dr. Wojciech Pisula and Alexey Mavrinskiy at Max-Planck Institute for Polymer Research. The method for the sample preparation is explained in detail in chapter 2 (Section 2.6).

Polymers $\mathbf{P_{11}}$ and $\mathbf{P_{12}}$ were extruded at 230°C and at 270°C, respectively. At these temperatures the materials became deformable enough to achieve a suitable macroscopic

alignment by the shear forces during extrusion. The filaments were positioned vertically towards the 2D detector.

The polymer **P_{11}** X-ray pattern is depicted in Figure 3.19. The equatorial reflections (marked as "1") in the wide-angle scattering range correspond to the stacking distance of 0.44 nm due to the non-covalent interactions between polymer backbones (represent the indication for the lamellae packing). The two other reflections in the small-angle scattering range (marked as "2") are attributed to spacing between lamellae structures in which the polymers are packed. The d-spacing for the reflection "2" is 1.89 nm for **P_{11}**. In chapter 2 it was shown that the presence of arylene groups between the triphenylene repeating units in the TP-arylene-based co-polymers **P_2**, **P_4** and **P_5** led to a high degree of molecular organization (see section 2.6). For polymer **P_{11}** the arylene groups were replaced by the fluorenylene group. The effect of this replacement was obvious in the 2D-WAXS pattern of **P_{11}** that exhibited quite pronounced reflexes (located on the equatorial axis), which were not strong as those of **P_2**, **P_4** and **P_5**. In addition, in the small-angle region no second-order reflexes were observed. These results give the indication that polymer **P_{11}** showed a primary degree of orientation (order) however, the polymer was of lower degree of molecular order compared to **P_2**, **P_4** and **P_5**. This can be associated with the high steric demand of the branched alkyl chains as compared to linear alkyl substituents.

The X-ray pattern of **P_{12}** (Figure 3.20) reveals only two weak reflections in the small-angle region which correspond to the lamellae organization (marked by red arrows). Due to the very weak reflexes we were not able to obtain more information out of this 2D-WAXS pattern. The low intensity and the lack of other scattering intensities indicate poor ordering of the polymer chains. The inferior organization of **P_{12}** in comparison to **P_{11}** can be attributed to the bulky side chains attached to the fluorenylene unit (expected to be out-of-plane), and to the presence of the aryl groups on the periphery of the triphenylene block that could reduce the molecular ordering.

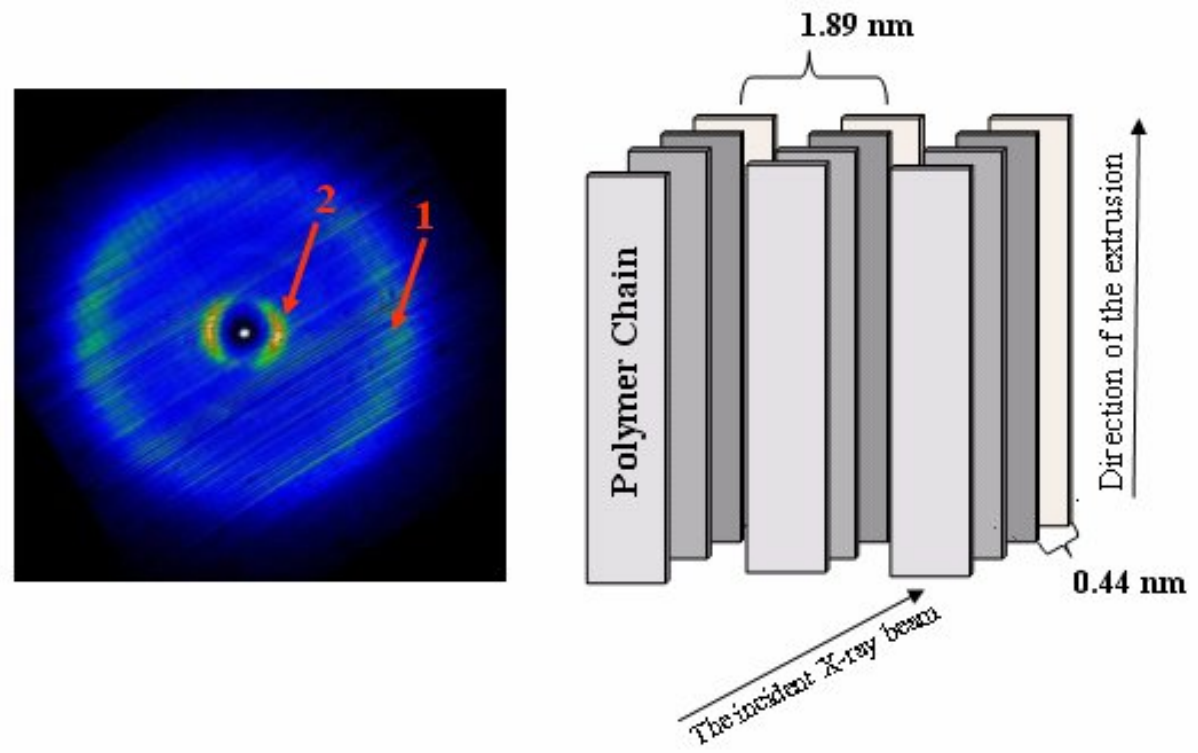

Figure 3.19 X-ray pattern and schematic illustration of supramolecular organization of $\mathbf{P_{11}}$.

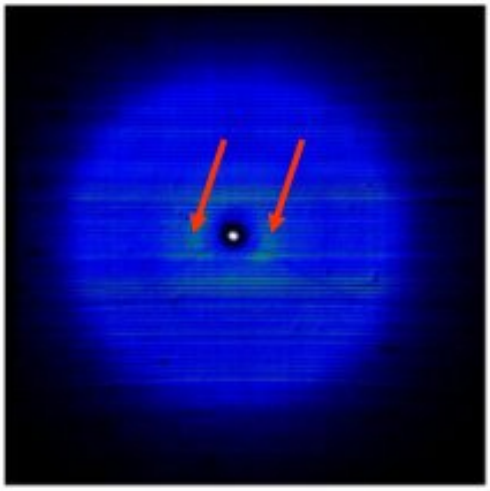

Figure 3.20 2D-WAXS pattern of $\mathbf{P_{12}}$.

3.3.7 Application of Triphenylene-Fluorene co-polymers (P_{11} and P_{12}) in polymeric light emitting diodes (PLEDs)

The PLED performances of polymers **P_{11}** and **P_{12}** were studied by Moussa Saleh and Young-Seo Park, at the group of professor Jang-Joo Kim at Seoul National University.

The device fabrication followed the same procedure described in chapter 2 (section 2.7). The hypothetical band diagram of the devices of polymers **P_{11}** and **P_{12}** is shown in Figure 3.21. In these devices only the polymer formed the emitting layer (EML) without any other additives.

The general device setup was: ITO (150 nm) / PEDOT: PSS (40 nm) / Polymer (80 nm) / Ca/Ag (10 nm/100 nm). After spin coating the polymer toluene solutions, the devices were dried at 150^{o}C under N_2 for 10 min. Finally the deposition of Ca / Ag cathode finished the device fabrication.

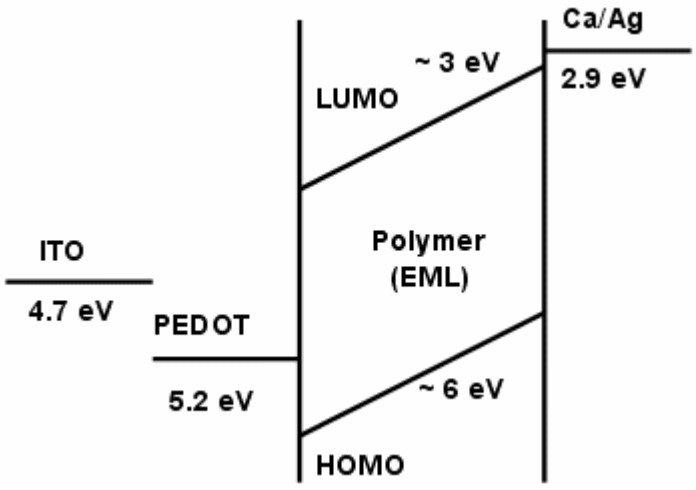

Figure 3.21 Hypothetical band diagram of the PLEDs of polymers **P_{11}** and **P_{12}**.

As seen in Figures 3.22a, polymer **P_{11}** demonstrated the common behavior of a PLED device. The current density increased exponentially by the increase of the applied bias voltage. The device showed turn-on voltage around 6 V. Figures 3.22b depicts that the PLED exhibited a Max.η_L of 0.14 cd / A corresponding to a bias of 9.6 V. Such rather low

luminance efficiency and quite high turn on voltage can be attributed to the large hole injection barrier between PEDOT:PSS (5.2 eV) and the HOMO energy level of the polymer (5.89 eV). Consequently, the injection of the holes into the EML is expected to be hindered, which result in different ratios of the holes and electrons in the polymer layer that resulted in the low efficiency of the PLED. Therefore, the use of a hole-transporting layer between the anode and the EML seems to be crucial to afford good energy level matching between the HOMO energy level of the polymer and the potential of the electrode. The fabrication of such optimized device is ongoing.

Figure 3.23 exhibits the recorded EL spectrum for polymer **P_{11}**. The spectrum was characterized by a maximum at 528 nm that corresponds to a green emission. Similar electroluminescence behavior with the emission around 530 nm was reported in the **PF**-type polymers, which was ascribed to the formation of keto-type defects in **PF** derivatives.[5] It was found that an oxidative degradation process, which is happening during the synthesis of the polymer was the reason for the formation of such defects due to the reduced chemical stability of the relatively weakly bound, acidic methylene bridge hydrogen (C-9) on the monomer units. Further studies showed that the keto-defects can be formed as a result of the electro-oxidation of the acidic methylene bridge hydrogen of the fluorene unit.

Therefore, polymer **P_{11}** that contains the 9,9-dialkylated-fluorene units in its backbone can suffer from an electro-oxidation at the methylene bridge hydrogen on the fluorene unit.[5,20] That was the reason for such green emission at 530 nm. In addition, **P_{11}** showed CIE color coordinates of x = 0.29, y = 0.46 with 0.052 % as the Max. ELQE. Based on the obtained results it was clear that **P_{11}** was not suitable for blue-PLED applications.

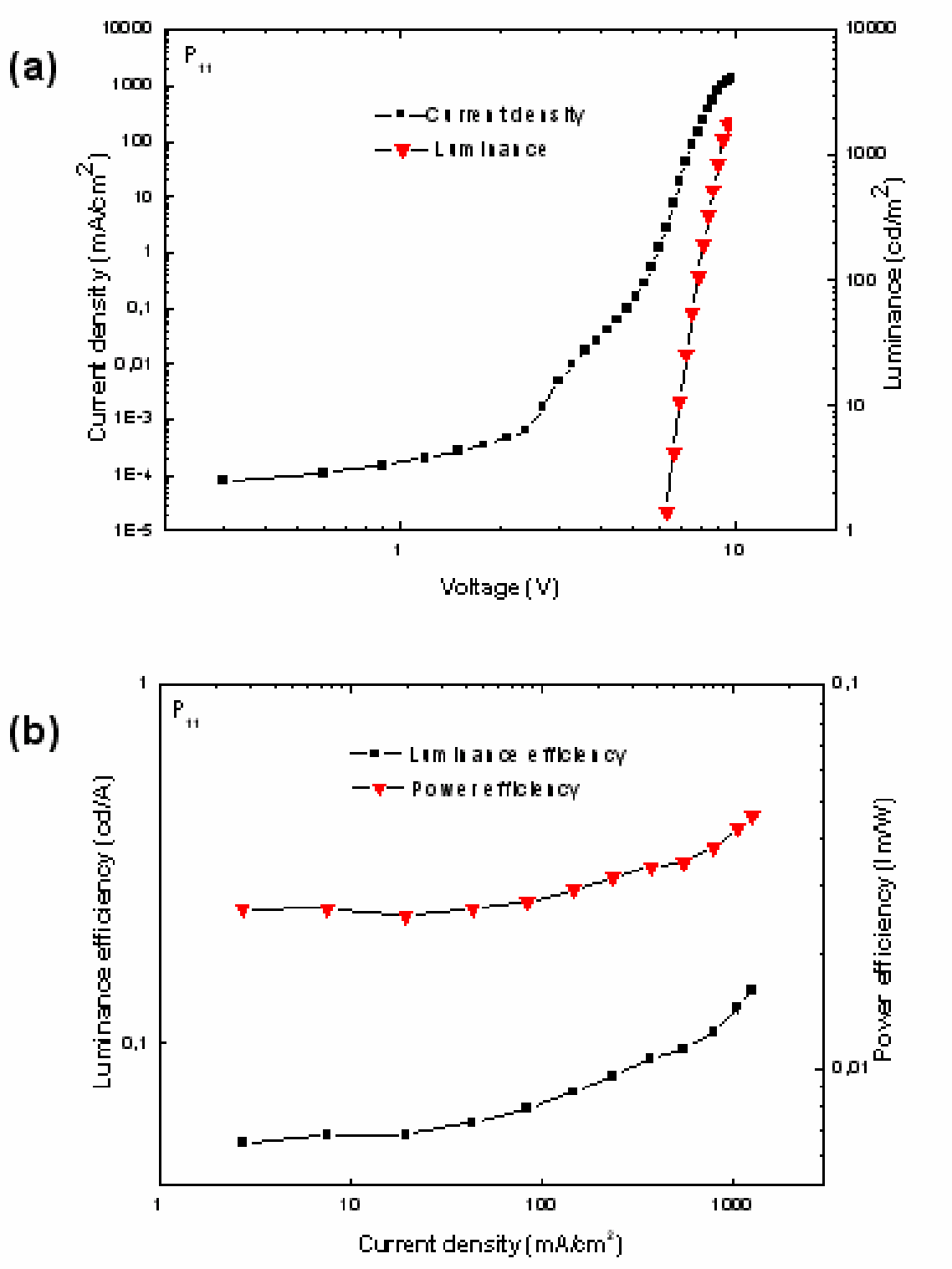

Figure 3.22 Current density–voltage–luminance characteristic of the device of $\mathbf{P_{11}}$ (a). Luminance efficiency and power efficiency of the PLED of $\mathbf{P_{11}}$ (b).

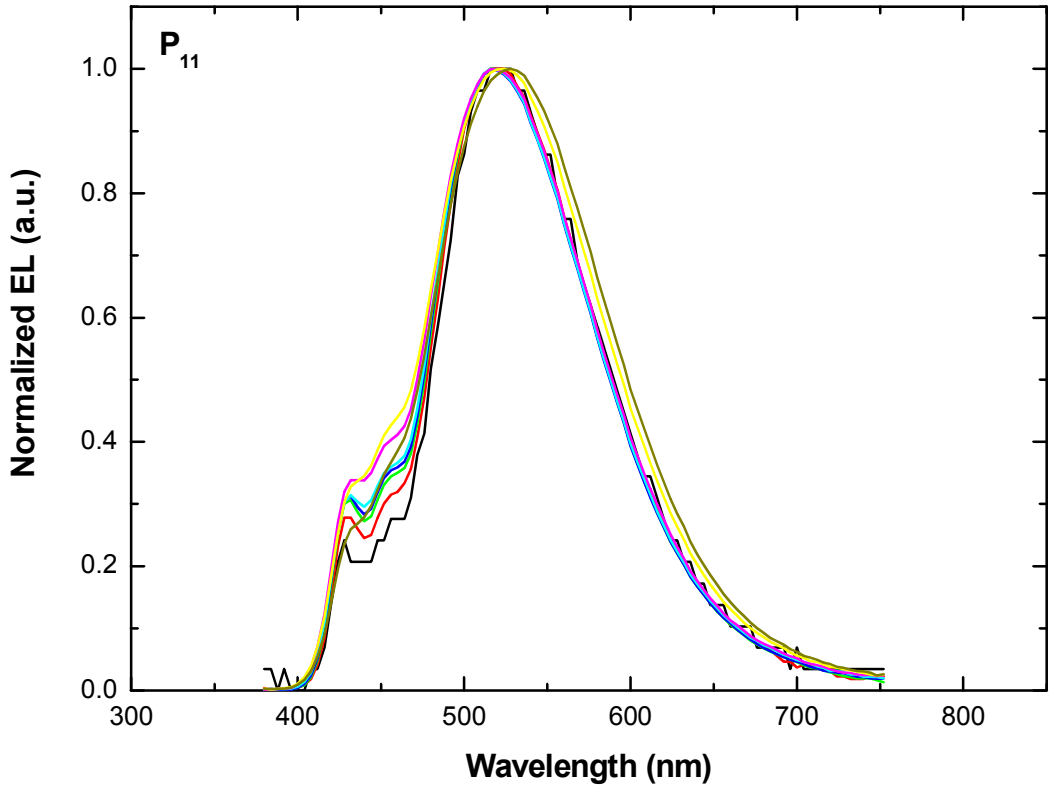

Figure 3.23 Normalized EL spectra of the device of $\mathbf{P_{11}}$.

The characteristics of the PLED device fabricated from polymer $\mathbf{P_{12}}$ (Figure 3.24) were similar to those of polymer $\mathbf{P_{11}}$. As common for a PLED the device showed as an exponential increase in the current density with the increase of the applied voltage, and showed a turn-on voltage of 6 V. The device depicted a maximum luminance efficiency of 0.083 cd / A corresponding to a bias of 8.7 V (Figure 3.24b). Such low device performances (Max.η_L and V_{on}) can be ascribed to the high hole- injection barrier between the anode (5.2 eV) and the HOMO energy level of the EML (5.93 eV) (for more details see the explanation of the device performance of $\mathbf{P_{11}}$), which reflects the importance of the use of a hole-transporting layer in this device structure to ease the hole-injection process and consequently improve the device efficiency. Moreover, it was noticed that the Max.η_L of $\mathbf{P_{12}}$ was lower than that of $\mathbf{P_{11}}$, which can be attributed to the inferior organization of $\mathbf{P_{12}}$ in comparison to $\mathbf{P_{11}}$ as a result of the high

steric hindrance caused by the phenyl groups at the periphery of the triphenylene block (previously proved by the 2D-WAXS). The higher organization of polymer **P_{11}**, should facilitate the charge carrier mobility and improve the electron and hole balance in the device, which result in better luminance efficiency.

Measuring the EL spectrum of **P_{12}** (Figure 3.25) resulted in a maximum at 516 nm, which corresponded to a green emission. Since polymer **P_{12}** also contains the same 9,9-dialkylated-fluorene unit in its backbone as **P_{11}** polymer, such green emission can be also attributed to the keto-defects formed due to the electro-oxidation of the methylene bridge hydrogen on the fluorene unit (for more details see the explanation of the device performance of **P_{11}**).[5,20] In addition, **P_{12}** exhibited CIE color coordinates of x = 0.27 and y = 0.42 with Maximum ELQE of 0.032 %. From these results polymer **P_{12}** can not be used as an active layer in blue-PLEDs.

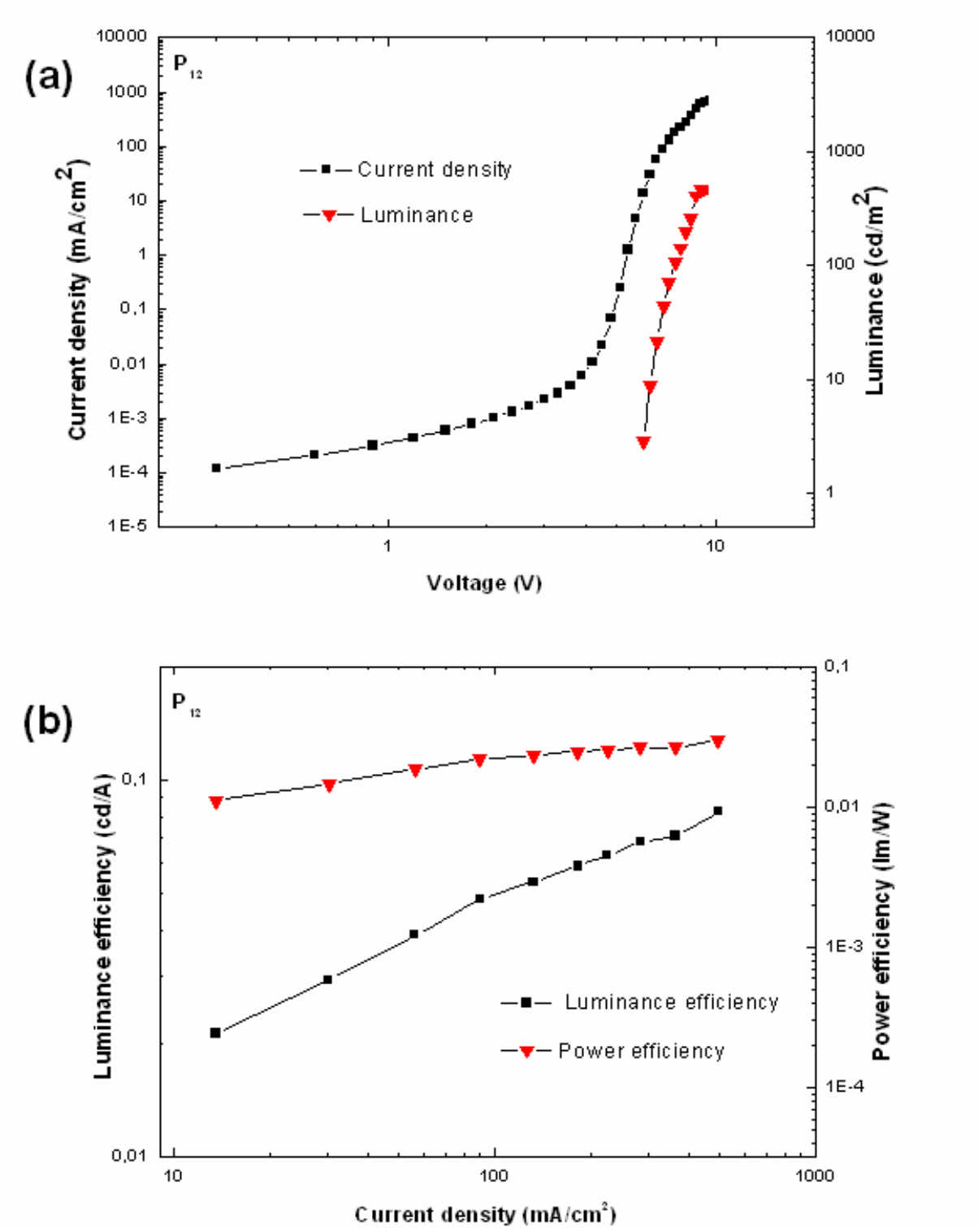

Figure 3.24 Current density–voltage–luminance characteristic of the device of **P_{12}** (a). Luminance efficiency and power efficiency of the PLED of **P_{12}** (b).

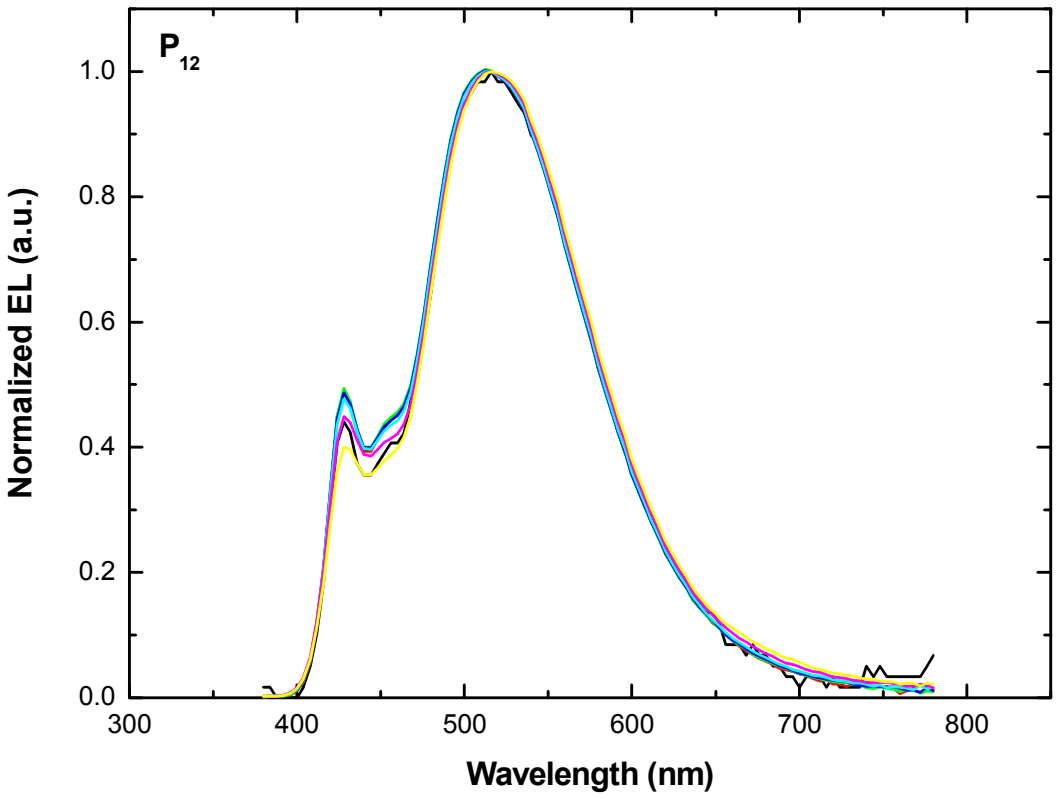

Figure 3.25 Normalized EL spectra of the device of $\mathbf{P_{12}}$.

3.4 Triphenylene-Carbazole co-polymer (P_{13})

3.4.1 Synthesis and characterization

Our third candidate to be coupled with the triphenylene moiety in one polymeric chain was the carbazole chromophore. That was also studied as a promising blue emitter in PLEDs due to its emission in the range of 420-440 nm, where the human eye is most sensitive for the blue color.[7,8]

The synthesis of polymer was accomplished by using the MA-palladium-catalyzed Suzuki-Miyaura coupling (50 W / 100°C / 1 h) of monomer **5e** (described in chapter 2) and 9-(2-decyl-tetradecyl)-2,7-bis-(4,4,5,5-tetramethyl-[1,3,2]dioxaborolan-2-yl)-9H-carbazole **(15)** to afford $\mathbf{P_{13}}$ in 56 % reaction yield (Scheme 3.4). The synthesis, work up and purification followed the same procedure described in chapter 2 for the synthesis of polymer $\mathbf{P_1}$-$\mathbf{P_6}$. Compound **15** was received from Dr. Gao Peng and was synthesized according to literature procedure.[21]

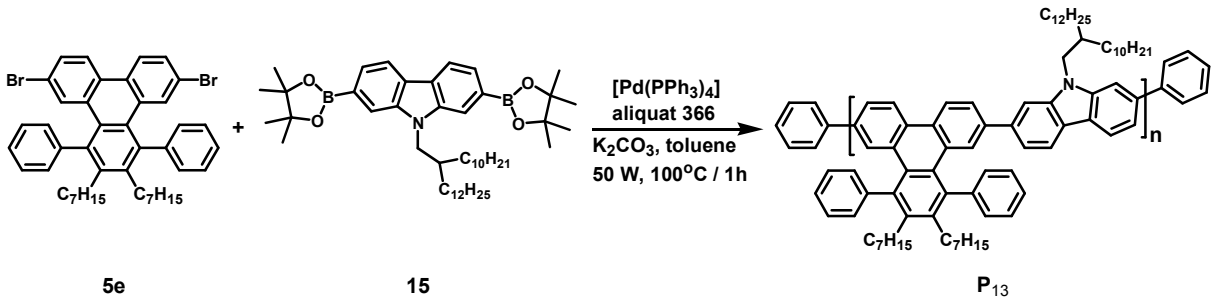

Scheme 3.4 Synthesis of polymer $\mathbf{P_{13}}$ via Suzuki-Miyaura coupling reaction.

The GPC analysis of $\mathbf{P_{13}}$ using PPP as a standard showed molecular weight of M_w = 10 $\times 10^3$ g mol^{-1}, with PDI of 1.5. The resulting polymer was of high solubility in common organic solvents (>10 mg / 1 ml) like DCM, THF, chloroform, and toluene. Such solubility allowed for structure characterization. ^{1}HNMR spectrum of $\mathbf{P_{13}}$ (Figure 3.26) showed a broad peak from 8.22 to 7.28 ppm, assigned to the 22 aromatic protons, and a second broad peak

from 1.53 to 0.74 ppm for the 79 aliphatic protons. That was perfectly matching with the number of the aromatic and aliphatic protons in the polymer.

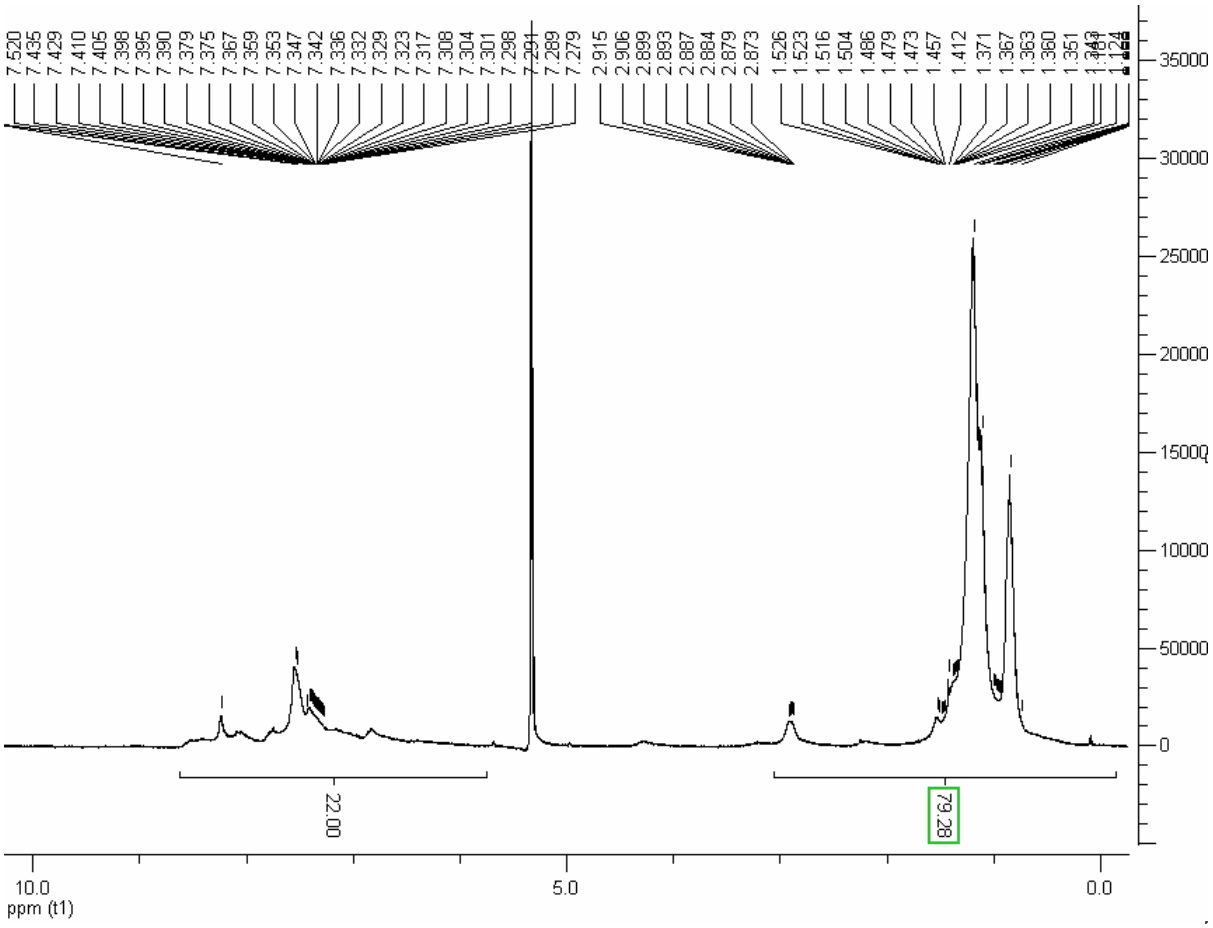

Figure 3.26 ^{1}HNMR spectrum for polymer $\mathbf{P_{13}}$ measured in DCM at 25^{o}C.

3.4.2 Photophysical properties of polymer $\mathbf{P_{13}}$

The UV-Vis absorption and PL spectroscopy in both solutions (THF) and films were measured for polymer $\mathbf{P_{13}}$. The thin film was prepared by spin coating from toluene solutions ($\sim 1 \times 10^{-5}$ M) at 1000 rpm over quartz substrates.

As shown in Figures 3.27 and 3.28, the UV-Vis absorption spectra for polymer $\mathbf{P_{13}}$ in solution and film were similar to demonstrate absorption maxima of 390 and 391 nm, respectively. These values were in between the reported absorption maxima of the homo-triphenylene polymer $\mathbf{P_7}$ (394 nm in solution and 401 nm in film) and those of the poly(*N*-

octadecyl-2,7-carbazole) (**POCD**)[22] which demonstrated absorption maximum at 374 nm in solution and 380 nm in film.

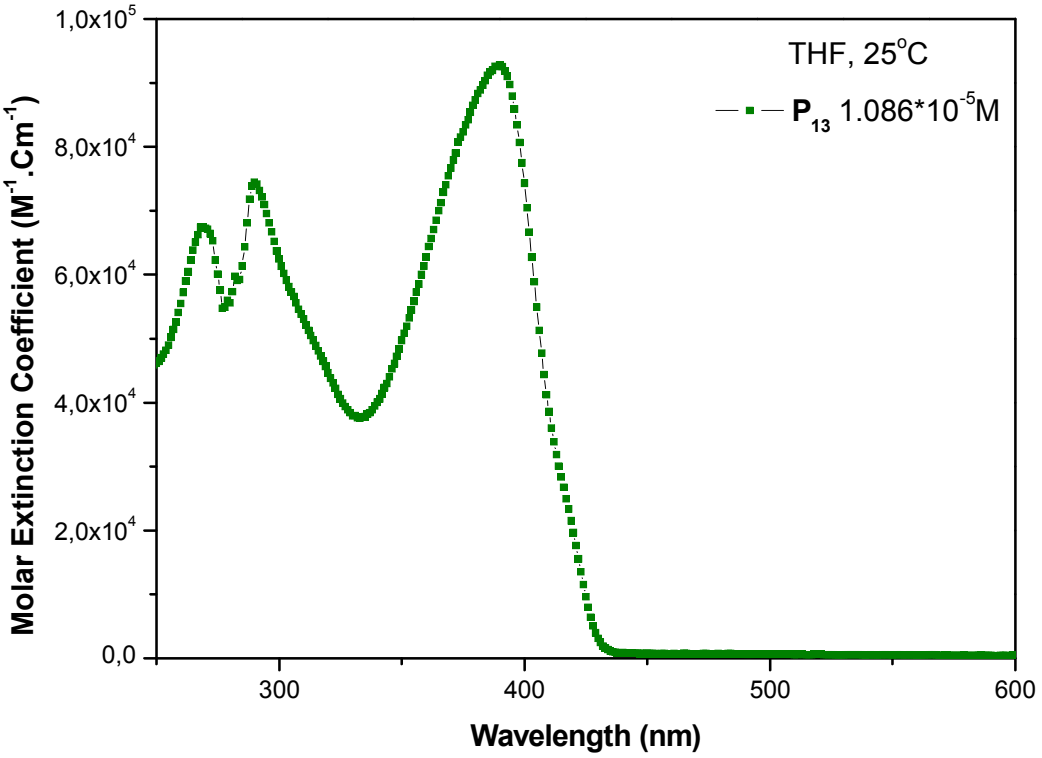

Figure 3.27 UV-Vis spectra of polymer $\mathbf{P_{13}}$ in THF at 25°C.

Polymer $\mathbf{P_{13}}$ exhibited a maximum solution PL at 425 nm with another lower energy maximum at 445 nm this maximum was red-shifted compared to the solution PL of $\mathbf{P_7}$ and POCD (418 nm).[22] The PL spectrum in film was bathochromically-shifted compared to the solution PL, and exhibited emission maximum at 434 nm with pronounced low energy peak at 459 nm. A solid state related broadening was also obvious in film PL spectrum (Figure 3.29).

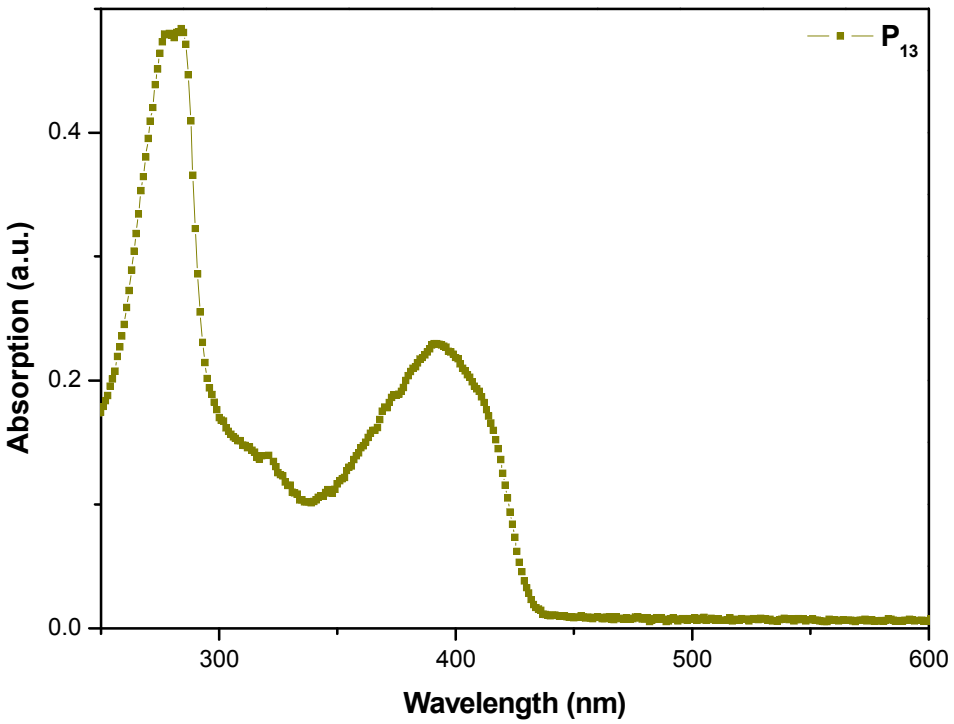

Figure 3.28 UV-Vis spectra of polymer $\mathbf{P_{13}}$ in thin film.

As previously discussed in this chapter the presence of two emitting moieties (chromophors) in one conjugated system can lead to Förster energy transfer (FRET). Therefore, FRET can occur in polymer $\mathbf{P_{13}}$ due to the existence of the two chromophors triphenylene and carbazole in one conjugated polymer chain. As a general rule, FRET can be detected by the appearance of the emission of the acceptor or by quenching the donor's PL.[12]

In order to study the possible FRET in $\mathbf{P_{13}}$ the emission spectrum of the co-polymer was compared with the PL spectrum of the homo-triphenylene polymer $\mathbf{P_7}$ (consists only of the triphenylene unit used in $\mathbf{P_{13}}$, see chapter 2). This comparison was reasonable since the solution PL of the two polymers was measured at nearly the same excitation wavelength (~390 nm). Consequently, the solution PL spectra of $\mathbf{P_{13}}$ and of $\mathbf{P_7}$ (Figure 3.30) showed that the PL spectra of $\mathbf{P_{13}}$ was different from that of $\mathbf{P_7}$ and even different from the carbazole

homo-polymer **POCD**,[22] which was in accordance with the different absorption spectra obtained for the three polymers. Such differences in the PL spectra can be attributed to the delocalization of the singlet states over the backbone of polymer $\mathbf{P_{13}}$. Thus, it was not possible to differentiate one emitting chromophore.

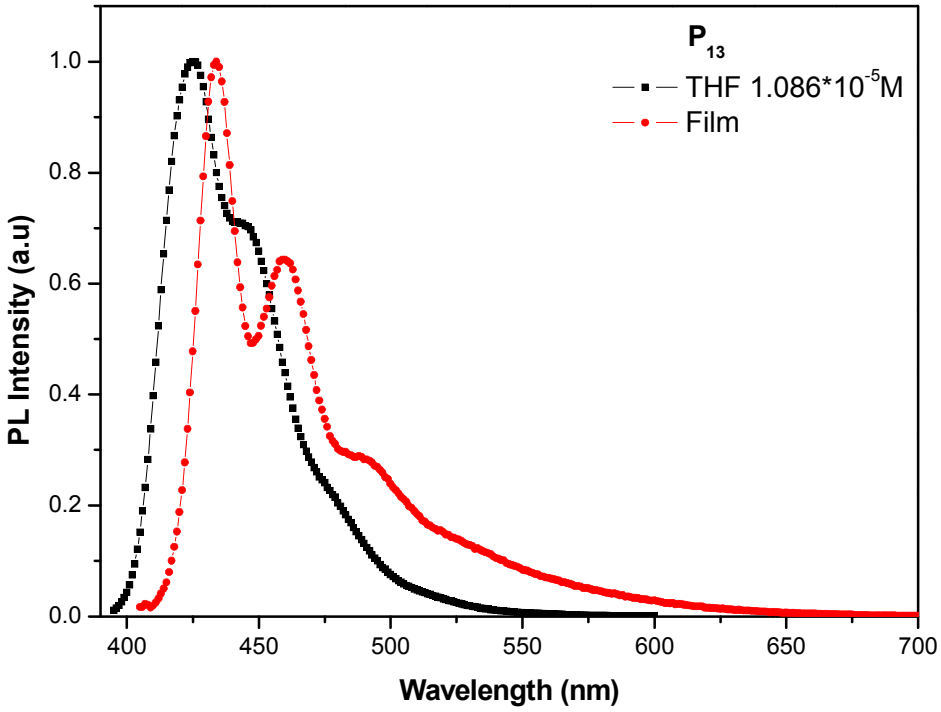

Figure 3.29 PL spectra of polymers $\mathbf{P_{13}}$ in solution and in thin film.

The quantum efficiencies (Φ_{PL}) of polymers $\mathbf{P_{13}}$ was measured in solution, which was upon excitation at 365 nm in THF, using 9,10-diphenylanthracene[15] as a standard found to be 1 (for detailed explanation of the measurement see chapter 2, section 2.3.2.3). This value was higher than that of **PODC** and poly(*N*-aryl-2,7-carbazole) **Pm*p*EHC**, which showed quantum efficiencies of 0.8 and 0.75, respectively.[8,9] The film PL quantum efficiency of polymer $\mathbf{P_{13}}$ was also measured using an integrating sphere[19] Polymer $\mathbf{P_{13}}$ exhibited PL quantum yield of

52 %. This low quantum yield values in film compared to solution can be attributed to excimer formation, which can be detected from the increased intensity of the emission peaks at the lower energy region of the film emission spectrum compared to the solution PL (Figure 3.29).

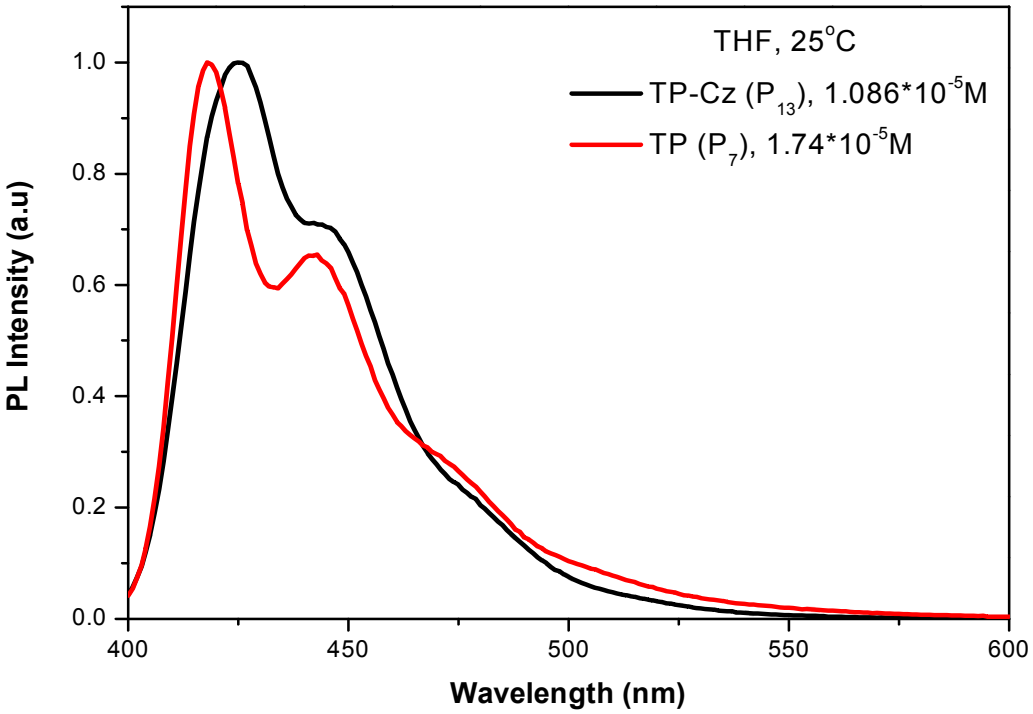

Figure 3.30 Emission spectra of polymer **P_{13}** compared to polymer **P_7**.

3.4.3 Electrochemical properties of polymer P_{13}

To investigate the redox properties, cyclic voltammogram was recorded for polymer **P_{13}** thin films against Ag/AgCl with a ferrocene standard (Figure 3.31).The polymer showed only anodic peak with irreversible oxidation, which can be ascribed to the electron rich nature of the polymer due to the presence of several alkyl chains on the edges of the polymers that

can work as an electron source, which may make it easier to oxidize rather than being reduced. Again, the HOMO and LUMO levels were calculated as described by *Janietz et al*.[16]

The irreversible oxidation peak of polymer **P_{13}** was at 1.62 V with onset oxidation potential of 1.47 V. The HOMO and LUMO values were at 5.87 and 3.0 eV, respectively with optical band gap of 2.87 eV. These electrochemical properties of **P_{13}** was very comparable to those of **Pm*p*EHC**, which exhibited HOMO of 5.6 eV and LUMO of 2.7 eV.[9]

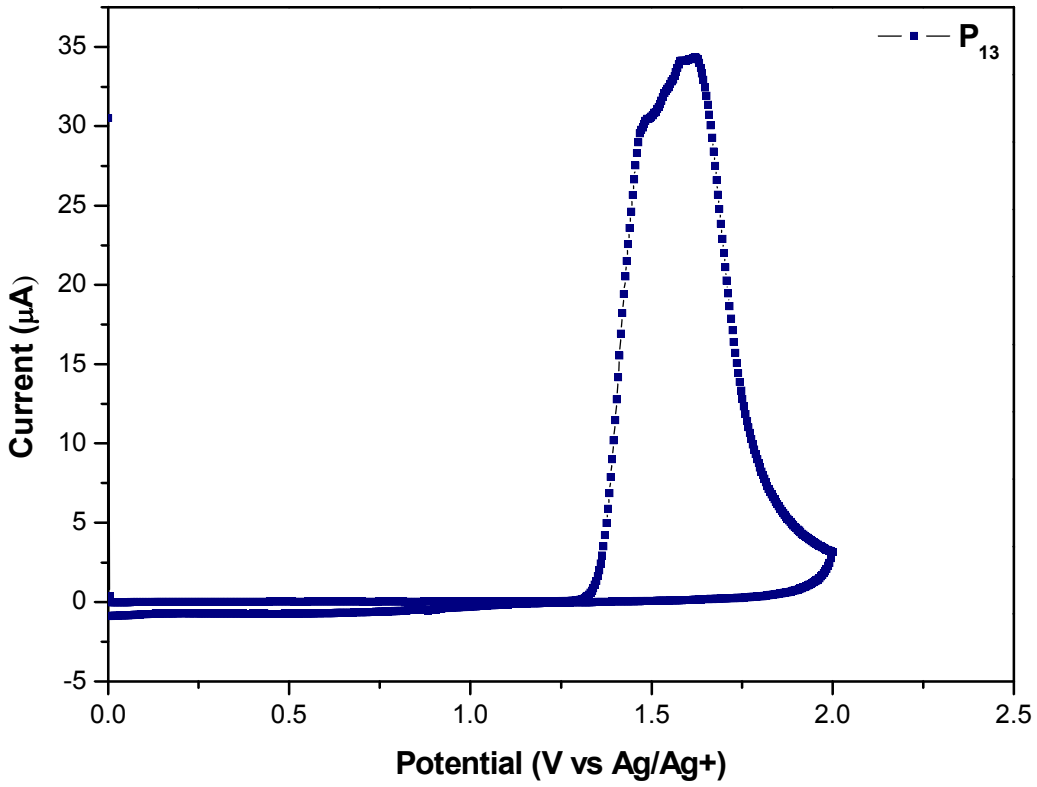

Figure 3.31 Cyclic voltammogram of drop caste film of **P_{13}** from toluene solution on Pt-electrode in 0.1 M $TBAClO_4$ in acetonitrile solution vs Ag/Ag^+. Scanning rate100 mV/s.

3.4.4 Differential scanning calorimetry

As the phase transition temperatures at which the material can form a liquid crystalline phase or even an isotropic melt is very important material property. DSC for polymer **P_{13}** was

investigated. The polymer demonstrated no significant peaks in the DSC curve, and no phase transition was recorded for **P_{13}** during the DSC measurements in the temperature range of –150°C to 300°C. Figure 3.32 displays the DSC curves for polymer **P_{13}**.

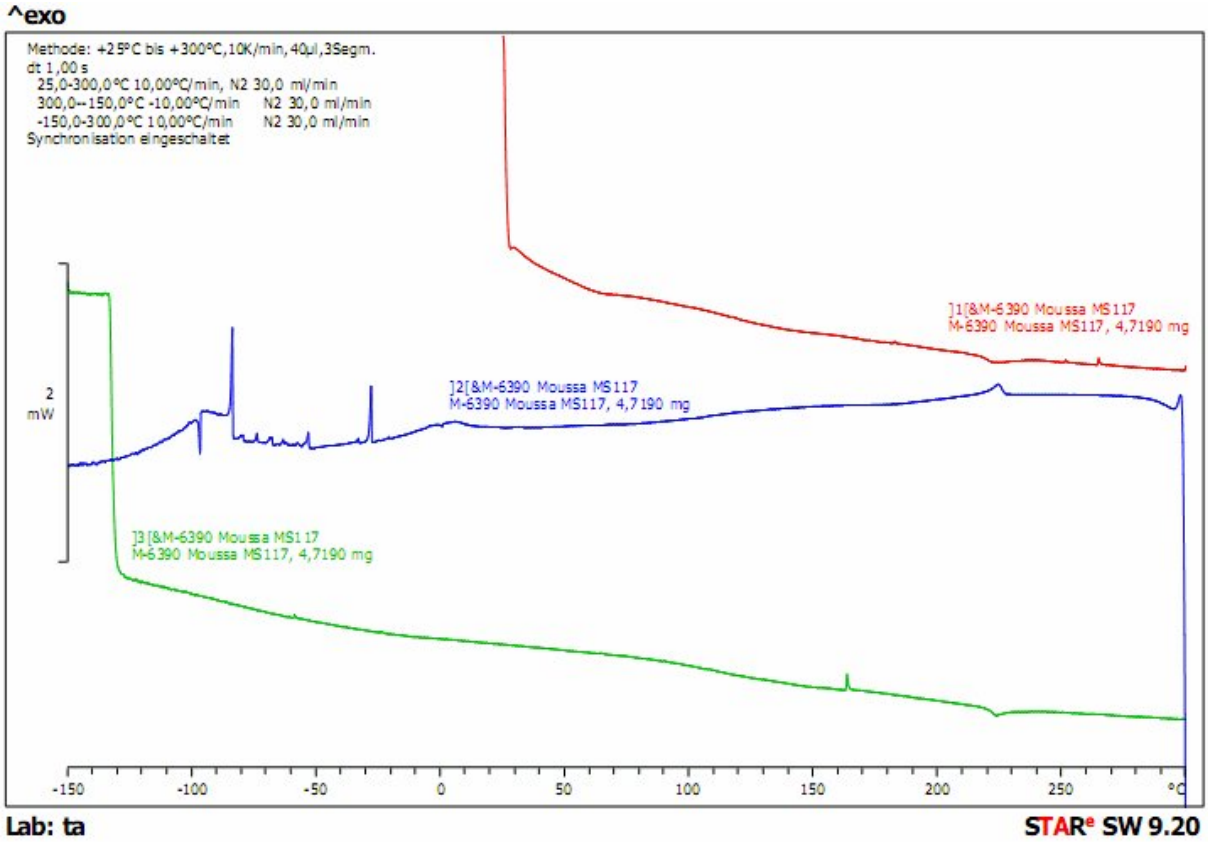

Figure 3.32 DSC curve for polymer **P_{13}**.

3.4.5 Thermogravimetric analysis

TGA analysis was used to study the thermal stability of polymer **P_{13}**. The experiment was done under nitrogen atmosphere by measuring the sample weight loss while heating at a rate of 10°C / min. **P_{13}** depicted good thermal stabilities with onset degradation temperatures above 300°C, which can be attributed to the loss of the alkyl chains on the polymer backbone. These values were comparable to those of polymers **P_1**-**P_{12}** described in chapter 2 and 3, but lower than those reported for the Poly(3,6-dihexyl)2,7-carbazole **27PCH** that exhibited thermal stabilities up to 415°C.[23] The TGA curve of polymer **P_{13}** (Figure 3.33) revealed a

thermal stability of the polymer up to 320°C, however after this temperature a degradation process was noticed till a temperature of 580°C. The measured total weight loss was about 46 %, which was close to the alkyl chains' weight percentage (49 %) in the repeating unit of the polymer. Consequently, the reported weight loss can be ascribed to the loss of the alkyl chains from the polymer chains.

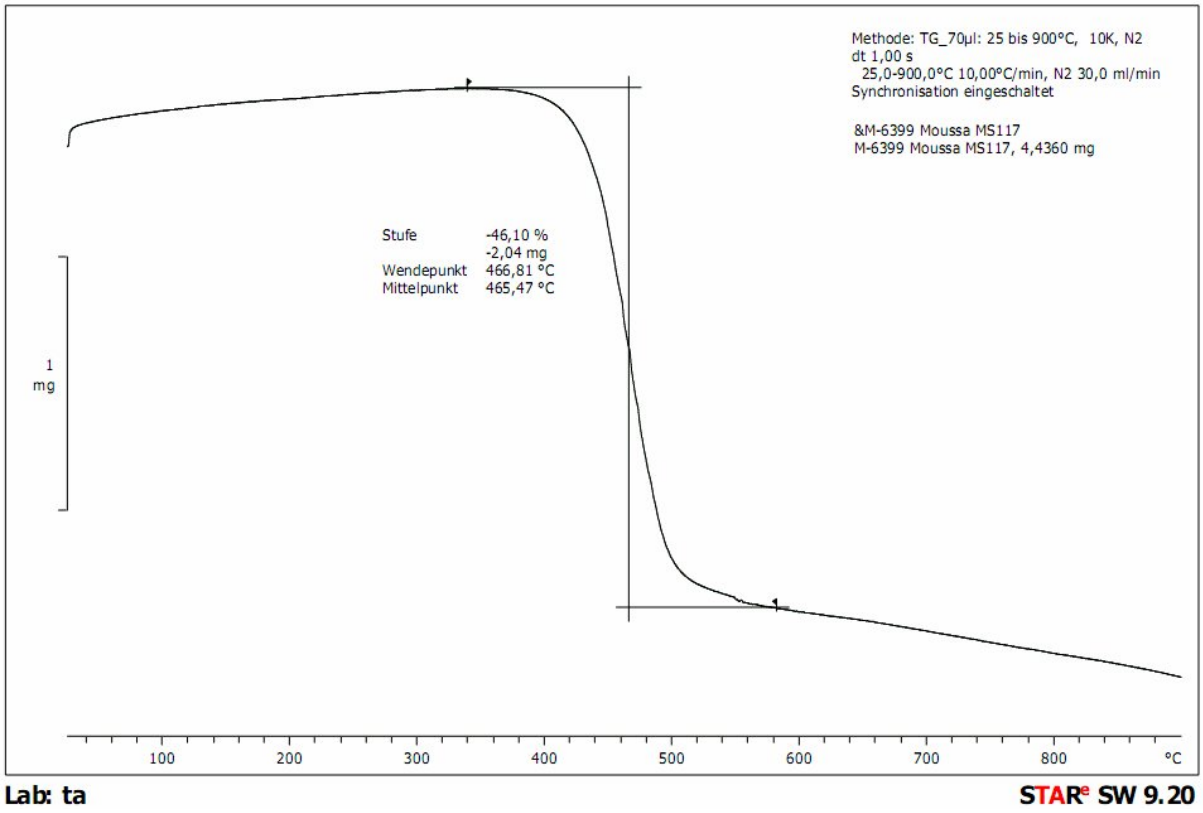

Figure 3.33 Thermogravimetric analysis results of polymer $\mathbf{P_{13}}$.

3.4.6 Supramolecular organization of polymer ($\mathbf{P_{13}}$)

The supramolecular organization of polymers $\mathbf{P_{13}}$ in solid-state was studied by using 2D-WAXS on extruded filaments. The method for the sample preparation is described in chapter 2 (Section 2.6). The Polymer was extruded at 230°C. At such temperature the polymer became plastically deformable and was extruded as thin filament, which was positioned vertically towards the 2D detector. Polymer $\mathbf{P_{13}}$ revealed quite similar X-ray patterns (Figure 3.34) as polymer $\mathbf{P_{11}}$ (containing the same triphenylene unit) indicating an identical

organization. Similar to the X-ray pattern for **P_{11}** the equatorial reflections in **P_{13}** (marked as "1") in the wide-angle scattering range attributed to 0.44 nm stacking distance, which was due to the non-covalent interactions between polymer backbones, which represent the sign for the lamellae packing. The other two reflections in the small-angle scattering range (marked as "2") were ascribed to the spacing between lamellae structures in which the polymers are packed. The d-spacing for the reflection "2" was 1.79 nm.

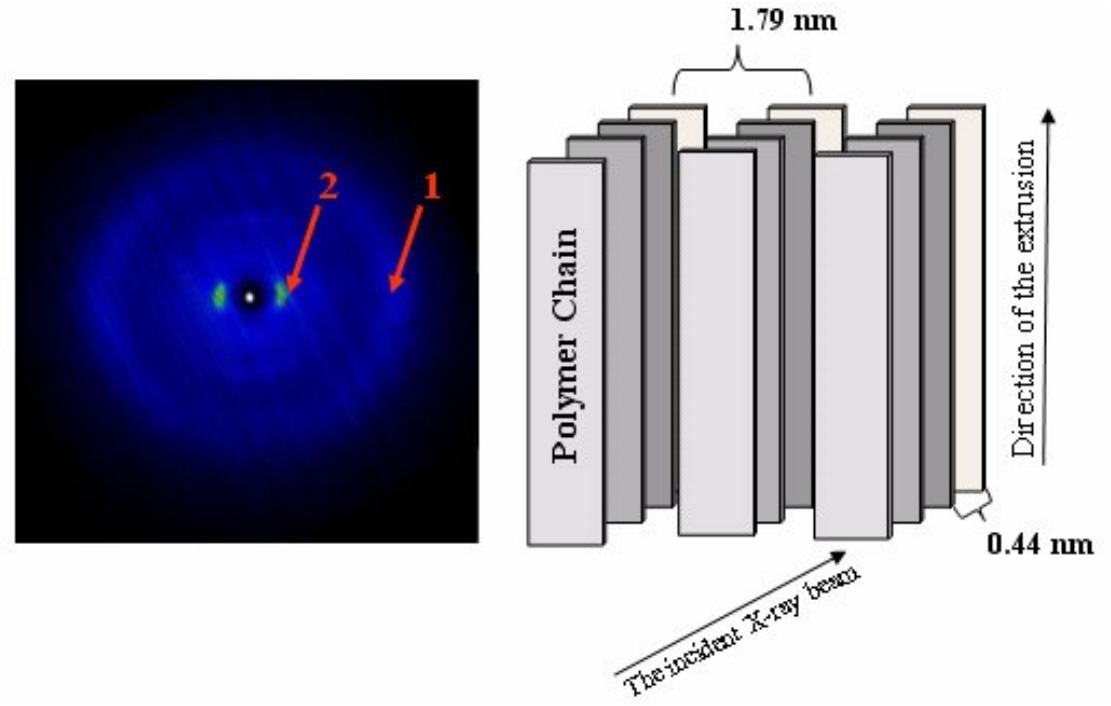

Figure 3.34 X-ray pattern and schematic illustration of supramolecular organization of **P_{13}**.

Comparing these 2D-WAXS results with those of the previously described co-polymers (refer to chapter 2, section 2.6), where the presence of the arylene groups between the triphenylene repeating units led to a high degree of ordering (organization) indicates that: replacing the arylene groups by the carbazolylene units saved the good arrangement in these compounds. However, the absence of the second-ordere reflections indicates a weaker ordering as compared to the triphenylene-arylene-based co-polymers. This can be associated with the high steric demand of the branched alkyl chains as compared to linear alkyl substituents.

3.4.7 Performance of polymer P_{13} in polymeric light emitting diodes (PLEDs)

These studies were performed by Moussa Saleh and Young-Seo Park at the OLED centre at Seoul National University. The electroluminescent property of the material was tested by incorporating the polymer (EML) into a device, similar in structure and fabrication procedure to the one presented in figure 3.21. The toluene solution of polymer **P_{13}** was deposited by spin-coating, followed by heating at 150^{o}C under N_2 for 10 min. The cathode (Ca) was vacuum deposited to give a 10 nm thick layer covered with a 100 nm thick silver layer.

The PLED device fabricated from polymer **P_{13}** (Figure 3.35a) depicts the usual behavior of PLEDs, where the current density increases exponentially by the increase of the applied bias voltage. The device exhibited a turn-on voltage of 4.5 V. The Max.η_L was found to be 0.013 cd/A corresponding to a bias of 11.7 V (Figure 3.35b). As previously discussed for polymers **P_{11}** and **P_{12}** (have the same device structure), the reason for such poor luminance efficiency can be ascribed to the large hole injection barrier between PEDOT:PSS (5.2 eV) and the HOMO energy level of **P_{13}** (5.87 eV) that hinder the hole-injection into the EML. Accordingly, unbalanced ratio of electrons and holes will be introduced to the polymer, which results in such low device efficiency. That can be solved by using a hole-transporting layer between the anode and the EML. In addition, this weak device performance was in agreement with the low degree of ordering of polymer **P_{13}** (see 2D-WAXS pattern) that can result in reduced charge carrier mobility.

Figure 3.36 displays the EL spectrum of the device of **P_{13}**, the PLED exhibited greenish-blue EL with maximum peak at 432 nm, which was accompanied with a broad shoulder between 500 and 600 nm. The reason of such broad shoulder is not yet clear and needs further studies. The device reveled CIE color coordinate of x = 0.23 and y = 2.0, with Max.ELQE of 0.006 %. Although, the device performance and the EL spectrum of **P_{13}** was not so promising, the device needs first to be reconstructed using a proper hole transporting

layer before we can give a final assessment about the quality of polymer **P_{13}** as an active layer in blue-PLEDs.

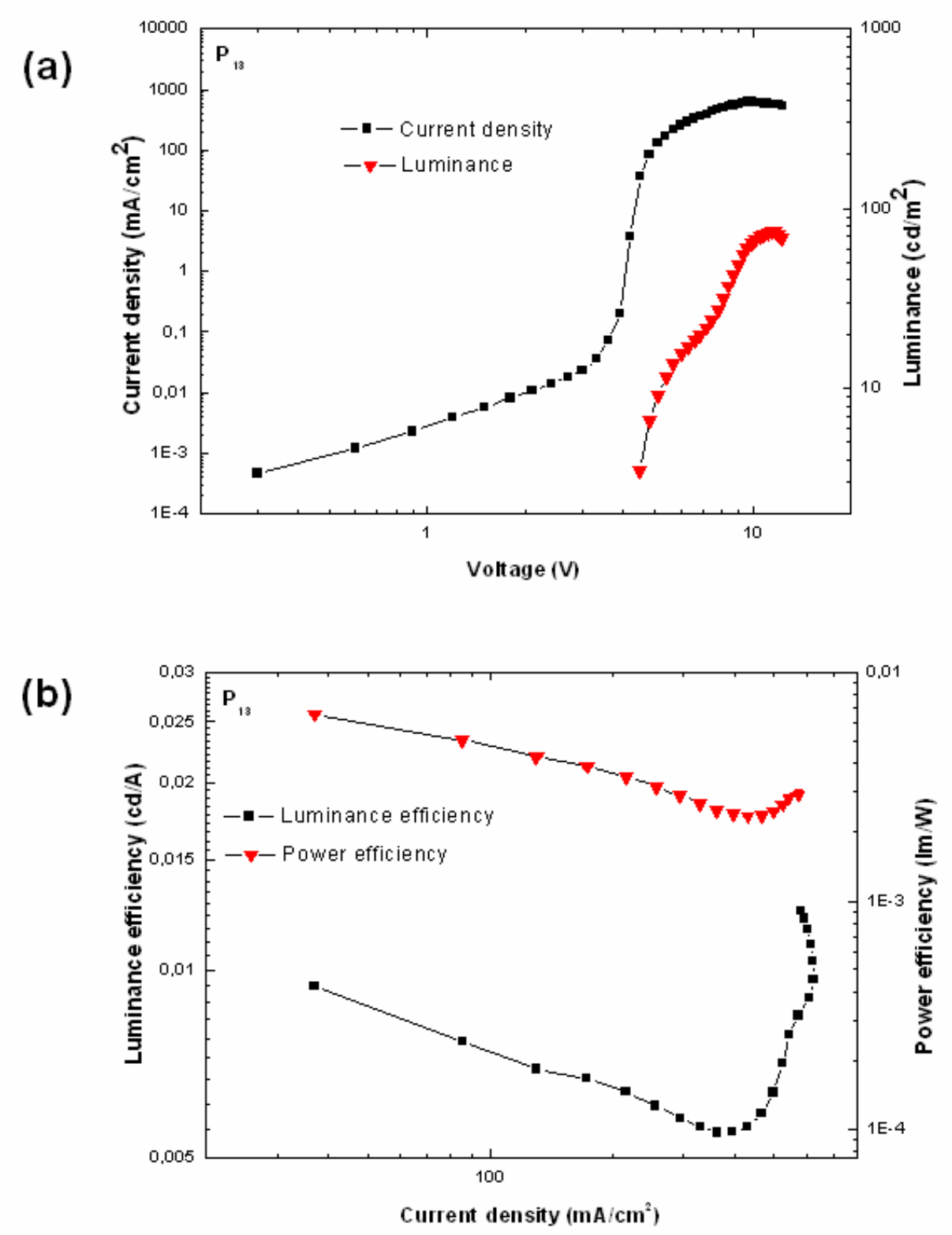

Figure 3.35 Current density–voltage–luminance characteristic of the device of **P_{13}** (a). Luminance efficiency and power efficiency of the PLED of **P_{13}** (b).

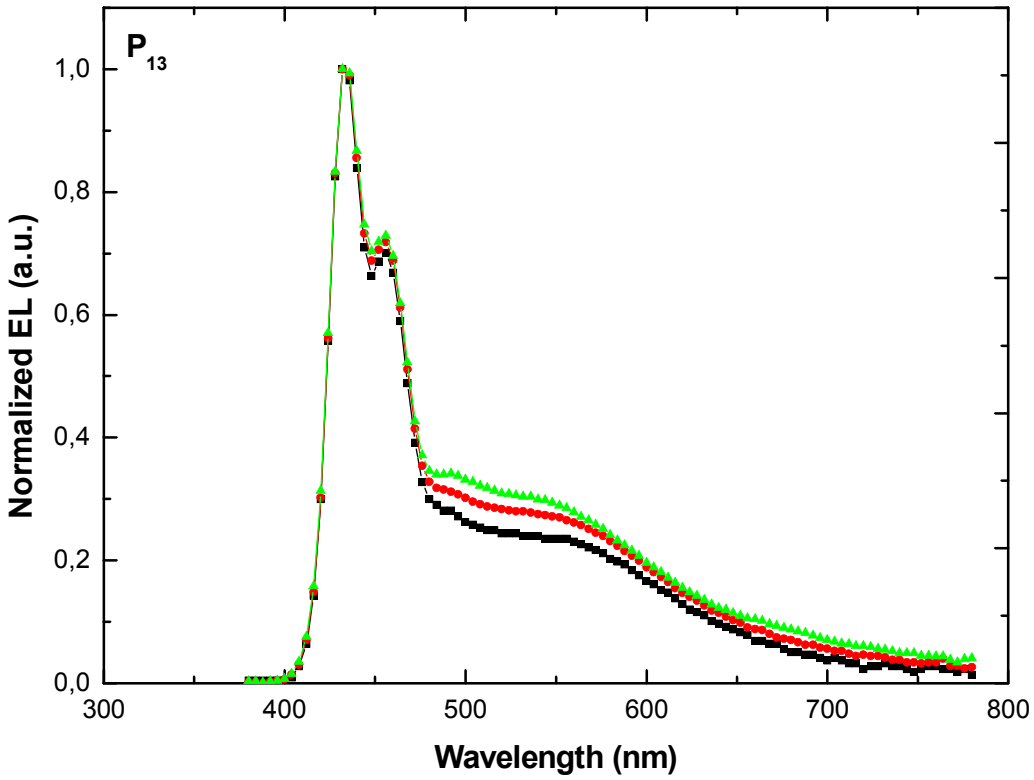

Figure 3.36 Normalized EL spectra of the device of $\mathbf{P_{13}}$.

3.5 Conclusions

The study presented here report for the first time the combination of the triphenylene(**TP**) chromophore with the pyrene (**Py**), fluorene (**F**), and carbazole (**Cz**) chromophores to afford four novel TP-Py ($\mathbf{P_{10}}$), TP-Fs ($\mathbf{P_{11}}$ and $\mathbf{P_{12}}$), and TP-Cz ($\mathbf{P_{13}}$) polymers for the applications in blue-PLEDs . The polymers synthesis was accomplished by using the MA-Suzuki-Miyaura and Yamamoto polycondensation reactions.

Polymer $\mathbf{P_{10}}$ exhibited deep blue emission in solution with emission maxima centered around 442 nm that was in agreement with the solution emission maximum (441 nm) of the Tetraalkoxypyrene polymer (**PPyr2**).[10b] Polymers $\mathbf{P_{11}}$, $\mathbf{P_{12}}$ as well as $\mathbf{P_{13}}$ showed also blue PL

in solution with their maxima around 420 nm, which was identical to the PL of **PFO** in case of $\mathbf{P_{11}}$ and $\mathbf{P_{12}}$, while different from that of the homo-carbazole polymer **PODC** in case of $\mathbf{P_{13}}$. It was also proven that Förster energy transfer was possible in polymer $\mathbf{P_{10}}$, with the triphenylene moiety in the polymer backbone working as donors, while the pyrene chromophors served as acceptors. However, FRET was not clear for $\mathbf{P_{11}}$, $\mathbf{P_{12}}$, and $\mathbf{P_{13}}$. The film emission maxima for all polymers were centered about 430 nm, but with pronounced low energy bands that extended up to 650 nm in all cases (can be attributed to excimer formation) and with different spectral shapes that can be attributed to the different moieties on the polymer backbones. The effect of the reduced number of benzene rings around the triphenylene moiety was not clear in the film PL of polymer $\mathbf{P_{11}}$, since it did not show extra red-shift and the spectra were comparable to that of polymer $\mathbf{P_{12}}$ with more aryl units around the triphenylene units. This behavior was probably the result of the effect of the bulky alkyl chains on the fluorene moiety that prevented aggregation in $\mathbf{P_{11}}$. The 2D-WAXS investigations displayed more ordered structure of $\mathbf{P_{11}}$ compared to $\mathbf{P_{12}}$. Such higher degree of ordering was reflected by the more intense reflexes in the small-angle scattering range of the 2D-WAXS pattern of $\mathbf{P_{11}}$. On the other hand, very weak reflexes were recorded for $\mathbf{P_{12}}$ in the same range (Figure 3.19 and 3.20). The low degree of ordering in $\mathbf{P_{12}}$ in comparison to $\mathbf{P_{11}}$ can be ascribed to the existence of the bulky alkyl side chains attached to the fluorenylene units which are expect to be arranged out-of-plane together with the high steric hindrance of the aryl units around t the triphenylene units. Polymer $\mathbf{P_{13}}$ depicted also strong reflexes in the small-angle scattering range of the 2D-WAXS pattern as $\mathbf{P_{11}}$, which gave an indication for a well arranged structure. Finally, all polymers were used in the fabrication of blue PLEDs. The overall obtained PLED results revealed that polymer $\mathbf{P_{10}}$ (TP-Py) with its deep blue EL (x = 0.16, y = 0.12) and Max.η_L of 0.22 cd/A can be considered as good emitter for blue-PLED. Moreover, the efficiency of the device can be improved by choosing more proper hole-transporting material to be used in the device. While polymers $\mathbf{P_{11}}$ and $\mathbf{P_{12}}$ exhibited green EL

(due to the formation of keto-defects on the acidic methylene bridge hydrogen on the fluorene unit) with Max.η_L of 0.14 and 0.083 cd/A, respectively, polymer **P_{13}** showed greenish-blue EL with Max.η_L of 0.013 cd/A. The low device efficiency of polymers **P_{11}**, **P_{12}**, and **P_{13}** were attributed to the high hole-injection barrier between the anode and the HOMO energy level of the polymers due to the absence of a hole-transporting layer. Based on these results polymers **P_{11}** and **P_{12}** (TP-Fs) can not be used as blue emitters in PLED (emit only green color). On the other hand, a final judgment about the quality of polymer **P_{13}** (Tp-Cz) can not be given at the moment. **P_{13}** needs first to be incorporated in a device contains a hole-transporting layer in order to balance the holes and electron ratio in the EML, since in some cases the higher electron transport in the EML can result in a stronger emission at longer wavelength (as explained for devices 1-4 of polymer **P_2** in chapter 2).

3.6 References

(1) Leclerc, M. *J. Polym. Sci.*, *Part A: Polym. Chem*. **2001**, 39, 2867–2873.

(2) Bernius, M.; Inbasekaran, M.; Woo, E.; Wu, W.; Wujkowski, L. *Thin Solid Films* **2000**, 363, 55–57.

(3) Inagi, S.; Hayashi, S.; Fuchigami, T. *Chem. Commun*. **2009**, 1718.

(4) Neher, D. Macromol. Rapid. Commun. **2001**, 22, 1365.

(5) a) Scherf, U.; List, E. J. W. *Adv. Mater*. **2002**, 14, 477–487, b) Oldridge, L.; Kastler, M.; Müllen, K. *Chem. Commun*., **2006**, 885.

(6) Jegadesan, S.; Sindhu, S.; Advincula, R. C.; Valiyaveettil, S. *Langmuir* **2006**, 22, 780.

(7) Morin, J.-F.; Leclerc, M.; Ades, D.; Siove, A. *Macromol. Rapid. Commun*. **2005**, 26, 761–778.

(8) Morin, J. F.; Leclerc, M. *Macromolecules* **2001**, 34, 4680–4682.

(9) Koguchi, R; Kobayashi, N.; Shinnai, T.; Oikawa, K.; Tsuchiya,K.; Kijima, M. Macromol. Chem. Phys. **2008**, 4, 439-449.

(10) a) Kawano, S.; Baumgarten, M.; Müllen, K.; Murer, P.; Schäfer,T.; Saleh, M. Novel Polymers, International Publication Number **WO 2010/006852 A1**. b) Kawano, S.; Yang, C.; Ribas, M.; Baluschev, S.; Baumgarten, M.; Müllen, K. Macromolecules **2008**, 41, 7933-7937.

(11) Qin, T. "New Design of Polyphenylene Dendrimers for Full-Color Light-Emitting Diodes" PhD. Thesis, University of Mainz, 2010.

(12) Gronheid, R.; Hofkens, J.; Kohn, F.; Weil, T.; Reuther, E.; Müllen, K.; De Schryver, F. C. J.Am. Chem. Soc. **2002**, 124, 2418.

(13) Qin, T. S. ; Zhou, G.; Scheiber, H.; Bauer, R. E.; Baumgarten, M.; Anson, C. E. ; List, E. J. W.; Müllen, K. Angew. Chem., Int. Ed. **2008**, 47,8292.

(14) Schlüter, A. D. J. Polym. Sci. Part A: Polym. Chem. **2001**, 39, 1533-1556.

(15) Joshi, H. S.; Jamshidi, R.; Tor, Y. Angew. Chem.Int. Ed. **1999**, 38, 18.

(16) Janietz, S.; Bradley, D. D. C.; Grell, M.; Giebeler, C.; Inbasekaran, M.; Woo, E. P. Appl. Phys.Lett. **1998**, 73, 2453-2455.

(17) Fabre, B. Electrochem. Commun.**2001**, 3, 549-552.

(18) Su, H-J.; Wu, F-I.; Shu, C-F. Macromolecules **2004**, 37, 7197-7202.

(19) Jeong**,** W.-I.; Kim, S.-Y.; Kim, J-J.; Kang, J.-W. Chem. Phys. **2009** 355, 25–30.

(20) List, E. J. W.; Guentner, R.; de Freitas, P. S.; Scherf, U. *AdvancedMaterials* **2002**, *14*, 374-378.

(21) Gao, P.; Feng,X.; Yang, X.; Enkelmann, V.; Baumgarten, M.; Müllen, K. J. Org. Chem. **2008**, *73*, 9207–9213.

(22) Morin, J. F.; Leclerc, M. *Macromolecules* **2002**, 35, 8413.

(23) Lévesque, I.; Bertrand, P.-O.; Blouin, N.; Leclerc, M.; Zecchin, S.; Zotti, G.; Ratcliffe, C.-I.; Klug, D.-D.; Gao, X.; Gao, F.; Tse, J. *Chem. Mater*. **2007**, 19, 2133.

Chapter 4

From Triphenylene-based Polymers to Graphene Nanoribbons

As mentioned in chapter 1 (general motivation section), the concept of graphene nanoribbons as well as a novel synthesis of several nano-graphene ribbons from a series of triphenylene-based polymers will be presented here.

The target molecules were fabricated by subjecting the precursor molecules to oxidative cyclodehydrogenation reaction conditions.

4.1 Introduction

Polycyclic aromatic hydrocarbons (**PAHs**) are chemical compounds that consist of fused aromatic rings and do not contain heteroatoms or carry substituents. **PAHs** occur in oil, coal, and tar deposits, and are produced as byproducts of fuel burning. In graphene the **PAH** motif is extended to large two-dimensional (2D) sheets.[1] Graphene is a monolayer of carbon atoms packed into a 2D honeycomb lattice, and can be considered as the basic structure element of several carbon allotropes such as graphite, fullerenes, and carbon nanotubes. However, when graphenes found as thin strips it is known as graphene nanoribbons (**GNRs**). In addition, graphene has emerged as a promising candidate material for nanoelectronics applications and graphene-based devices since it exhibits impressive electronic and mechanical properties (charge-carrier mobility = 250 000 cm^2 V^{-1} s^{-1} at room temperature, thermal conductivity = 5000 W m^{-1} K^{-1}, and mechanical stiffness = 1 TPa).[2-7]

GNRs were originally introduced as a theoretical model by Mitsutaka Fujita and coworkers to examine the edge and nanoscale size effect in graphene.[8-10] However, the first single-layer graphene nanosheets were first characterized in 2004, when a research group at

the University of Manchester led by Andrey K. Geim succeeded in isolating and studying the ultimate flatland-graphene by mechanical exfoliation (the "scotch-tape" method) of bulk graphite.[11] These achievement has opened the way to other production techniques by which **GNRs** have been prepared starting from graphite, graphene, or graphene oxide. These techniques include lithographic, [12-14] chemical,[15,16] sonochemical,[17] and chemical vapor deposition[18] methods. Moreover, two groups have recently separately reported very elegant methods for the production of **GNRs** based on the longitudinal unzipping of multiwalled carbon nanotubes (MWCNTs).[19,20]

Although, all the previously mentioned methods exhibited recognized success in the generation of **GNRs**, the uncontrollable character of these methods, the harsh conditions, or in some case the inferior electronic characteristics have strongly restricted the quality of the resulting graphenes, and consequently limited their applications. Other alternative method for the production of graphene-type molecules was the use of the organic synthesis, which led to the synthesis of different size graphenes.[21-25] In 2003 Müllen and coworkers reported the first ribbonlike graphite framework from branched polyphenylenes by oxidative cyclodehydrogenation using $FeCl_3$.[26] The kink-ribbon (Scheme 4.1) was ~1 nm wide, and showed insolubility in organic solvents. Therefore, solid state analytical methods were conducted. The solid-state UV-Vis spectroscopy demonstrated a wide and unstructured absorption band covering the visible range of the electronic spectrum (λ_{max} ~ 800 nm) that confirmed the highly extended conjugated framework. Raman spectroscopy was also recorded for the ribbon and the profile of the visible Raman spectrum was characterized by two strong bands (at 1603 and 1322 cm^{-1}), corresponding to the G and D bands of graphite.[26]

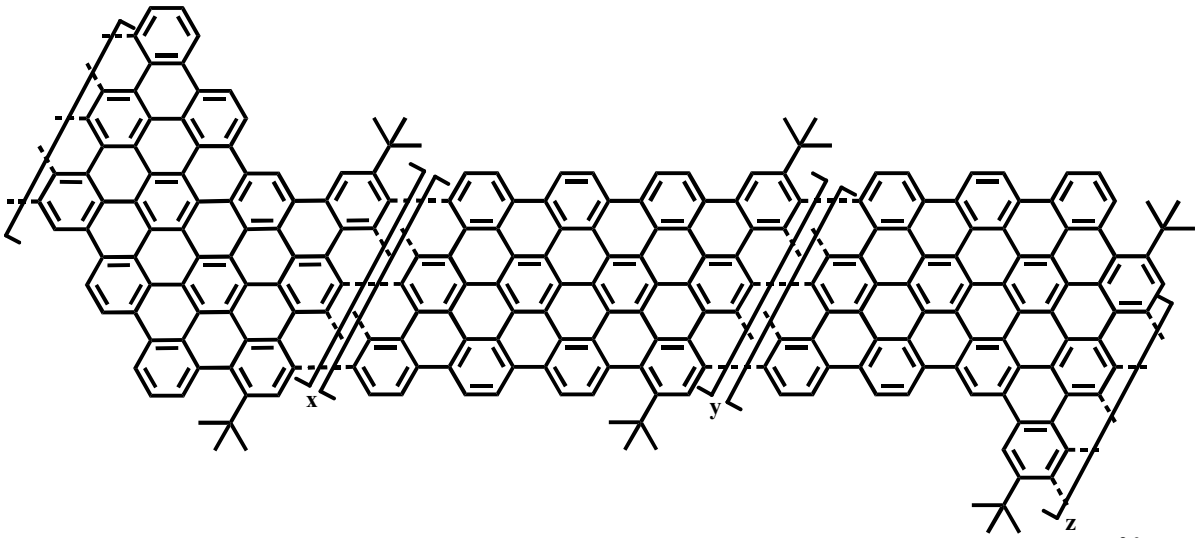

Scheme 4.1 Ribbonlike graphitic framework reported by Müllen and coworkers.[26]

After this work and particularly in 2008, the same group presented a novel method for the synthesis of linear 2D-graphene nanoribbons. The obtained **GNRs** (Scheme 4.2) showed good solubility in THF, and exhibited lengths up to 12 nm, which were never achieved before using the bottom up synthetic approach. The material was studied by several analytical methods such as MALDI-TOF mass spectroscopy (MS), scanning electron microscopy (SEM) scanning tunneling microscope (STM), transmission electron microscopy (TEM), and UV-Vis spectroscopy. The reported absorption maximum (λ_{max}) for the ribbons (in THF) was at 485 nm, which was 200 nm bathochromically shifted compared to the used precursor polymers. While MALDI-TOF spectra showed clearly molecular weights corresponding to the fused **GNRs**, the STM, SEM, and TEM studies depicted a well ordered-stacking for graphene layers with interlayer distance (d-spacing) of 3.4 Å, which revealed the formation of **GNRs**.[22]

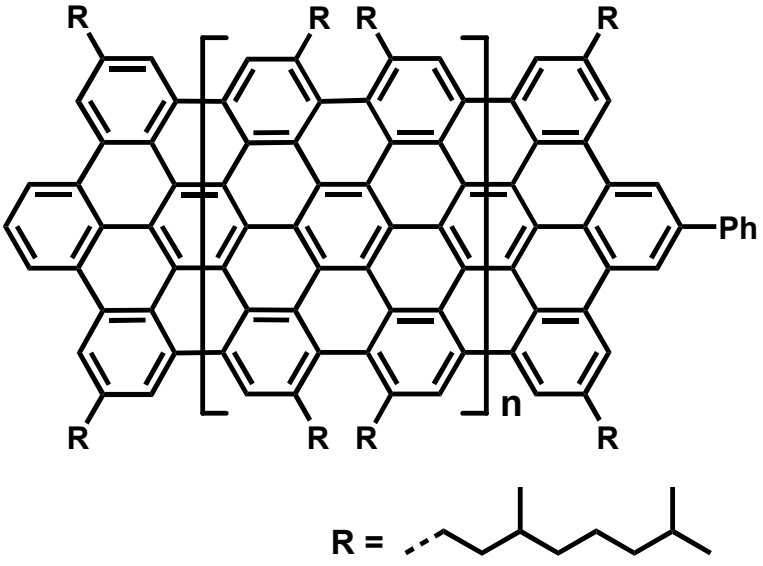

Scheme 4.2 Linear **GNRs** reported by Müllen and coworkers.[22]

Following the above demonstrated work by our group, we present here a novel synthesis of **2D-GNRs** starting from the previously described conjugated TP-based polymers (chapter 2).

The synthesis of the **GNRs** followed a bottom-up approach and was achieved by utilizing two major routes:

i) *Solution route*: By oxidative cyclodehydrogenation of the precursor polymers using Scholl reaction conditions.

ii) *Surface route*: Using surface-assisted coupling of monomer precursors into linear polyphenylenes followed by their subsequent cyclodehydrogenation.

The two methods will be described and discussed in the next sections.

4.2 Synthesis of GNRs using Scholl reaction conditions

4.2.1 Synthesis of 6,11-Bis-(4-tert-butyl-phenyl)-1,2,3,4-tetraphenyl-triphenylene (model compound)

The synthesis toward the desired **GNRs** started with the study of the suitable cyclodehydrogenation reaction conditions for the model compound 6,11-Bis-(4-tert-butyl-phenyl)-1,2,3,4-tetraphenyl-triphenylene **(17)** (Scheme 4.3). The scheme depicts the MA-palladium-catalyzed Suzuki-Miyaura coupling reaction of compound **5d** (described in chapter 2) and 4-tert-butylbenzeneboronic acid **(16)** (commercially available) that afforded compound **17** in a yield of 43 %. Such moderate yield was attributed to the loss of some of the product during the purification using column chromatography, due to the presence of other unidentified side products that were formed during the coupling reaction and were similar in polarity to compound **17**, which made the separation process quite difficult. Subsequently several intramolecular oxidative cyclodehydrogenation reactions were carried out in DCM using $FeCl_3$ as an oxidant at 25°C. The initial attempts were carried out by reacting compound **17** with $FeCl_3$ (3equivalent / 1H) in DCM at 25°C for 1.5 hours, and for 5 hours, however the target product was not detected when using MALDI-TOF MS.

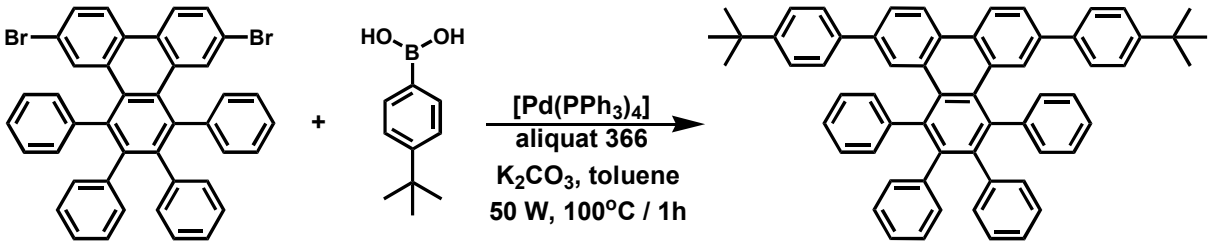

Scheme 4.3 Synthesis of 6,11-Bis-(4-tert-butyl-phenyl)-1,2,3,4-tetraphenyl-triphenylene **(17)** via MA-Suzuki-Miyaura coupling.

Only treating precursor **17** with $FeCl_3$ (6 equivalent / 1H) at 25°C for 5 hours afforded the final semi-triangle-shaped discotic graphene molecule **18** in 90 % yield (Scheme 4.4). Compound **18** was insoluble in common organic solvents, nevertheless when the material was heated (in 1,2,4-trichlorobenzene (TCB)) and sonicated in ultrasonic bath for 1 hour, a suspension of the material was formed. Such poor solubility in organic solvents reflects the great tendency of the compounds toward aggregate formation, which reduce the solubility in a dramatic way. Therefore the product was characterized by using MALDI-TOF MS (tetracyanoquinodimethane (TCNQ) matrix) using a solid-state sample preparation method that showed a single species (at 782 m/z) with isotopic distributions, which was in accordance with the calculated mass of compound **18** (Figure 4.1a). Because of the high carbon content of the PAH, combustion was incomplete (soot formation), which resulted in values lower than expected for the carbon content.

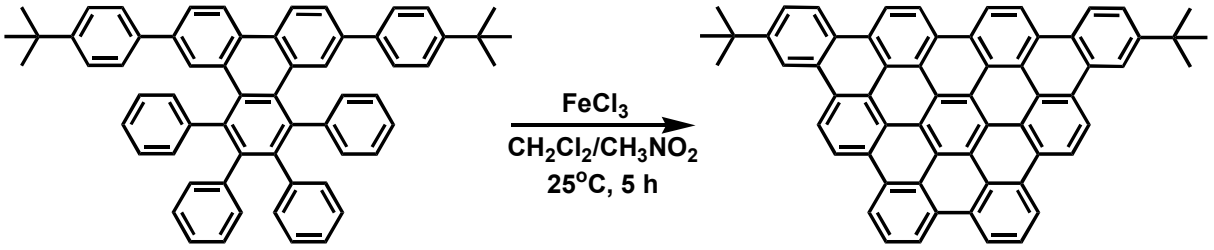

17 **18**

Scheme 4.4 Synthesis of semi-triangle-shaped discotic graphene molecule **18**.

The UV-Vis absorption of **18** (Figure 4.2) was studied using a suspension of the compound in TCB. The spectrum exhibited three types of bands α (not detected due to low intensity), β (at 330 nm), and p (at 385 nm) that are typical for large PAHs.[24b] Moreover, the recorded absorption maximum (λ_{max}) at 330 nm was 29 nm bathochromically shifted compared to that of the corresponding precursor molecule **17** (λ_{max} = 301 nm). Such red-shift suggests a higher conjugation in compound **18** compared to its precursor molecule **17** as result

of the formed fused structure. In contrast to the PAH triangle molecule C_{60} H_{24} (Figure 4.1b) that was synthesized by Feng et al.,[24b] a 70 nm blue-shift of the absorption maximum was observed for **18**, which can be attributed to the lower conjugation in **18** compared to the triangle molecule C_{60} H_{24}.[24b]

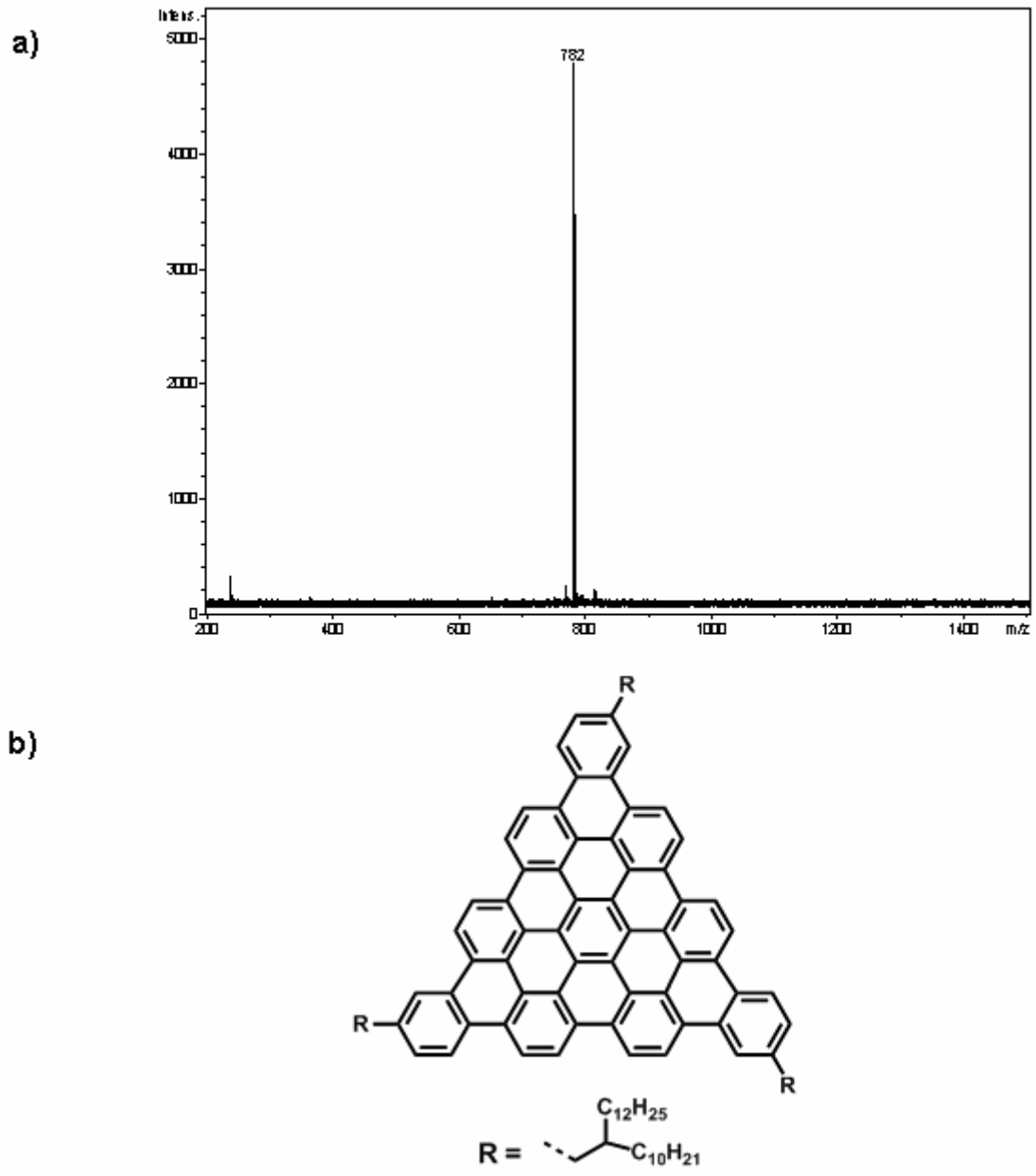

Figure 4.1 a) MALDI-TOF MS obtained by applying the dry sample preparation with TCNQ as matrix to a sample containing a significant amount of target molecule **18**. b) Molecular structure of the PAH triangle molecule C_{60} H_{24}.

The success in synthesizing the model compound **18** using the intramolecular oxidative cyclodehydrogenation reaction showed that, using 3 equivalents (per hydrogen) from the oxidant $FeCl_3$ were not enough to accomplish the cyclodehydrogenation reaction in this system. However, when 6 equivalents were used at 25°C the fully fused molecule **18** was generated. Knowing the proper Scholl reaction conditions for our small TP-based molecule, motivated us to apply the same reaction conditions for some of the previously synthesized conjugated TP-based polymers (chapter 2) in order to generate more extended aromatic **GNRs**.

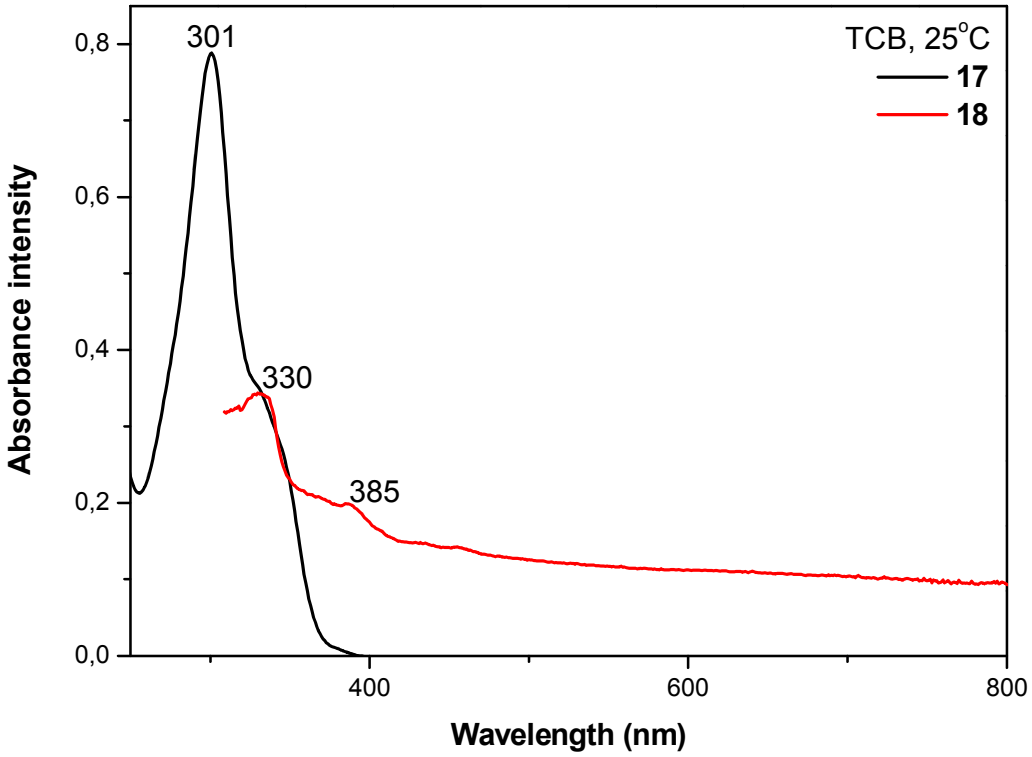

Figure 4.2 UV-Vis spectra of the PAH **18** (red line) and its corresponding precursor molecule **17** (black line) in TCB at 25°C.

4.2.2 Synthesis of GNR-20

The synthesis started with the preparation of the related precursor polymer. Using the nickel (0) mediated MA-Yamamoto polymerization reaction (Scheme 4.5) of monomer **5d** (refer to Chapter 2) at 80^{o}C and by using a microwave power of 80 W for one hour the homopolymers $\mathbf{P_{14}}$ was obtained in 88 % reaction yield. The polymer was insoluble in common organic solvents like THF, dichloromethane, and toluene. The insolubility can be attributed to the absence of any linear or branched alkyl chains at adjacent positions of the aromatic periphery, which are known to reduce aggregation in solution and enhance the solubility if present. While $\mathbf{P_{14}}$ was insoluble in common organic solvents it showed slight solubility when heated in TCB. However, it was not possible to detect the average molecular weight using the GPC analysis. Instead MALDI-TOF MS (TCNQ matrix) was utilized to determine the average molecular weight of the polymer. The MALDI mass spectrum of polymer $\mathbf{P_{14}}$ (Figure 4.3) consisted of a series of peaks with nominal masses corresponding to the integer multiples of the repeating units. The highest defined peak at about 11000 *m*/*z* was corresponding to 20 repeating units in the polymer backbone.

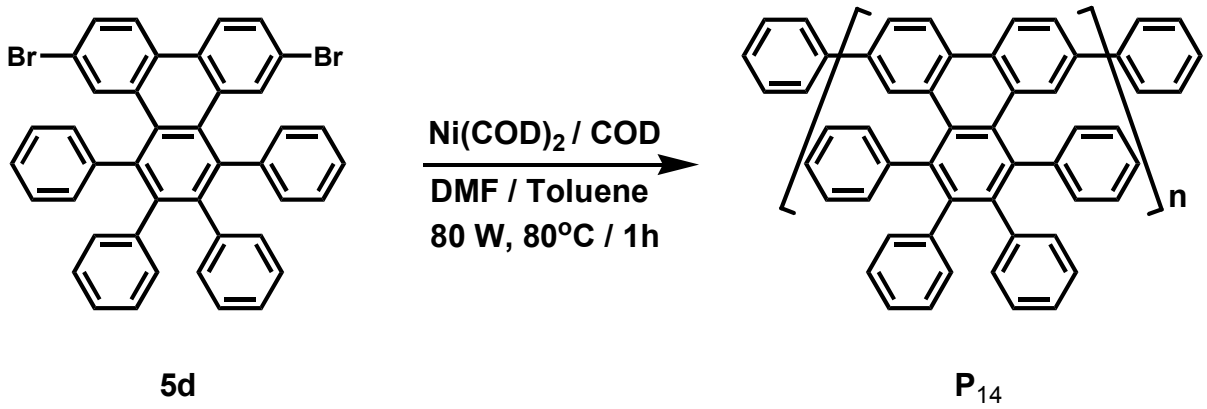

Scheme 4.5 Synthetic route of polymer $\mathbf{P_{14}}$ via Yamamoto coupling reaction.

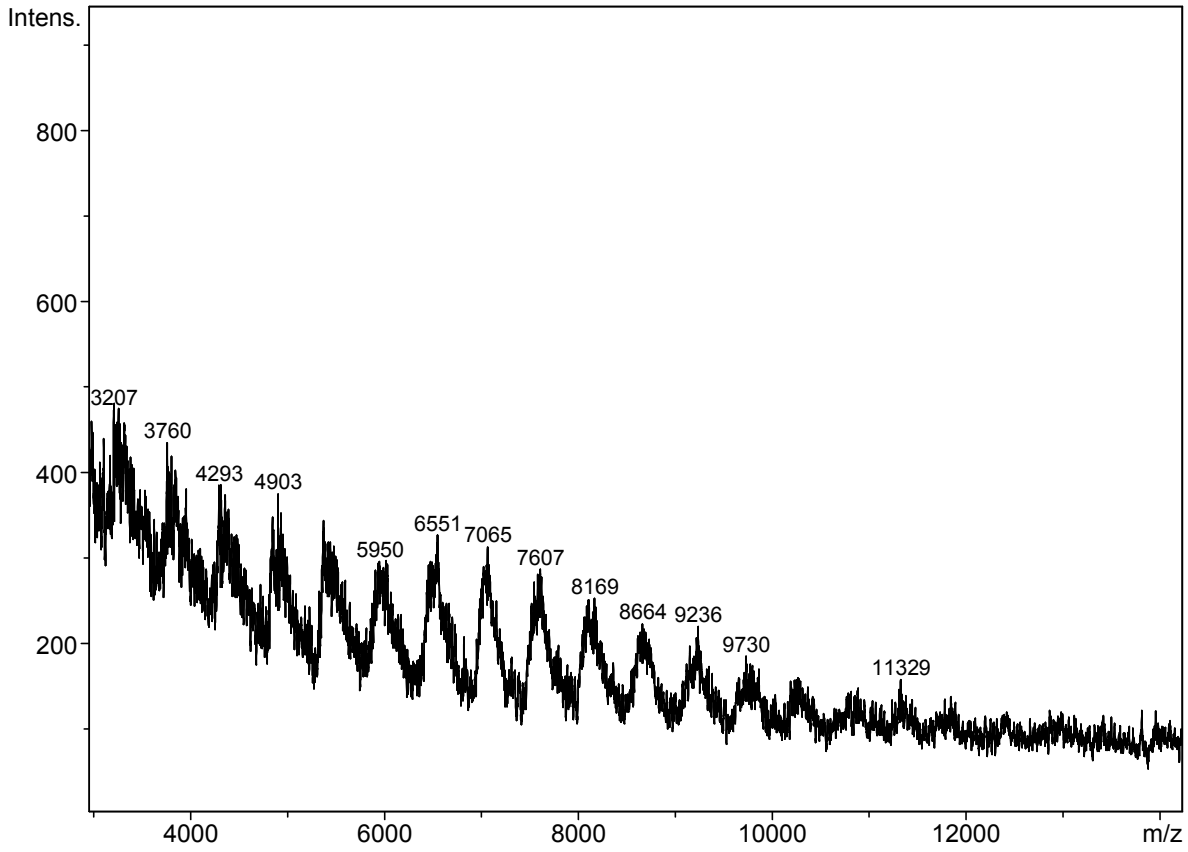

Figure 4.3 MALDI-TOF MS obtained by applying the dry sample preparation with TCNQ as matrix to a sample containing a significant amount of polymer $\mathbf{P_{14}}$.

In a mixture of CH_2Cl_2 / CS_2 the polymer was stirred and poor solubility of $\mathbf{P_{14}}$ in this solvents mixture was observed. As a result, the intramolecular Scholl reaction (Scheme 4.6) of the soluble part of $\mathbf{P_{14}}$ with $FeCl_3$ as oxidative reagent in CH_2Cl_2 / CS_2 at room temperature for 24 hours provided a black solid in 88 % yield.

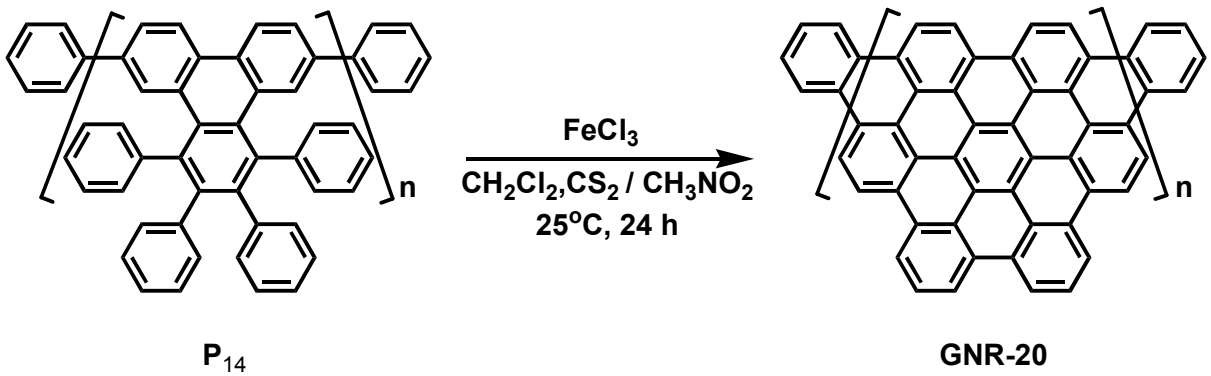

Scheme 4.6 Synthesis of **GNR-20**.

The black solid was as its precursor polymer **P_{14}** insoluble in the common organic solvents, while when heated and sonicated in TCB for about an hour it formed a suspension. The suspension of TCB was used to study the UV-Vis absorption of the material.

As shown in Figure 4.4, a broad absorption, with a continuum-like appearance in the visible range and an approximate maximum of 650 nm was observed for the formed black solid. The broad and unstructured profile of the absorption spectrum can be explained by the large number of electronic transitions taking place in this giant PAH.

Although, the UV-Vis absorption spectrum of the obtained material proposed that the obtained material was **GNR-20**, additional structure elucidation was required. However, due to the insolubility of **GNR-20** in common organic solvents further solution-based characterization methods were not possible and solid state-based analytical techniques were the only possible tool. Elemental analysis, which is usually used to test the purity of solid compounds was used, however the results exhibited inaccurate carbon content (33.53 % less than the expected value) that can be attributed to the incomplete combustion under soot formation of this high carbon content PAH. Raman spectroscopy is one of the solid state-based methods that demonstrated a great success in the determination of the extended π-conjugation and ordering of cyclodehydrogenated products and so it was utilized here.[26] The spectrum was recorded from a solid sample of **GNR-20** using 768 nm excitation laser wavelength. The first-order Raman spectrum was characterized by two relevant features, a first broad band situated approximately at 1327 cm^{-1} and a second more defined band located nearly at 1597 cm^{-1} (Figure 4.5). The investigations of vibronic frequencies and Raman intensities of several all-benzenoid PAHs (such as the graphite nanoribbons reported by J. Wu) of different, but well-defined structure and size revealed as common features a band near 1600 cm^{-1} that is known as the G band and other band near 1300 cm^{-1}, which is defined as the D band.[26] Generally speaking, the G band is the only feature observed in the first-order Raman spectrum of highly ordered, crystalline graphite, while the D peak results from imperfections

(mainly due to incomplete cyclodehydrogenation) and small conjugated domains with finite size.[26] Therefore, from the obtained Raman spectrum for **GNR-20** the band located at 1597 cm^{-1} can be assigned to the G band and that positioned at 1327 cm^{-1} to the D band.

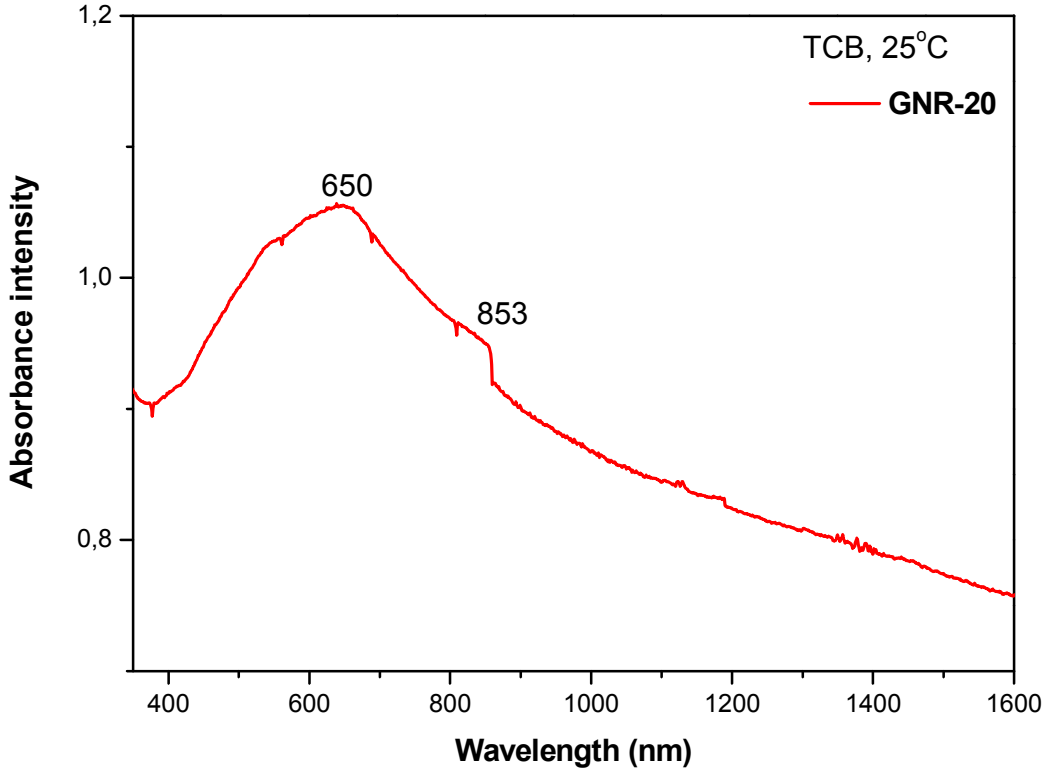

Figure 4.4 UV-Vis spectrum of **GNR-20**.

These results supported the thought that the Scholl reaction of $\mathbf{P_{14}}$ afforded the **GNR-20**. However due to the low intensities of the spectral peaks, it was not possible to perform in depth structure investigations such as determining the width of the GNR, which can be achieved from the integrated areas under the D and G bands (A (D) / A (G)).

To perform complete structural investigations, micro-Raman analysis was conducted. The method resulted in well resolved spectral signals, which provided a clear evidence for the formation of the **GNR-20** and allowed for complete structural analysis. The micro-Raman results of **GNR-20** will be presented and discussed later in a separate section within this

chapter together with the results of other two GNRs, which will be introduced soon, in order to have a direct comparison between the three systems.

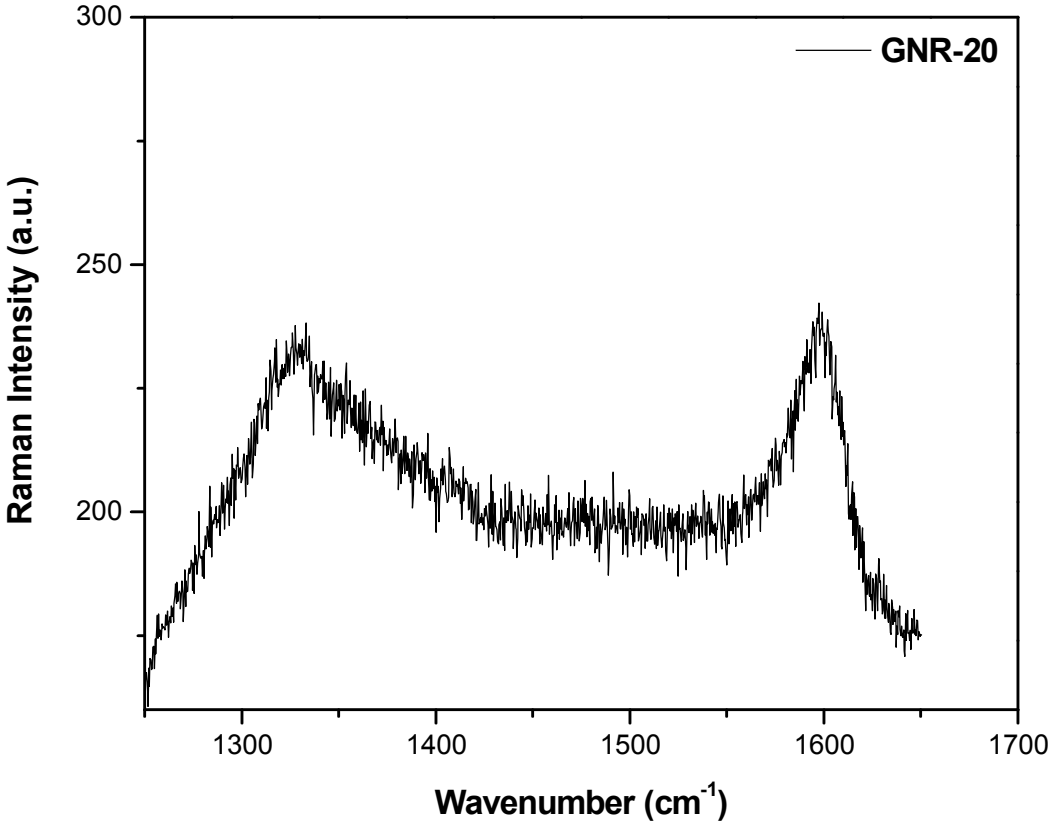

Figure 4.5 Raman spectrum of **GNR-20** using 768 nm excitation laser wavelength.

4.2.3 Synthesis of GNR-21

In order to improve the solubility of the desired **GNRs** for better later characterization, other alkyl substituted precursors were needed. Polymer **P_9** (described in chapter 2) with its long branched alkyl chains demonstrated a very good solubility (10mg / 1ml solvent) in common organic solvent and was our first candidate. Moreover, the high molecular weight (M_w = 77 × 10^3, PDI = 2.0) of **P_9** held a promise for producing large soluble **GNRs**. Thus polymer **P_9** was subjected to the Scholl reaction conditions ($FeCl_3$, CH_2Cl_2, and 25^oC) for 24 hours (Scheme 4.7) to result in a black solid in 80 % yield.

Although the product contains long branched alkyl chains on its aromatic margins that were expected to give rise to a soluble material, the obtained compound was insoluble in the common organic solvents that can be ascribed to high tendency of the material to form aggregation as result of the anticipated extended planar structure of **GNR-21**. However by sonicating and heating the material in TCB for 1 hour a suspension from the material was formed. Such suspension was used to study the UV-Vis absorption characteristics.

The absorption spectrum (Figure 4.6) of the compound showed absorption over the complete visible range of the electronic spectrum, with a maximum of the band at approximately 528 nm, which depicted a significant red-shift of about 133 nm compared to the absorption maximum of its precursor polymer **P$_9$** (λ_{max} = 395 nm), which was expected due to the increased degree of conjugation in the product. These results were in agreement with the general behavior of large PAHs such as **C$_{222}$**, which was reported by C. D. Simpson in the Müllen group[23b] and acquired UV-Vis spectrum that covered the complete visible range of the electronic spectrum and exhibited a bathochromically-shifted absorption maximum at about 765 nm. Moreover, these results reflect the effect of introducing the long branched alkyl chains to the edges of the molecule on the optical properties. While **GNR-20**, which has the same structure as **GNR-21** but without any alkyl chains on it periphery showed absorption maximum at about 650 nm, the blue-shifted absorption of **GNR-21** (λ_{max} = 528 nm) suggested that the existence of the alkyl chains reduced the extent of the molecular aggregation in **GNR-21** compared to **GNR-20**.

These obtained spectroscopic results gave a clue that the $FeCl_3$ mediated intramolecular oxidative cyclodehydrogenation of polymer **P$_9$** indeed gave rise to more extended aromatic system that could be the desired product **GNR-21**. However, a full structure proof was still missing , and due to the insolubility of **GNR-21** in common organic solvents, the success of the cyclodehydrogenation could no be proven by any other solution-based analysis methods. For instance solution NMR spectroscopy was completely out of the

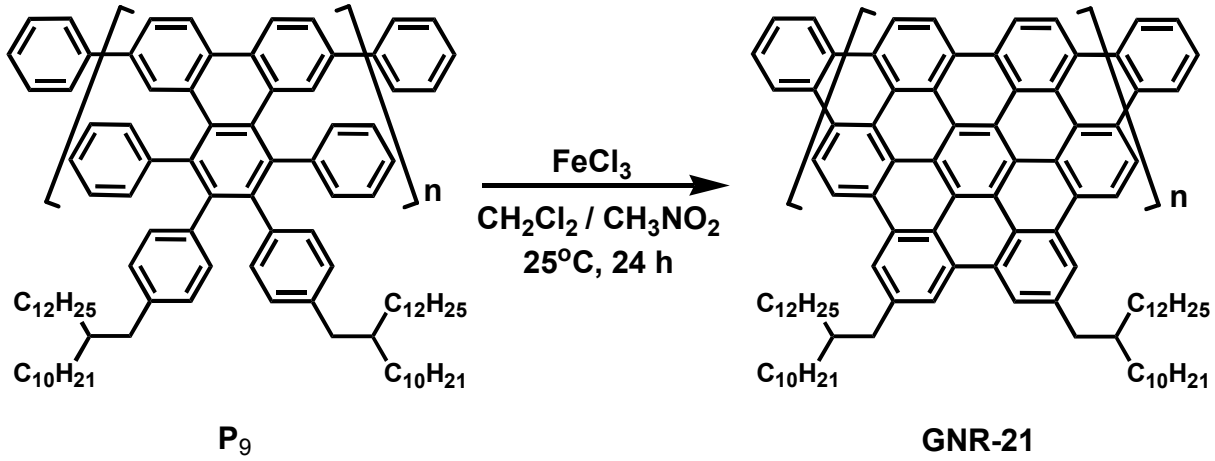

Scheme 4.7 Synthesis of **GNR-21.**

question. Also elementary analysis, a method usually very well suitable for solid materials, could not be used since incomplete combustion under soot formation of this high carbon content type of molecules leads to inaccurate results. Even leaving the combustion problem

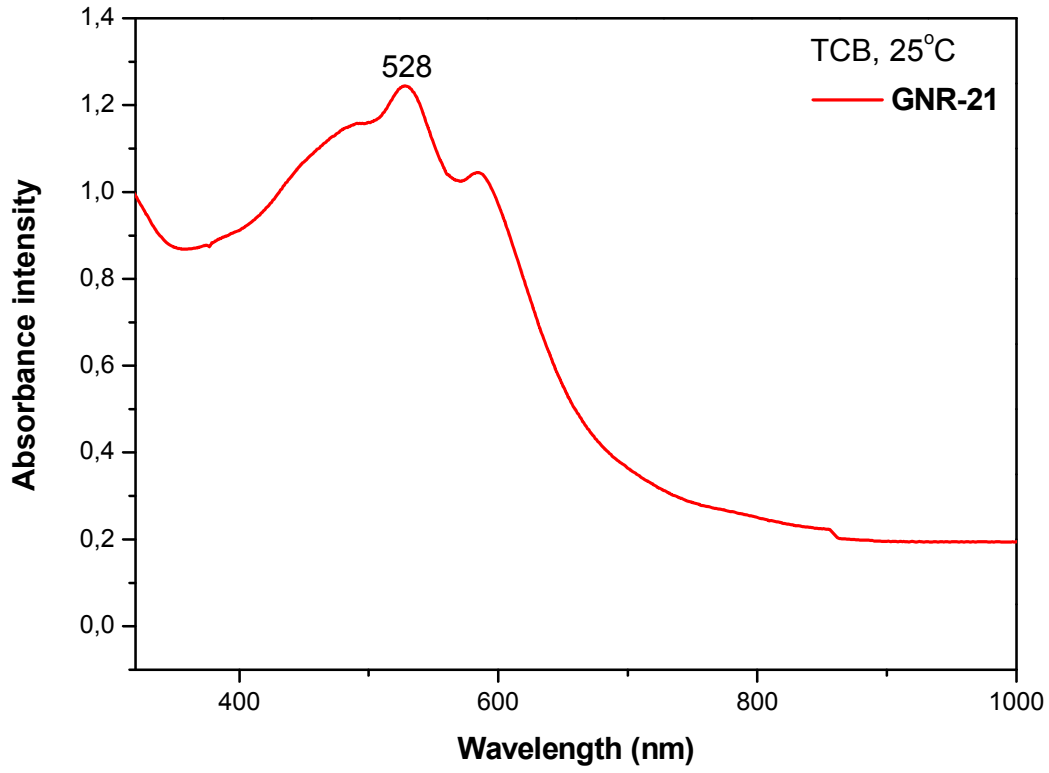

Figure 4.6 UV-Vis spectrum of **GNR-21**.

aside, the accuracy of the method is not high enough to distinguish between the molecular composition of a mixture of the precursor polymer and for example a partially fused GNR. Consequently, Raman spectroscopy for a solid sample of **GNR-21** was measured utilizing excitation laser of 768 nm wavelength. As in the case of **GNR-20** the Raman spectrum of **GNR-21** showed similar characters to the fully-benzenoid graphite nanoribbon reported by J. Wu. [26] The spectrum revealed two bands, a broad band was centered at around 1334 cm^{-1} and a more intense one located nearly at 1605 cm^{-1}, which can be ascribed to the D and G bands, respectively (Figure 4.7). These two bands as previously mentioned are characteristic features for all-benzenoid PAHs.

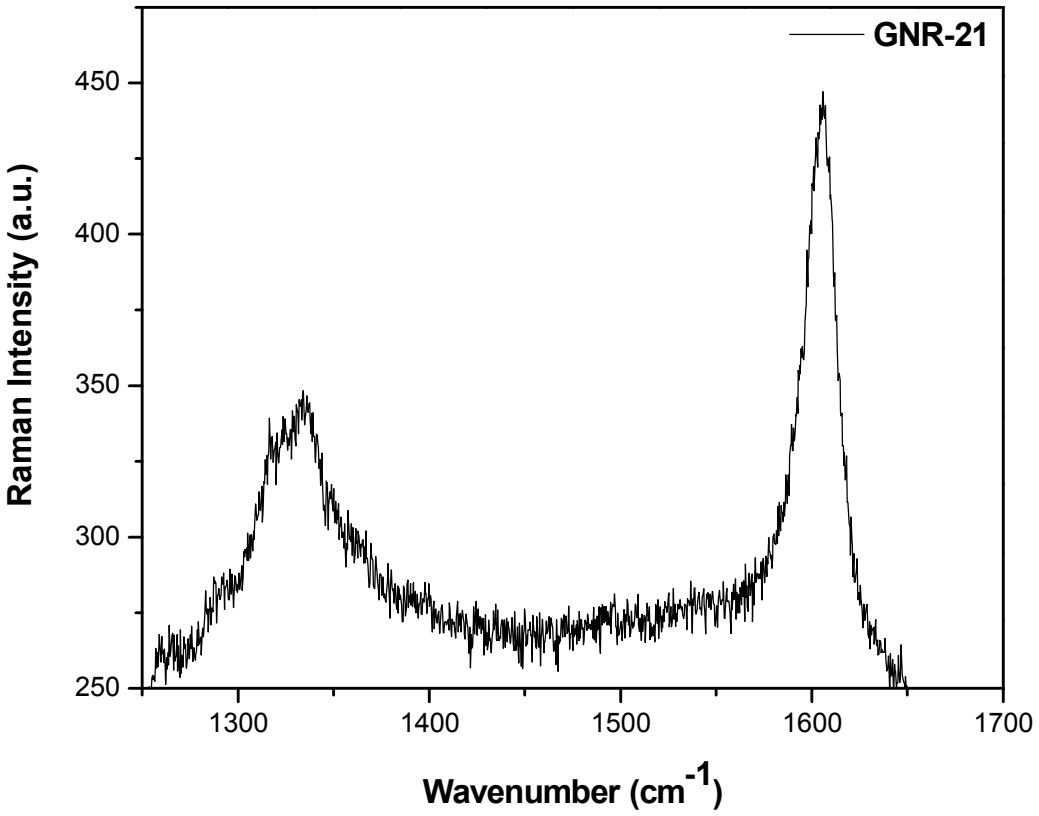

Figure 4.7 Raman spectrum of **GNR-21** using 768 nm excitation laser wavelength.

Thus, the Raman spectra together with the obtained UV-Vis absorption results suggested that the cyclodehydrogenation reaction of polymer **P_9** gave the target molecule **GNR-21**. Nevertheless, the two methods did not afford a complete structure analysis. Consequently, micro-Raman analysis was performed for **GNR-21** and the obtained results (presented later in this chapter) clearly proved the formation of the desired graphene nanoribbon.

Following that, and by using a suspension of **GNR-21** in TCB that was drop-casted onto copper-grid substrate the morphology of the obtained sample was studied by transmission electron microscopy (TEM) (Figure 4.8). In the larger areas, disordered graphite structures were observed. However, an ordered graphite layer structure surrounded by amorphous zones was also found. A typical example is shown in Figure 4.8a discloses an ordered graphite structure which extends approximately over 5 nm width and 25 nm length with an interlayer distance of 3.34 Å, which was comparable to the typical distance of π-π stacking (3.4 Å) of the nanographenes.[27,28]

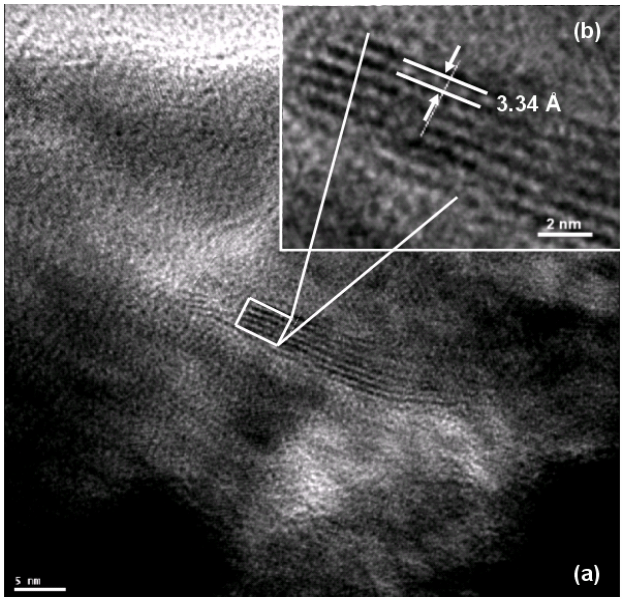

Figure 4.8 (a) TEM images of the **GNR-21** sample, where an ordered graphite layer structure is marked by a square; (b) magnification of the marked area showing interplanar distance of 3.34 Å.

4.2.4 Synthesis of GNR-22

While polymers $\mathbf{P_{14}}$ and $\mathbf{P_9}$, which have the same number of aryl groups around the TP-moiety afforded poorly soluble compounds (**GNR-20** and **GNR-21**, respectively), polymer $\mathbf{P_7}$ (described in chapter 2) with the less number of aryl units on the TP-unit could result in better soluble **GNRs**. $\mathbf{P_7}$ exhibited very good solubility (10mg / 1ml solvent) in common organic solvent and was of high molecular weight ($M_w = 224 \times 10^3$, PDI = 2.7).

The cyclodehydrogenation reaction of $\mathbf{P_7}$ (Scheme 4.8) with $FeCl_3$ (6 equivalent / 1H) afforded a black solid in 85 % yield. Similar to compound **GNR-21**, the obtained product **GNR-22** was insoluble in the common organic solvents, and formed a suspension in TCB when sonicated and heated for 1 hour.

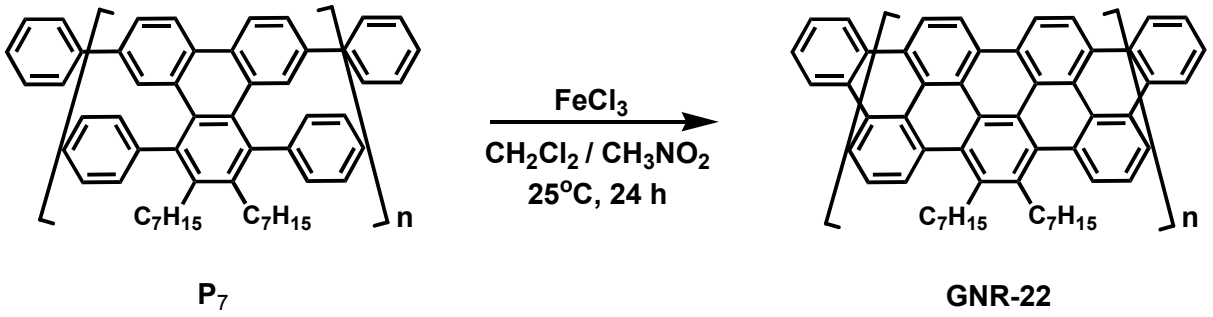

$\mathbf{P_7}$ **GNR-22**

Scheme 4.8 Synthesis of **GNR-22**.

Investigation of the UV-Vis absorption of a suspension of **GNR-22** (Figure 4.9) showed similar behavior to **GNR-20** and **GNR-21** as well as to the previously described polyphenylene-based ribbonlike graphite system and C_{222} PAH.[26, 23b] The absorption spectrum disclosed again a broad absorption band that covered the complete visible range, which was attributed to the large number of electronic transitions occurring in this huge PAH. In addition the material exhibited approximate absorption maximum (λ_{max}) at 530 nm, which was 136 nm bathochromically-shifted from that of the precursor polymer $\mathbf{P_7}$ (λ_{max} = 394 nm).

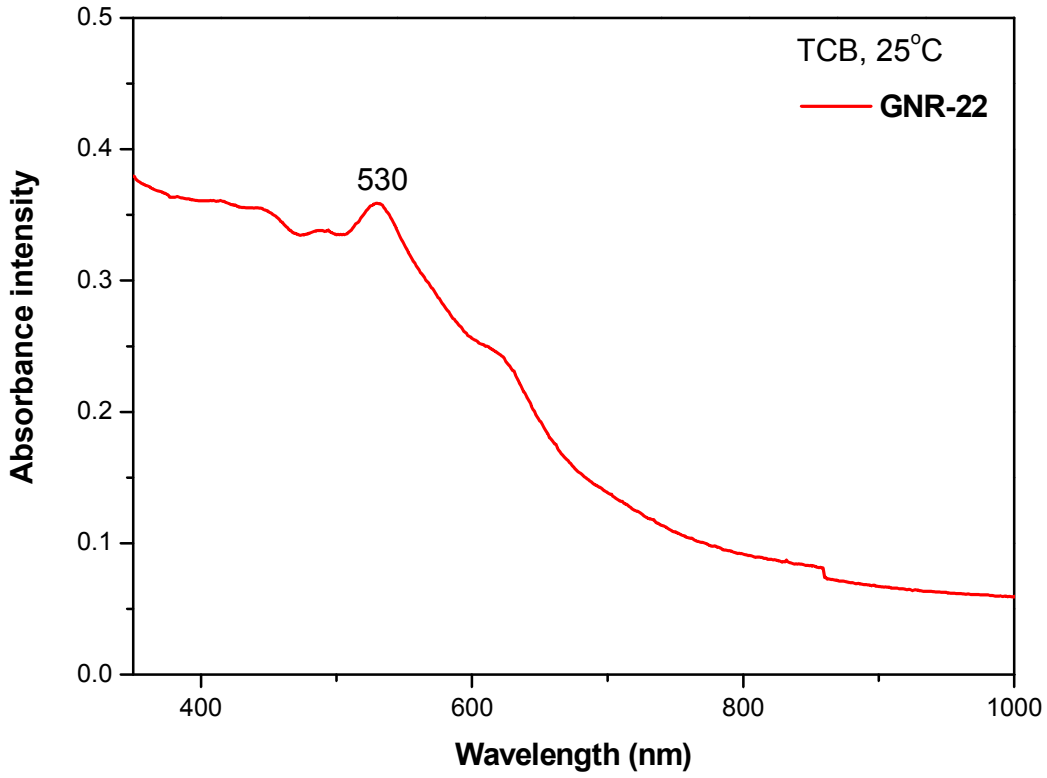

Figure 4.9 UV-Vis spectra of **GNR-22**.

As in the previous cases of **GNR-20** and **GNR-21**, the extremely poor solubility of **GNR-22** in organic solvents directed the investigation toward solid-state analysis methods.

Solid-state Raman spectroscopy was then used to study a solid sample of **GNR-22** by using laser beam as the excitation source (λ_{exc} = 768 nm). The Raman spectrum (Figure 4.10) was in agreement with the Raman vibronic frequencies of all-fused PAHs,[26] since it exhibited their two common features around 1334 cm^{-1} and 1605 cm^{-1}, which can be assigned to the D and G bands, respectively. The D and G band vibronic frequencies for **GNR-22** were at the same time comparable to those of **GNR-20** and **GNR-21**.

The UV-Vis absorption results of **GNR-22** showed that a more extended aromatic system has been formed, which can be seen from the absorption over the whole visible range.

Moreover, the Raman spectrum revealed the characteristic D and G bands for PAHs. These results proposed that the formed product from the Scholl reaction of polymer $\mathbf{P_7}$ was the desired PAH **GNR-22**. Even so, a complete structure elucidation was still demanded, which was done by using micro-Raman analysis (presented soon in this chapter).

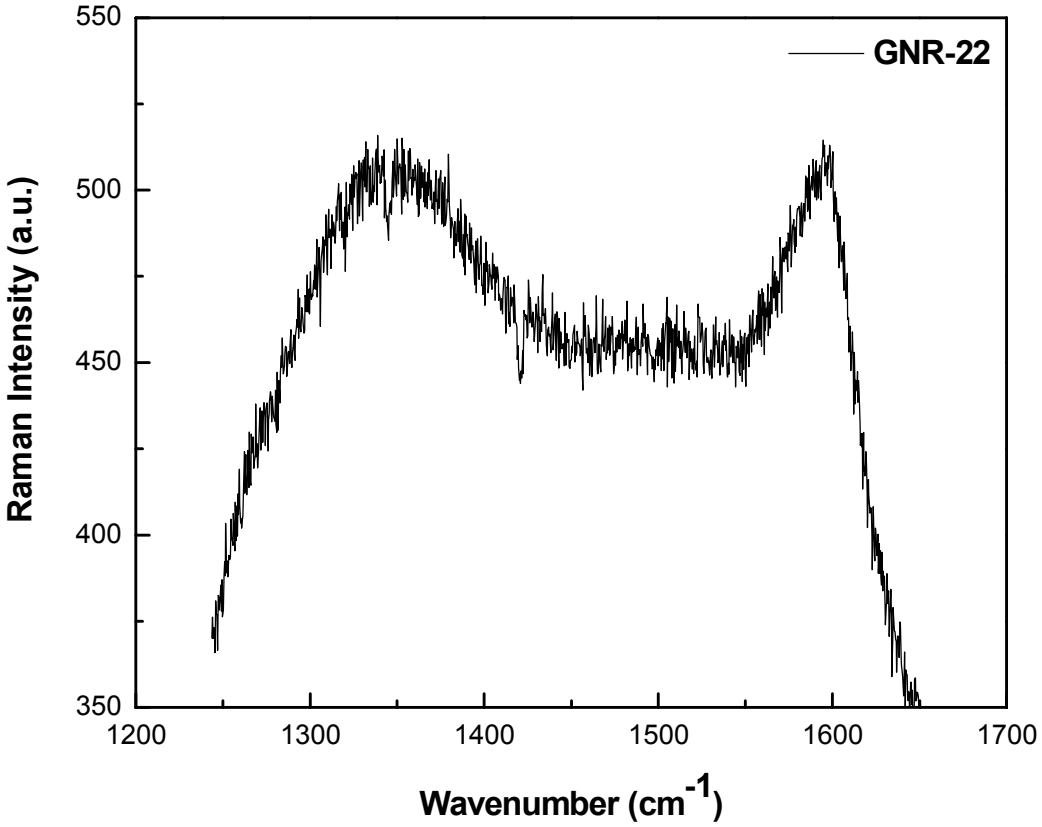

Figure 4.10 Raman spectrum of **GNR-22** using 768 nm excitation laser wavelength.

In order to study the morphology of the obtained material **GNR-22**, TEM studies were performed by using a drop-casted film from a suspension of the material in TCB onto copper-grid substrate. Figure 4.11 illustrates the TEM images of this object, in contrast to **GNR-21** the large areas disclosed more ordered graphite layer structures surrounded by amorphous regions, which was in agreement with the higher tendency of **GNR-22** toward aggregates formation compared to **GNR-21**. The marked area in the Figure shows a typical example of

highly ordered graphitic structure. The d-spacing of the lattice was calculated as 3.34 Å, in agreement with that of **GNR-21** and very close to the nanographenes' interplanar distance.[27,28] Moreover, the TEM image depicted a more extended graphite structure compared to **GNR-21** that was about 5 nm in width and 65 nm in length.

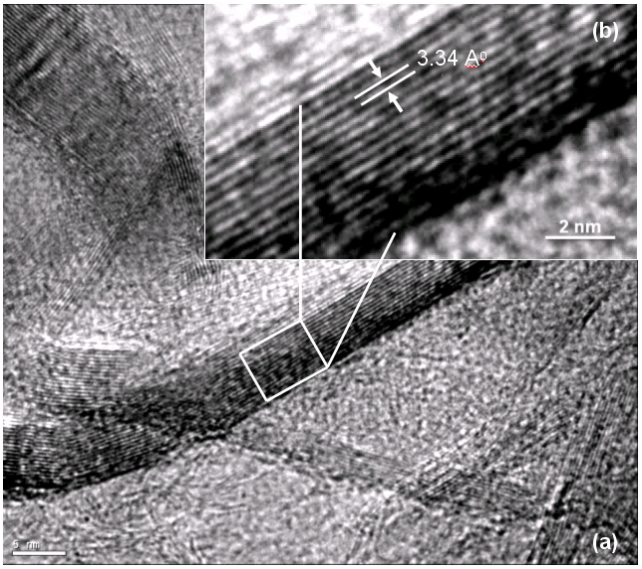

Figure 4.11 (a) TEM images of the **GNR-22** sample, where an ordered graphite layer structure is marked by a square; (b) magnification of the marked area showing interplanar distance of 3.34 Å.

4.2.5 Micro-Raman analysis

As formerly presented, the extreme poor solubility of the obtained **GNRs** in organic solvents hindered the usage of solution-based analysis techniques, which is needed to prove the success of the cyclodehydrogenation reaction and for structural elucidation. Although, UV-Vis absorption of the materials was measured in TCB, one should keep in mind that these measurements were done from suspension of the materials in TCB. Accordingly, the obtained absorption spectra can not perfectly represent the obtained product, since the highest molecular weight **GNRs** should not be soluble in TCB. Nevertheless, the observed absorption

spectra that expanded over the whole visible range proved that more extended aromatic systems were formed when compared to the precursor polymers. Solid-state Raman spectroscopy was also conducted and it is true that the vibronic spectra showed the characteristic D and G bands for full-aromatic PAHs, however the weak intensity of the spectral signal did not allow further structure clarification.

Another promising solid-state analytical method is micro-Raman spectroscopy. This method showed good results when applied for similar systems like soot[29] or thin diamond films[30] that gave us the motivation to apply this method on our systems to see if it will help in the characterization of our materials.

In the following sections a brief description of the measurement will be presented followed by a detailed discussion for the obtained results. The work was done in the group of Prof. Dr. Andreas Hirsch by Jan Englert at the University of Erlangen-Nürnberg.

In order to provide an evidence for the highly crystalline nature of the **GNRs**, we conducted micro-Raman investigations. Crystallites of ~1 mg of mass were investigated before and after the intramolecular oxidative cyclodehydrogenation reactions by placing them onto a common microscopy glass slides.

Upon irradiation with monochromatic laser light (λ = 532 nm) through a high spatial resolution objective, the spectrum of inelastically scattered photons was measured as a red-shift with respect to the incident laser energy. This directly allowed for the quantification of the excited vibrations or phonon in the material using the relationship $E_{vibration} = E_{Laser} - E_{Raman}$.[31]

Figures 4.12-4.14 depict a comparison between the recorded spectra from the precursor polymers (**P_{14}**, **P_9**, and **P_7**) with their graphene ribbons counterpart (**GNR-20**, **GNR-21** and **GNR-22**). The most obvious change is the appearance of sharp and well defined signals in the region of 1100 to 1700 cm^{-1} Stokes Shift after the Scholl reaction. In the same time all precursors only exhibit a broad fluorescence background extending over the whole

spectral range from 90 to 3500 cm^{-1}. The appearance of these distinct signals after planarization can be directly attributed to the formation of an expanded sp^2 hybridized carbon network, which according to the pronounced intensity and shape, must exhibits significant crystalline order.[32] The signal appearing around 1600 cm^{-1} was the result of the first order Raman allowed tangential in plane vibration of carbon atoms in the lattice and will be called G-band in analogy to graphite,[33] graphene[34] and carbon nanotubes.[35] Its appearance and frequency can be directly attributed to the generation of an extended sp^2-carbon network in analogy to other expanded sp^2 carbon allotropes.

As shown in Figures 4.12-4.14 the second area of interest in the spectrum is found at 1200 – 1450 cm^{-1} and is referred to as the D-band. This feature is commonly used to determine the amount of defects in the graphene basal plane and widely used (e.g. to estimate the degree of functionalization in single walled carbon nanotubes).[36] The D-band evolves from a double resonant scattering process. Upon irradiation of the sample an electron/hole pair (e^-/h^+) is generated at the edge of the Brillouin zone near the high symmetry point K. After a scattering event involving a phonon with high momentum ($\underline{q}$), h^+ and e^- are separated in k-space by the amount of $\underline{q}$ preventing recombination and emission of Stokes's shifted Raman light. Emission is only possible if a lattice defect is present and acts as elastic scattering site for electrons, overcoming the k-space separation and thus allowing radiative recombination of e^- and h^+.[37]

Experiments conducted upon single layer graphene edges by Casiraghi *et al.* provide evidence that even though the sp^2 network inside the carbon domain is defect free, the edges give rise to a D-band at Raman shifts of ~1350 cm^{-1}.[38] Such defect induced band can be still resolved at distances as far as 0.5 μm away from the nearest edge and is expected to be particularly strong for armchair edges.[39,40] The work of Cancado et al. suggested no D-band activation for zigzag edges because of momentum conservation.[39,40] The edge of a graphene flake or nanoribbons can be regarded as defect in the crystal lattice as its periodicity and symmetry is broken there.

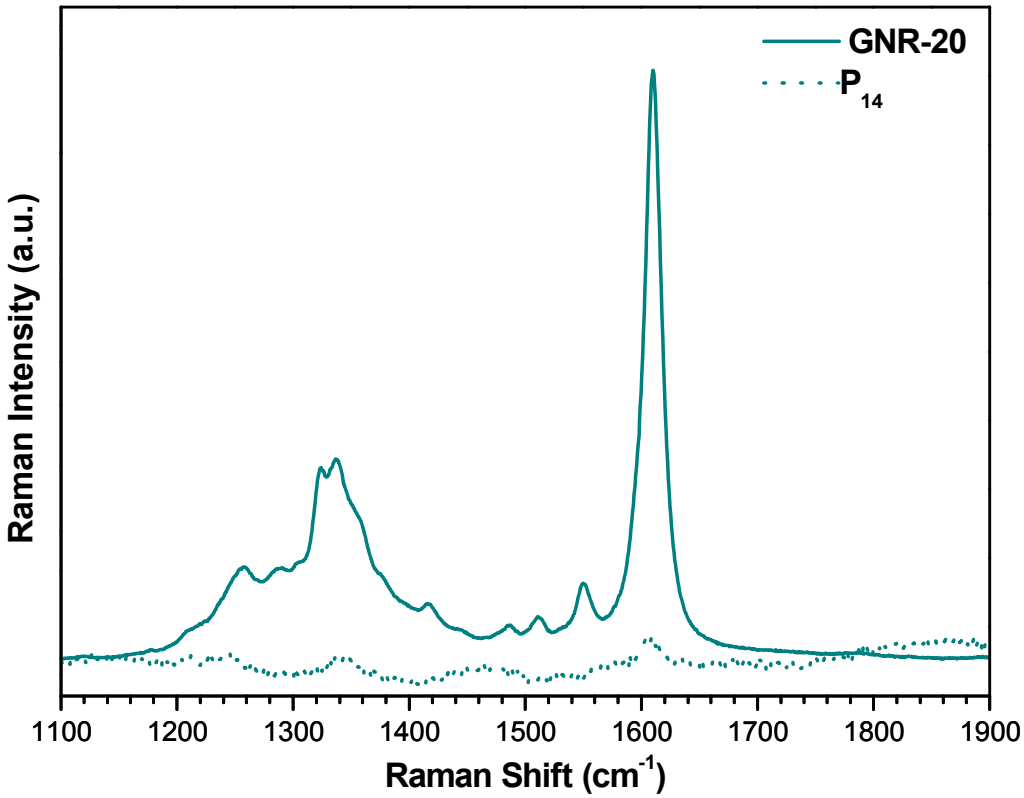

Figure 4.12 Raman spectrum of **GNR-20** at 532 nm excitation wavelength after baseline correction. The dashed line presents the spectrum recorded from polymer $\mathbf{P_{14}}$ after baseline subtraction and magnification.

Thus the edge can act as elastic scattering site for excited electrons in the Raman process and gives rise to the D-band, depending on its bonding motive (zigzag or armchair). For the synthesized **GNRs**, every e^-/h^+ pair generated upon irradiation will be in close proximity (maximum distance X Angström for **GNR-22** and Y Angström for **GNR-20/21**) to one armchair edge. As this distance is significantly smaller than the experimentally derived 0.5 µm minimally needed to exclude edge activated D-band, the presence of the D-band feature is attributed to edge scattering exclusively.

Further evidence for this assumption can be deduced from the integrated A(D) / A(G) areas for **GNR-22** and **GNR-20** and **GNR-21**. As the aspect ratio L_{Length} / L_{Width} increases for more narrow ribbons so does the ratio of edge sp^2 carbon atoms N_{Edge} over the number of plane sp^2 carbon atoms N_{Plane}. Under the assumption that the D-band is generated from the number of edge atoms N_{Edge} in the laser spot while the G-band is originating from the number of in plane carbons N_{Plane} an increased relative D-band intensity is to be expected for the narrow ribbon for **GNR-22** when compared to **GNR-20** and **GNR-21**, which both should yield comparable relative D-band intensities as their aspect ratio is identical. In order to test this hypothesis, the experimentally derived spectra from **GNR-20**, **GNR-21** and **GNR-22** were integrated between 1100 and 1450 cm^{-1}, yielding the arithmetic area of the complete D-band feature including fine structure. In order to exclude intensity fluctuations between the different samples originating from varying laser focus quality or laser intensity variations, all D-band areas were normalized to their respective G-band integrals, which were determined using the same procedure of arithmetic integration between 1460 and 1700 cm^{-1} yielding a characteristic A(D)/A(G) value for every **GNR** under investigation. Accordingly, for **GNR-22**, which is X Å smaller in width compared to **GNR-20** and **GNR-21**, that are both exhibiting widths of Y Å, a higher relative integrated D-band intensity is expected when compared to **GNR-20** and **GNR-21**. The experimental values were in accordance with this conclusion as a value of A(D)/A(G) = 1.32 was found for the narrow **GNR-22**, while lower A(D)/A(G) ratios of 1.13 and 1.17 were observed for the broader **GNR-20** and **GNR-21**, respectively. (However, to derive an empirical model for this correlation, a lot more different widths are needed to see if there is a good correlation between A(D)/A(G) and N_{edge}/N_{plane}).

Finally and by using the micro-Raman analysis method it was clearly proved that the intramolecular oxidative cyclodehydrogenation reactions of the precursor polymers (**P_7**, **P_9**, and **P_{14}**) afforded the desired two-dimensional graphene nanoribbons **GNR-20**, **GNR-21**, **and GNR-22**.

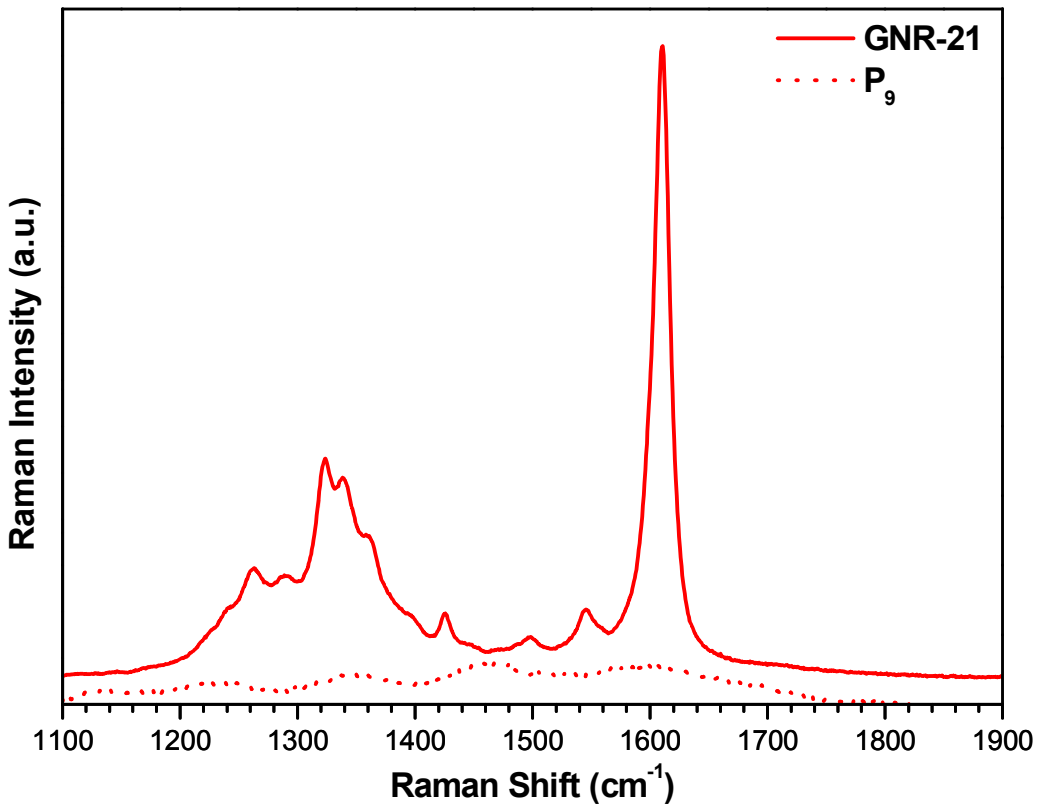

Figure 4.13 Raman spectrum of **GNR-21** at 532 nm excitation wavelength after baseline correction. The dashed line presents the spectrum recorded from polymer **P_9** after baseline subtraction and magnification.

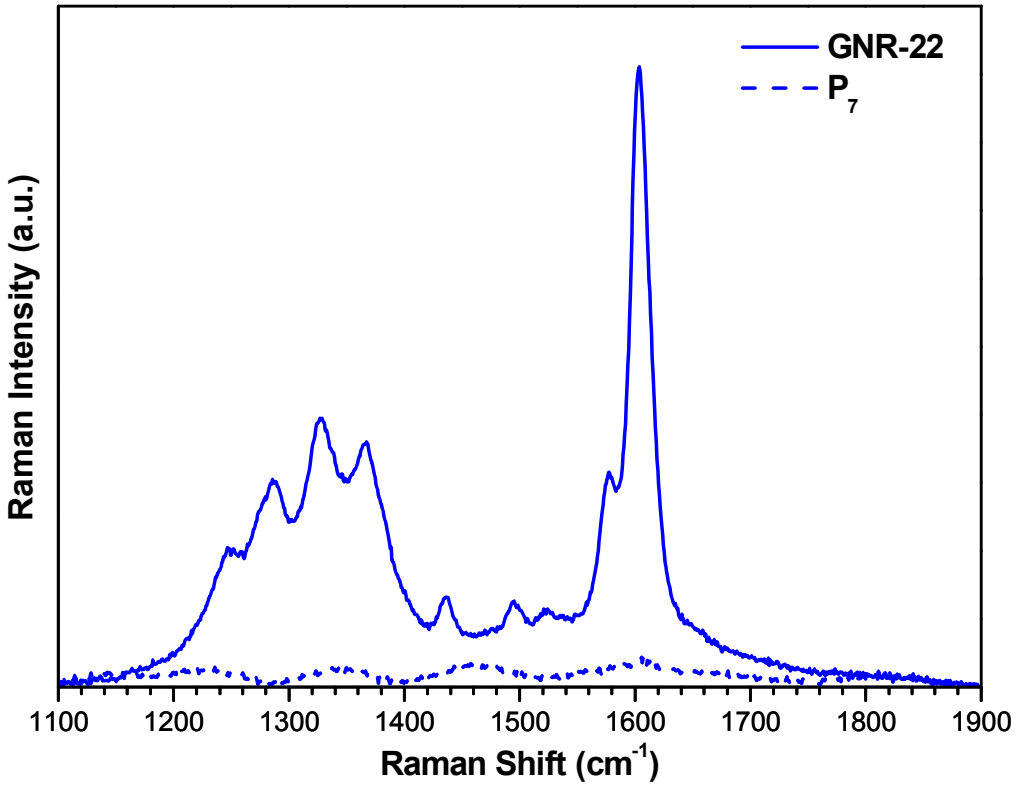

Figure 4.14 Raman spectrum of **GNR-22** at 532 nm excitation wavelength after baseline correction. The dashed line presents the spectrum recorded from polymer $\mathbf{P_7}$ after baseline subtraction and magnification.

4.3 Surface-mediated GNRs synthesis

The synthesis and characterization of graphene nanoribbons have recently attracted the attention of many research groups around the glob. This is because of the very promising properties such class of materials have, which make them suitable for future electronic applications.[41-43] In contrast to their two-dimensional parent material graphene that is known by its semimetallic properties,[11,44,45] GNRs are expected to acquire semiconducting behaviour when their widths are smaller than 10 nm, which can be attributed to quantum confinement and edge effects.[42,46] Several synthetic procedures such as lithographic[12,13] and chemical[17-20,47] methods have been reported for the fabrication of GNRs, in order to afford microscopic samples of GNRs. Nevertheless, these procedures were not successful in producing GNRs with defect- and disorder-free structure or in producing ribbons of well-defined edges and widths. Moreover, the chemical routes using the bottom-up approach for the synthesis of GNR in solution undergo from re-aggregation of the formed graphitic structures during cyclodehydrogenation of polyphenylene precursors, which makes further processing to regenerate single layer GNRs very complicated.[22] As a result, the needed structural accuracy to tune the precise electronic properties of GNRs has not been accomplished hitherto.

In this work the synthesis of GNRs using a new bottom-up approach will be presented and discussed. The advantage of this method compared to the other reported methods is the possibility to produce GNRs of defined structures. The principle of the method described here depends on utilizing difunctionalized precursor monomers, which are supposed to interact in a specific way to produce finally nanostructured graphene systems. This was achieved by using two alternative thermal activation steps, in the first one the precursor monomers were adsorbed on a surface and coupled together to form linear polymer chains, which were by the second activation step planarized into GNRs by cyclodehydrogenation.

4.3.1 Synthesis of precursor monomers

For the surface-supported GNRs synthesis two different precursors were considered, monomer 10,10'-dibromo-9,9'-bianthracene **(25)** and **5d** (described in chapter 2) (Scheme 4.9 a and b).

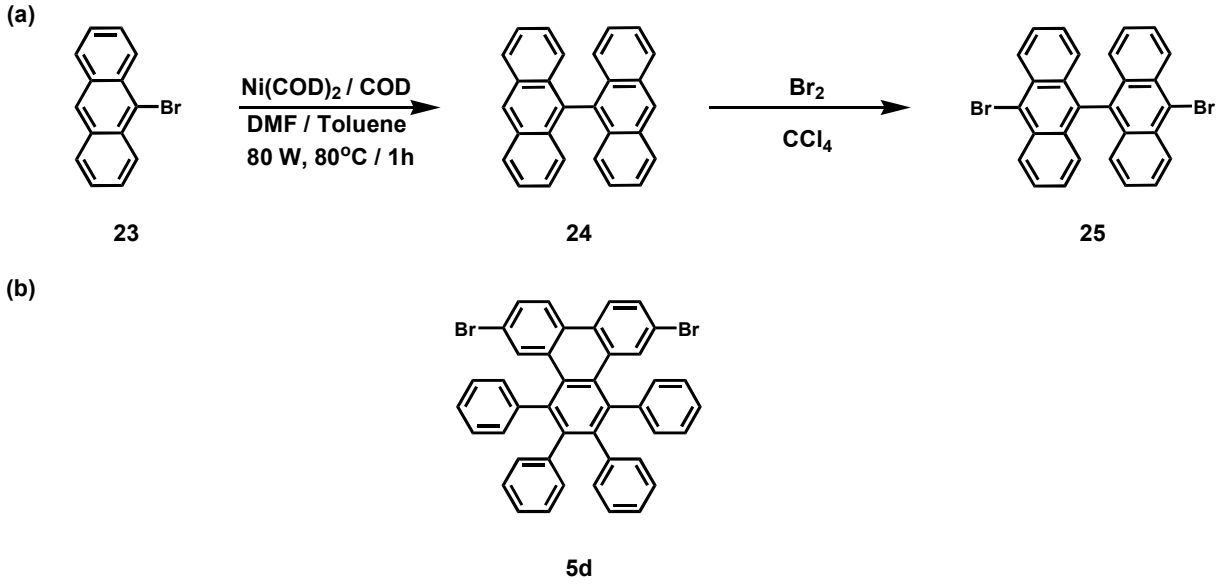

Scheme 4.9 a) synthesis of 10,10'-dibromo-9,9'-bianthracene **(25),** b) molecular structure of 6,11-dibromo-1,2,3,4-tetraphenyltriphenylene **(5d)**.

The synthesis of monomer **25** (Scheme 4.9) started with the nickel (0) mediated MA-Yamamoto coupling reaction of 9-bromoanthracene **(23)** using bis(cyclooctadiene)nickel(0) as catalyst and 1:1 mixture of dimethylformamide / toluene as solvent at 80^{o}C for 1 hour. The reaction afforded 9,9'-bianthracene **(24)** as a light yellow solid in 22 % yield. Such low reaction yield can be attributed to the high steric demands arising during the coupling of two anthracene units together, due to the presence of four hydrogen atoms on the peripheries of the anthracene moieties in a very close proximity. Following that compound **24** was subjected to bromination reaction using bromine to result in the target molecule 10,10'-dibromo-9,9'-bianthracene **(25)** as a light yellow solid in 55 % yield. Proton NMR spectroscopy has been used as an efficient tool to evaluate the purity of the product. The^{1}H-NMR spectrum of **25** that

was recorded in CD_2Cl_2 at room temperature is shown in Figure 4.15. Three kinds of protons (Ha, Hb, and Hc) were recognized in the aromatic region of the spectrum. The aromatic signals assigned to the four protons Ha were found as doublets (J = 8.88 Hz) due to their nearness to only one other proton (Hb), and experienced a down-field shift around 8.71 ppm. Furthermore, the four Hb protons exhibited signals of multiple splitting as a result of the increased number of neighbouring protons (Ha and Hc), and a more up-field chemical shift of 7.63-7.57 ppm compared to the signal of Ha, due to the reduced deshielding effect from the bromine atoms on Hb. Likewise, the eight protons of Hc were of multiple split in their aromatic signals, and acquired a chemical shift of 7.23-7.05 ppm.

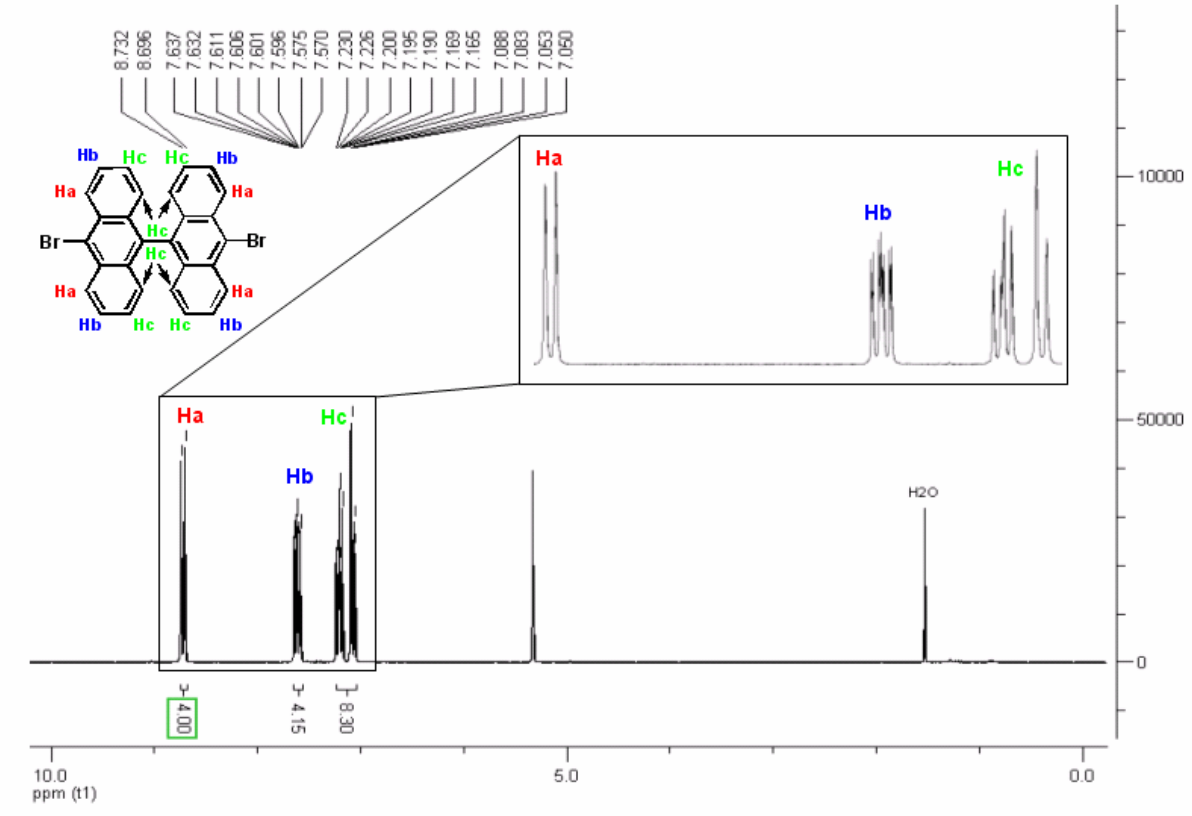

Figure 4.15 ^{1}H-NMR spectrum of compound **25** in CD_2Cl_2 at 25^{o}C (250 MHZ).

Elemental analysis of monomer **25** was also measured and exhibited carbon and hydrogen contents of 64.60 % and 2.23 %, respectively. These values were about 1 % lower

than the theoritical calculated values (C = 65.65 % and H = 3.15 %) that can be attributed to the incomplete combustion (soot formation) of such molecule. However, these results proved that 10-bromo-9,9'-bianthracene did not exist as impurities in the sample, since it shoud lead to higher carbon and hydrogen contents (C = 77.61 % and H = 3.95 %) in the sample. The ^{1}H-NMR spectrum of **5d** is shown in chapter 2.

4.3.2 Synthesis of GNRs

In this section the surface assisted GNR production process will be presented. The work was done by the group of Prof. Dr. Roman Fasel at the Empa, Swiss Federal Laboratories for Materials Science and Technology, Switzerland.

As mentioned above the surface-mediated synthesis of the GNR presented here were done by using two alternate thermal activation steps. The schematic representation shown in Figure 4.10 demonstrates the basic steps for these processes. In the first step the dibromo-functionalized precursor monomers were given enough thermal energy to sublime on top of a solid substrate where they lost their halogen atoms to form a kind of surface-stabilized biradical reactive intermediates. Following that, and due to the high thermal activation energy that was given to the biradicals, linear polymer chains were produced through radical addition.[48] At this point it is important to mention that, the formation of the polymer chains was not coincidence but was strictly imprinted by the specific chemical functionality pattern of the monomers.

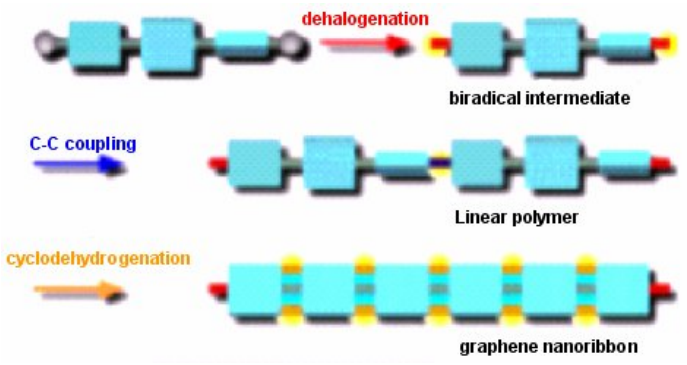

Figure 4.10 Schematic illustrations for the basic steps for surface-supported GNR synthesis.

After the generation of the linear polymer and with the assist of a second thermal activation step a surface-mediated cyclodehydrogenation occurred, which resulted in the formation of extended full-aromatic systems whose structures were again strictly defined by the design of the precursors.

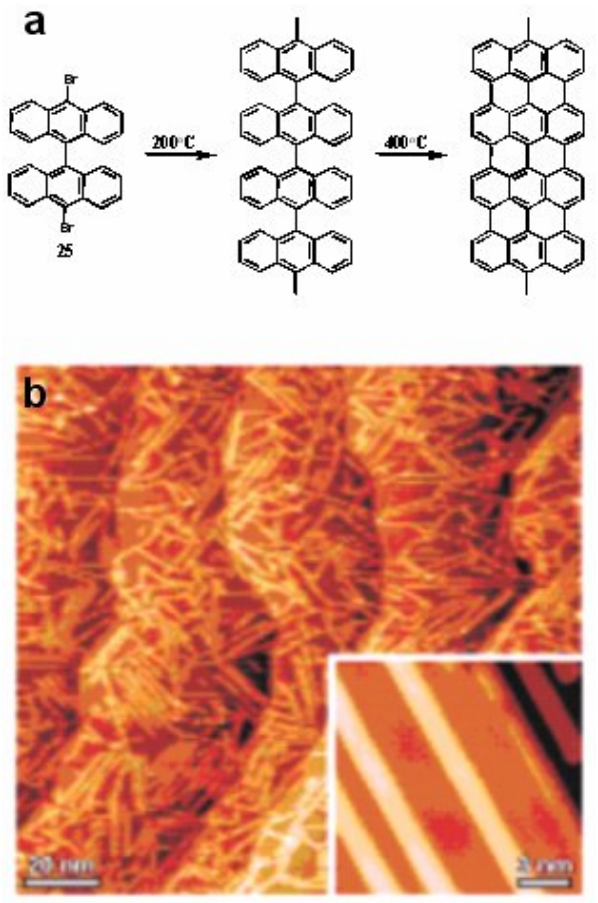

Figure 4.11 Straight GNRs from 10,10'-dibromo-9,9'-bianthryl monomers (**25**). **a)** Reaction scheme from monomer **25** to straight $N = 7$ GNRs. **b)** Overview STM image after cyclodehydrogenation at 400°C, showing straight $N = 7$ GNRs ($T = 300$ K, $U = -3$ V, $I = 0.03$ nA, inset: $T = 35$ K, $U = -1.5$ V, $I = 0.5$ nA).

Figure 4.11a depicts the molecular structure of an armchair GNR with $N = 7$ (N is the number of carbon atom pairs across the ribbon), which was formed after the thermal activation of the precursor monomer **25** on a Au(111) surface. Moreover, Figure 4.11b shows

the STM images for the formed GNR. In the first activation step monomer **25** was annealed till 200°C, as a result the monomer molecules were probably dehalogenated to form reactive biradicals. At the same temperature the formed intermediates were given enough thermal energy to diffuse across the surface to form by intermolecular colligation through radical addition linear polymer chains in which the monomers were coupled by single covalent C-C bonds.

The generation of the desired GNR was then accomplished by further annealing of the sample to 400°C. At this temperature the intramolecular cyclodehydrogenation of the formed polymer chains afforded armchair ribbon with $N = 7$ (Figure. 4.11b).

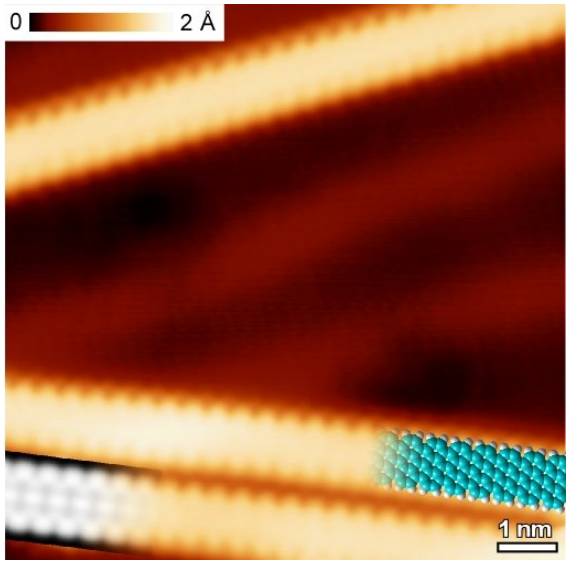

Figure 4.12 High resolution STM image with partly overlaid molecular model of the ribbon (T = 5 K, U = -0.1 V, I = 0.2 nA). Bottom left: DFT-based STM simulation of the N = 7 ribbon shown as grey scale image.

STM simulations were also in perfect agreement with experimental images (Figure 4.12), giving further evidence for the identification of the reaction products as atomically precise $N = 7$ GNRs with fully hydrogen-terminated armchair edges.

The uniform width of the produced GNRs is also reflected in the Raman spectrum of Figure 4.13 taken from a densely packed layer of $N = 7$ armchair GNRs grown on a 200 nm

Au(111) film on a mica substrate. Besides the D and G peaks[49] and several other peaks appearing due to the finite width and low symmetry of the ribbons, the width-specific radial-breathing-like mode (RBLM)[50] is seen as a sharp peak at 396 cm^{-1}, in excellent agreement with our calculation (394 cm^{-1}). This implies that the RBLM is indeed a sensitive probe of GNR width (N = 6 and N = 8 GNRs have RBLM frequencies about 50 cm^{-1} higher and lower, respectively).[50]

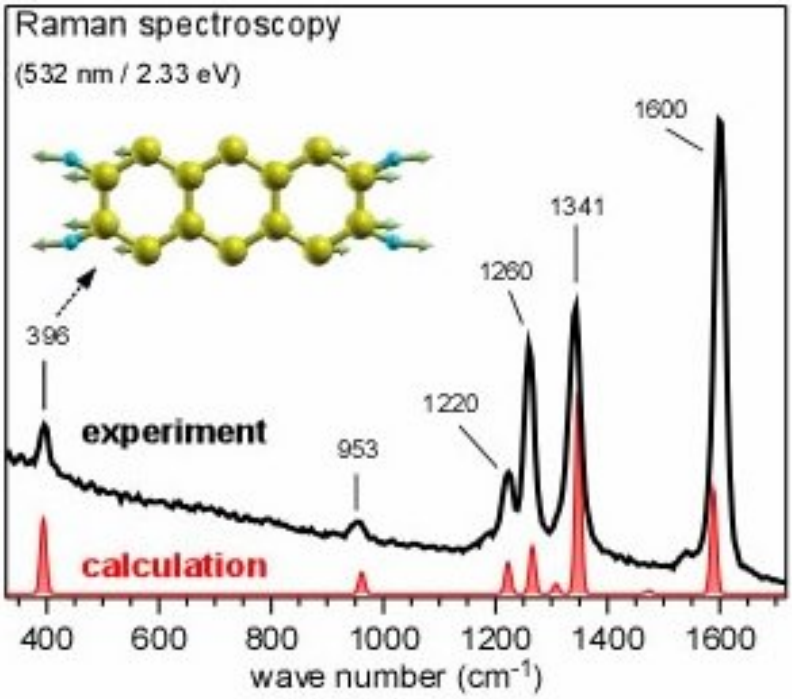

Figure 4.13 Raman spectrum (532 nm) of straight N = 7 GNRs. The peak at 396 cm^{-1} is characteristic for the 0.74 nm width of the N = 7 ribbons. The inset shows the atomic displacements characteristic for the RBLM mode at 396 cm^{-1}.

The above results showed that the topology of the obtained GNRs was determined by the functionality pattern of the precursor monomers. Based on that, other ribbons with different and more sophisticated structures should be also accessible. For example, the thermal activation of monomer 6,11-dibromo-1,2,3,4-tetraphenyltriphenylene **(5d)** resulted in

chevron-type GNRs with pure armchair edge structure. The ribbons exhibited alternating widths of $N = 6$ and $N = 9$ (Figure 4.14). The synthesis of the GNRs started by annealing **5d** at

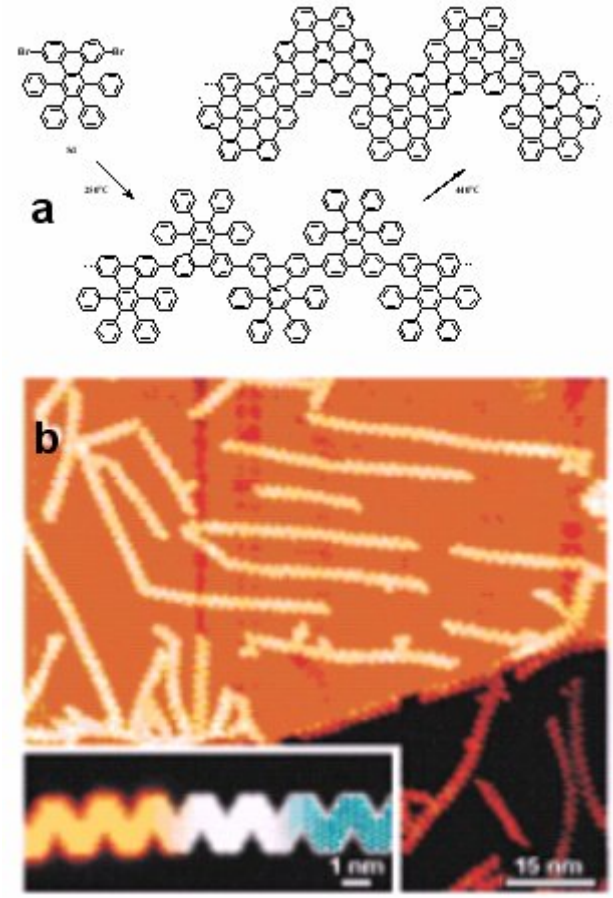

Figure 4.14 Chevron-type GNRs. **a)** Reaction scheme from 6,11-dibromo-1,2,3,4-tetraphenyltriphenylene monomer **(5d)** to chevron-type GNRs. **b)** Overview STM image of chevron-type GNRs fabricated on a Au(111) surface ($T = 35$ K, $U = -2$ V, $I = 0.02$ nA). Inset: High resolution STM image ($T = 77$ K, $U = -2$ V, $I = 0.5$ nA) and DFT-based simulation of the STM image (greyscale) with partly overlaid molecular model of the ribbon (blue: carbon, white: hydrogen).

250°C to form kink-structure polymer chains that formed the fully-aromatic GNR by applying a second annealing step at 440°C. The structure of the GNR was also proved from the comparison with the model structure and with DFT STM simulations (Figure 4.14b); the

results confirmed that the structure of the chevron-type ribbon reflects the one imposed by the colligated and cyclodehydrogenated monomer **5d**.

In order to investigate the degree of selectivity of the precursor monomers coupling on the gold substrate, the straight $N = 7$ GNRs and the chevron-type $N = 6$ / $N = 9$ GNRs have been grown sequentially on a Ag(111) surface (Figure 4.15 a). In this experiment both precursor monomers (**25** and **5d**) were deposited on the surface at the same time and the

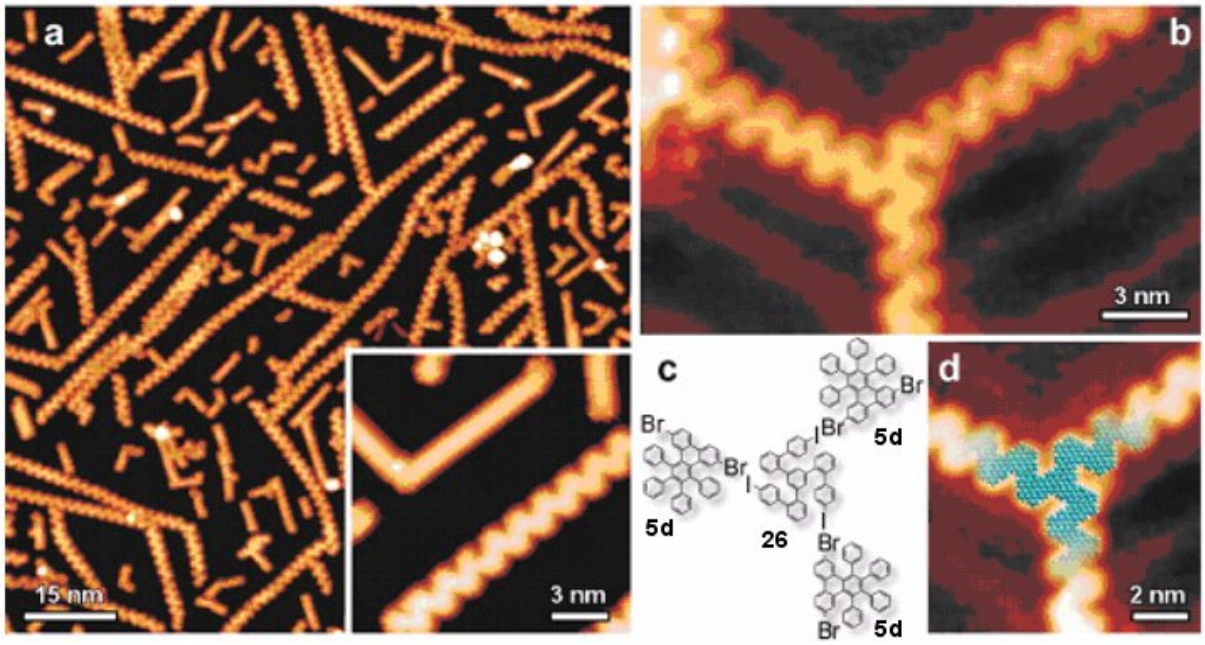

Figure 4.15 Versatility of bottom-up GNR synthesis. a) STM image of coexisting straight $N = 7$ and chevron-type GNRs sequentially grown on Ag(111) ($T = 5$ K, $U = -2$ V, $I = 0.1$ nA). **b)** Threefold GNR junction obtained from a 1,3,5-tris(4''-iodo-2'-biphenyl)benzene monomer **(26)** at the nodal point and monomer 5d for the ribbon arms: STM image on Au(111) ($T = 115$ K, $U = -2$ V, $I = 0.02$ nA). 5d and 26 have been deposited simultaneously at 250°C followed by annealing to 440°C to induce cyclodehydrogentation. **c)** Schematic model of the junction fabrication process with components 26 and 5d. **d)** Model (blue: carbon, white: hydrogen) of the colligated and dehydrogenated molecules forming the threefold junction overlaid on the STM image from **b**.

thermal activation sequence then applied to the sample. Interestingly, both GNRs have been formed, which suggests that the intermolecular coupling reaction is selective, and the design of the two monomers only allows homomolecular reactions, whereas heteromolecular coupling is sterically hindered.

The opposite case, the addition of a small number of tri-halogen-functionalized monomers specifically designed for heteromolecular coupling to the precursor monomer **5d**, is illustrated in Figure 4.15b-d. The C_3 symmetric 1,3,5-tris(4''-iodo-2'-biphenyl)benzene **(26)** (reported by Feng et al.)[51] has been chosen because it provides no steric hindrance against radical addition to **5d**. An STM image of a threefold GNR junction resulting from this fabrication process is shown in Figure 4.15b. The underlying fabrication principle – the use of two different precursor monomers suitably designed for facile heteromolecular coupling and cyclodehydrogenation – should also enable the controlled growth of GNR heterojunctions.

In summary, this work presents a novel way for the synthesis of well-defined GNRs by using a surface-mediated route. This in situ synthetic method allowed for a full structural elucidation of the obtained GNRs, which is of great importance to explore their many predicted technologically highly interesting properties. Moreover, the demonstrated in depth monolayer structural investigations have never been achieved for the GNRs synthesized via solution-mediated routes due to the high tendency of the formed products to aggegate.[22]

4.4 References

(1) Fetzer, J. C. *The Chemistry and Analysis of the Large Polycyclic Aromatic Hydrocarbons*. New York: Wiley, **2000**.

(2) Ohta, T.; Bostwick, A.; Seyller, T.; Horn, K.; Rotenberg, E. *Science* **2006**, 313 , 951.

(3) Zhang, Y.; Tan, Y.-W.; Stormer, H.-L.; Kim, P. *Nature.* **2005**, 438, 201.

(4) Berger, C.; Song, Z.; Li, X.; Wu, X.; Brown, N.; Naud, C.; Mayou, D.; Li, T.; Hass, J.; Marchenkov, A.; Conrad, E.; First, P.; De, W. *Science.* **2006**, 312, 1191.

(5) a) Noorden, R. V. *Nature.* **2006**, 442, 228. b) Compton, C. O.; Nguyen, T. S. *Small.* **2010**, 6, 711.

(6) Geim, A. K.; Novoselov, K. S. *Nat. Mater*. **2007**, 6,183.

(7) De Heer, Walt A.; Berger, Claire; Conrad, Ed; First, Phillip; Murali, Raghunath; Meindl, James."Pionics: The emerging science and technology of graphene-based nanoelectronics," *in Intl. Electron Dev ices Meeting Te chnical Digest*. **2007**,199.

(8) Fujita M.;Wakabayashi, K.; Nakada, K.; Kusakabe, K. *J. Phys. Soc. Jpn.* **1996***,* 65, 1920.

(9) Nakada, K.; Fujita, M.; Dresselhaus, G.; Dresselhaus, M. S. *Phys. Rev. B.* **1996***,* 54, 17954.

(10) Wakabayashi, K.; Fujita, M.; Ajiki, H.; Sigrist, M. *Phys. Rev. B*. **1999***,* 59, 8271.

(11) Novoselov, K. S. ; Geim, A. K. ; Morozov, S. V. ; Jiang, D.; Zhang, Y.; Dubonos, S. V.; Grigorieva, I. V.; Firsov**,** A. A. *Science.* **2004**, 306, 666**.**

(12) Han, M. Y.; Ozyilmaz, B.; Zhang, Y. B.; Kim, P. *Phys. Rev. Lett* .**2007**, 98, 206805.

(13) Chen, Z.; Lin, Y. M.; Rooks, M. J.; Avouris, P. *Phys. E*. **2007**, 40, 228..

(14) Tapaszt, L.; Dobrik, G.; Lambin, P.; Biro, L. P.; *Nat. Nanotechnol.* **2008**, 3, 397.

(15) Datta, S. S.; Strachan, D. R.; Khamis, S. M. ; Johnson, A . T. C. *Nano Lett.* **2008**, 8 , 1912.

(16) Ci, L. J. Xu, Z.; Gao, W.; Ding, F.; Yakobson, B. I.; Ajayan, P. M. *Nano Res.* **2008**, 1, 116.

(17) Li, X. L.; Wang, X.; Zhang, L .; Lee, S.; Dai, H . *Science* **2008**, 319, 1229.

(18) Campos-Delgado, J.; Romo-Herrera, J. M .; Jia, X. ; Cullen, D. A.; Muramatsu, H.; Kim, Y. A. ; Hayashi, T.; Ren, Z. ; Smith, D. J. ; Okuno, Y. ; Ohba, T.; Kanoh, H.; Kaneko, K.; Endo, M . ; Terrones, H .; Dresselhaus, M. S. ; Terrones, M . *Nano Lett*. **2008**, 8, 2773.

(19) Jiao, L.; Zhang, L .; Wang, X .; Diankov, G.; Dai, H . *Nature* **2009**, 458, 877.

(20) Kosynkin, D. V. ; Higginbotham, A. L.; Sinitskii, A. ; Lomeda, J. R.; Dimiev, A.; Price, B. K.; Tour, J. M . *Nature* **2009**, 458, 872.

(21) Scott, L. T. *Angew. Chem., Int. Ed.* **2004**, 43, 4994.

(22) Yang, X.; Dou, X.; Rouhanipour, A.; Zhi, L .; Räder, H. J.; Müllen, K . *J. Am. Chem. Soc.* **2008**, 130, 4216.

(23) a) Tahara, K.; Tobe, Y. *Chem. ReV*. **2006***,* 106, 5274. b) Simpson, C. D.; Brand, J. D.; Berresheim, A. J.; Przybilla, L.; Räder, H. J.; Müllen, K. *Chem. Eur. J.* **2002**, 8, 6.

(24) a) Wu, J.; Pisula, W.; Müllen, K.*Chem. Re*V. **2007**, 107, 718. b) Feng, X.; Liu, M.; Pisula, W.; Takase, M.; Li, J.; Müllen, K. *Adv. Mater*. **2008**, 20, 2684.

(25) Lambert, C. *Angew. Chem., Int. Ed.* **2005**, 44, 7337.

(26) Wu, J.; Gherghel, L.; Simpson, D. C.; Watson, D. M.; Kolb, U.; Li, J.; Wang, Z.; Müllen, K. *Macromolecules* **2003**, 36,7082.

(27) Zhi, L.; Wu, J.; Li, J.; Kolb, U.; Müllen, K. *Angew. Chem., Int. Ed.* **2005**, 44, 2120.

(28) Zhi, L.; Gorelik, T.; Wu, J.; Kolb, U.; Müllen, K. *J. Am. Chem. Soc.* **2005**, 127, 12792.

(29) Sadezky, A. ; Muckenhuber, H.; Grothe, H.; Niessner, R.; Pöschl, U. *Carbon* **2005**, 43, 1731.

(30) Huong, P. V. *Diamond Relat. Mater.* **1991**, 1, 33.

(31) Raman, C. V.; Krishnan, K. S. *Nature* **1928**, 121, 501.

(32) Dresselhaus, M. S. ; Jorio, A.; Hofmann, M. ; Dresselhaus, G. ; Saito, R. *Nano Lett.* **2010**, 10, 751.

(33) Reich, S.; Thomsen, C. *Philos. Trans. R. Soc. London, Ser. A* **2004**, 362, 2271.

(34) Ferrari, A.; Meyer, J.; Scardaci, V.; Casiraghi, C.; Lazzeri, M.; Mauri, F. ; Piscanec, S.; Jiang, D.; Novoselov, K.; Roth, S. *Phys. Rev. Lett.* **2006**, 97, 187401.

(35) Rao, A. M.; Richter, E.; Bandow, S.; Chase, B.; Eklund, P. C.; Williams, K. A.; Fang, S.; Subbaswamy, K. R.; Menon, M.; Thess, A.; Smalley, R. E.; Dresselhaus, G.; Dresselhaus, M. S. *Science* **1997**, 275, 187.

(36) Graupner, R. *J. Raman Spectrosc.* **2007**, 38, 673.

(37) Reich, S.; Thomsen, C. *Philos. Trans. R. Soc. London*, Ser. A **2004**, 362, 2271.

(38) Casiraghi, C. ; Hartschuh, A. ; Qian, H.; Piscanec, S.; Georgi, C.; Fasoli, A.; Novoselov, K. S.; Basko, D. M.; Ferrari, A. C. *Nano Lett.* **2009**, 9, 1433.

(39) Cançado, L. G.; Pimenta, M. A.; Neves, B. R. A.; Dantas, M. S. S.; Jorio, A. *Phys. Rev. Lett.* **2004**, 93, 247401.

(40) Cançado, L. G.; Pimenta, M. A.; Neves, B. R. A.; Medeiros-Ribeiro, G. ; Enoki, T.; Kobayashi, Y. ; Takai, K. ; Fukui, K.-i.; Dresselhaus, M. S.; Saito, R.; Jorio, A. *Phys. Rev. Lett.* **2004**, 93, 047403.

(41) Wakabayashi, K. *Phys. Rev. B.* **2001**, 64, 125428 .

(42) Barone, V.; Hod, O.; Scuseria, G.E. *Nano Lett.* **2006**, 6, 2748.

(43) Son, Y.W.; Cohen, M.L.; Louie, S.G. *Nature* **2006**, 444, 347.

(44) Mohr, M.; Papagelis, K.; Maultzsch, J.; Thomsen, C. *Condens. Matter*. **2009**,1.

(45) Geim, A.K. *Science* **2009**, 324, 1530.

(46) Yang, L.; Park, C. H.; Son, Y.W.; Cohen, M. L.; Louie, S.G. *Phys. Rev. Lett.* **2007**, 99, 186801.

(47) Elías, A.L.; Me´ndez,A.; Meneses-Rodrı´guez, D.; Gonza´lez, V.; Gonza´lez, D.; Ci, L.; Sandoval, E.; Ajayan, P.; Terrones, H.; Terrones, M. *Nano Lett.* **2009**, 10, 366.

(48) Sevincli, H.; Topsakal, M.; Ciraci, S. *Phys. Rev. B* **2008**, 78, 245402.

(49) Malard, L.M.; Pimenta, M.A.; Dresselhaus, G.; Dresselhaus, M.S. *Phys. Rep.* **2009**, 473, 51.

(51) Feng, X.; Wu, J.; Enkelmann, V.; Müllen, K. *Org. Lett.* **2006**, 8, 1145.

Chapter 5

Outlook and Conclusion Remarks

As introduced earlier in the motivation, the main goals of this thesis were the design, synthesis, characterization of novel conjugated triphenylene-based polymers for blue polymeric light emitting diodes, and the synthesis of their graphene nanoribbons counterparts for electronic applications.

In chapter 2, a novel synthetic strategy of blue light-emitting conjugated polytriphenylenes was presented. The synthetic strategy started from the key building bloke 2,7-dibromophenanthrene-9,10-dione towards the versatile synthesis of a novel series of monomers (**5a-5g**), which by using the microwave assisted palladium-catalyzed Suzuki-Miyaura and the nickel-catalysed Yamamoto polycondensation reactions afforded a series of soluble 1,2,3,4-tetraphenyltriphenylene, 2,3-bis(4-octylphenyl)-1,4-diphenyltriphenylene, 2-heptyl-1,3,4-triphenyltriphenylene, 2-decyl-3-(4-octylphenyl)-1,4-diphenyltriphenylene, 2,3-diheptyl-1,4-diphenyltriphenylene, 2,3-bis(4-dodecylphenyl)-1,4-diphenyltriphenylene, and 2,3-bis(4-(2-decyltetradecyl)phenyl)-1,4-diphenyltriphenylene-based co- and homo-polymers (**P_1-P_9**). From the UV-Vis absorption and PL spectra it was found that all polymers depict similar behavior in solution but not in thin films, which was attributed to the number of aryl units around the triphenylene moiety. While the more aryl substituted polymers **P_1**, **P_2**, **P_3**, **P_4**, **P_6**, **P_8** and **P_9** demonstrated deep blue emission with PL maxima around 430 nm, the less aryl substituted polymers **P_5** and **P_7** depicted large bathochromic shifts (30-40 nm) compared to this value. Based on that, it can be concluded that decreasing the number of aryl units around the triphenylene moiety was not favored since it lead to polymer aggregates.

According to the 2D-WAX studies it was also found that a well-aligned macroscopic organization was related to the triphenylene-*alt*-arylene copolymer when compared to the homopolymers. This dissimilarity in the macroscopic organization was ascribed to the reduced / increased twist the polymer's backbone as a result of the existence / absence of extra arylene groups between the triphenylene units in the polymer chain.

The thermal stability of the polymers were also tested using the TGA analysis, and all polymers exhibited good thermal stability up to 300^{o}C.

Following that some of the polymers were tested as active materials in blue-PLED devices. The fabricated devices showed the best performances only upon using hole-transporting, electron-transporting, and hole-blocking materials in the device structure.

In chapter 3, in order to achieve even higher blue-PLED device efficiency, the triphenylene moiety was coupled with other blue emitter of high quantum yield. For that, new TP-Py (**P_{10}**), TP-F (**P_{11}** and **P_{12}**), and TP-Cz (**P_{13}**) copolymers were synthesized using the same routes used for polymers **P_1-P_9**. The four polymers exhibited blue emission in solution and in thin films but with pronounced low energy bands (up to 650 nm) in the film case. Since the four systems composed of two blue chromophores, it was found that Förster energy transfer was possible to occur. This behavior was observed in polymer **P_{10}** with the triphenylene moiety in the polymer acting as donors and the pyrene unit serving as an energy acceptor. On the other hand the Förster energy transfer was not clear in polymers **P_{11}**, **P_{12}**, and **P_{13}**.

It was also proved that polymers **P_{11}** and **P_{13}** were of higher supramolecular organization compared to **P_{12}** polymer when studied by 2D-WAXS. The poorer organization of **P_{12}** was attributed to the presence of the bulky alkyl side chains attached to the fluorenylene unit which are expect to be out-of-plane arranged together with the high steric hindrance of the aryl units around t the triphenylene units. The thermal stabilities of polymers **P_{10}-P_{13}** were in agreement with those of polymers **P_1-P_9** (stable up to 300^{o}C).

Testing the polymers as emissive layers in blue-PLED devices revealed that only polymer **P_{10}** (TP-Py) was of deep blue emission with descent luminescence efficiency (Max.η_L = 0.22 cd/A). Polymers **P_{11}**, **P_{12}**, and **P_{13}** showed green and greenish-blue emission, respectively. Thus, it can be concluded that polymers **P_{11}**and **P_{12}** can not considered as suitable emitters for blue-PLED. On the other hand **P_{10}** and **P_{13}** are proper blue emitters for PLEDs, however the device structure need further improvement to get ride of the associated green emission in the emission of **P_{13}** and to enhance the device performances in both cases.

These results proved that coupling the triphenylene unit with other chromophore in one conjugated systems is an effective method to tune the final polymer properties. Consequently, this study can be extended in the future by applying other chromophors than those presented here.

In chapter 4, the synthesis of novel graphene nanoribbons was presented. The synthetic protocols depended on the transformation of the triphenylene-based conjugated polymers into 2D-planarized graphene nanoribbons by means of chemical and surface-mediated cyclodehydrogenation routes.

In the solution route, the polymers were subjected to intramolecular oxidative cyclodehydrogenation by using Scholl reaction. The obtained materials after the cyclodehydrogenation reactions were either insoluble or of poor solubility. Therefore, the conventional characterization techniques were not able to give enough information about the structure of the formed materials. Even using solid state-based analytical methods (solid-state UV-Vis, IR, and conventional FT-Raman spectroscopy) did not help, since the weak intensity of the spectral signals hindered the structure elucidation.

Only using the micro-Raman analysis provided the obvious evidence of the formation of the desired **2D-GNRs**. The clear proof was achieved by proving that the D-bands in the Raman spectra were dedicated exclusively to the **GNRs**' edge (armchair structures) effects.

Further evidence was attained from the integrated area (A) under the D and G bands in the Raman spectra. The A(D) / A(G) aspect ration is normally expected to be larger for narrow **GNRs** compared to broader ribbons. The experimentally derived values showed that the narrow **GNR-22** showed aspect ratio of 1.32, while the broader ribbons **GNR-20** and **GNR-21** yield A(D)/A(G) values of 1.13 and 1.17 respectively.

The other way for the generation of **GNRs** was the surface-mediated cyclodehydrogenation route that was accomplished by firstly synthesizing functionalized precursor monomers that were functionalized in order to specifically interact with each other. Following the monomer's synthesis two subsequent thermal activation steps were conducted, in the first step the surface-adsorbed monomers were coupled to linear polymer chains, while in the second step the polymers were planarized into **GNRs** by cyclodehydrogenation. Most important is the modest temperatures used in our **GNR** fabrication method (< 450° C) that make the process compatible with current CMOS technology. Moreover, all fabrication steps from substrate preparation to the final cyclodehydrogenation were performed in situ, which allows for an investigation of the intrinsic properties of the resulting **GNRs** on clean and well-defined substrates. Several analytical methods such as STM, Raman spectroscopy, line profile analysis, and XPS analysis were applied to study the formed **GNRs**. All of these methods provided obvious confirmation that the desired **GNRs** were excellently formed and were of high chemical stability.

With possible molecular monomer precursors being virtually unlimited, this bottom-up approach of **GNR** fabrication will allow a manifold engineering of chemical and electronic properties and thus allow the so far elusive realization of theoretically predicted structures such as intraribbon quantum dots,[1] superlattice structures,[2] or magnetic devices based on specific **GNR** edge states.[3]

References

(1) Huang, L., Lai, Y.C., Ferry, D.K., Akis, R., & Goodnick, S.M., Transmission and scarring in graphene quantum dots. *J. Phys.: Condens. Matter* **21**, 344203 (2009).

(2) Sevincli, H., Topsakal, M., & Ciraci, S., Superlattice structures of graphene-based armchair nanoribbons. *Phys. Rev. B* **78**, 245402 (2008).

(3) Son, Y.W., Cohen, M.L., & Louie, S.G. Half-metallic graphene nanoribbons. *Nature* **444**, 347-349 (2006).

Chapter 6

Experimental Section

6.1 Reagents and analysis instruments

Materials:

All starting materials, solvents and catalysts for chemical reactions otherwise mentioned were purchased from Aldrich, Acros, Fluka, ABCR, TCI, Strem, and Alfa Aesar and used as received without purification. Only 2,7-dibromophenanthrene-9,10-dione (**1**) was received from Ciba Inc.

Chromatography:

Preparative column chromatography was performed on silica gel from Merck with particle size of 0.063-0.200 mm (Geduran Si 60). For analytical thin layer chromatography (TLC) silica gel coated substrates 60 F254 from Merck were used. Compounds were detected by fluorescence quenching at 254 nm and self-fluorescence at 366 nm. Gel-permeation chromatography (GPC) analysis was performed with SDV (PSS) columns (10^6, 10^4, and 500 Å porosity) connected to RI and UV (254 nm) detectors against polystyrene standards, and calibrated for 1,4-polyparaphenylene (PPP) using THF as an eluting solvent.

NMR Spectroscopy:

^{1}HNMR and ^{13}C-NMR spectra were recorded in deuterated solvents on a Bruker DPX250 or Bruker AMX 300 spectrometer with use of the solvent proton or carbon signal as an internal standard.

Mass spectrometry:

FD mass spectra were obtained on a VG Instruments ZAB 2-SE-FPD spectrometer. MALDI-TOF mass spectra were measured on a Bruker Reflex IITOF spectrometer using a 337 nm nitrogen laser and 7,7,8,8-tetracyanoquinodimethane (TCNQ) as matrix. The mass instrument is not dedicated to isotopic measurements, and the deviations of relative intensities of peaks, from those calculated, can be more than 10%.

UV/Vis spectroscopy:

UV/Vis spectra were recorded at room temperature on a Perkin-Elmer Lambda 9 spectrophotometer.

Photoluminescence spectroscopy:

Photoluminescence (PL) spectra were recorded on a SPEX–Fluorolog II (212) spectrometer.

Cyclic voltammetry:

Cyclic voltammetry measurements were conducted for drop casted polymer films from toluene solution using scanning rate 100 mVs^{-1} at room temperature under argon protection with 0.1 M tetrabutylammonium perchlorate ($TBAClO_4$) in acetonitrile solution as the supporting electrolyte. A platinum electrode was used as the working electrode and an Ag/Ag^+ electrode as the reference electrode.

Elemental analysis: Elemental analyses were carried out on a Foss Heraeus Vario EL as a service of the Institute for Organic Chemistry, Johannes-Gutenberg-University of Mainz. Because of the high carbon content of large PAHs and some other compounds, combustion may be incomplete (soot formation), resulting in values lower than expected for the carbon content.

Differential scanning calorimetry (DSC) and thermogravimetric analysis (TGA): DSC was measured on a Mettler DSC 30 with heating and cooling rates of 10°C / min in the range from -150 °C to 250 °C. For TGA a Mettler TG 50 thermogravimetric analyzer was used.

Two-dimensional wide-angle X-ray scattering (2D-WAXS):

2D-WAXS measurements of oriented filaments were conducted using a rotating anode (Rigaku 18 kW) X-ray beam (CuKa, pinhole collimation, double graphite monochromator) and CCD camera. The patterns were recorded with vertical orientation of the filament axis and with the beam perpendicular to the filament.

Transmission electron microscope (TEM):

TEM studies were conducted on a Philips Tecnai F20 electron microscope at an operating voltage of 200 kV.

Scanning Tunneling Microscopy (STM):

STM images were done using a variable-temperature STM (VT-STM) and a low-temperature STM (LT-STM), both from Omicron Nanotechnology GmbH, Germany. Images were taken in the constant current mode under ultra-high vacuum conditions at sample temperatures of 298 K (room temperature), 115 K (LN_2 cooling) or 35 K (LHe cooling) in the VT-STM and 77 K or 5 K in the LT-STM. The WSxM software (Horcas, I. et al., *Rev. Sci. Instrum.* **2007**, 78, 013705) was used to analyze the STM images.

Micro-Raman spectroscopy:

Micro-Raman investigations were carried out using micro-Raman system consists of an optical microscope (Olympus) equipped with 100x/0.9 NA objective housed in a Horiba Jobin Yvon (HJY) LabRAM Aramis Raman system.

Raman spectroscopy:

The Raman studies were performed using a confocal Raman microscope CRM200 (WiTec Wissenschaftliche Instrumente und Technologie GmbH, Ulm) that was operated at an excitation laser wavelength of 532.3 nm. Laser light was provided via a single-mode optical fibre, supporting only a single transversal mode. A 100X objective of 0.8NA and a multi-mode fiber acted as a pinhole of 100 μm in diameter established confocal conditions. Raman spectra were recorded at 2 mW laser intensity with an integration time of 30 s.

X-ray photoelectron spectroscopy (XPS):

Photoemission experiments were performed on an Omicron ESCA system equipped with an EA-125 analyzer that was operated at a base pressure of 2 x 10^{-10} mbar. For XPS experiments a monochromatized X-Ray source (Al K_α 1486.7 eV) was used and all spectra were recorded at room temperature. Overview XPS spectra were measured with a pass energy of 80 eV , high-resolution spectra of the C1s core level with a pass energy of 10 eV.

Simulation of STM images for GNRs:

Large scale simulations with the CP2K suite were performed to simulate the STM images. Assuming that no chemical bonds between the molecules and the substrate are being formed a combined approach was used by modeling the surface via empirical potentials and the molecule–surface interaction through a potential that reproduces the van der Waals interaction in the form of C6/R6 and the core repulsion in an exponential form. The molecules on the other hand were treated with the empirical density functional based tight binding (DFTB) method. This approach has proven to be successful in the description of similar systems. The STM images were simulated according to the Tersoff-Hamann approach with an additional rolling ball algorithm to include tip effects. The integrated density of states between the Fermi energy and the Fermi energy plus a given bias were extracted from a Gaussian and plane waves (GPW) approach for the given geometries.

Calculation of the band structure and Raman spectra for GNRs:

DFT calculations were performed using the Quantum-Espresso code employing the PBE-GGA as the exchange correlation functional in the Kohn-Sham equations. The lattice constant of bulk graphene of 2.470 Å was used, and a slice of at least 8.5 Å was left between the ribbons in the super-cell geometry and the vacuum side. The integral over the first Brillouin zone was taken by using 32 and 10 equidistant k-points along the ribbons. The static Raman coefficients were calculated using the second-order response approach of Lazzeri and Mauri.

PLED device fabrication

The device fabrication was carried out by Moussa Saleh and Young-Seo Park at the Department of Materials Science and Engineering the ‘‘OLED Center’’, in the group of Prof. Dr. Jang-Joo Kim, Seoul National University in Seoul, S. Korea.

The ITO covered glass substrates for the PLEDs were thoroughly cleaned in acetone and isopropyl alcohol and were exposed to an oxygen plasma dry cleaning step using UV Ozone cleaner (185 nm, Nippon laser& Electronic Lab.). Following that PEDOT:PSS layers were spin coated under ambient conditions and dried at 200^{o}C for 5 min and cooled slowly for 40 min. The emissive polymer (containing HTL and ETL) films were spin-cast from toluene solution and dried under argon atmosphere, followed by the thermal deposition of a hole-blocking layer. Metal electrodes were thermally deposited in a vacuum coating mounted in a glove box under a vacuum of $<5 \times 10^{-7}$ Torr.

The current/luminance/voltage (IVL) characteristics were recorded using PR-650 Spectra Colorimeter (LMS) for recording the current/voltage characteristics while recording the electoluminance.

6.2 General synthetic routes

5,10-dibromo-1,3-diphenyl-2H-cyclopenta[l]phenanthren-2-one (3)

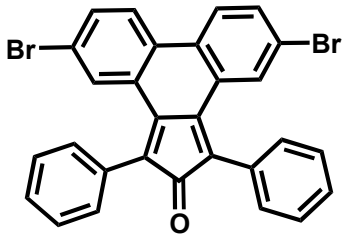

In a dry and inert 100 ml Schlenk flask equipped with magnetic stirrer and septum 2,7-dibromophenanthrene-9,10-dione 1 (10 g, 27.3 mmol), 1,3-diphenylpropan-2-one (2) (6.3 g, 30 mmol), and 30 ml of dry ethanol were combined. To the resulting slurry 0.76 g potassium

hydroxide dissolved in 25 ml methanol was added drop wise. The reaction mixture was vigorously stirred under argon for 1 h at 80°C. During the reaction a dark green precipitate formed. The product was filtered off, washed with excess ethanol and dried under reduced pressure to give 6 g (40 %) of **3**, which was used without further purification.

1-(dodec-1-ynyl)-4-octylbenzene (4b)

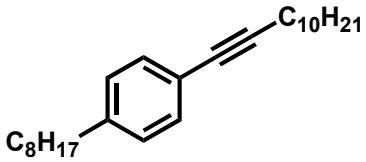

A solution of 1-dodecyne (1.2 g, 7 mmol), 1-bromo-4-octyl-benzene 6 (1.6 g, 6 mmol), CuI (0.115 g, 0.6 mmol), in piperidine (20 ml) was placed in 100 ml Schlenk flask the mixture was degassed by three "freeze–pump–thaw" cycles, and then $Pd(PPh_3)_4$ (0.35 g, 0.3 mmol) was added. The resulting mixture was degassed again by three "freeze–pump–thaw" cycles. The mixture was stirred at 50^{o}C for 3 days. The mixture was extracted with dichloromethane, and the extract was washed with brine and then dried over $MgSO_4$. The crude product obtained was purified by chromatography on silica gel with pure hexane as the eluent. The product **4b** was isolated as yellow oil (1.5 g, 70 %).

^{1}H NMR (250 MH_Z, CD_2Cl_2): δ = 7.28 (d, *J* = 8.08 Hz, 2H), 7.10 (d, *J* = 8.09 Hz, 2H), 2.59 (t, *J* = 7.5 Hz, 2H), 2.40 (t, *J* = 6.9 Hz, 2H), 1.6-0.86 (m, 34H).

^{13}C NMR (62.5 MHZ, CD_2Cl_2): δ = 143.26, 131.9, 128.9, 121.9, 90.3, 81, 36.4, 32.6, 32.5, 32, 30.3, 30.2, 30.1, 30, 29.9, 29.8, 29.6, 29.5, 23.4, 19.9, 14.5.

FD-MS: m/z calc.:354.6, found: 354.7 ($C_{26}H_{42}$).

Elemental analysis (%) calcd for $C_{26}H_{42}$: C 88.06, H 11.94; found: C 87.73, H 12.0

Trimethyl-(4-octylphenyl)ethynyl) silane (7)

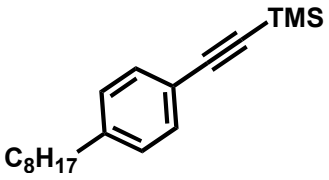

A degassed solution of 1-bromo-4-octyl-benzene 6 (2 g, 7.43 mmol), CuI (0.136 g, 0.715 mmol), $Pd(PPh_3)_4$ (0.43 g, 0.37 mmol) in piperidine (48 ml), was heated up to 50°C then ethynyltrimethylsilane (1.483 g, 15.1 mmol) was added drop wise. The resulting mixture was stirred at 80°C for 24 h under argon atmosphere. The reaction mixture was poured into a saturated NH_4Cl solution and extracted with DCM. The organic phase was washed with half concentrated ammonium chloride solution and water. After removing the solvent the residue was purified by column chromatography on silica gel with hexane to afford **7** as yellow oil (1.93 g, 91 %).

^{1}H NMR (250 MHZ, CD_2Cl_2): δ = 7.36 (d, *J* = 8.04 Hz, 2H), 7.13 (d, *J* = 8.04 Hz, 2H), 2.61 (t, *J* = 7.50 Hz, 2H), 1.62 -0.25 (m, 24H).

FD-MS: m/z calc.:286.5, found: 286.7 ($C_{19}H_{30}Si$).

1-ethynyl-4-octylbenzene (8)

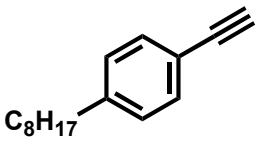

To a solution of 7 (1.9 g, 6.73 mmol) in THF (2 ml), tetrabutylammonium fluoride (TBAF) 0.1 M in THF (2.11 g, 8 mmol) was added drop wise. After stirring at room temperature for 1h the reaction was quenched by water (10 ml). The organic phase was extracted by DCM, washed with brine, dried over $MgSO_4$ and concentrated under reduced pressure. The residue was purified by column chromatography on silica gel with hexane to afford **8** as yellow oil (0.9 g, 62 %).

^{1}H NMR (250 MHZ, CD_2Cl_2): δ = 7.4 (d, *J* = 8.17 Hz, 2H), 7.15 (d, *J* = 8.18 Hz, 2H), 3.1 (s, 1 H), 2.62 (t, *J* = 7.48 Hz, 2H), 1.62 -0.86 (m, 15H).

1,2-bis(4-octylphenyl)ethyne (4c)

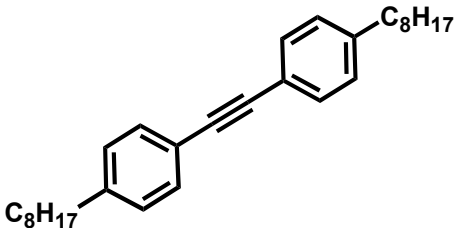

A solution of 1-ethynyl-4-octylbenzene (**8**) (0.9 g, 4.2 mmol), 1-bromo-4-octyl-benzene (**6**) (1.35 g, 5 mmol), CuI (0.08 g, 0.42 mmol) in piperidine (14 ml) was placed in 100 ml schlenk flask the mixture was degassed by three "freeze–pump–thaw" cycles, and then $Pd(PPh_3)_4$ (0.24 g, 0.21 mmol) was added. The resulting mixture was degassed again by three "freeze–pump–thaw" cycles. The mixture was stirred at 80^{o}C for 2 days. The mixture was extracted with DCM, and the extract was washed with brine and then dried over $MgSO_4$. The crude product so obtained was purified by chromatography on silica gel with pure hexane as the eluent. The product **4c** was isolated as a white solid (1 g, 59 %).

^{1}HNMR (250 MHZ, CD_2Cl_2): δ = 7.45 (d, *J* = 8.04 Hz, 4H), 7.19 (d, *J* = 8.07 Hz, 4H), 2.65 (t, *J* = 7.6 Hz, 4H), 1.62-1.59 (m, 4H), 1.32-1.31 (m, 20H), 0.90 (t, *J* = 7.30 Hz, 6 H).

^{13}C NMR (62.5 MHZ, CD_2Cl_2): δ = 144.1, 131.8, 129, 121, 89.3, 36.4, 32.4, 31.8, 30, 29.8, 23.2, 14.4.

FD-MS: m/z calc.:402.6, found: 402 ($C_{30}H_{42}$).

Elemental analysis (%) calcd for $C_{30}H_{42}$: C 89.49, H 10.51; found: C 89.01, H 10.34.

1,2-bis(4-(2-decyltetradecyl)phenyl)ethyne (4g)

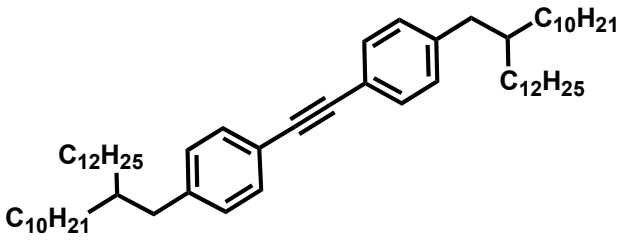

In a dry schlenk flask zinc dust (4.6 g, 72 mmol), iodine (0.16g, 2.4 mmol), alkyl halide **10** (20 g, 48 mmol) in dimethylacetamide (90 ml) were stirred under argon for 24 h at 80°C. The formed Negishi reagent was then transferred via a cannula to an argon filled flask that was previously charged with the tolane **11** (3.2 g, 9.5 mmol) and the catalyst $PdCl_2$(dppf). Following that the reaction mixture was stirred at 50°C overnight. The mixture was extracted with DCM, and washed with diluted HCl solution. The crude product was then purified using chromatography on silica gel with pure hexane as the eluent. The product **4g** was isolated as yellow oil (6.5 g, 80 %).

^{1}HNMR (250 MHZ, CD_2Cl_2): δ = 7.42 (d, *J* = 8.16 Hz, 4H), 7.14 (d, *J* = 8.17 Hz, 4H), 2.55 (d, *J* = 6.98 Hz, 4H), 1.73-0.84 (m, 94H).

FD-MS: m/z calc.:851.5, found: 850.5 ($C_{62}H_{106}$).

6,11-dibromo-2-heptyl-1,3,4-triphenyltriphenylene (5a)

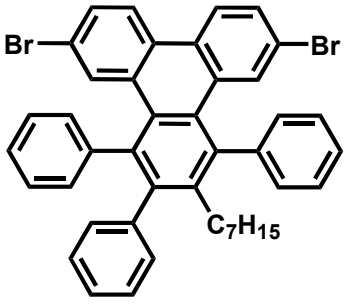

5,10-dibromo-1,3-diphenyl-2H-cyclopenta[l]phenanthren-2-one (**3**) (0.37 g, 0.7 mmol), 1-phenyl-1-nonyne (**4a**) (0.14 g, 0.7 mmol) and 3.0 ml of diphenylether were placed in 50 ml schlenk flask, which was purged with argon and sealed. The reaction mixture left to reflux for 12 h. The solvent was removed under reduced pressure and the product was finally purified by

chromatography on silica gel with Hexane: DCM (20:1), to give compound **5a** as a light yellow solid (0.250 g, 50 %).

^{1}H NMR (250 MHZ, CD_2Cl_2): δ = 8.24-8.20 (m, 2H), 7.77 (d, *J* = 1.9 Hz, 1H), 7.68 (d, *J* = 1.9 Hz, 1H), 7.51-7.38 (m, 7H), 7.22-7.03 (m,10H), 2.48 (t, *J* = 8.33 Hz, 2H), 1.26-0.76 (m,13H).

FD-MS: m/z calc.:712.5, found: 712.4 ($C_{43}H_{36}Br_2$).

6,11-dibromo-2-decyl-3-(4-octylphenyl)-1,4-diphenyltriphenylene (5b)

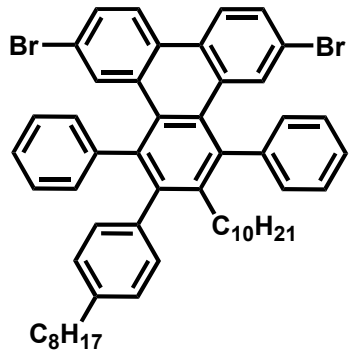

Compound **3** (2 g, 3.7 mmol), compound (**4b**) (1.0 g, 2.8 mmol) and 23 ml of diphenylether were placed in a microwave tube, which was purged with argon and sealed. The reaction was carried out in a CEM Discover microwave at 300 W and activated cooling, keeping the temperature between 230°C and 250°C for 12 h. The solvent was removed under reduced pressure. The product was finally purified by chromatography on silica gel with Hexane: DCM (20:1), to give compound **5b** as a light yellow solid (0.650 g, 27 %).

^{1}H NMR (250 MHZ, CD_2Cl_2): δ = 8.22-8.16 (m, 2H), 7.78 (d, *J* = 1.94 Hz, 1H), 7.70 (d, *J* = 1.93 Hz, 1H), 7.50-7.39 (m, 7H), 7.15-6.98 (m, 9H), 2.60-2.49 (m, 4H), 1.53-0.86 (m, 34H).

^{13}C NMR (62.5 MHZ, CD_2Cl_2): δ = 143.1, 143, 142.9, 141.5, 141.2, 138.6, 138.4, 138, 133, 132.8, 132.4, 131.8, 131, 130.6, 130, 129.7, 129.6, 129.5, 129.4, 129.3, 128.5, 128, 127.8, 126.9, 125.1, 125, 120.5, 120.4, 36, 32.5, 32, 31.1, 30.2, 30.1, 29.9, 29.8, 29.5, 29.2, 23.3, 14.4.

FD-MS: m/z calc.:866.8, found: 867.3 ($C_{54}H_{58}Br_2$).

Elemental analysis (%) calcd for $C_{54}H_{58}Br_2$: C 74.82, H 6.74; found: C 74.75, H 7.0.

6,11-dibromo-2,3-bis(4-octylphenyl)-1,4-diphenyltriphenylene (5c)

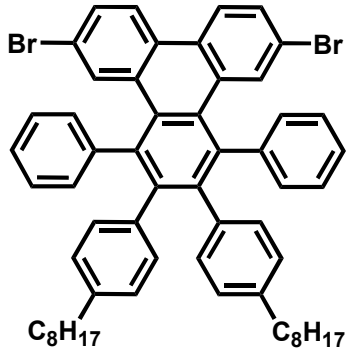

Compound **3** (0.54 g, 1mmol), compound **4c** (0.402 g, 1 mmol) and 0.5 ml diphenylether were placed in 10 ml schlenk flask, the mixture was degassed and left to reflux for 12 h. The solvent was removed under reduced pressure and the product was purified by chromatography on silica gel with Hexane: DCM (10:1), to give compound **5c** as light yellow oil (0.165 g, 18 %).

^{1}H NMR (250 MHZ, CD_2Cl_2): δ = 8.23 (d, *J* = 8.73 Hz, 2H), 7.65 (d, *J* = 1.77 Hz, 2H), 7.49 (d, *J* = 8.66 Hz, 2H), 7.17-7.04 (m, 10H), 6.71 (d, *J* = 7.92 Hz, 4H), 6.60 (d, *J* = 7.96, 4H), 2.40 (t, *J* = 7.37 Hz, 4H), 1.52-1.43 (m, 4H), 1.27-1.17(m, 20H), 0.88(t, *J* = 6.85 Hz, 6H) .

^{13}C NMR (62.5 MHZ, CD_2Cl_2): δ = 142.7, 142.2, 140.5, 138, 137.7, 133.2, 132.9, 132.5, 131.7, 130.6, 130, 129.9, 128.7, 127.2, 127.1, 125.1, 120.4, 35.8, 32.5, 31.9, 30, 29.9, 29.3, 23.2, 14.4.

FD-MS: m/z calc.:914.8, found: 914.6 ($C_{58}H_{58}Br_2$).

Elemental analysis (%) calcd for $C_{58}H_{58}Br_2$: C 76.14, H 6.39; found: C 74.42, H 6.22.

6,11-dibromo-1,2,3,4-tetraphenyltriphenylene (5d)

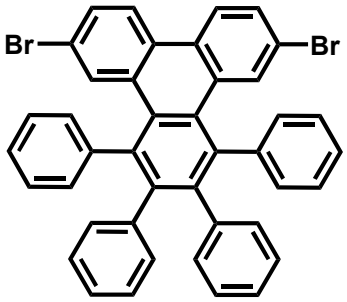

A solution of **3** (4 g, 7.4 mmol) and 1 equivalent of 1,2-diphenylethyne (**4d**) (1.32 g, 7.4 mmol) in diphenylether (30 ml) was placed in a microwave tube. The same reaction conditions and work up as in **5b** were applied here. The product was finally purified by chromatography on silica gel with hexane: DCM (10:1), to give compound **5d** as a light yellow solid (1.3 g, 25 %).

^{1}H NMR (250 MHZ, CD_2Cl_2): δ = 8.24 (d, *J* = 8.73, 2H), 7.67 (d, *J* = 1.74 Hz, 2H), 7.51 (d, *J* = 8.65 Hz, 2H), 7.19-6.73 (m, 20H).

^{13}C NMR (62.5 MHZ, CD_2Cl_2): δ = 142.6, 141.9, 140.6, 138.1, 133.1, 132.8, 132.4, 131.9, 130.7, 130.1, 130, 128.7, 127.2, 127.1, 125.9, 125.1, 120.5.

FD-MS: m/z calc.:690.4, found: 690 ($C_{42}H_{26}Br_2$).

6,11-dibromo-2,3-diheptyl-1,4-diphenyltriphenylene (5e)

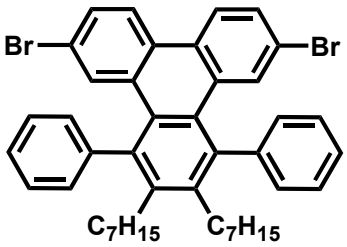

A solution of **3** (5 g, 9.3 mmol) and 8-hexadecyne (**4e**) (2.1 g, 9.3 mmol) in diphenylether (20 ml) was placed in a microwave tube. The same reaction conditions and work up as in **5b** were applied here. The product was finally purified by chromatography on silica gel with hexane: DCM (20:1), to give compound **5e** as a light yellow solid (0.706 g, 10 %).

^{1}H NMR (250 MHZ, CD_2CL_2): δ = 8.15 (d, *J* = 8.73Hz, 2H), 7.72 (s, 2H), 7.50-7.35

(m, 12H), 2.9 (t, *J* = 7.5 Hz, 4H), 1.27-1.10 (m, 20H), 0.83 (t, *J* = 7.17 Hz, 6H).

^{13}C NMR (62.5 MHZ, CD_2Cl_2): δ = 143.2, 141.2, 138.8, 133, 132.7, 132.1, 129.9, 129.7, 129.4, 129.2, 127.8, 124.9, 120.3, 32.1, 31.5, 30.8, 30.2, 29.2, 23.1, 14.3.

FD-MS: m/z calc.:734.6, found: 734.6 ($C_{44}H_{46}Br_2$).

Elemental analysis (%) calcd for $C_{44}H_{46}Br_2$: C 71.94, H 6.31; found: C 71.65, H 6.34.

6,11-dibromo-2,3-bis(4-dodecylphenyl)-1,4-diphenyltriphenylene (5f)

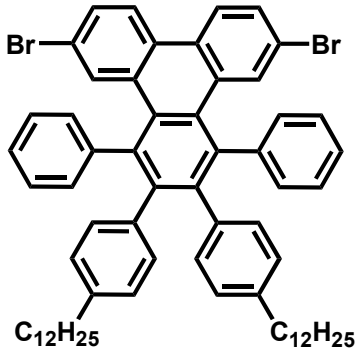

Compound **3** (2 g, 3.7 mmol), 1,2-bis(4-dodecylphenyl)ethyne (**4f**) (1.7 g, 3.3 mmol) and 23 ml diphenylether were placed in 50 ml schlenk flask. The same reaction conditions and work up as in **5c** were applied here. The product was purified by chromatography on silica gel with Hexane: DCM (20:1), to give compound **5f** as light yellow oil (0.54 g, 16 %).

^{1}H NMR (250 MHZ, CD_2Cl_2): δ = 8.02 (d, *J* = 8.74 Hz, 2H), 7.47 (d, *J* = 1.64 Hz, 2H), 7.29 (d, *J* = 8.57 Hz, 2H), 7.03-6.86 (m, 10H), 6.54-6.40 (m, 8H), 2.25 (t, *J* = 7.23 Hz, 4H), 1.32-0.99 (m, 40H), 0.72 (t, *J* = 5.48 Hz, 6H) .

FD-MS: m/z calc.:1027.1, found: 1027 ($C_{66}H_{74}Br_2$).

6,11-dibromo-2,3-bis(4-(2-decyltetradecyl)phenyl)-1,4-diphenyltriphenylene (5g)

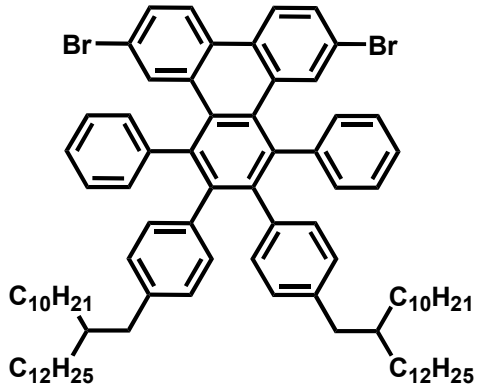

Compound **3** (0.63 g, 1.2 mmol), compound **4g** (0.5 g, 0.6 mmol) and 2.5 ml diphenylether were placed in 10 ml schlenk flask. The same reaction conditions, work up, and purification methode as in **5c** were applied here to provide compound **5g** as light yellow oil (0.16 g, 20 %). ^{1}H NMR (250 MHZ, CD_2Cl_2): δ = 8.23 (d, *J* = 8.78 Hz, 2H), 7.66 (d, *J* = 1.95 Hz, 2H), 7.49 (d, *J* = 8.61 Hz, 2H), 7.19-7.04 (m, 10H), 6.69-6.57 (m, 8H), 2.34 (d, *J* = 7.0 Hz, 4H), 1.53-0.85 (m, 94H).

FD-MS: m/z calc.:1363.7, found: 1362 ($C_{90}H_{122}Br_2$).

Elemental analysis (%) calcd for $C_{90}H_{122}Br_2$: C 79.26, H 9.02; found: C 79.57, H 9.26.

2,2'-(9,10,11,12-tetraphenyltriphenylene-2,7-diyl)bis(4,4,5,5-tetramethyl-1,3,2-dioxaborolane) (12)

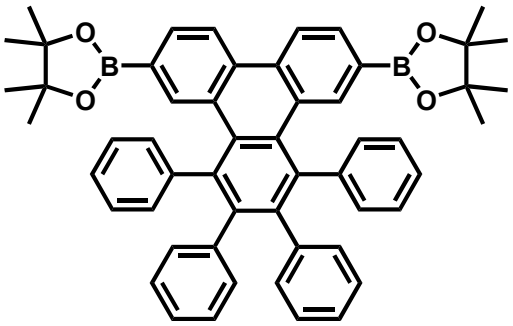

In 100 ml dry schlenk flask, **5d** (1.1 g, 1.6 mmol), bis(pinacolato)diboron (0.9 g, 3.5 mmol), potassium acetate (0.46 g, 4.7 mmol), [$PdCl_2$(dppf)]CH_2Cl_2 (0.065 g, 4.7 mmol), and 17.5 ml

dioxane were charged. The mixture was degassed and stirred at 95°C for 20 h. The crude product was extracted by DCM. The product was purified by chromatography on silica gel with Hexane: DCM (1:1), to afford compound **12** as light yellow solid (0.495 g, 40 %).

^{1}H NMR (250 MHZ, CD_2Cl_2): δ = 8.43 (d, *J* = 8.05 Hz, 2H), 8.11 (d, *J* = 0.82 Hz, 2H), 7.71 (d, *J* = 8.03 Hz, 2H), 7.1-6.7 (m, 20H), 1.22 (s, 24H).

FD-MS: m/z calc.:784.5, found: 784 ($C_{54}H_{50}Br_2O_4$).

6,11-bis(4-tert-butylphenyl)-1,2,3,4-tetraphenyltriphenylene (17)

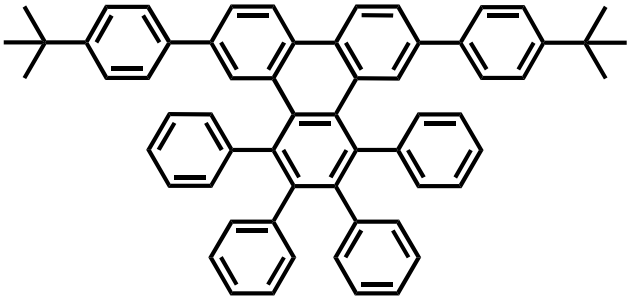

In 35 ml microwave vial, monomer **5d** (0.1 g, 0.145 mmol), 4-tert-butylbenzeneboronic acid (0.065 g, 0.36 mmol), aqueous K_2CO_3 (1 ml / 2M), aliquat 336 (0.02 g, 0.05 mmol), $Pd(PPh_3)_4$ (0.008 g, 0.007 mmol), and toluene (2 ml) were charged. The reaction mixture was stirred under argon atmosphere in a CEM Discover microwave at 50 W under activated cooling; keeping the temperature at 100°C for 1 h. The crude product was extracted with DCM, and finally purified with chromatography on silica gel with petroleum ether: DCM (8:1), to afford compound **17** as light yellow solid (0.05 g, 43 %).

^{1}H NMR (250 MHZ, CD_2Cl_2): δ = 8.5 (d, *J* = 8.5 Hz, 2H), 8.1 (d, *J* = 1.75 Hz, 2H), 7.7 (d, *J* = 8.4 Hz, 2H), 7.3-6.7 (m, 28H), 1.32 (s, 18H).

FD-MS: m/z calc.:797.1, found: 796 ($C_{62}H_{52}$).

Synthesis of Polymers

The general procedure of polymerization was preceded through the microwave assisted Suzuki and Yamamoto coupling reactions.

Suzuki Synthesis

Typical route for the formation of triphenylene based polymers type P_1 (TP A).

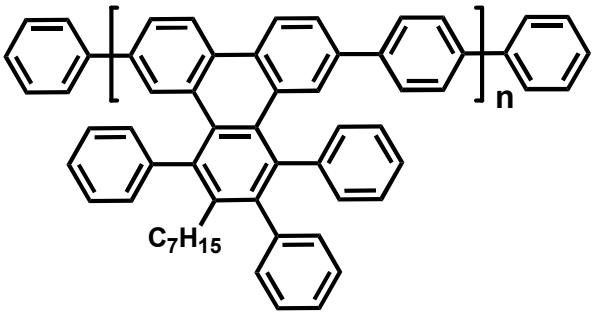

A suspension of monomer **5a** (0.099 g, 0.14 mmol), 1,4-bis(4,4,5,5-tetramethyl-1,3,2-dioxaborolan-2-yl)benzene (0.046 g, 0.14 mmol), aqueous K_2CO_3 (1 ml / 2M), aliquat 336 (0.02 g, 0.05 mmol), and $Pd(PPh_3)_4$ (0.008 g, 0.007 mmol) in toluene (2 ml) was charged in a microwave tube equipped with a magnetic stirrer bar, which was purged with argon and sealed. The mixture was vigorously stirred in a CEM Discover microwave at 50 W and activated cooling; keeping the temperature at 100°C for 1 h. Sequentially bromobenzene (0.132 g, 0.84 mmol), and benzene boronic acid (0.1 g, 0.84 mmol) in degassed toluene (2 ml) were added to the reaction mixture and stirred at 100°C for ½ h each. At room temperature the organic layer was extracted and washed with aqueous sodium cyanide (1 %, 2 × 50 ml). The organic layer was extracted again with toluene and the solution was concentrated in vacuo until a high viscous solution was obtained. The polymer was precipitated by the slow addition to 300 ml methanol. The polymer filtered off and sequentially washed with methanol, water, acetone, and methanol. The polymer was dissolved again in toluene and vigorously stirred in aqueous sodium cyanide (1 %, 100 ml) at 90°C for 2 h. The organic phase was extracted, concentrated, and finally poured into excess of methanol. The polymer was filtered off, and the oligomeric fractions were removed by extraction (2 days / Soxhlet apparatus / ethyl acetate).

The isolated yield of polymer $\mathbf{P_1}$ was (0.06 g, 68 %). GPC analysis*:* $Mw = 19 \times 10^3$ g mol^{-1}, PDI = 1.9 (PPP standard).

Synthesis of polymer (P_2)

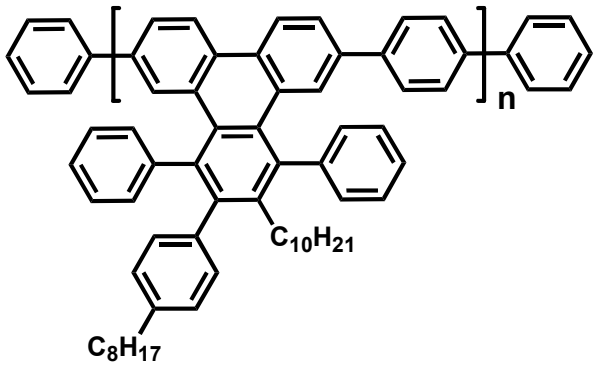

Prepared according to TP A; **5b** (0.234 g, 0.270 mmol), 1,4-bis(4,4,5,5-tetramethyl-1,3,2-dioxaborolan-2-yl)benzene (0.089 g, 0.270 mmol), aqueous K_2CO_3 (2 ml / 2M), aliquat 336 (0.04 g, 0.1 mmol), and $Pd(PPh_3)_4$ (0.015 g, 0.0135 mmol) in toluene (3 ml) was heated at 100°C for 1h. Bromobenzene (0.38g, 2.453 mmol), and benzene boronic acid (0.19 g, 1.584 mmol) in degassed toluene (2 ml) were added to the reaction mixture and stirred at 100°C for ½ h each. The isolated yield of polymer P_2 was (0.105 g, 55 %).

^{1}H NMR (250 MHZ, CD_2Cl_2): δ = 7.95-6.4 (m, 24H), 2.8-2.4 (m, 4H), 1.4-1.1 (m, 23H), 0.98-0.84 (m, 11H).

GPC analysis*: Mw* = 36 × 10^3 g mol^{-1}, PDI = 1.4 (PPP standard).

Synthesis of polymer (P_3)

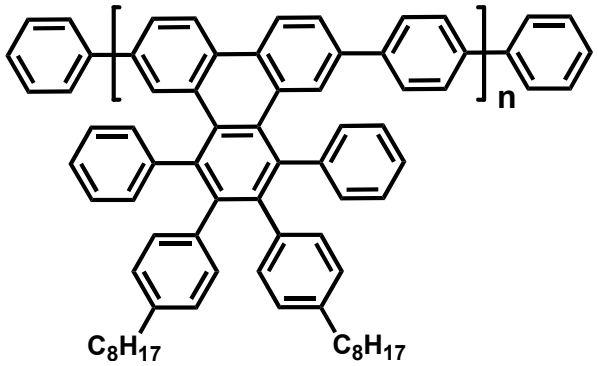

Prepared according to TP A; **5c** (0.099 g, 0.11 mmol), 1,4-bis(4,4,5,5-tetramethyl-1,3,2-dioxaborolan-2-yl)benzene (0.036 g, 0.11 mmol), aqueous K_2CO_3 (1 ml / 2M), aliquat 336 (0.02 g, 0.05 mmol), and $Pd(PPh_3)_4$ (0.006 g, 0.005 mmol) in toluene (3 ml) was heated at

100°C for 1 h. Bromobenzene (0.153g, 0.97 mmol), and benzene boronic acid (0.08 g, 0.65 mmol) in degassed toluene (1 ml) were added to the reaction mixture and stirred at 100°C for ½ h each. The isolated yield of polymer **P_3** was (0.061 g, 67 %).

^{1}H NMR (250 MHZ, CD_2Cl_2): δ = 8.3-6.3 (m, 28H), 2.5-2.4 (m, 4H), 1.3-0.9 (m, 30H).

GPC analysis*: Mw* = 15 × 10^3 g mol^{-1}, PDI = 1.9 (PPP standard).

Synthesis of polymer (P_4)

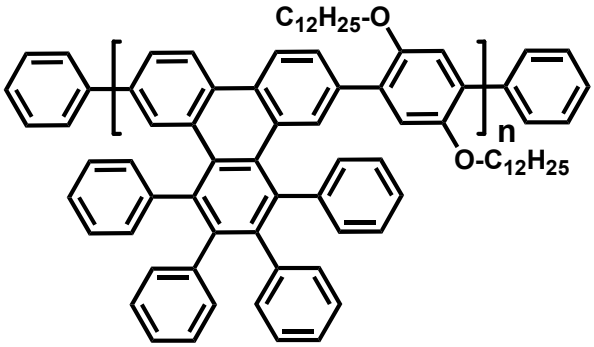

Prepared according to TP A; **5d** (0.273 g, 0.395 mmol), 2,5-bis(dodecyloxy)-1,4-bis(4,4,5,5-tetramethyl-1,3,2-dioxaborolan-2-yl)benzene (0.276 g, 0.395 mmol), aqueous K_2CO_3 (3 ml / 2M), aliquat 336 (0.04g, 0.1 mmol), and $Pd(PPh_3)_4$ (0.023 g, 0.02 mmol) in toluene (4 ml) was heated at 100°C for 1 h. Bromobenzene (0.56 g, 3.55 mmol), and benzene boronic acid (0.28 g, 2.3 mmol) in degassed toluene (3 ml) were added to the reaction mixture and stirred at 100°C for ½ h each. Finally the oligomeric fractions were removed by extraction (1 days / Soxhlet apparatus/acetone). The isolated yield of polymer **P_4** was (0.250 g, 65 %).

^{1}H NMR (250 MHZ, CD_2Cl_2): δ = 8.5-5.9 (m, 28H), 4-3.1 (m, 4H), 1.5-1 (m, 40H), 0.8 (t, *J* = 6.6Hz, 6H).

GPC analysis*: Mw* = 18 × 10^3 g mol^{-1}, PDI = 1.6 (PPP standard).

Synthesis of polymer (P_5)

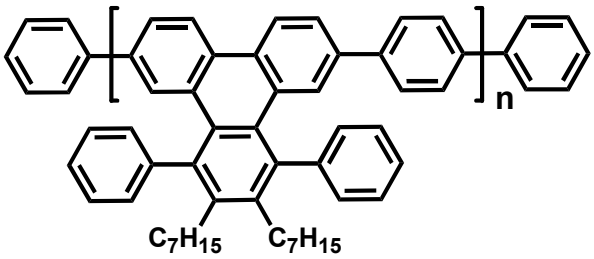

Prepared according to TP A; **5e** (0.289 g, 0.394 mmol),), 1,4-bis(4,4,5,5-tetramethyl-1,3,2-dioxaborolan-2-yl)benzene (0.13 g, 0.394 mmol), aqueous K_2CO_3 (3 ml / 2M), aliquat 336 (0.04 g, 0.1mmol), and $Pd(PPh_3)_4$ (0.023 g, 0.02 mmol) in toluene (4 ml) was heated at 100°C for 1 h. Bromobenzene (0.56 g, 3.58 mmol), and benzene boronic acid (0.28 g, 2.3 mmol) in degassed toluene (3 ml) were added to the reaction mixture and stirred at 100°C for ½ h each. The isolated yield of polymer **P_5** was (0.209 g, 81.5 %). GPC analysis*: Mw* = 63 × 10^3 g mol^{-1}, PDI = 3.6 (PPP standard).

Synthesis of polymer (P_6)

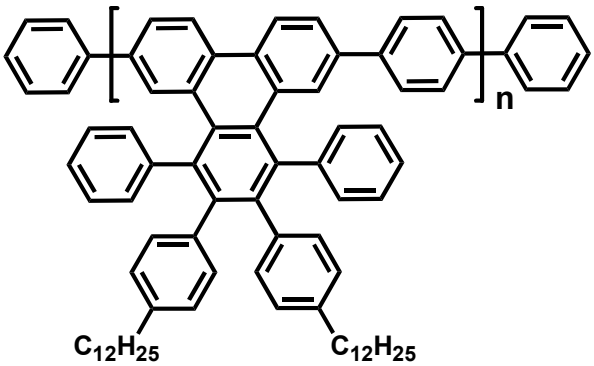

Prepared according to TP A; **5f** (0.17 g, 0.165 mmol),), 1,4-bis(4,4,5,5-tetramethyl-1,3,2-dioxaborolan-2-yl)benzene (0.054 g, 0.165 mmol), aqueous K_2CO_3 (1.3 ml / 2M), aliquat 336 (0.04 g, 0.1mmol), and $Pd(PPh_3)_4$ (0.01 g, 0.009 mmol) in toluene (2 ml) was heated at 100°C for 1 h. Bromobenzene (0.24 g, 1.5 mmol), and benzene boronic acid (0.12 g, 0.96 mmol) in degassed toluene (2 ml) were added to the reaction mixture and stirred at 100°C for ½ h each. The isolated yield of polymer **P_6** was (0.78 g, 50 %). GPC analysis*: Mw* = 19 × 10^3 g mol^{-1}, PDI = 1.5 (PPP standard).

Synthesis of polymer (P_{10})

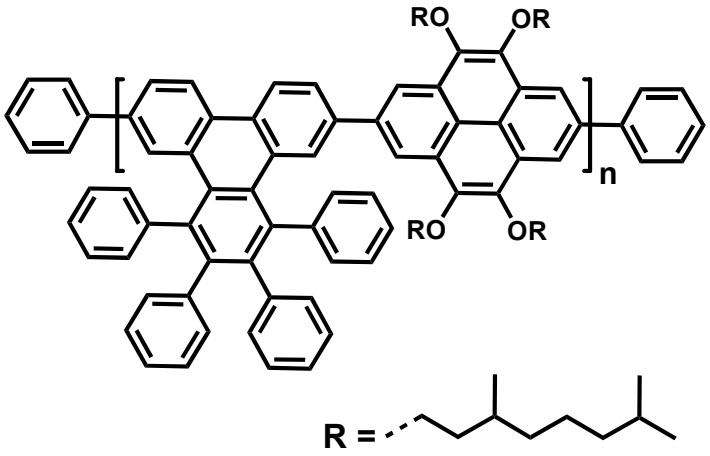

Prepared according to TP A; compound **12** (0.309 g, 0.39 mmol),), 2,7-dibromo-4,5,9,10-tetrakis(3,7-dimethyloctyloxy)pyrene **13** (0.387 g, 0.393 mmol), aqueous K_2CO_3 (3 ml / 2M), aliquat 336 (0.04 g, 0.1 mmol), and $Pd(PPh_3)_4$ (0.023 g, 0.0197 mmol) in toluene (4.5 mL) was heated at 100°C for 1 h. Sequentially bromobenzene (0.56 g, 3.6 mmol), and benzene boronic acid (0.28 g, 2.3 mmol) in degassed toluene (3 ml) were added to the reaction mixture and stirred at 100°C for ½ h each. The isolated yield of polymer **P_{10}** was (0.285 g, 53 %).

^{1}H NMR (250 MHZ, CD_2Cl_2): δ = 8.8-6.8 (m, 30H), 4.6-4.2 (m, 8H), 2.1-0.75 (m, 78H).

GPC analysis*: Mw* = 12 × 10^3 g mol^{-1}, PDI = 1.3 (PPP standard).

Synthesis of polymer (P_{13})

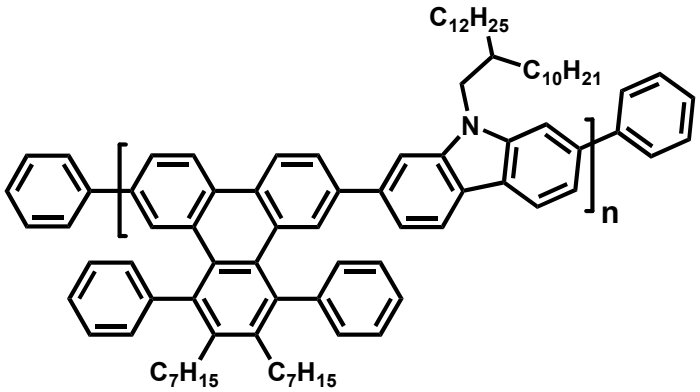

Prepared according to TP A; compound **5e** (0.1 g, 0.136 mmol), 9-(2-decyltetradecyl)-2,7-bis(4,4,5,5-tetramethyl-1,3,2-dioxaborolan-2-yl)-9H-carbazole (**15)** (0.102 g, 0.136 mmol),

aqueous K_2CO_3 (1 ml / 2M), aliquat 336 (0.04 g, 0.1 mmol), and $Pd(PPh_3)_4$ (0.008 g, 0.007 mmol) in toluene (1.5 mL) was heated at 100°C for 1 h. Sequentially bromobenzene (0.2 g, 1.24 mmol), and benzene boronic acid (0.1 g, 0.8 mmol) in degassed toluene (2 ml) were added to the reaction mixture and stirred at 100°C for ½ h each. The isolated yield of polymer **P_{13}** was (0.082 g, 56 %).

^{1}H NMR (250 MHZ, CD_2Cl_2): δ = 8.4-6.6 (m, 22H), 2.9-0.7 (m, 81H).

GPC analysis*: Mw* = 10 × 10^3 g mol^{-1}, PDI = 1.5 (PPP standard).

Yamamoto synthesis

Typical route for the formation of triphenylene based polymers type P_7 (TP B).

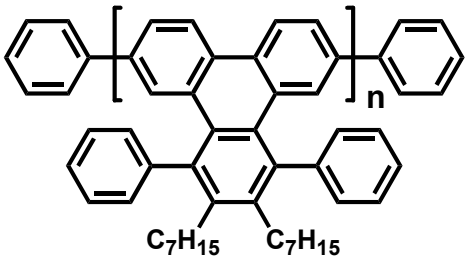

Bis(1,5-cyclooctadiene)nickel (0.179 g, 0.653 mmol), 1,5-cyclooctadiene (0.071 g, 0.653 mmol), and 2,2'-bipyridine (0.102 g, 0.653 mmol) were dissolved in dry toluene (3 ml) and dry *N*,*N*dimethylformamide (3 ml) and charged under argon in a microwave tube equipped with a magnetic stirrer bar. The mixture was heated at 80°C for 30 min to generate the catalyst. A solution of **5e** (0.2 g, 0.272 mmol) in dry toluene (4 ml) was added. The mixture was vigorously stirred in a CEM Discover microwave at 80 W and activated cooling; keeping the temperature at 80°C for 1 h. Bromobenzene (0.4 g, 2.56 mmol) was added, and the mixture was heated at 80°C for additional ½ h. The mixture was then poured into a mixture of methanol and concentrated hydrochloric acid (1:1, 400 ml) and stirred for 4 h. The precipitated yellow polymer was again dissolved in toluene (10 ml) and stirred in a saturated aqueous EDTA solution (200 ml) for 12 h. The organic layer was extracted and the polymer reprecipitated again in methanol, filtrated, sequentially washed with methanol, water, acetone,

and methanol. The isolated yield of polymer **P$_7$** was (0.146 g, 93 %).GPC analysis*: Mw* = 224 × 10^3 g mol^{-1}, PDI = 2.7 (PPP standard).

Synthesis of polymer (P$_8$)

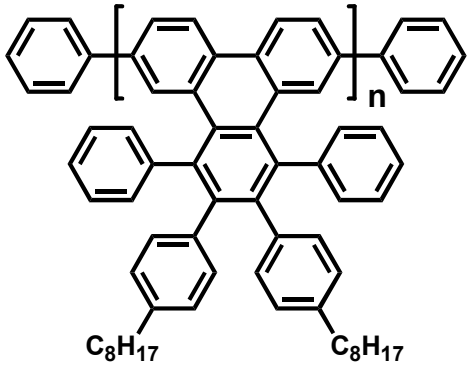

Prepared according to TP B. A solution of Bis(1,5-cyclooctadiene)nickel (0.144 g, 0.524 mmol), 1,5-cyclooctadiene (0.057 g, 0.524 mmol), and 2,2'-bipyridine (0.082 g, 0.524 mmol) in dry toluene (2 ml) and dry *N*,*N*-dimethylformamide (2 ml) was heated at 80^{o}C for 30 min. **5c** (0.2 g, 0.22 mmol) in dry toluene (3 ml) was added to the reaction mixture and heated at 80°C for 1 h. Bromobenzene (0.33 g, 2.1 mmol) was added, and the mixture was heated at 80°C for additional ½ h. . The isolated yield of polymer **P$_8$** was (0.151 g, 91 %).

^{1}H NMR (300 MHZ, CD_2Cl_2): δ = 8.2-7.7 (m, 2H), 7.6-6.8 (m, 12H), 6.7-6.4 (m, 10H), 2.5-2 (m, 4H), 1.4-1.1 (m, 24H), 0.9-0.8 (m, 6H).

GPC analysis*: Mw* = 112 × 10^3 g mol^{-1}, PDI = 2.7 (PPP standard).

Synthesis of polymer (P_9)

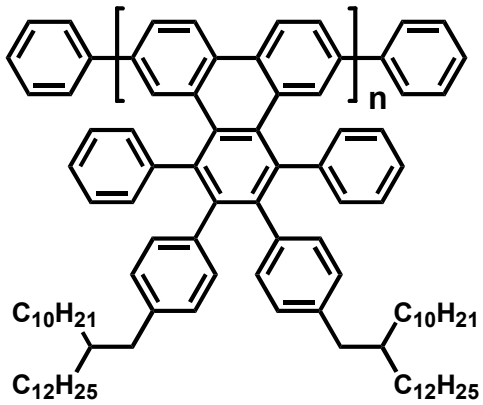

Prepared according to TP B; A solution of Bis(1,5-cyclooctadiene)nickel (0.076 g, 0.28 mmol), 1,5-cyclooctadiene (0.03 g, 0.28 mmol), and 2,2'-bipyridine (0.043 g, 0.28 mmol) in dry toluene (1 ml) and dry *N*,*N*-dimethylformamide (1 ml) was heated at 80°C for 30 min. **5g** (0.16 g, 0.12 mmol) in dry toluene (2 ml) was added to the reaction mixture and heated at 80°C for 1 h. Bromobenzene (0.33 g, 2.1 mmol) was added, and the mixture was heated at 80°C for additional ½ h. . The isolated yield of polymer **P_9** was (0.11 g, 79 %).

^{1}H NMR (300 MHZ, CD_2Cl_2): δ = 8.3-7.8 (m, 2H), 7.3-6.3 (m, 22H), 2.6-1.5 (m, 4H), 1.5-0.8 (m, 96H).

GPC analysis*: Mw* = 77 × 10^3 g mol^{-1}, PDI = 2.0 (PPP standard).

Synthesis of polymer (P_{11})

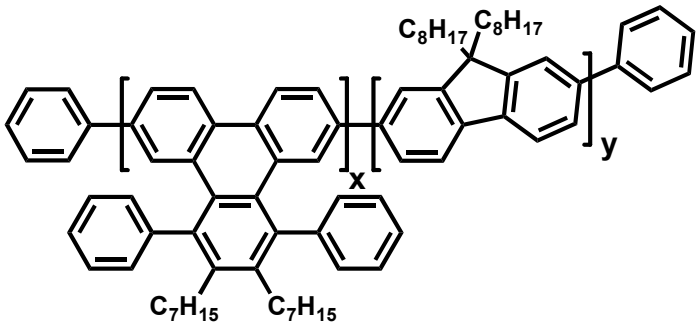

Prepared according to TP B; (1,5-cyclooctadiene) nickel (0.179 g, 0.653 mmol), cyclooctadiene (0.07 g, 0.653 mmol), and 2, 2'-bipyridine (0.1 g, 0.653 mmol) in dry toluene (2.7 ml) and dry *N*,*N*-dimethylformamide (2.7 ml) was charged under argon in a microwave

tube equipped with a magnetic stirrer bar and heated at 80°C for 30 min. A solution of **5e** (0.1 g, 0.136 mmol) and 2,7-dibromo-9,9-dioctyl-9H-fluorene **(14)** (0.074, 0.136 mmol) in dry toluene (4 ml) was added to the reaction mixture and heated at 80°C for 1 h. Bromobenzene (0.27 ml, 2.57 mmol) was added, and the mixture was heated at 80°C for additional ½ h.

The isolated yield of polymer $\mathbf{P_{11}}$ was (0.1 g, 80 %).

^{1}H NMR (250 MHZ, CD_2Cl_2): δ = 8.3-6.8 (m, 22H), 1.4-0.82 (m, 64H).

GPC analysis*: Mw* = 100 × 10^3 g mol^{-1}, PDI = 2.3 (PPP standard).

Synthesis of polymer (P_{12})

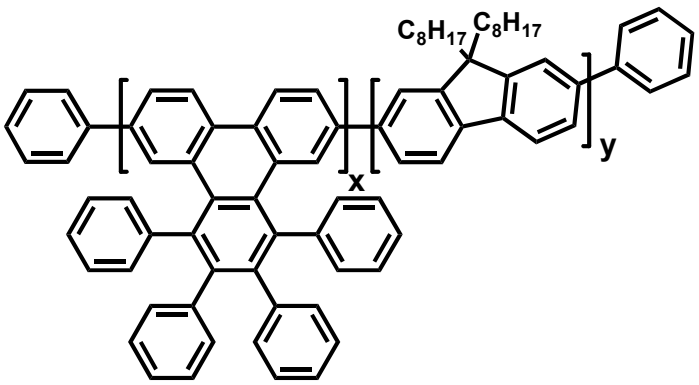

Prepared according to TP B; (1,5-cyclooctadiene) nickel (0.233 g, 0.85 mmol), cyclooctadiene (0.092 g, 0.85 mmol), and 2, 2'-bipyridine (0.132 g, 0.85 mmol) in dry toluene (3.5 ml) and dry *N*,*N*-dimethylformamide (3.5 ml) was charged under argon in a microwave tube equipped with a magnetic stirrer bar and heated at 80°C for 30 min. A solution of **5d** (0.122 g, 0.177 mmol) and **14** (0.097, 0.177 mmol) in dry toluene (5 ml) was added to the reaction mixture and heated at 80°C for 1 h. Bromobenzene (0.27 ml, 2.57 mmol) was added, and the mixture was heated at 80°C for ½ h.

The isolated yield of polymer $\mathbf{P_{12}}$ was (0.126 g, 78 %).

^{1}H NMR (250 MHZ, CD_2Cl_2): δ = 7.7-6.7 (m, 32H), 2.4-0.8 (m, 34H).

GPC analysis*: Mw* = 19 × 10^3 g mol^{-1}, PDI = 1.6 (PPP standard).

Synthesis of polymer (P_{14})

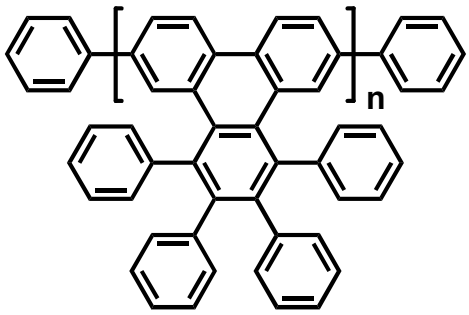

Prepared according to TP B; (1,5-cyclooctadiene) nickel (0.191 g, 0.69 mmol), cyclooctadiene (0.075 g, 0.69 mmol), and 2, 2'-bipyridine (0.11 g, 0.69 mmol) in dry toluene (3 ml) and dry *N*,*N*-dimethylformamide (3 ml) was charged under argon in a microwave tube equipped with a magnetic stirrer bar and heated at 80°C for 30 min. A solution of **5d** (0.2 g, 0.29 mmol) in dry toluene (4 ml) was added to the reaction mixture and heated at 80°C for 1 h. Bromobenzene (0.28 ml, 2.6 mmol) was added, and the mixture was heated at 80°C for ½ h. The isolated yield of polymer **P_{14}** was (0.135 g, 88 %).

MALDI-TOF-MS (TCNQ as matrix): m/z: up to 11000.

Synthesis of graphene molecule 18

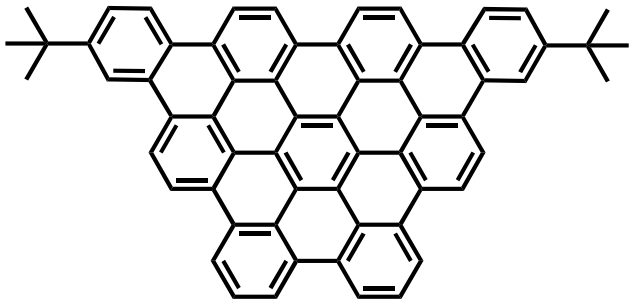

Compound **17** (0.01 g, 0.0125 mmol) was dissolved in 10 ml DCM, the solution was degassed by bubbling through argon for 20 min, and then $FeCl_3$ (0.170 g, 1.05 mmol) in CH_3NO_2 (0.9 ml) was added dropwise. After being stirred for 5 h at room temperature, the reaction was quenched by adding 50 ml methanol. The brown precipitate was collected, washed by methanol repeatedly and dried under vacuum to afford compound **18** (0.009, 90 %).

MALDI-TOF-MS (TCNQ as matrix): m/z calc.: 782.97, found: 782 ($C_{62}H_{38}$).

Synthesis of GNR-20

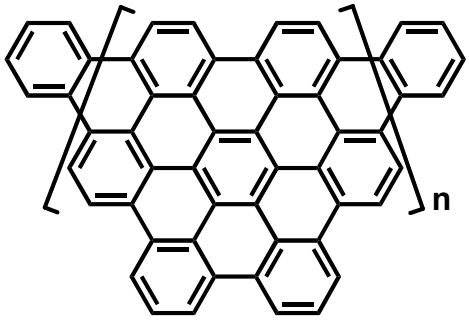

Polymer **P_{14}** (0.05 g, 0.094 mmol) was dissolved in 50 ml DCM / CS_2 solvent mixture (1:1). The solution was flashed with argon for 20 min. Following that $FeCl_3$ (1.28 g, 7.91 mmol) in CH_3NO_2 (6.5 ml) was slowly added. The reaction mixture was stirred for 24 h at room temperature. Finally, the reaction was quenched by adding 100 ml methanol. The black precipitate was collected, washed by methanol repeatedly and dried under vacuum to afford **GNR-20** (43 mg, 88 %).

Elemental analysis (%) calcd for the repeating unit $C_{42}H_{16}$: C 96.53, H 3.47; found: C 64.66, H 2.07.

Synthesis of GNR-21

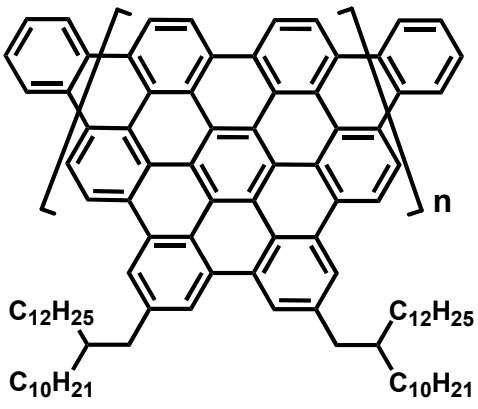

Following the synthetic procedure of **GNR-20**, Polymer **P_9** (0.02 g, 0.017 mmol) was dissolved in 20 ml DCM, followed by the addition of $FeCl_3$ (0.226 g, 1.39 mmol) in CH_3NO_2 (1.1 ml). Finally, the reaction mixture was stirred at room temperature for 24 h to afford **GNR-21** as a black (16 mg, 80 %).

Elemental analysis (%) calcd for the repeating unit $C_{90}H_{114}$: C 90.39, H 9.61; found: C 83.66, H 7.97.

Synthesis of GNR-22

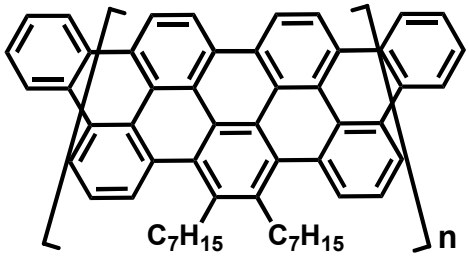

Applying the same Scholl reaction conditions for **GNR-20**, graphene nanoribbon **GNR-22** was synthesized. Polymer $\mathbf{P_7}$ (0.01 g, 0.0174 mmol) was dissolved in 10 ml DCM, $FeCl_3$ (0.135 g, 0.83 mmol) in CH_3NO_2 (0.7ml) was then added to the polymer solution and the whole mixture left to stir at room temperature for 24 h. Finally, **GNR-22** was isolated as a black (8.5 mg, 85 %).

9,9'-bianthracene (24)

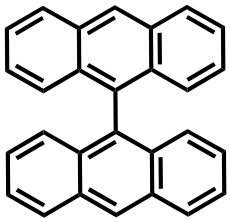

Bis(1,5-cyclooctadiene)nickel (2.56 g, 9.31 mmol), 1,5-cyclooctadiene (1 g, 9.31 mmol), and 2,2'-bipyridine (1.45 g, 9.31 mmol) were dissolved in dry toluene (4 ml) and dry *N*,*N*-dimethylformamide (4 ml) and stored under argon in a microwave tube. The mixture was stirred and heated to 80°C for 30 min to produce the catalyst. A solution of 9-bromoanthracene (**23**) (1 g, 3.9 mmol) was added to 12 ml of a mixture of dry toluene and dry *N*,*N*-dimethylformamide (1:1). The mixture was then continuously stirred in a CEM Discover

microwave oven at 80 W holding the temperature at 80°C for 1h. The mixture was afterwards rinsed in methanol/concentrated hydrochloric acid (1:1) and the solvent was removed under reduced pressure. The product was finally purified by chromatography on silica gel with hexane: DCM (20:1), yielding compound **24** as a light yellow solid (0.308 g, 22 %).

^{1}H NMR (250 MH_Z, CD_2Cl_2): δ = 8.72 (s, 2H), 8.18 (d, *J* = 8.58 Hz, 4H), 7.49-7.43 (m, 4H), 7.18-7.02 (m, 8H).

^{13}C NMR (62.5 MHZ, CD_2CL_2): δ = 133.3, 132, 131.9, 129, 127.6, 126.9, 126.2, 125.7.

FD-MS: m/z calc.:354.4, found: 354 ($C_{28}H_{18}$).

10,10'-dibromo-9,9'-bianthracene (25)

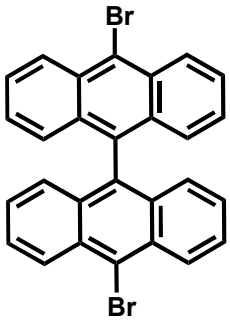

A solution of bromine (0.15 g, 0.93 mmol) in CCl_4 (7.5 mL) was added drop-wise for 10 min to a solution of 9,9'-bianthracene **24** (0.15 g, 0.42 mmol) in CCl_4 (8 ml) at 0^{o}C (ice bath). The ice bath was removed and after 24 h of further reaction time the organic layer was extracted and the solvent was removed under reduced pressure. The product was finally purified by chromatography on silica gel with hexane : DCM (20:1), yielding compound **25** as a light yellow solid (0.12 g, 55.3 %).

^{1}H NMR (250 MH_Z, CD_2Cl_2): δ = 8.71 (d, *J* = 8.88 Hz, 4H), 7.63-7.57 (m, 4H), 7.23-7.05 (m, 8H).

^{13}C NMR (62.5 MHZ, CD_2CL_2): δ = 133.6, 132.5, 130.8, 128.4, 127.7, 127.3, 126.7, 124.1.

FD-MS: m/z calc.:512.2, found: 512 ($C_{28}H_{16}Br_2$).

Elemental analysis (%) calcd for $C_{28}H_{16}Br_2$: C 65.65, H 3.15; found: C 64.60, H 2.23.

Publication

1. Jinming Cai, Pascal Ruffieux, Rached Jaafar, Marco Bieri, Thomas Braun, Stephan Blankenburg, Matthias Muoth, Ari P. Seitsonen, **Moussa Saleh**, Xinliang Feng, Klaus Müllen & Roman Fasel, "*Atomically precise bottom-up fabrication of graphene nanoribbons*" **Nature**, **2010**, 466, 470 (*The authors contributed equally to this work*).
2. **Saleh, M**.; Baumgarten, M.; Mavrinskiy, A.; Schäfer, T.; Müllen, K. "*Triphenylene-Based Polymers for Blue Polymeric Light Emitting Diodes*" **Macromol**. **2010**, 43 (1), 137.
3. **Saleh, M**.; Park, Y.-S.; Baumgarten, M.; Kim, J.-J.; Müllen, K. "*Conjugated Triphenylene Polymers for Blue OLED Devices"* **Macromol. Rap. Commun**. **2009**, 30, 1279.
4. **Moussa Saleh**, Jan Englert, Feng Xinliang, Klaus Müllen "*Extended zigzage-type grapheme nanoribbons"* In preparation and to be submitted to **Nature Chemistry**.

Patent

1. Kawano, S-I; Baumgarten, M; Müllen, K; Murer, P; Schäfer, T; **Saleh, M.** "*Novel Polymers"* WO 2010/006852 A1.